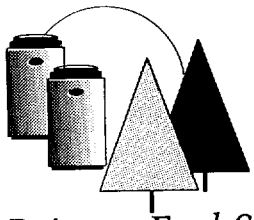

Private Fuel Storage, L.L.C.

7677 East Berry Ave., Englewood, CO 80111-2137
Phone 303-741-7009 Fax: 303-741-7806
John L. Donnell, P.E., Project Director

April 5, 2001

U.S. Nuclear Regulatory Commission
ATTN: Document Control Desk
Washington, D.C. 20555-0001

CALCULATION PACKAGE AND REPORT SUBMITTAL
DOCKET NO. 72-22 / TAC NO. L22462
PRIVATE FUEL STORAGE FACILITY
PRIVATE FUEL STORAGE L.L.C.

The calculations and reports listed below have been revised by Geomatrix Consultants, Inc. for the Private Fuel Storage Facility (PFSF) and are enclosed for your use.

1. Calculation No. 05996.02 – G(PO18) – 2, Revision 1, entitled "Soil and foundation parameters for dynamic soil-structure interaction analysis, 2000-year return period design ground motions"

2. Calculation No. 05996.02 – G(PO18) – 3, Revision 1, entitled "Development of Time Histories for 2000-year return period design spectra"

3. Fault Evaluation Study And Seismic Hazard Assessment, Rev 1, March 2001

Page replacement instructions:

- Replace the cover page for Volume I, II, and III with the enclosed Revision 1 cover pages
- Replace the Table of Contents in Volume I (pages i through vi) with the enclosed Revision 1 replacement pages
- In Volume I Chapter 6, replace pages 88 through 93 with Revision I pages 88 through 93-A
- In Volume I, replace the References (pages 110 through 118) with Revision I replace References (pages 110 through 120)
- In Volume I, add the new enclosed Revision 1 Table 6-4
- In Volume I, replace Figures 6-8 through 6-24 with Revision I replace Figures 6-8 through 6-26
- Replace Volume III – Appendix F in its entirety with the enclosed Revision 1 Appendix F

NMSSDI public

4. Development of Design Basis Ground Motions for the Private Fuel Storage Facility, Revision 1, March 2001.

   Page replacement instructions:
   - Replace the entire March 1999 document with the enclosed Revision 1, March 2001 document

These calculations and reports were revised to update the PFSF design ground motion as discussed in License Amendment #22. If you have any questions regarding this submittal, please contact me at 303-741-7009.

Sincerely

John L. Donnell
Project Director
Private Fuel Storage L.L.C.

Enclosure

cc:
Mark Delligatti-1/1
John Parkyn-1/0
Jay Silberg-1/0
Sherwin Turk-1/0
Asadul Chowdhury-1/1
Greg Zimmerman-1/0
Scott Northard-1/0
Denise Chancellor-1/1
Richard E. Condit-1/0
John Paul Kennedy-1/0
Joro Walker-1/0
Utah Document File (D. Bird)-1/1

STONE & WEBSTER ENGINEERING CORPORATION

CALCULATION TITLE PAGE

*SEE INSTRUCTIONS ON REVERSE SIDE

▲ 5010.64 (FRONT)

CLIENT & PROJECT	Private Fuel Storage Facility, LLC Private Fuel Storage Facility, Skull Valley, UT	PAGE 1 OF ~~23~~ 32
CALCULATION TITLE (Indicative of the Objective): Soil and foundation parameters for dynamic soil-structure interaction analyses, 2,000-year return period design ground motions		QA CATEGORY (✓) ☒ I – NUCLEAR SAFETY RELATED ☐ II ☐ III ☐ OTHER

CALCULATION IDENTIFICATION NUMBER				OPTIONAL WORK PACKAGE NO.
J.O. OR W.O. NO.	DIVISION & GROUP	CURRENT CALC. NO.	OPTIONAL TASK CODE	
05996.02	Geotechnical	G(PO18)-2	N/A	N/A

* APPROVALS – SIGNATURE & DATE			REV. NO. OR NEW CALC. NO.	SUPERSEDES * CALC. NO. OR REV. NO.	CONFIRMATION * REQUIRED (✓)	
PREPARER(S)/DATE(S)	REVIEWER(S)/DATE(S)	INDEPENDENT REVIEWER(S)/DATE(S)			YES	NO
Robert R. Youngs 8/10/99	C.Y. Chang 8/10/99	C.Y. Chang 8/10/99	0	N/A		X
Robert R. Youngs 3/21/01	Chin-Man Mok 3/21/01	Chin-Man Mok 3/21/01	1	05996.02-G(PO18)-2, Rev 0		

DISTRIBUTION *

GROUP	NAME & LOCATION	COPY SENT (✓)	GROUP	NAME & LOCATION	COPY SENT (✓)
RECORDS MGT. FILES (OR FIRE FILE IF NONE)	Geomatrix Consultants, Inc. Oakland, California	original ☐ ☐			☐ ☐ ☐

CALCULATION SUMMARY ▲ 5010.62	J.O./W.O./CALCULATION NO. 05996.02-G(PO18)-2	REVISION 1	PAGE 2 OF 32
CLIENT / PROJECT: Private Fuel Storage Facility, LLC Private Fuel Storage Facility, Skull Valley, UT		QA CATEGORY / CODE CLASS: I	

SUBJECT / TITLE

Soil and foundation parameters for dynamic soil-structure interaction analyses

OBJECTIVE OF CALCULATION

(1) To develop strain-compatible dynamic soil parameters for SASSI analyses.
(2) To develop dynamic parameters for uncoupled soil spring, dashpot, and mass model.

CALCULATION METHOD / ASSUMPTIONS

(1) 1-D equivalent linear site response analysis using complete program "SHAKE." The purpose is to develop strain-compatible properties corresponding to the design earthquake for 2,000 year return period.

(2) Used weighted average to estimate equivalent homogenous and isotropic soil parameters consistent with strain-compatible properties developed in (1).

(3) Calculate equivalent soil spring, dashpot, and mass parameters to match with the analytical solution of vibration of rigid rectangular footing on homogenous isotropic elastic halspace.

SOURCES OF DATA / EQUATIONS

See list of references on Page 15 of 32.

Computer Programs:
1. SHAKE: A computer program for earthquake response analysis of horizontally layered sites rev. 01 GMX, Benchmarked against Stone & Webster's qualified version of SHAKE.

CONCLUSIONS

(1) Strain-compatible dynamic soil parameters were developed for horizontally layered system. These parameters will be used in SASSI analyses. Results are listed on page 23 of 32.

(2) Equivalent soil spring, dashpot, and mass parameters were developed, results are listed on page 24 of 32.

REVIEWER (S) COMMENTS	PREPARER	DATE
	Robert R. Youngs	3/21/01
	REVIEWER / CHECKER Chin Man Mok	DATE 3/21/01
	INDEPENDENT REVIEWER Chin Man Mok	DATE 3/21/01

STONE & WEBSTER ENGINEERING CORPORATION

CALCULATION SHEET

CALCULATION IDENTIFICATION NUMBER				PAGE 3 OF 32
J.O. OR W.O. NO.	DIVISION & GROUP	CALCULATION NO.	OPTIONAL TASK CODE	
05996.02	Geotechnical	G(PO18)-2	N/A	

RECORD OF REVISIONS

Revision 0 - Original Issue

Revision 1 - The revision was performed to incorporate new soil dynamic properties data and a new design ground motion level. The entire calculation was revised.

CALCULATION SHEET	J.O./W.O./CALCULATION NO. 05996.02-G(PO18)-2	REVISION 1	PAGE 4 OF 32
PREPARER/DATE Robert R. Youngs / 3/21/01	REVIEWER/CHECKER/DATE Chin Man Mok / 3/21/01	INDEPENDENT REVIEWER/DATE Chin Man Mok / 3/21/01	
SUBJECT / TITLE Soil and foundation parameters for dynamic soil-structure interaction analyses		QA CATEGORY / CODE CLASS I	

TABLE OF CONTENTS AND HISTORIC DATA
(Revisions, Additions, Deletions, Etc.)

PRIVATE FUEL STORAGE FACILITY
SKULL VALLEY, UTAH

SOIL AND FOUNDATION PARAMETERS FOR DYNAMIC SOIL-STRUCTURE INTERACTION ANALYSES

1.0 INTRODUCTION AND APPROACH

This calculation developed dynamic soil and foundation parameters for the Private Fuel Storage Facility located in Skull Valley, Utah. The calculation supersedes Geomatrix Calculation 05996.02-G(PO18)-2 Rev 0 and 05996.02G(PO18)-1 Rev 1. The reasons for the new calculation are new soil data and a revised design level ground motion.

The approach followed in this analysis matches that used in the previous calculation [Geomatrix Calculation 05996.02-G(PO18)-2 Rev 0] and involves the following steps:

1. Dynamic properties are developed for the subsurface soils at the Skull Valley site. These include profile layering, low-strain shear and compression wave velocities, unit weight, and strain-compatible shear modulus reduction and damping relationships. In this calculation package we provide uncertainties in the dynamic properties following the guidance provided in the Standard Review Plan Chapter 3.7.2 and in ASCE 4-86. These are presented in Section 2.

2. One-dimensional site response analyses are conducted using the properties defined in step 1 and time histories scaled to match the design ground motion response spectrum defined in Geomatrix (2001b). These are described in Section 3.0

3. Using the results of step 2, three profiles are developed for use in soil-structure-interaction (SSI) analyses based on the SASSI continuum model. These profiles represent best estimate and upper and lower range strain-compatible soil properties. These are described in Section 4.0

4. Using the results of step 2, three sets of dynamic soil profiles are developed for use in SSI analyses based on uncoupled soil spring-dashpot-mass models. These profiles represent best estimate and upper and lower range strain-compatible soil properties. These are described in Section 5.0

2.0 SUBSURFACE DYNAMIC PROPERTIES

General Stratigraphy

The general stratigraphy of the Skull Valley Private Fuel Storage site is described in Geomatrix (2001a). The upper few feet consists of eolian silty soil deposits. These are underlain by Lake Bonneville lacustrine soils to a depth of 45 to 55 feet. The soils above

a depth of 26 feet consist of predominately deep-water deposits of clayey silts and silty clays. Between a depth of 26 and 45 to 55 feet, near-shore deposits of very dense fine sand underlain by very dense silts with gravel and sand layers are encountered.

An erosional unconformity marked by the Promontory soil lies at a depth of 45 to 55 feet below the surface. The soils between this unconformity and a depth of 85 to 95 feet consist of the Little Valley lacustrine deposits, interbeded gravely and clayey sands and sandy silts. These soils are dense to hard with refusal conditions often encountered in site borings.

A second erosional unconformity at a depth of 85 to 95 feet marks the boundary between Quaternary and Tertiary sediments. Below this boundary lies the Salt Lake group, a mid to late Miocene sequence of semi-consolidated siltstones, claystones and sandstones. These sediments are presumed to continue to bedrock, which is a west dipping surface lying at a depth of 600 to 800 feet beneath the site. Ground water is estimated to lie at a depth of approximately 125 feet. The underlying bedrock consists of hard limestone and dolomite.

Best Estimate Dynamic Properties

Attachment A contains a listing of seismic cone velocity measurements and down-hole velocity measurements obtained at the site. Figure 1 shows a plot of these data for the to 35 feet of the soil profile where the measurements overlap. The seismic cone data represent interval velocities taken at ~1 meter intervals. The down-hole shear wave velocity measurements represent pseudo-interval velocities at a 2.5-foot spacing. The down-hole compression wave velocities represent the layer averages defined in the down-hole velocity report.

The Table 1 defines the best estimate dynamic properties for the subsurface materials. The basis for the parameters is described below. The subsurface stratigraphy in the upper 100 feet was defined based on the cross sections presented in PFS (2000) (copies are included in Attachment A), the description given above, and the velocity data shown on Figure 1. The top 5 feet of the soils consist of eolian silts that are to be replaced by soil cement over the entire site area. Between a depth of 5 and 26 feet, the soils consist of lacustrine silty clays and clayey silts. The layering shown in Table 1 reflects the steps in shear wave velocity noted in the data shown on Figure 1, the increases in cone penetration resistance shown on the cross section in Attachment A, and the variation in soil unit weights. Table 2 of this calculation lists the moist unit weight data from the Canister Transfer Building (CTB) from Tables 3 and 4 of Stone & Webster (2000, reproduced in Attachment A) sorted by depth. There is a clear increase in the moist unit weight values at a depth of ~ 12 ft and a decrease at a depth of ~ 18 ft. Below ~ 26 ft the layering shown in Table 1 is based on the shear wave velocity layering from the down-hole velocity measurements and the cross sections developed in PFS (2000). The depth of the Tertiary sediments is assessed from the results presented in Geosphere Midwest (1997).

The average wave velocities listed in Table 1 for the depth range of 0 to 35 feet are based on a statistical analysis of the seismic cone and down-hole interval velocity data.

Attachment 2 lists two small computer programs used to compute these averages. The listing of these programs, the input files and the output files are given in Attachment B and are included in directory \CONESTAT on the attached diskette. The programs read in the interval velocity data and a prescribed layering. Each cone penetration test or down-hole boring is considered a separate velocity profile. For each layer within each profile, the average velocity is computed as the harmonic mean of all velocity measurements within the layer. The harmonic mean is equivalent to computing the average velocity by summing the travel times for each depth increment represented by a test within a soil layer and then dividing the layer thickness by the total travel time. The arithmetic average of the layer velocities across the 17 test locations are listed as the average velocities in Table 1 and are shown on Figure 1.

For the depth range of 35 to 50 feet the velocity listed in Table 1 is based on the harmonic mean of the downhole velocity measurements in boring CTB-05 between 35 and 55 feet (see Attachment B, listing of output file VS7L-ALL.out). For depths between 55 and 125 feet, the velocities are based on the down-hole velocity measurements in boring CTB-05a (listed in Attachment A) and represent the recommended layer averages. In the zone of overlap between the measurements in borings CTB-05 and CTB-05a, the values from boring CTB-05 were selected because they were taken in a cased boring and the quality of the results above ~ 45 feet in boring CTB-05a were reported to be poor (Northland Geophysical, 2001).

Geosphere Midwest (1997) conducted a shallow refraction survey of the site. In the shear wave survey Geosphere Midwest (1997, their Figures 2 and 4) identified two layers; a surficial layer with a shear wave velocity ranging from approximately 700 to 790 ft/sec, and a second layer at a depth of 40 to 55 feet with a shear wave velocity ranging generally from 1,700 to 2,400 ft/sec. The maximum depth of penetration of the shear wave survey was estimated to be 80 to 90 feet. In the compression wave survey Geosphere Midwest (1997, their Figures 1 and 3) identified three layers; a surface layer with a compression wave velocity generally in the range of 1,100 to 1,300 ft/sec, a second layer at a depth of 35 to 45 feet with a compression wave velocity in the range of 2,200 to 3,500 ft/sec, and a third layer lying at a variable depth of 90 to 125 feet with a compression wave velocity generally ranging from 5,200 to 5,900 ft/sec. The third layer was interpreted to possibly represent the location of saturated sediments. Bay Geophysical Associates (1999) conducted a second shallow refraction survey on the site to locate evidence of offsets in the shallow stratigraphy. Their Table 1 [reproduced as Table 5-2 in Geomatrix (2001a)] specifies an average shear wave velocity of 800 ft/sec for the material above the Promontory soil (depth ~45 feet and 1,100 ft/sec for the material above the Quaternary/Tertiary boundary (depth ~85 feet). These values are generally consistent with the values from Geosphere Midwest (1997). The average shear wave velocity from the surface to a depth of 85 feet computed using the Geosphere Midwest (1997) results is:

$$V(avg)=85ft/(45ft/750ft/sec+40ft/2000ft/sec)=1,063 \text{ ft/sec}$$

The results of the geophysical surveys are consistent with the more detailed seismic cone and down-hole velocity measurements. The following table computes the average velocity as a function of depth for the top 100 feet of the soil profile using the best estimate velocity profile listed in Table 1.

Calculation of Average Velocities versus Depth

Layer	Thickness (ft)	Layer Vs (fps)	Total Depth (ft)	Layer Travel Time* (sec)	Total Travel Time (sec)	Average Velocity** (fps)
1	5	560	5	0.008929	0.008929	560
2	5	580	10	0.008621	0.017549	570
3	2	727	12	0.002751	0.020300	591
4	6	854	18	0.007026	0.027326	659
5	8	871	26	0.009185	0.036511	712
6	9	1,022	35	0.008806	0.045317	772
7	15	1,190	50	0.012605	0.057922	863
8	40	1,800	90	0.022222	0.080144	1123
9	10	2,900	100	0.003448	0.083593	1196

*Layer travel time is equal to the layer thickness divided by the layer velocity.
**Average velocity is equal to the total depth divided by the total travel time.

The velocities for depths below a depth of 100 have not been measured at the site. Two alternative velocity profiles were considered for the Tertiary sediments (Table 1). The first considers the velocity to be constant for the entire depth range. The second considers that the velocity increases with depth. Two steps were placed in the velocity profile at approximately equal intervals. The velocity at the base of the profile of 5,000 fps was chosen to represent the upper range on reported velocities for the Salt Lake Group and semi-consolidated sediments in the Salt Lake Valley (Ivan Wong, 1999, personal communication; Wong and Silva, 1993; see Attachment A). The compression wave velocities in the Tertiary sediments were selected to provide a Poisson's ratio of 0.25 consistent with the value for older sediments in the Salt Lake Valley (Williams and others, 1993). The velocity profile for the crustal rocks below the Tertiary sediments was set equal to the crustal velocity model used for earthquake location in Utah (see Attachment A).

The eolian silts are to be replaced throughout the site area by soil cement to a sufficient distance that the soil-cement layer can be considered part of the free-field soil profile.

The initial design parameters for this material indicate a target minimum compacted unit weight of 100 pcf, a target undrained strength of 100 to 250 psi, and a target shear wave velocity in excess of 1,500 fps (Attachment A). Appendix F of Geomatrix (2001a)

indicates that the surface motions are not sensitive to increases in the shear wave velocity in the soil cement layer above 1,500 fps. Therefore, a value of 1,500 fps was selected as the best estimate shear wave velocity for the soil cement layer. The compression wave velocity was computed using a Poisson's ratio of 0.175, the midpoint in reported values for concrete.

The unit weights for the soil layers in Table 1 were derived as follows. The data presented in Table 2 of Stone & Webster (2000, reproduced in Attachment A) give a mean moist unit weight of 78 pcf for the silts and clays in the pad area in for depths up to ~ 12 ft. Data from the CTB listed in Table 2 of this calculation for the same depth range give and average unit weight of 86 pcf. A moist unit weight of 80 pcf was assigned to this layer to reflect the larger data set for the pad emplacement area. For the depth range of 12 to 18 feet, data given in Table 2 indicate and average moist unit weight of 105 pcf. A value of 100 was assigned to this layer to reflect the slightly lower values found at shallower depths in the pad emplacement area than in the CTB area. For the silts in the depth range of 18 to 26 feet variable unit weights are reported. The data given in Table 2 suggest average values in the range of 93 to 99 pcf. A conservative value of 94 pcf was assigned to this layer. Below 26 feet the soils become dense sands. The moist unit weights for the silts just above this layer indicate a moist unit weight of 115 pcf and this value was assigned to the sands and silts in the depth range of 26 to 50 feet. Below a depth of 50 feet, the soils are older and consist of dense sands. It was assumed that they have a slightly higher unit weight that the shallower materials and a moist unit weight of 120 pcf was assigned to these materials, corresponding to a dry unit weight of about 115 pcf and a moisture content of about 5%. The density for the Tertiary sediments was set at 135 pcf, increasing to 145 pcf below the water table. These values are consistent with unit weights reported in Wong and Silva (1993) for semi-consolidated sediments. The unit weights of the crustal rocks are consistent with the densities assumed for these materials by Wong and Silva (1993).

Upper and Lower Range Dynamic Properties

The U.S. Nuclear Regulatory Commission's Standard Review Plan, Chapter 3.7, stipulates that SSI analyses must be performed using a range of properties. If the site dynamic parameters are not well known, then the low-strain shear modulus is to be varied by multiplying and dividing by a factor of 2. The American Society of Civil Engineers (ASCE, 1986) recommends that the low-strain shear modulus is to be varied by multiplying and dividing by a factor of 1+COV of the site modulus data, with a minimum COV of 0.5 to be used. In terms of wave velocities, these factors translate into factors of $\sqrt{2}$=1.414 and the $\sqrt{1.5}$=1.225, respectively.

Table 4 presents the statistics of the shear wave velocity data listed in Table 3a. These values are taken from the calculations shown in Attachment B. The coefficients of variation for the soils up to a depth of 35 feet are 0.13 or less. Thus, it is judged that the velocities in this depth range are well known and the ASCE minimum criterion of a factor of $\sqrt{1.5}$ was used to vary the velocities. For the soil cement layer and for all other

sediment layers above the basement rock at 700-feet depth, the Standard Review Plan requirement of a factor of $\sqrt{2}$ was applied. Tables 5a and 5b list the properties of the resulting soil profiles. For the low range profile, only the constant Tertiary velocity case was considered because is represents the lower range of the two best estimate cases and for the high range profile, only the increasing Tertiary velocity case was considered. In addition, the velocity in the Tertiary sediments was limited to that of the shallow crustal velocity used for the underlying limestone bedrock.

Strain-Compatible Modulus Reduction and Damping Relationships.

Figure 2 shows the strain-compatible shear modulus reduction and damping ratio curves used for the soils in the depth range of 0 to 90 feet. The curves for the depth range of 0-12 ft and 12-26 feet are based on two resonant column tests performed on samples from the site (test data presented in Attachment A). The test results for the sample at a depth of 7.9 feet were applied to the depth range of 5 to 12 feet, which represents the range of lower velocities in the silty soils; and the test results for the sample at a depth of 20.8 feet were applied to the depth range of 12 to 26 feet, which represents the range of higher velocities in the silty soils. The test results for the shallow silty and clayey soils were also applied to the soil cement layer. Modulus reduction and damping curves developed for a sand-cement mixture reported by Dupas and Pecker (1979) are similar to those for sand. Therefore, it was assumed that the curves for a silt-cement mixture would be similar to those for the silt.

For the sandy soils below a depth of 26 feet, the relationships used by Silva and others (1998) to calibrate ground motion models for alluvial soils in California were selected. Silva and others (1998) developed two alternative sets of relationships. The curves selected for this analysis represent the stiffer (less modulus reduction and lower damping) set. This set was selected because of the low level of modulus reduction and low damping exhibited by the site test data. The Tertiary sediments below a depth of 85 feet are assumed to remain linear.

The damping in the linear Tertiary sediments was computed assuming that the shallow crustal damping corresponds to a κ value of 0.04 seconds and using the crustal model for the site. Anderson and Hough (1984) have show that the high frequency attenuation of ground motions in the near surface can be modeled by the attenuation parameter κ. The κ value of 0.04 seconds was selected by Wong and Silva (1993) to represent shallow crustal damping for all types of sites in Utah and is consistent with the average value observed for soft rock sites in California. Silva and Darragh (1996) indicate that κ is related to the near surface shear wave quality factor, Q_s by the expression:

$$\kappa = \frac{H}{Q_s V_s} \qquad (1)$$

where H is the portion of the crust over which the energy loss occurs and V_s is the average shear wave velocity over H. The appropriate value of H is 1 to 2 km (Silva and Darragh,

1996). For this calculation H was set equal to 1.4 km, the point where there is a large step in the crustal velocity model.

Q_s is, in turn, related to the material damping, λ, used in liner viscoelastic wave propagation modeling (such as the site response analyses performed for this study using the program SHAKE) by the expression:

$$\lambda = \frac{1}{2Q_s} \tag{2}$$

The κ value of 0.04 seconds represents the total damping in the upper portion of the crustal profile, including the soils. To calculate the damping to be applied to the Tertiary and shallow crustal rocks, the κ contributed by the low strain damping in the soils above a depth of 90 feet is removed. The following table shows this calculation for the best estimate profile. Equation **(2)** is used to compute the value of Q_s for each layer from the low strain damping shown on Figure 2, and Equation **(1)** is used to compute the layer contribution to κ.

layer	h(ft)	Total h(ft)	Vs(fps)	Lambda	Qs	kappa(sec)
1	5	5	562	0.009	55.6	0.00016
2	5	10	528	0.009	55.6	0.00017
3	2	12	727	0.009	55.6	0.00005
4	6	18	854	0.008	62.5	0.00011
5	8	26	871	0.008	62.5	0.00015
6	9	35	1022	0.010	50.0	0.00018
7	15	50	1190	0.010	50.0	0.00025
8	40	90	1800	0.006	83.3	0.00027
					Total	0.0013

The κ value of 0.0013 seconds is subtracted from the total of 0.04 seconds to define the portion assigned to the Tertiary and shallow crustal rocks.

Silva and Darragh (1996) found that Q_s for WUS rocks is proportional to shear wave velocity. Using the assumption that $Q_s \propto V_S$, damping values are computed for the two best estimate profiles in the following tables. The calculation is performed by substituting for Q_s the term γV_S in Equation **(1)**, resulting in the following expression for the total κ.

$$\kappa = \frac{1}{\gamma} \sum_i \frac{H_i}{V_{s\,i}^2} \tag{3}$$

In the following tables the value of $H_i / V_{s\,i}^2$ is summed for all layers and then Equation **(3)** is used to solve for the value of γ that produces the desired value of κ. The appropriate values of Q_s are then computed as γV_S and Equation **(2)** is used to compute the value of damping to use for each layer in the SHAKE computation.

Best Estimate Constant Tertiary Velocity

		total kappa=	0.0387	gamma=	14.37		
layer	h(km)	Th(km)	Vs(km/s)	h/Vs^2	Qs	damping	kappa
1	0.185	0.186	0.88392	0.237	12.7	0.0394	0.0165
2	1.214	1.4	1.95	0.319	28.0	0.0178	0.0222
			Sum=	0.556		Sum =	0.0387

Best Estimate Increasing Tertiary Velocity

		total kappa=	0.0387	gamma=	12.05		
layer	h(km)	Th(km)	Vs(km/s)	h/Vs^2	Qs	damping	kappa
1	0.06166667	0.06166667	0.88392	0.079	10.6	0.0470	0.0066
2	0.06166667	0.12333333	1.2192	0.041	14.7	0.0340	0.0034
3	0.06166667	0.185	1.524	0.027	18.4	0.0272	0.0022
4	1.214	1.40	1.95	-0.319	23.5	0.0213	0.0265
			Sum=	0.466		Sum =	0.0387

The following spread sheets list the damping values computed for the upper and lower range profiles. These values are based on the range of velocities considered representative of the Tertiary velocity uncertainty documented in Appendix F of Geomatrix (2001a) rather than the range listed in Table 5a and 5b required by the Standard Review Plan variation in shear modulus. Thus, the velocities represent changes from the best estimate by factors of $\sqrt{1.5}$.

Low Range Constant Tertiary Velocity

		total kappa=	0.0386	gamma=	17.47		
layer	h(km)	Th(km)	Vs(km/s)	h/Vs^2	Qs	damping	kappa
1	0.185	0.186	0.7217	0.355	12.6	0.0397	0.0203
2	1.214	1.4	1.95	0.319	34.1	0.0147	0.0183
			Sum=	0.674		Sum =	0.0386

High Range Increasing Tertiary Velocity

		total kappa=	0.0387	gamma=	10.80		
layer	h(km)	Th(km)	Vs(km/s)	h/Vs^2	Qs	damping	kappa
1	0.06166667	0.06166667	1.0826	0.053	11.7	0.0428	0.0049
2	0.06166667	0.12333333	1.4932	0.028	16.1	0.0310	0.0026
3	0.06166667	0.185	1.8335	0.018	19.8	0.0253	0.0017
4	1.214	1.40	1.95	0.319	21.1	0.0237	0.0296
			Sum=	0.418		Sum =	0.0387

3.0 SITE RESPONSE ANALYSES

The site response analyses were conducted using Geomatrix's in-house version of program SHAKE. This program has been benchmarked against Stone & Webster's verified version of SHAKE. Documentation of this verification is located in the project files.

The input ground motion is specified to be the horizontal 2,000-year return period time histories developed by Geomatrix (2001b) which are specified at the free surface. Both horizontal components were used to perform the calculations. A total of 8 site response analyses were performed (4 velocity profiles × 2 input time histories). The input and output files are located in Attachment C. Figures 3, 4, and 5 show the strain-compatible shear wave velocity and damping values obtained for the low range, best estimate, and high range velocity profiles, respectively. The results are show to a depth of 200 feet only because the sediments are assumed to remain linear below a depth of 100 feet. For each velocity profile, the geometric mean of the strain-compatible modulus and the average of the damping in each layer were computed as described in Attachment C. Figures 6, 7, and 8 show these values.

4.0 IDEALIZED SOIL PROFILE FOR SASSI ANALYSES

Based on the strain-compatible profiles obtained from one-dimensional site response analysis, idealized horizontally layered soil profiles were developed in support of the SSI analyses based on SASSI continuum model. The dynamic properties for these idealized layers are presented in Table 6. The details of this idealization are in spreadsheet SV-SSIFEB01.XLS in Attachment D. The compressional-wave velocity profile is assumed to be equal to the low-strain values (no reduction in bulk modulus). The damping ratios for compressional-waves are assumed to be the same as those for shear-waves, and are limited to be not greater than 10% (Geomatrix, 1996).

5.0 SOIL PARAMETERS FOR SPRING, DASHPOT, AND MASS MODEL

The equivalent single layer shear modulus, Young's modulus, damping ratio, and unit weight of the soil were computed as a weighted average of the values within 30 feet below the surface (the minimum width of the canister storage pads). The weighting factors were assumed to decrease linearly with increasing depth, to zero at a depth of 30 feet. These values are computed using the spreadsheet SV-SSIFEB01.XLS in Attachment D and are listed in Table 7. The storage pads extend approximately 3 feet below grade. To account for this embedment, the top 3 feet of the soil-cement is removed from the computation of the soil springs for the best estimate properties. To account for the variation in the soil-cement thickness across the site (~± 2 feet) the lower range properties have the minimum thickness below the pad (planned to be 1 foot) and the upper range properties have 4 feet of soil-cement.

Based on Table 3.1 of Newmark and Rosenblueth (1971) (see Attachment D) for a surface rectangular foundation of 30 feet by 67 feet, the equivalent dynamic soil

parameters were computed (see spreadsheet SV-SSIFEB01.XLS in Attachment D). These are:

A = area of foundation (30 ft × 67 ft)

ρ = mass density = unit weight/acceleration of gravity

E = Young's modulus = $G(1+\mu)$ where μ is Poisson's ratio and G is the shear modulus

Vertical Mode

$$
\begin{aligned}
h &= 0.27\sqrt{A} \\
M &= Ah\rho \\
m &= M / A = h\rho \\
K_V &= \frac{E\sqrt{A}C_S}{1-\mu^2} \\
k_V &= K_V / A = \frac{EC_s}{\sqrt{A}\left(1-\mu^2\right)} \\
C &= 5.42\sqrt{K_V \rho h^3} \\
c &= C / A = 5.42\sqrt{k_V A\rho h^3} / A
\end{aligned}
\qquad \textbf{(4)}
$$

where m is the mass constant/unit area, k_V is the spring constant/unit area, and c is the dashpot constant/unit area. Constant C_S is interpolated from Table 3.1 of Newmark and Rosenblueth (1971) for an aspect ratio of 67/30=2.23 as 1.099.

Horizontal Mode

$$
\begin{aligned}
h &= 0.05\sqrt{A} \\
M &= Ah\rho \\
m &= M / A = h\rho \\
K_H &= \frac{E\sqrt{A}k_T}{1-\mu^2} \\
k_H &= K_H / A = \frac{Ek_T}{\sqrt{A}\left(1-\mu^2\right)} \\
C &= 41.1\sqrt{K_H \rho h^3} \\
c &= C / A = 41.1\sqrt{k_H A\rho h^3} / A
\end{aligned}
\qquad \textbf{(5)}
$$

where m is the mass constant/unit area, k_H is the spring constant/unit area, and c is the dashpot constant/unit area. Constant k_T is interpolated from Table 3.1 of Newmark and Rosenblueth (1971) for an aspect ratio of 67/30=2.23 and Poisson's ratio.

Rocking Mode

$$
\begin{aligned}
h &= 0.35\sqrt{A} \\
M &= Ah\tilde{n} \\
m &= M / A = h\tilde{n} \\
K_R &= \frac{EIk_{\delta}}{\sqrt{A}\left(1-\dot{\imath}^{2}\right)} \\
I &= LB^3 / 12 \\
k_R &= K_V / I = \frac{Ek_{\delta}}{\sqrt{A}\left(1-\dot{\imath}^{2}\right)} \\
C &= 0.97\sqrt{K_R \tilde{n} h^5} \\
c &= C / I = {0.97\sqrt{K_R \tilde{n} h^5}} \Big/ {LB^3 / 12}
\end{aligned}
\qquad (6)
$$

where m is the mass constant/unit area, k_R is the spring constant/unit area, and c is the dashpot constant/unit area. Constant k_ϕ is interpolated from Table 3.1 of Newmark and Rosenblueth (1971) for an aspect ratio of 67/30 = 2.23.

The resulting parameters are presented in Table 7.

As this calculation was being finalized, it was determined that the maximum thickness of soil cement under the pads is to be 2 feet. Use of a maximum soil-cement thickness of 2 feet instead of 4 feet results in slightly lower values than those given in Table 7 for the upper range dynamic properties. Thus, use of the upper range dynamic properties given in Table 7 in dynamic response calculations is conservative.

6.0 REFERENCES

American Society of Civil Engineers (ASCE), 1986, Seismic analysis of safety-related nuclear structures and commentary on standard for seismic analysis of safety-related nuclear structures: ASCE Standard 4-86.

Anderson, J.G., and Hough, S.E., 1984, A model for the shape of the Fourier amplitude spectrum of acceleration at high frequencies: Bulletin of the Seismological Society of America, v. 74, p. 1969-1994.

Bay Geophysical Associates, Inc., 1999, Shearwave reflection survey: Prepared for Stone & Webster Engineering Corporation, January.

Dupas, J.-M., and Pecker, A., 1979, Static and dynamic properties of sand-cement: Journal of the Geotechnical Engineering Division, ASCE, v. 105, n. GT3, p. 419-436.

Electric Power Research Institute (EPRI), 1993, Guidelines for determining design basis ground motions: Electric Power Research Institute Report EPRITR-102293.

Geomatrix Consultants, Inc., 1996, Recommendations of site response analyses of vertical excitation, Richmond-San Rafael Bridge seismic retrofit design: report prepared for

Geomatrix Consultants, Inc., 2001a, Fault evaluation study and seismic hazard assessment, Private Fuel Storage Facility, Skull Valley, Utah, Rev 01: report prepared for Stone & Webster Engineering Corporation, March.

Geomatrix Consultants, Inc., 2001b, Development of design ground motions for the Private Fuel Storage Facility, Skull Valley, Utah, Rev.01: report prepared for Stone & Webster Engineering Corporation, March.

Geosphere, 1997, Seismic survey of Private Fuel Storage Facility: Geosphere Midwest, Midland, MI, January, 1997.

Newmark, N.M. and Rosenblueth, E., 1971, *Fundamentals of Earthquake Engineering*, Prentice Hall, Inc.

Northland Geophysical, LLC, 2001, Rev. 1 of report on downhole seismic geophysical testing, Private Fuel Storage Facility, Skull Valley, Utah, ESSOW No. 05996.02-G011: report prepared for Private Fuel Storage, January 31.

Private Fuel Storage Limited Liability Company (PFS), 2000, Safety Analysis Report for Private Fuel Storage Facility, Revision 8, Docket No. 72-22, La Crosse, WI.

Silva, W., 1986, Soil response to earthquake ground motion: Report prepared for the Electric Power Research Institute, Research Project RP2556-07, September.

Silva, W.J. and R.B. Darragh, 1996, Engineering characterization of strong ground motion recorded at rock sites: Report submitted to the Electric Power Research Institute, EPRI RP 2556-48.

Silva, W.C., Abrahamson, N., Toro, G., and Costantino, C., 1998, Description and validation of the stochastic ground motion model: Report submitted to Brookhaven National Laboratory, Associated Universities, Inc., New York.

Stone and Webster, 2000, Document basis for geotechnical parameters provided in geotechnical design criteria: Stone and Webster Engineering Corporation, Calculation 05996.02-G(B)-05, Rev. 2, June 15.

Williams, R.A., King, K.W., and Tinsley, J.C., 1993, Site response estimates in Salt Lake Valley, Utah, from borehole seismic velocities: Bulletin of the Seismological Society of America, v. 83, p. 862-889.

Wong, I., and Silva, W.J., 1993, Site-specific strong ground motion estimates for the Salt Lake Valley, Utah: Utah Geological Survey Miscellaneous Publication 93-9, 34 p.

Table 1
Best Estimate Dynamic Properties for Skull Valley PFSF Site
Constant Tertiary Sediment Velocity

Layer	Depth to Base of Layer (ft)	Average Layer Shear Wave Velocity (fps)	Average Layer Compression Wave Velocity (fps)	Unit Weight (pcf)
Eolian silts* replaced by Soil cement	5±2 5±2	560* 1,500	1,117* 2,390	-- 100
Silty clay/clayey silt	10±1	528	1,131	80
Silty clay/clayey silt	12±1	727	1,260	80
Silty clay/clayey silt	18±1	854	1,472	100
Silty clay/clayey silt	26±1	871	1,440	94
Sand	35±1	1,022	1,667	115
Sands and silts	50±5	1,190	2,085	115
Dense sands and silty sands capped by Promontory Soil	90±5	1,800	3,400	120
Tertiary Salt Lake group – unsaturated	125	2,900	5,023	135
Tertiary Salt Lake group – saturated	700±100	2,900	5,023	145
Shallow crustal rocks	4,593	6,398	11,155	165
Crustal rocks	15 km	11,122	19,357	170

Increasing Tertiary Sediment Velocity

Layer	Depth to Base of Layer (ft)	Average Layer Shear Wave Velocity (fps)	Average Layer Compression Wave Velocity (fps)	Unit Weight (pcf)
Eolian silts* replaced by Soil cement	5±2 5±2	560* 1,500	1,117* 2,390	-- 100
Silty clay/clayey silt	10±1	528	1,131	80
Silty clay/clayey silt	12±1	727	1,260	80
Silty clay/clayey silt	18±1	854	1,472	100
Silty clay/clayey silt	26±1	871	1,440	94
Sand	35±1	1,022	1,667	115
Sands and silts	50±5	1,190	2,085	115
Dense sands and silty sands capped by Promontory Soil	90±5	1,800	3,400	120
Tertiary Salt Lake group – unsaturated	125	2,900	5,023	135
Tertiary Salt Lake group – saturated	300±30	2,900	5,023	145
Tertiary Salt Lake group – saturated	500±70	4,000	6928	145
Tertiary Salt Lake group – saturated	700±100	5,000	8660	145
Shallow crustal rocks	4,593	6,398	11,155	165
Crustal rocks	15 km	11,122	19,357	170

Table 2

Moist Unit Weights from CTB area (Tables 3 and 4 of Stone & Webster, 2000)

S&W Table Number	Boring	Sample	Depth (ft)	Moist Unit Wt (pcf)	
3	CTB-S	U-1AA	5.3	73.2	
3	CTB-N	U-1B	5.7	100.6	
3	CTB-S	U-1B	5.8	78	
3	CTB-S	U-1D	6.6	84.8	
3	CTB-4	U-1C	7	95.7	
3	CTB-4	U-1D	7.5	74.9	
3	CTB-6	U-3B	7.6	81.2	
3	CTB-N	U-2B	7.7	74.6	
3	CTB-6	U-3C	7.9	88.5	
3	CTB-1	U-3C	8.1	86.4	
3	CTB-6	U-3D	8.3	85.7	
3	CTB-N	U-2C	8.3	86.3	
4	CTB-7	U-3D	8.3	102.3	
3	CTB-S	U-2D	8.4	90	
3	CTB-1	U-3D	8.7	91.9	
3	CTB-N	U-2D	8.7	78.8	
3	CTB-4	U-2D	9.5	87.7	
3	CTB-4	U-2E	9.9	94.1	
3	CTB-N	U-3C	9.9	86.1	
3	CTB-S	U-3C	10.1	89.5	
4	CTB-S	U-3D	10.4	84.7	
3	CTB-N	U-3D	10.5	86.3	86.4 (Average for E5:E26)
3	CTB-5	U-6C	10.8	101.8	
3	CTB-5	U-6D	11.1	111.3	
3	CTB-5	U-6E	11.3	118	
3	CTB-4	U-7D	13	101.3	
4	CTB-5	U-8D	15.4	105.8	
4	CTB-4	U-9E	16.9	98.4	
4	CTB-4	U-9F	17.1	101	105.4 (Average for E28:E34)
3	CTB-5	U-10D	19.4	94.5	
3	CTB-1	U-7C	21.1	83.8	
3	CTB-4	U-11D	21.2	89.8	
3	CTB-1	U-7D	21.7	91.2	
3	CTB-5	U-12B	23.2	93.6	
3	CTB-5	U-12C	23.6	96.4	
3	CTB-5	U-12D	23.9	93.7	
3	CTB-4	U-13D	25.2	101.4	93.1 (Average for E36:E43)
3	CTB-5	U-14D	27	113.9	99.0 (Average for E36:E46)
3	CTB-5	U-14E	27.4	114.7	
3	CTB-4	U-15C	28	115.5	114.7 (Average for E44:E46)

Table 3a
Layer Shear Wave Velocities for Individual Cone Penetration Tests or Borings

Depth Range (ft)	Shear Wave Velocity (fps)for Cone Penetration Test / Boring								
	CPT 01	CPT 03	CPT 06	CPT 13	CPT 15	CPT 16	CPT 18	CPT 20	CPT 21
0-5	596	644	545	592	496	588	499	525	625
5-10	452	457	571	534	545	543	474	491	434
10-12	594	647	789	653	562	623	650	789	702
12-18	825	777	763	905	879	848	761	948	856
18-26	877	950	877	883	886	840	877	898	863
26-35	1140	1078	-	-	-	-	-	-	1021
Depth Range (ft)	Shear Wave Velocity (fps)for Cone Penetration Test / Boring								
	CPT 22	CPT 31	CPT 33	CPT 34	CPT 36	CPT 37	CPT 38	Boring CTB 05	
0-5	605	559	508	443	612	-	-	585	
5-10	518	526	559	449	709	581	499	636	
10-12	759	906	869	679	731	741	803	853	
12-18	885	912	903	898	890	839	808	823	
18-26	810	902	881	873	866	828	865	835	
26-35	-	-	986	-	-	912	957	1059	
								1191	

Table 3b
Layer Compression Wave Velocities for Individual Cone Penetration Tests or Borings

Depth Range (ft)	Compression Wave Velocity (fps)for Cone Penetration Test / Boring								
	CPT 01	CPT 03	CPT 06	CPT 13	CPT 15	CPT 16	CPT 18	CPT 20	CPT 21
0-5	1145	1271	1052	1027	1362	1272	1124	813	1128
5-10	1058	1053	1236	1015	1320	1094	1139	1415	1110
10-12	1087	1070	1235	1274	1161	1083	1517	1522	1170
12-18	1529	1456	1312	1464	1447	1422	1407	1528	1582
18-26	1289	1343	2105	1390	1394	1347	1691	1446	1408
26-35	1798	1879	-	-	-	-	-	-	1962
Depth Range (ft)	Compression Wave Velocity (fps)for Cone Penetration Test / Boring								
	CPT 22	CPT 31	CPT 33	CPT 34	CPT 36	CPT 37	CPT 38	Boring CTB 05	
0-5	1282	852	1058	1003	1368	-	-	990	
5-10	1379	1140	1023	1046	959	1083	1168	990	
10-12	1148	1280	1337	1205	1377	1182	1330	1440	
12-18	1419	1688	1566	1505	1414	1312	1537	1440	
18-26	1308	1624	1275	1319	1439	1314	1345	1440	
26-35	-	-	1593	-	-	1461	1537	1440	

Table 4
Statistics of Shear Wave Velocities in Table 3a

Layer	Depth Range (ft)	Number of Velocity Profiles	Average Shear Wave Velocity (fps)	Standard Deviation in Shear Wave Velocity (fps)	Coefficient of Variation	90% Confidence Interval in Mean Velocity (fps)	Correlation Coefficient with Layer Above
1	0-5	15	560	57	0.10	±24	--
2	5-10	17	528	70	0.13	±28	0.13
3	10-12	17	727	100	0.14	±40	0.34
4	12-18	17	854	55	0.06	±22	0.21
5	18-26	17	871	32	0.04	±13	-0.05
6	26-35	7	1,022	78	0.08	±48	0.58

Table 5a
Low Range Dynamic Properties for Skull Valley PFSF Site

Layer	Depth to Base of Layer (ft)	Average Layer Shear Wave Velocity (fps)	Average Layer Compression Wave Velocity (fps)	Unit Weight (pcf)
Soil cement	5	1,061	1,690	100
Silty clay/clayey silt	10	431	923	80
Silty clay/clayey silt	12	594	1,029	80
Silty clay/clayey silt	18	697	1,202	100
Silty clay/clayey silt	26	712	1,176	94
Sand	35	834	1,361	115
Sands and silts	50	841	1,474	115
Dense sands and silty sands capped by Promontory Soil	90	1,273	2,404	120
Tertiary Salt Lake group – unsaturated	125	2,051	3,552	135
Tertiary Salt Lake group – saturated	700	2,051	3,552	145
Shallow crustal rocks	4,593	6,398	11,155	165
Crustal rocks	15 km	11,122	19,357	170

Table 5b
High Range Dynamic Properties for Skull Valley PFSF Site

Layer	Depth to Base of Layer (ft)	Average Layer Shear Wave Velocity (fps)	Average Layer Compression Wave Velocity (fps)	Unit Weight (pcf)
Soil cement	5	2,121	3,380	100
Silty clay/clayey silt	10	647	1,385	80
Silty clay/clayey silt	12	890	1,543	80
Silty clay/clayey silt	18	1,046	1,803	100
Silty clay/clayey silt	26	1,068	1,764	94
Sand	35	1,250	2,042	115
Sands and silts	50	1,683	2,949	115
Dense sands and silty sands capped by Promontory Soil	90	2,546	4,808	120
Tertiary Salt Lake group – unsaturated	125	4,101	7,104	135
Tertiary Salt Lake group – saturated	300	4,101	7,104	145
Tertiary Salt Lake group – saturated	500	5,657	9,798	145
Tertiary Salt Lake group – saturated	700	6,398	11,155	145
Shallow crustal rocks	4,593	6,398	11,155	165
Crustal rocks	15 km	11,122	19,357	170

Table 6
Dynamic Soil Properties for SASSI Model

High Range Properties

Shake Layers	Depth of Top (ft)	Depth of Bottom (ft)	Density (pcf)	Wave Velocity		Damping Ratio		Poisson's Ratio
				Vs (fps)	Vp (fps)	Shear (%)	Compression (%)	
1-2	0	5	100	2120	3380	0.91	0.91	0.176
3-4	5	10	80	557	1385	3.48	3.48	0.403
5	10	12	80	807	1543	2.69	2.69	0.312
6-7	12	18	100	983	1803	1.82	1.82	0.289
8-9	18	26	94	973	1764	2.31	2.31	0.281
10-12	26	35	115	1053	2042	5.07	5.07	0.319
13-15	35	50	115	1488	2949	4.04	4.04	0.329
16-23	50	90	120	2481	4808	1.21	1.21	0.318
24-26	90	125	135	4101	7104	4.28	4.28	0.250
27-35	125	300	145	4101	7104	4.28	4.28	0.250
36-39	300	500	145	5657	9798	3.10	3.10	0.250
40-41	500	700	145	6398	11155	2.53	2.53	0.255
	700		170	6398	11155	2.16	2.16	0.255

Best Estimate Properties

Shake Layers	Depth of Top (ft)	Depth of Bottom (ft)	Density (pcf)	Wave Velocity		Damping Ratio		Poisson's Ratio
				Vs (fps)	Vp (fps)	Shear (%)	Compression (%)	
1-2	0	5	100	1497	2390	0.94	0.94	0.177
3-4	5	10	80	415	1131	4.78	4.78	0.422
5	10	12	80	622	1260	3.60	3.60	0.339
6-7	12	18	100	779	1472	2.29	2.29	0.306
8-9	18	26	94	760	1440	3.01	3.01	0.307
10-12	26	35	115	818	1667	6.21	6.21	0.341
13-15	35	50	115	956	2085	6.13	6.13	0.367
16-23	50	90	120	1716	3400	1.74	1.74	0.329
24-26	90	125	135	2900	5023	4.32	4.32	0.250
27-35	125	300	145	2900	5023	4.32	4.32	0.250
36-39	300	500	145	3450	5976	3.67	3.67	0.250
40-41	500	700	145	3950	6842	3.33	3.33	0.250
	700		170	6398	11155	1.76	1.76	0.255

Low Range Properties

Shake Layers	Depth of Top (ft)	Depth of Bottom (ft)	Density (pcf)	Wave Velocity		Damping Ratio		Poisson's Ratio
				Vs (fps)	Vp (fps)	Shear (%)	Compression (%)	
1-2	0	5	100	1053	1690	1.08	1.08	0.183
3-4	5	10	80	298	923	6.57	6.57	0.442
5	10	12	80	622	1260	3.60	3.60	0.339
6-7	12	18	100	610	1202	2.97	2.97	0.327
8-9	18	26	94	593	1176	3.73	3.73	0.330
10-12	26	35	115	614	1361	8.09	8.09	0.372
13-15	35	50	115	565	1474	9.82	9.82	0.414
16-23	50	90	120	1191	2404	2.18	2.18	0.337
24-26	90	125	135	2051	3552	3.97	3.97	0.250
27-35	125	300	145	2051	3552	3.97	3.97	0.250
36-39	300	500	145	2051	3552	3.97	3.97	0.250
40-41	500	700	145	2051	3552	3.97	3.97	0.250
	700		170	6398	11155	2.16	2.16	0.255

Table 7
Dynamic Soil Properties for Spring-Dashpot-Mass Model

	Upper Range	Best Estimate	Lower Range	
Vp	2205	1527	1157	
Vs	1322	842	579	
G (ksf)	5015	2027	955	
beta S (%)	2.3	3.3	4.6	
E (ksf)	12234	5194	2546	
beta P (%)	2.3	3.3	4.6	
Poisson's Ratio	0.220	0.281	0.333	
Unit Wt. (pcf)	92.4	92.0	91.8	
A (30x67) sqft	2010	2010	2010	
Aspect Ratio	2.233	2.233	2.233	
Vertical Mode				
h	12.10	12.10	12.10	
m (pcf-sec^2)	**34.75**	**34.58**	**34.52**	mass/area (pcf-sec^2)
kv (kcf)	**315.20**	**138.29**	**70.23**	spring constant/area (kcf)
c (kcf-sec)	**4.84**	**3.20**	**2.28**	dashpot constant/area (kcf-sec)
Horizontal Mode				
h	2.24	2.24	2.24	
Kappa T	0.937	0.892	0.760	
m (pcf-sec^2)	**6.43**	**6.40**	**6.39**	mass/area (pcf-sec^2)
kh (kcf)	**268.79**	**112.24**	**48.52**	spring constant/area (kcf)
c (kcf-sec)	**2.70**	**1.74**	**1.14**	dashpot constant/area (kcf-sec)
Rocking Mode				
h	15.69	15.69	15.69	
Kr	112978035.57	49565892.37	25172167.30	
C	538785.878	356027.756	253487.104	
m (pcf-sec^2)	**45.04**	**44.83**	**44.75**	mass/area (pcf-sec^2)
kr (kcf)	**736.87**	**323.28**	**164.18**	spring constant/area (kcf)
c (kcf-sec)	**3.57**	**2.36**	**1.68**	dashpot constant/area (kcf-sec)

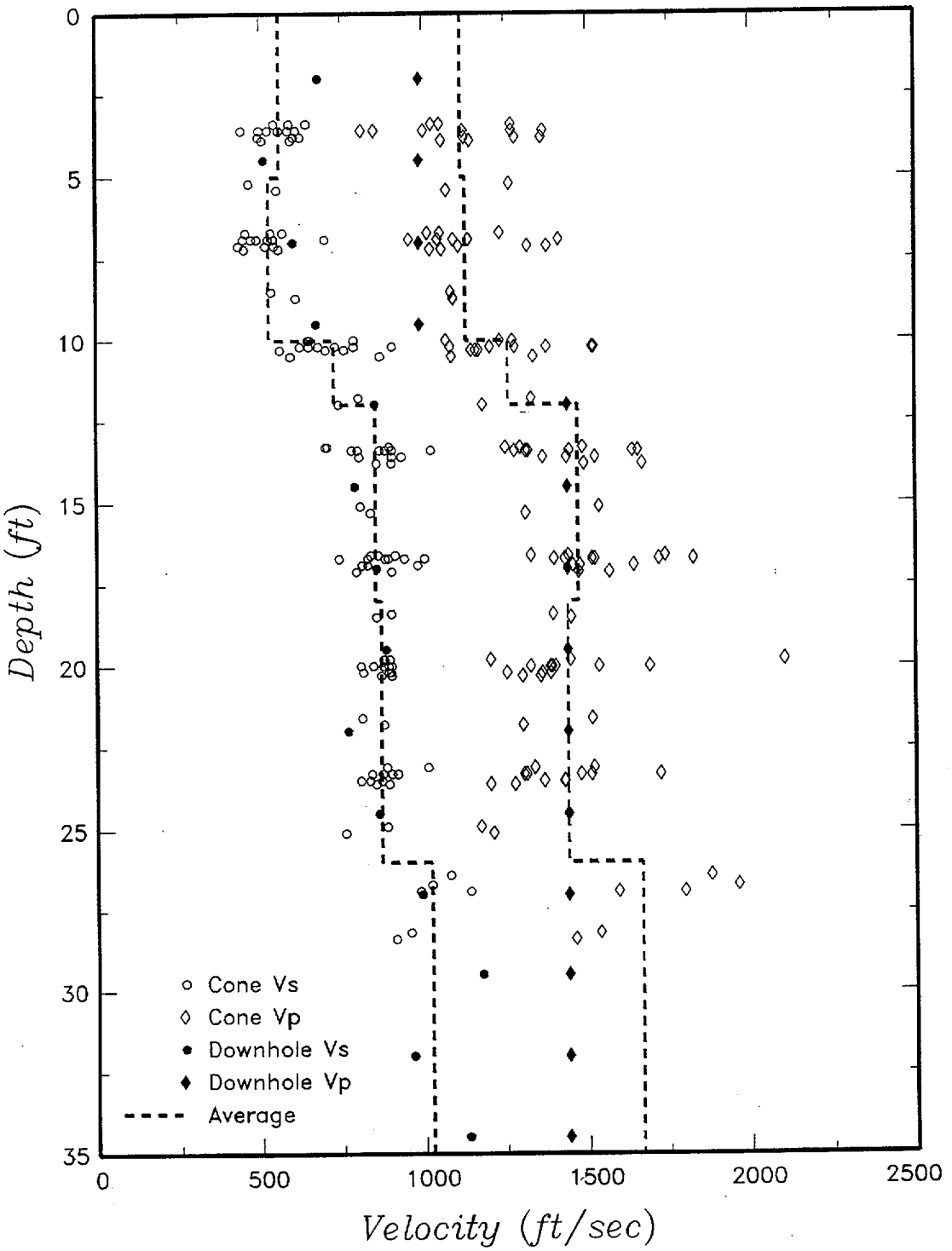

Figure 1 Site Velocity Measurements

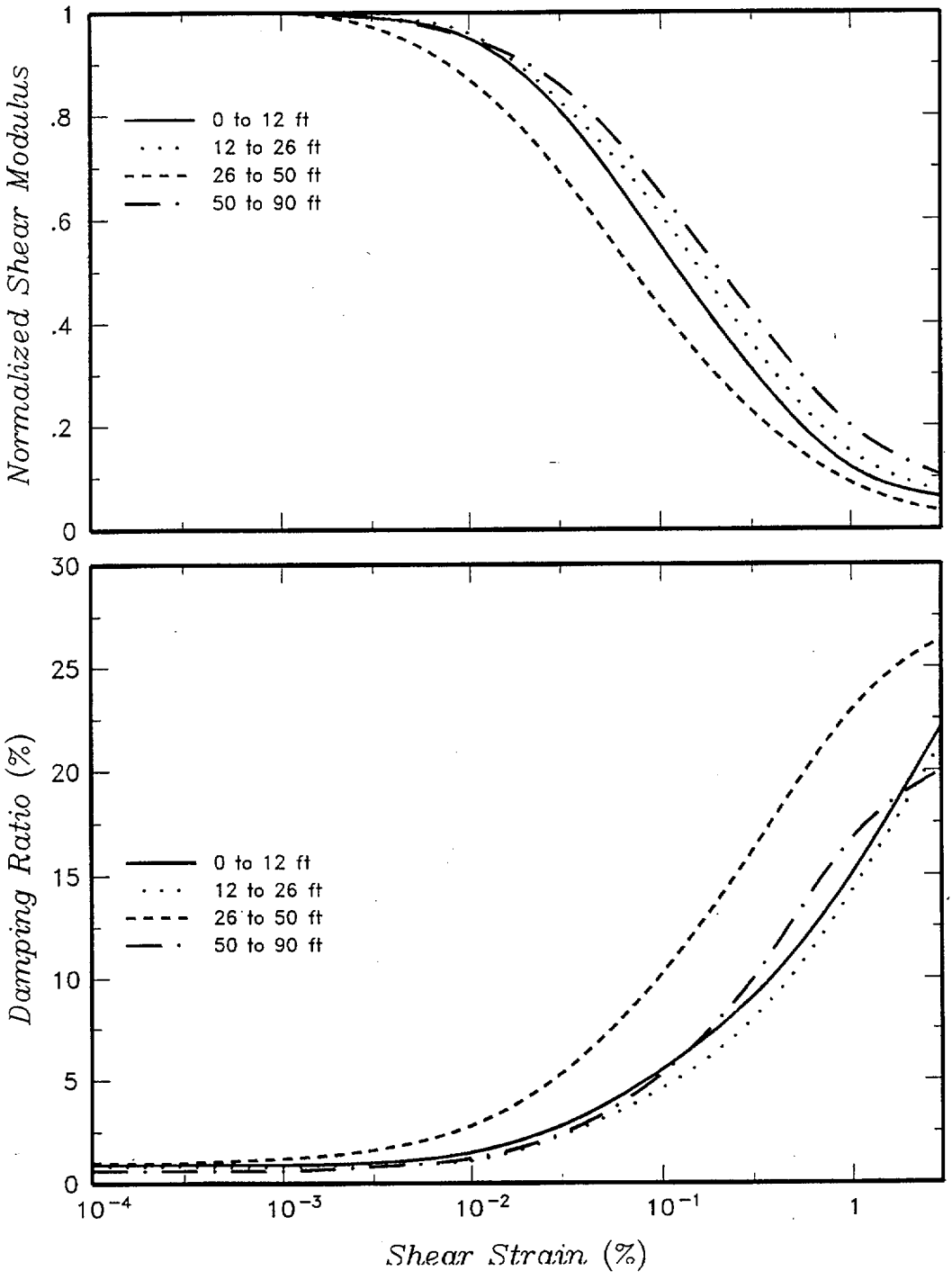

Figure 2 Modulus and Damping Relationships

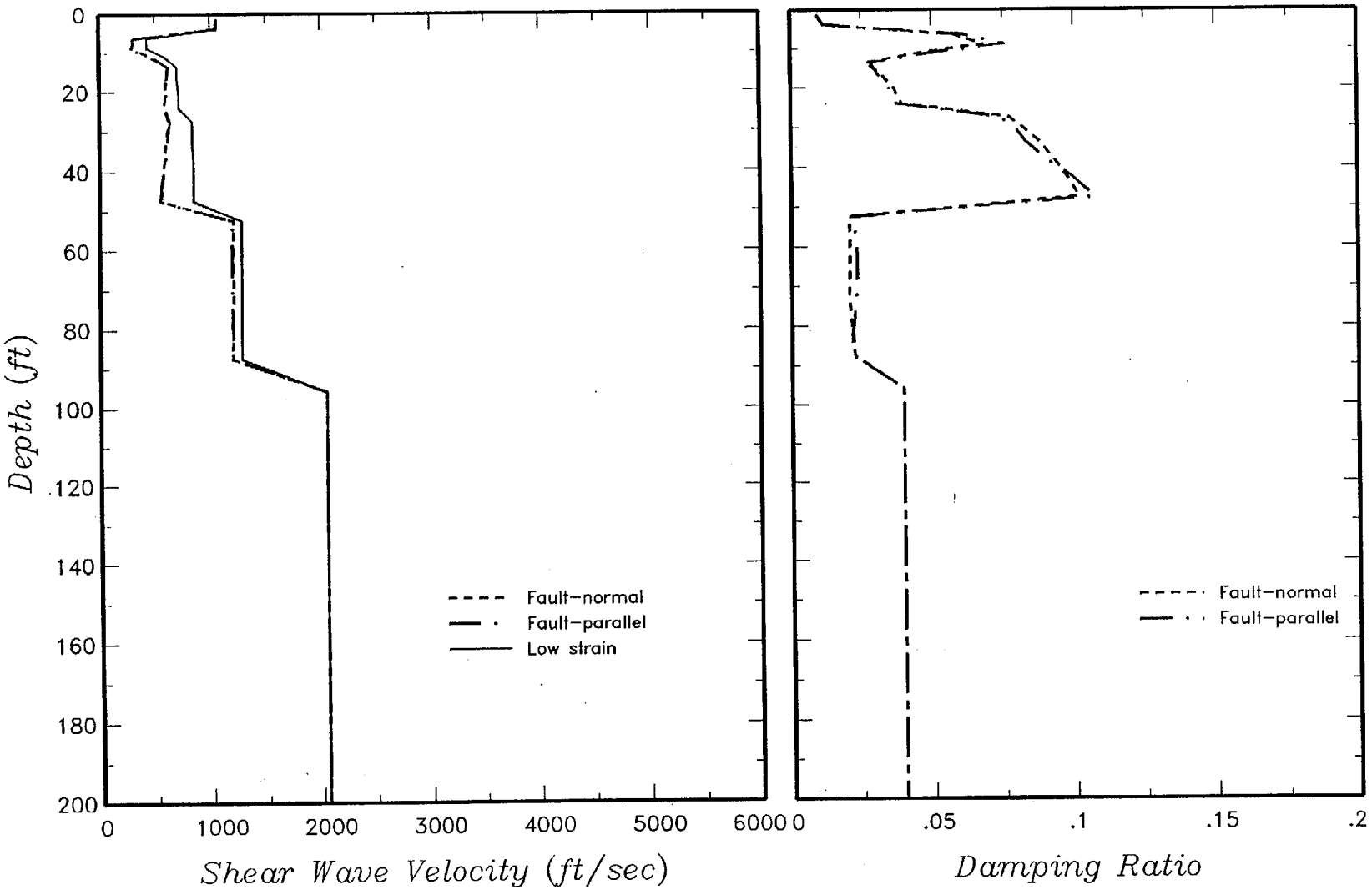

Figure 3 Strain-compatible velocity and damping for lower range properties 2,000-yr Return Period Input Motion

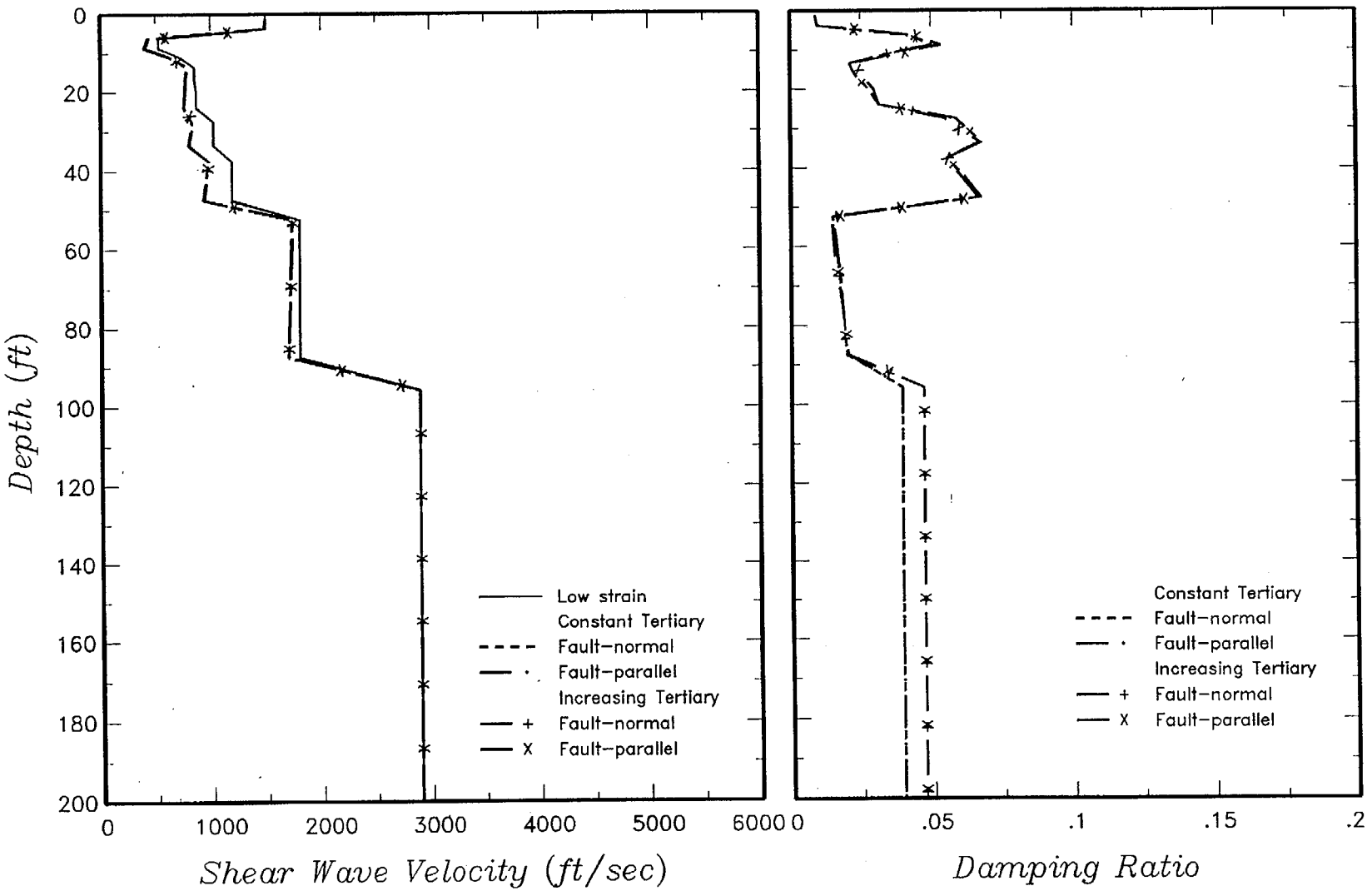

Figure 4 Strain-compatible velocity and damping for mean properties 2,000-yr Return Period Input Motion

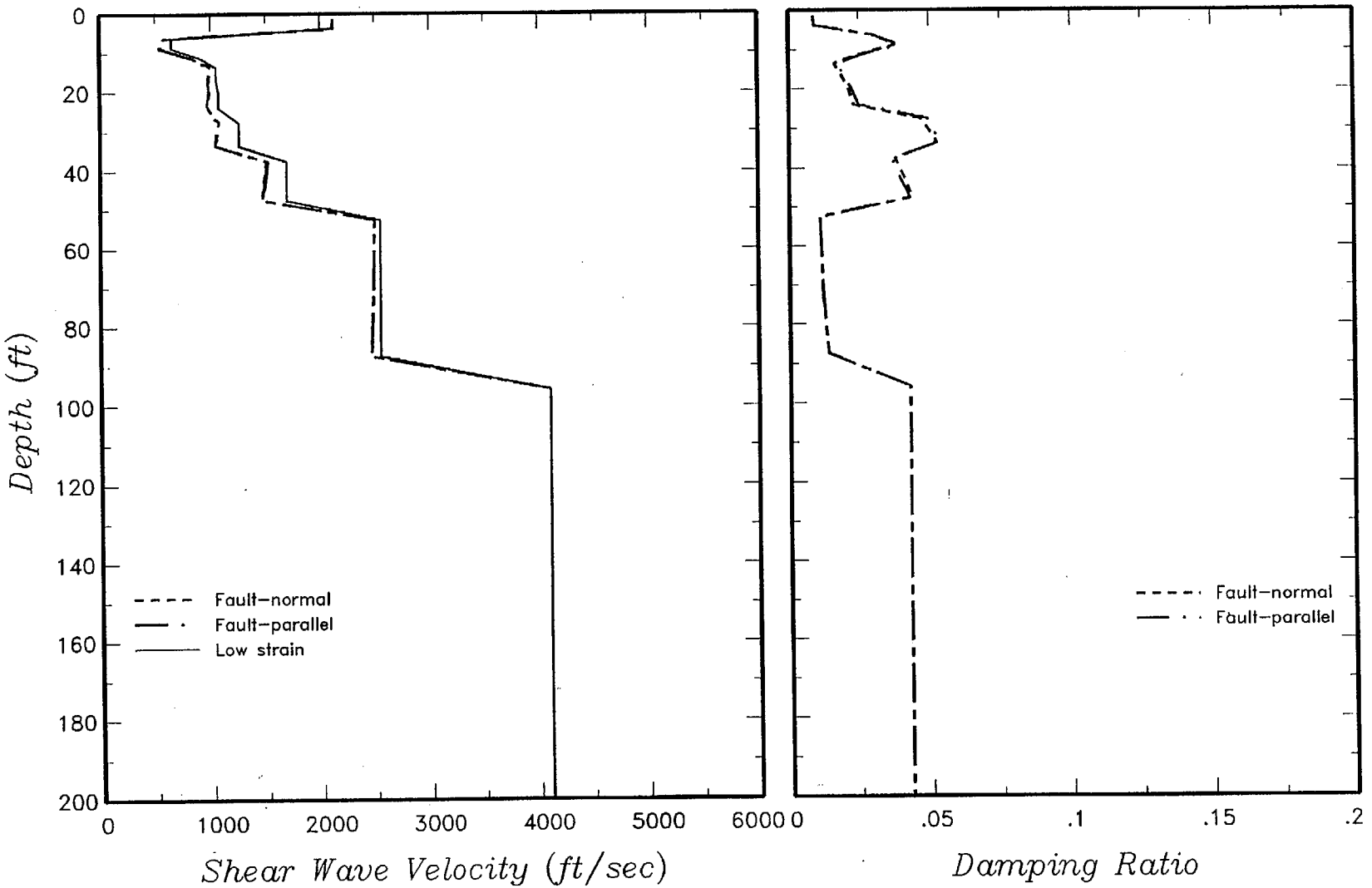

Figure 5 Strain–compatible velocity and damping for upper range properties 2,000–yr Return Period Input Motion

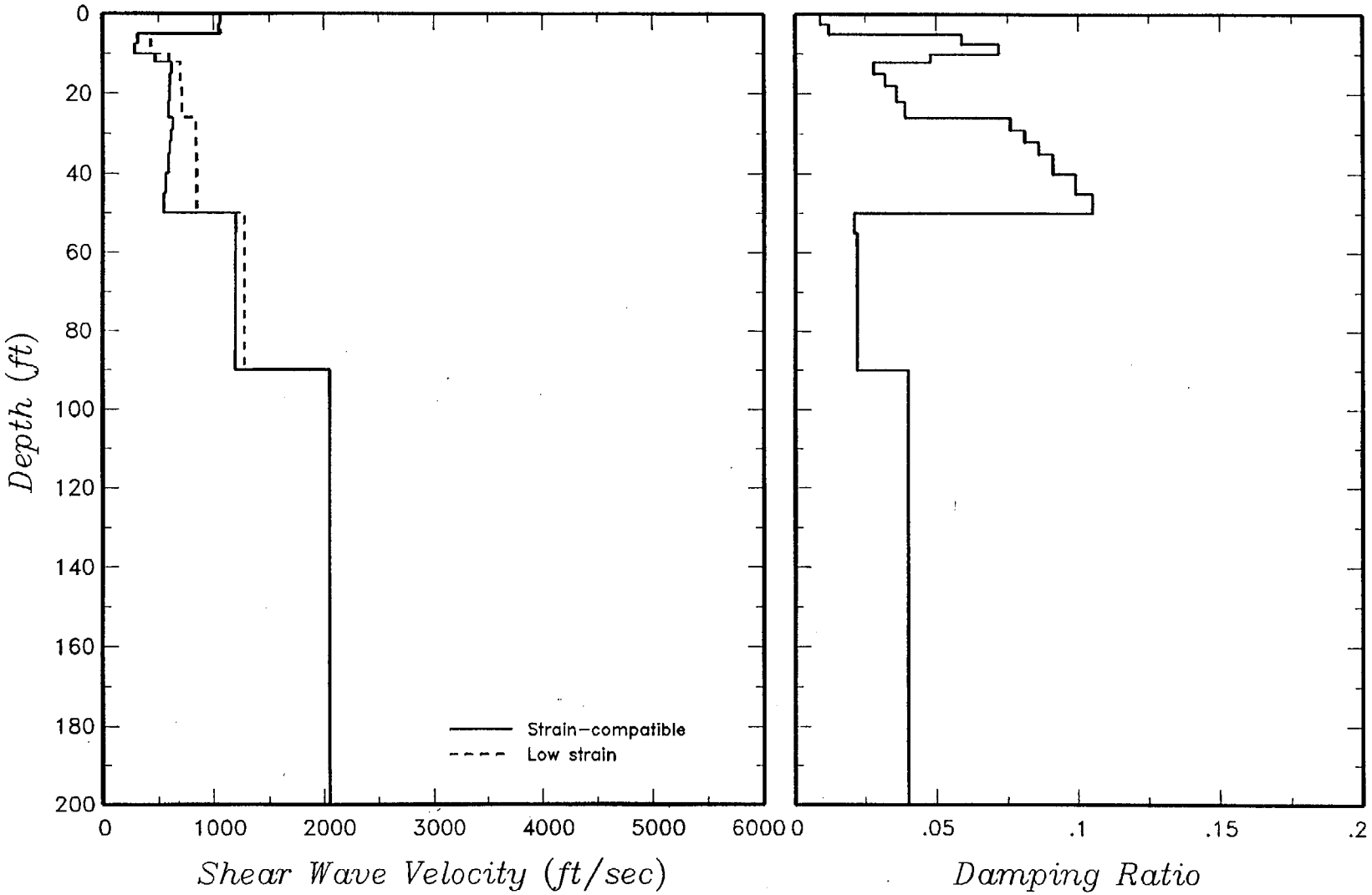

Figure 6 Average strain-compatible velocity and damping for low range properties – 2,000-yr Return Period Input Motion

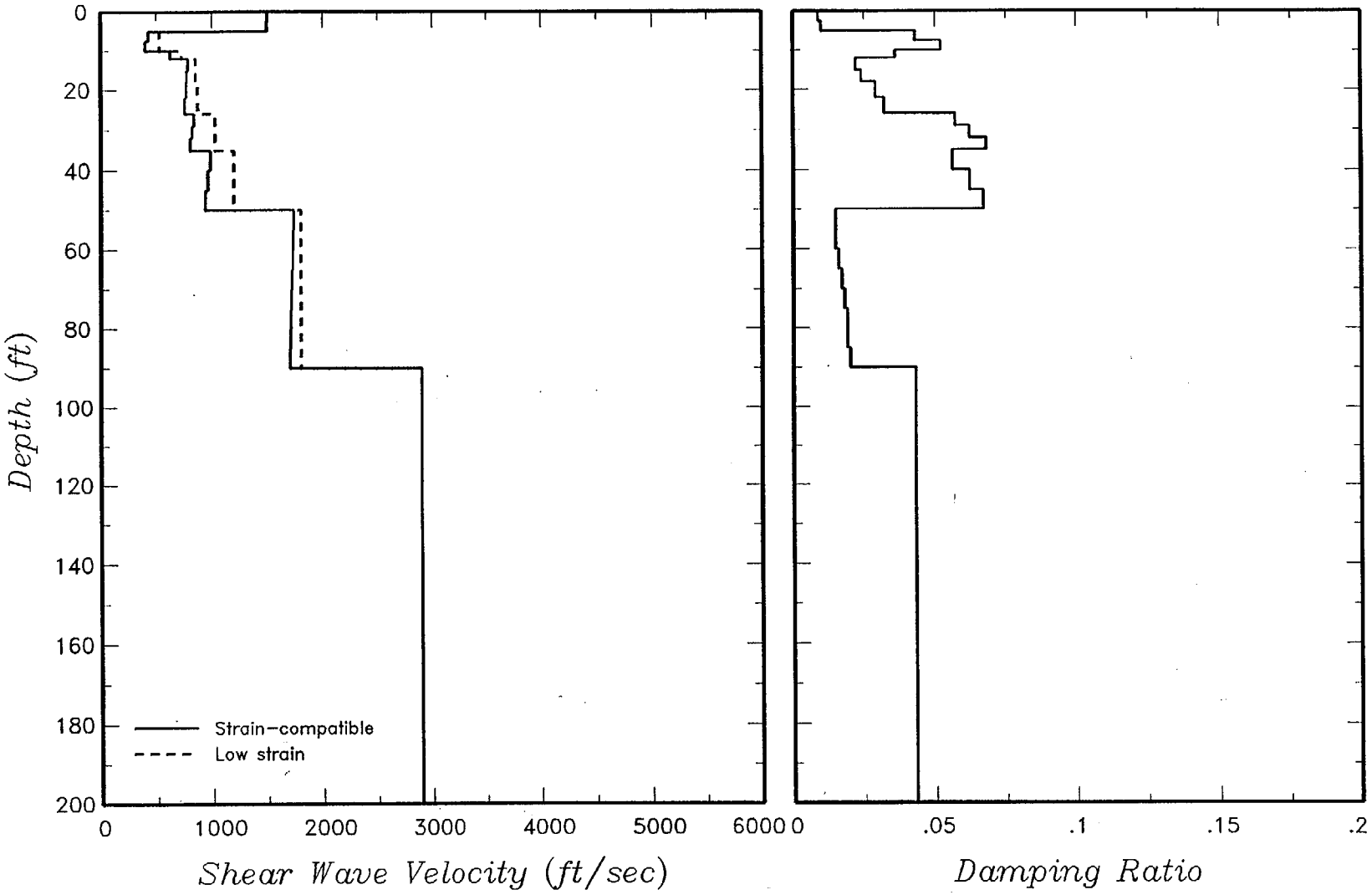

Figure 7 Average strain-compatible velocity and damping for best estimate properties – 2,000-yr Return Period Input Motion

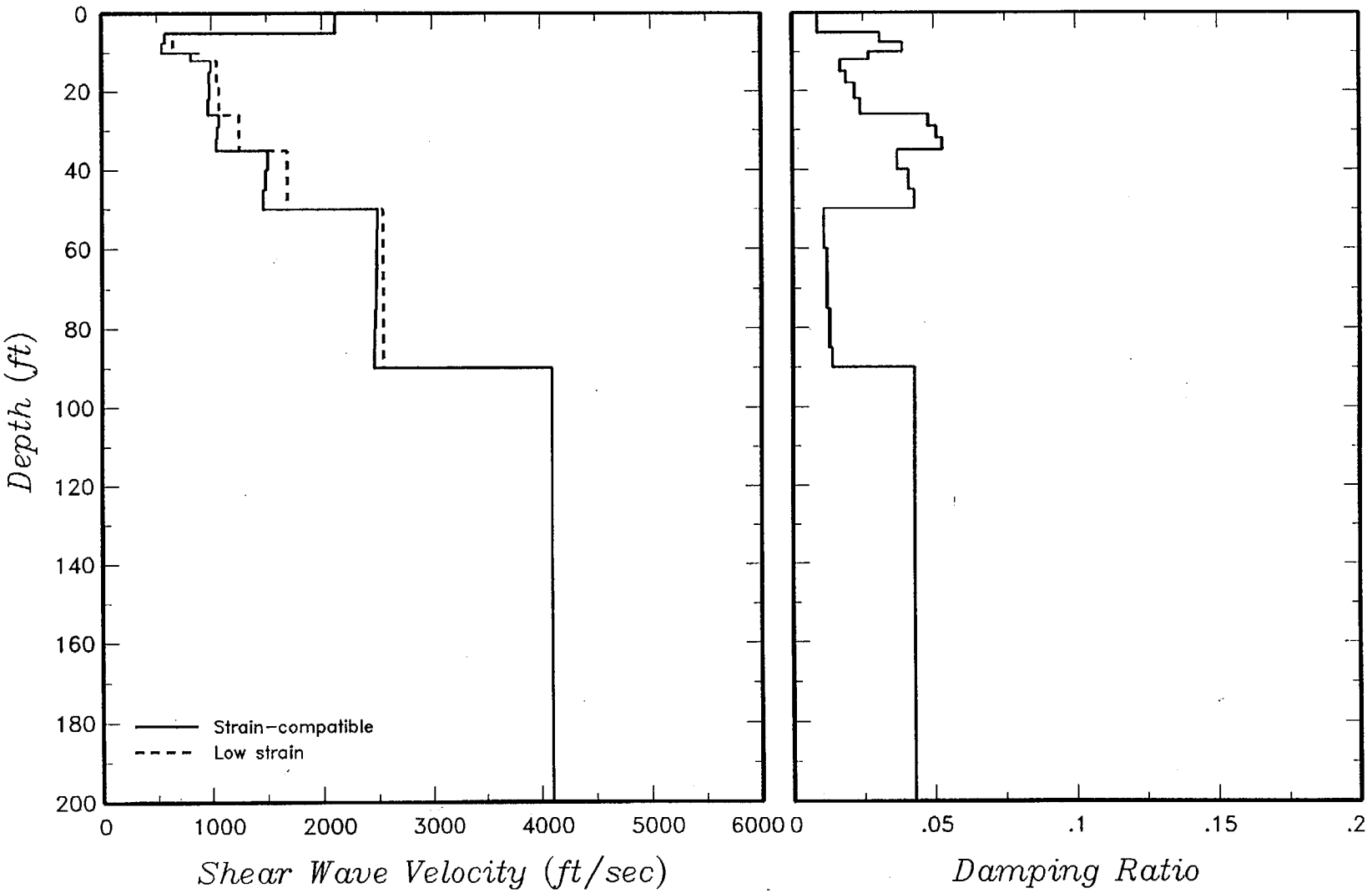

Figure 8 Average strain-compatible velocity and damping for high range properties – 2,000-yr Return Period Input Motion

Calculation 05996.02-G(PO18)-2, Rev. 1
Attachment A
Site Soil Properties Data

This attachment contains the following information:

SEISMIC LINE 2: REFLECTION SECTION ACROSS CENTER OF SITE

SURVEYED: DECEMBER 1996

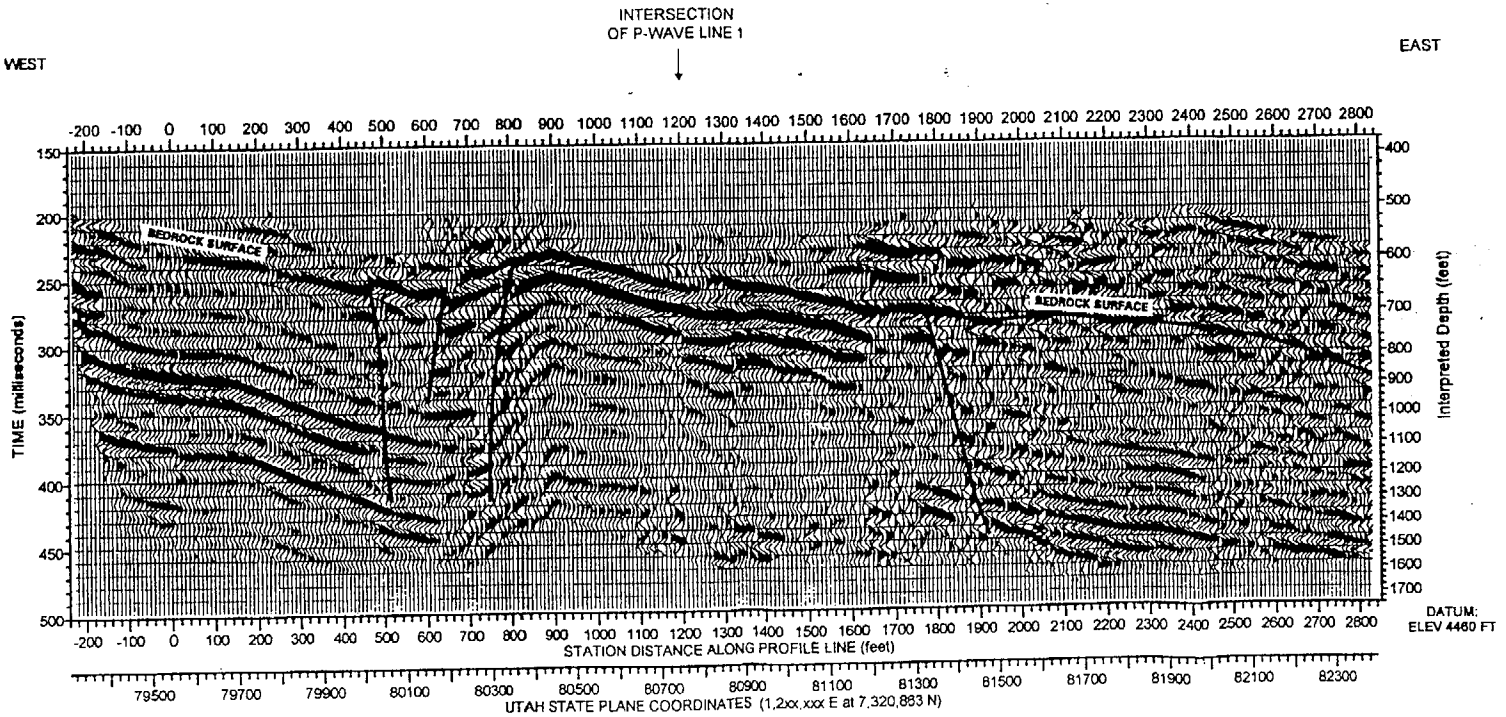

PFSF SITE, SKULL VALLEY, UTAH

GEOSPHERE MIDWEST

20

FIGURE 4.6

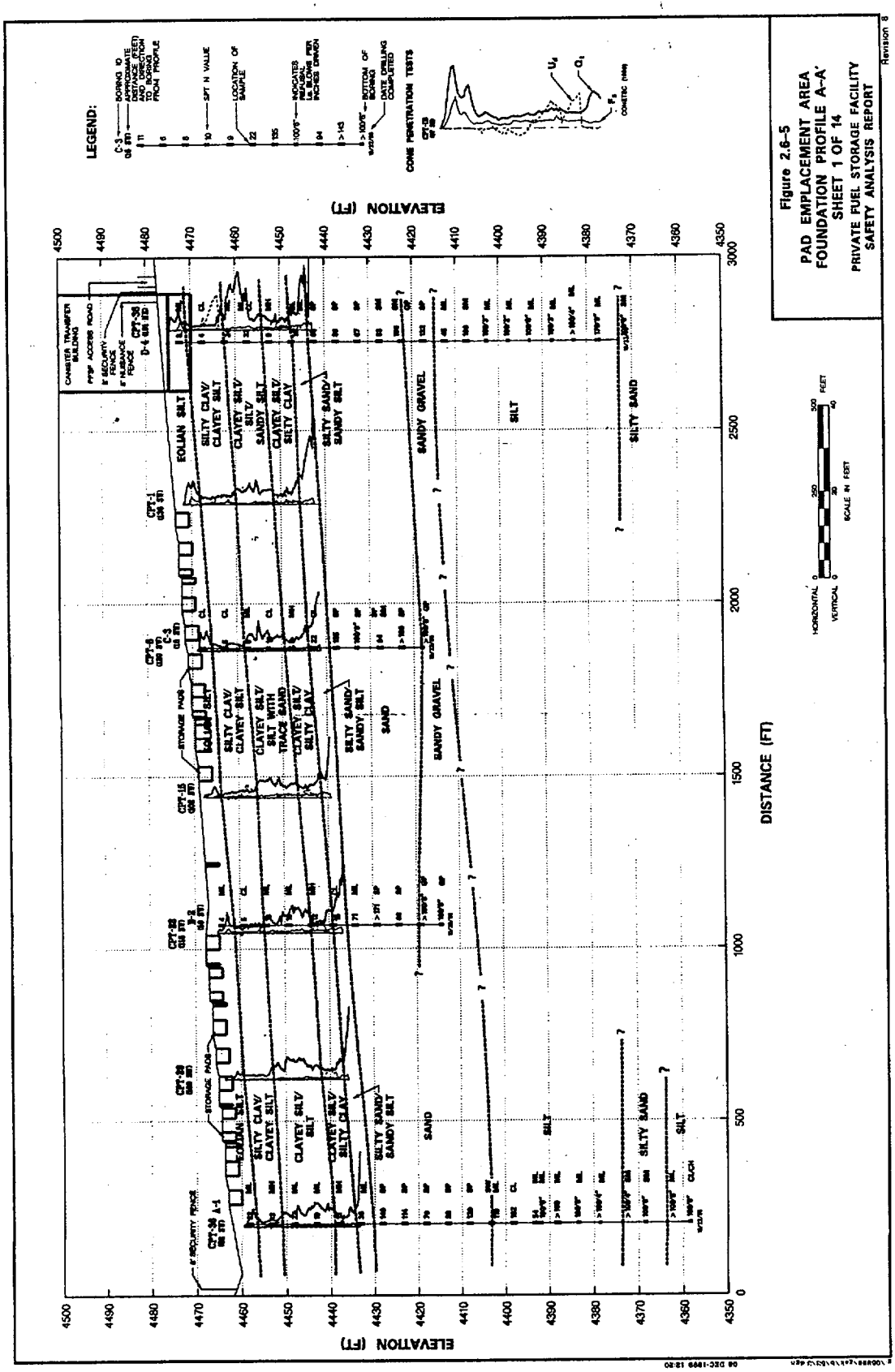
LEGEND:
CONE PENETRATION TESTS
ELEVATION (FT)
DISTANCE (FT)
CANISTER TRANSFER BUILDING
FFTF ACCESS ROAD
8' SECURITY FENCE
8' FENCE POST
STORAGE PADS
EOLIAN SILT
SILTY CLAY/ CLAYEY SILT
CLAYEY SILT/ SILTY/ SANDY SILT
CLAYEY SILT/ SILTY CLAY
SILTY SAND/ SANDY SILT
SANDY GRAVEL
SILT
SILTY SAND
CLAYEY SILT/ SILT WITH TRACE SAND
SAND
CLAYEY SILT
SILTY SAND
CLAYEY SILT/ SILTY CLAY
CLAYEY SILTY SILT
SILTY SAND/ SANDY SILT
CLAY
HORIZONTAL
VERTICAL
SCALE IN FEET
Figure 2.6-5
PAD EMPLACEMENT AREA
FOUNDATION PROFILE A-A'
SHEET 1 OF 14
PRIVATE FUEL STORAGE FACILITY
SAFETY ANALYSIS REPORT
Revision 8

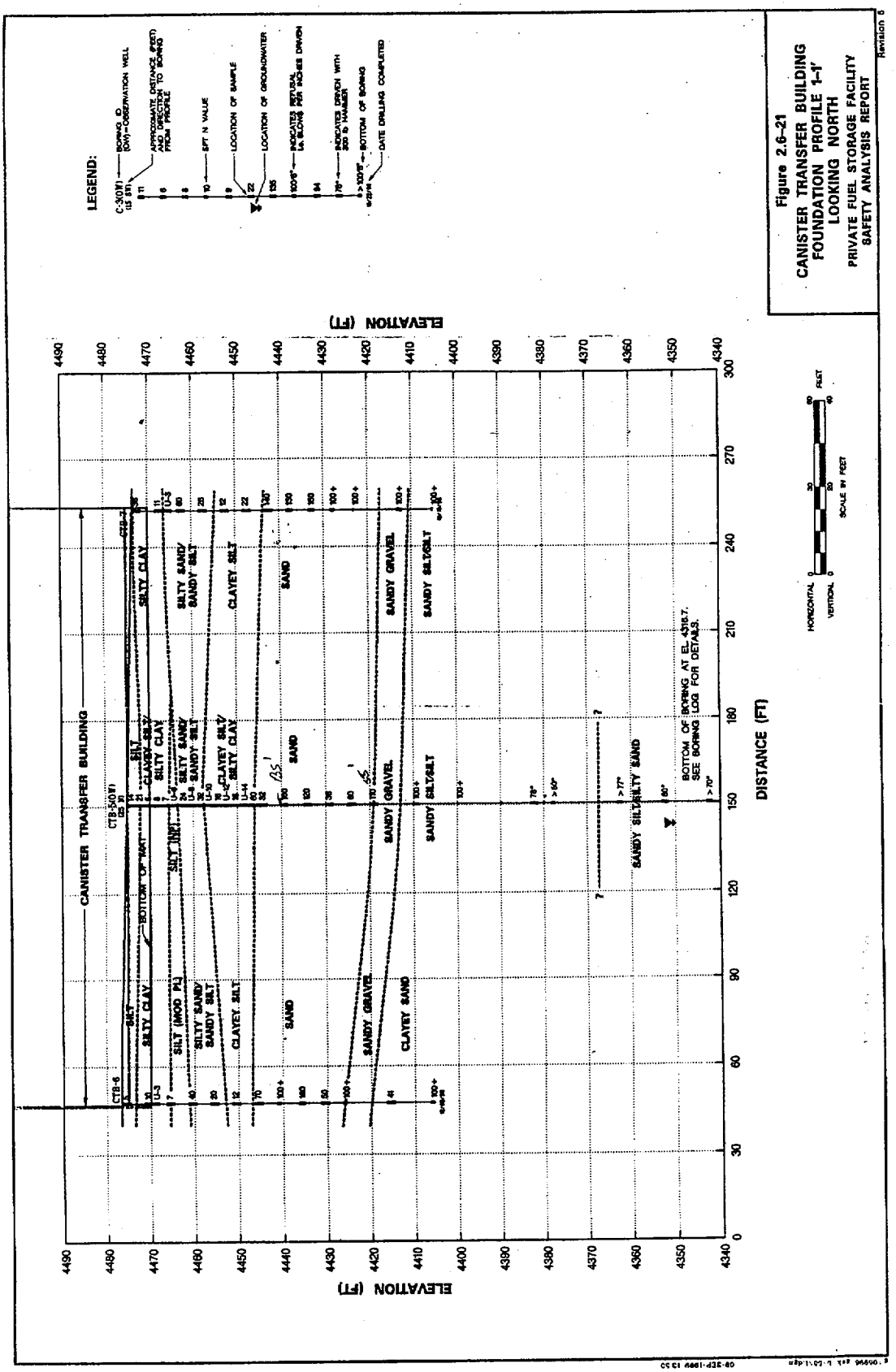
LEGEND:
CANISTER TRANSFER BUILDING
BOTTOM OF MAT
SILT
SILTY CLAY
SILT (WOOD PC)
SILTY SAND
SANDY SILT
CLAYEY SILT
SAND
SANDY GRAVEL
CLAYEY SAND
SANDY SILT/SILT
SANDY SILT/SILTY SAND
BOTTOM OF BORING AT EL. 4316.7. SEE BORING LOG FOR DETAILS.
ELEVATION (FT)
DISTANCE (FT)
HORIZONTAL
VERTICAL
SCALE IN FEET
Figure 2.6-21
CANISTER TRANSFER BUILDING
FOUNDATION PROFILE 1-1'
LOOKING NORTH
PRIVATE FUEL STORAGE FACILITY
SAFETY ANALYSIS REPORT
Revision 0

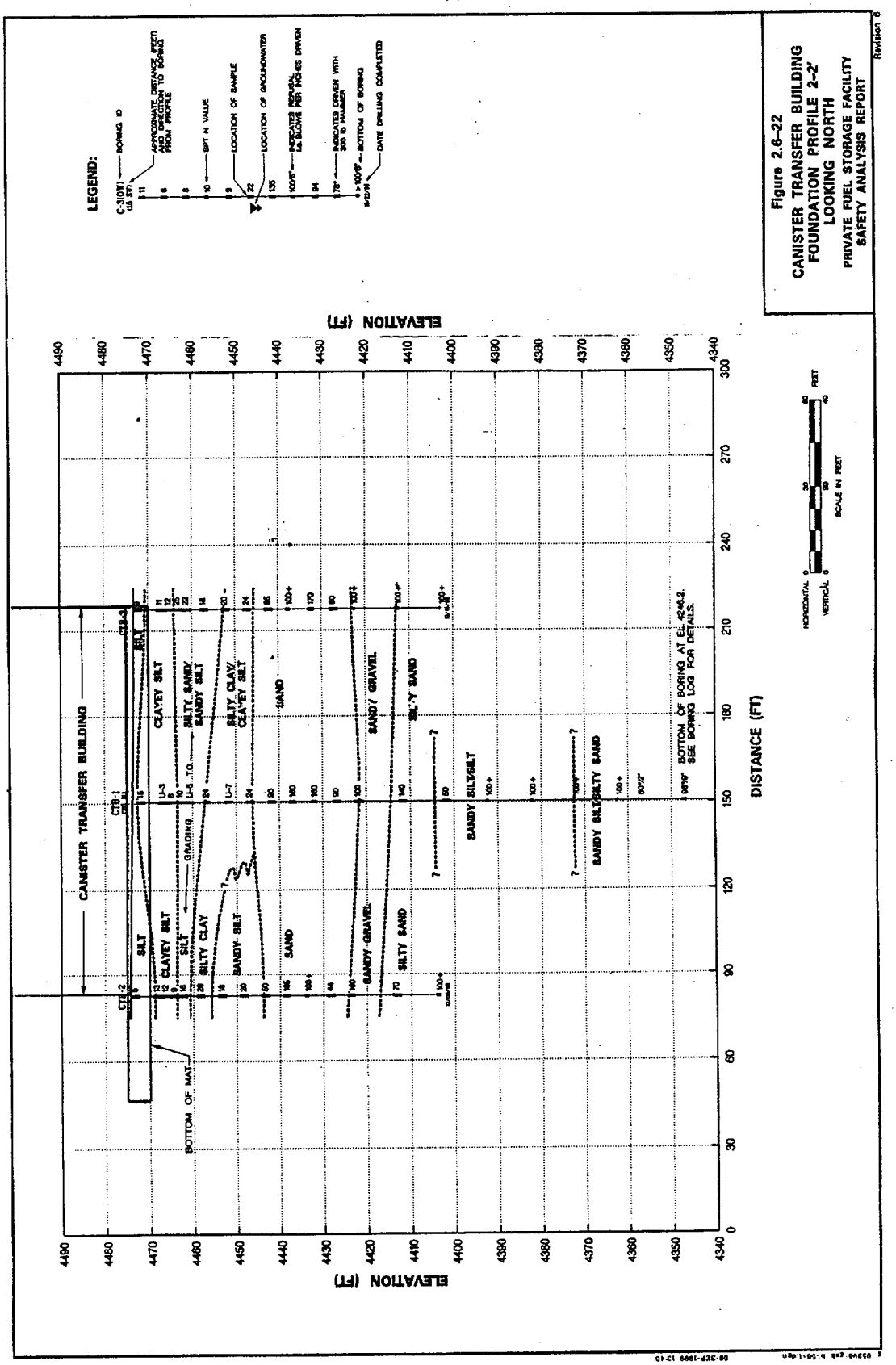

Figure 2.6-22
CANISTER TRANSFER BUILDING
FOUNDATION PROFILE 2-2'
LOOKING NORTH
PRIVATE FUEL STORAGE FACILITY
SAFETY ANALYSIS REPORT
Revision 0

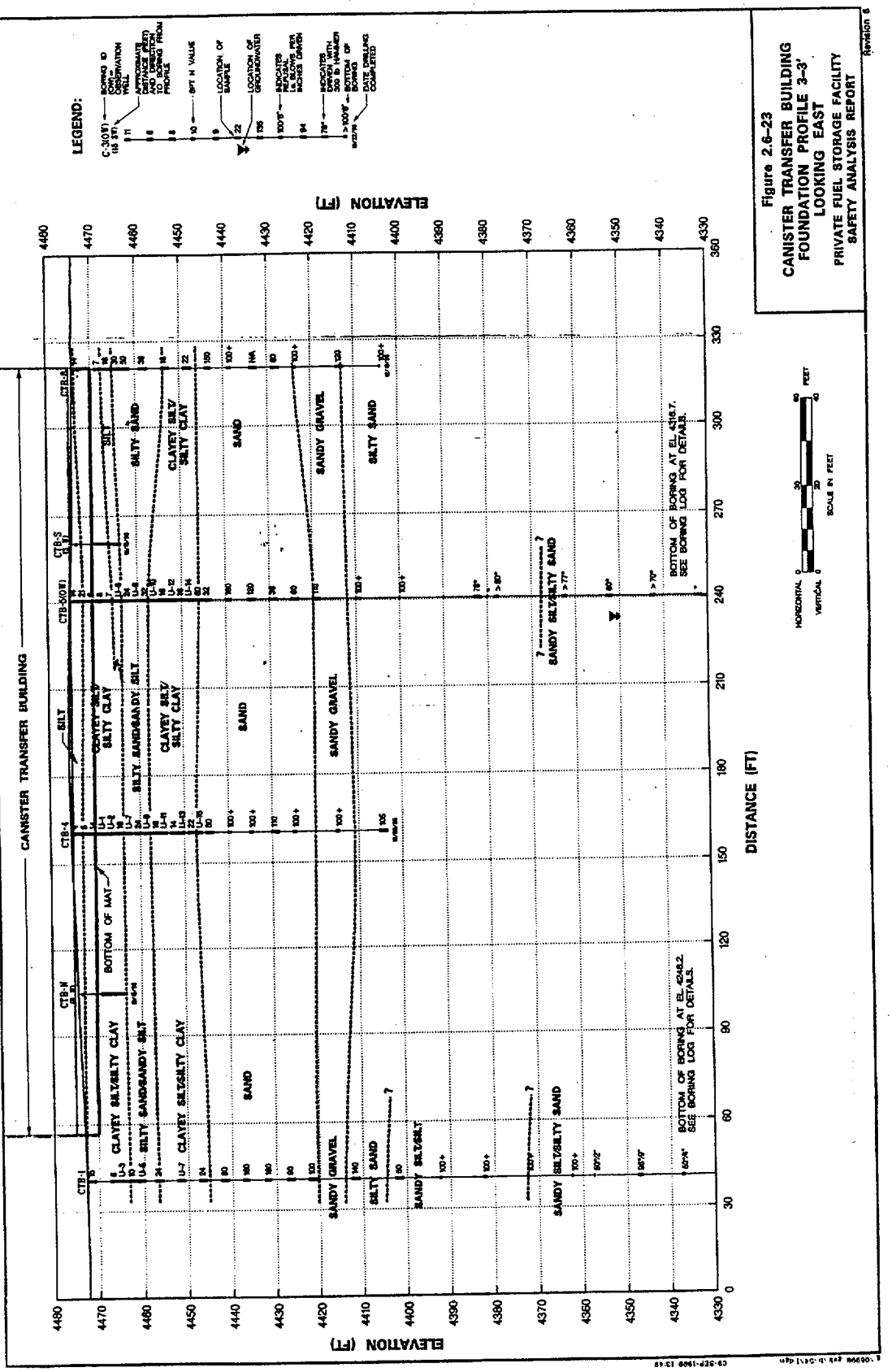
LEGEND:
CANISTER TRANSFER BUILDING
BOTTOM OF MAT
CTB-1
CTB-N
CTB-4
CTB-5
CTB-5(W)
CTB-6
SILT
CLAYEY SILTY CLAY
SILTY SAND/SANDY SILT
CLAYEY SILT/SILTY CLAY
SAND
SANDY GRAVEL
SILTY SAND
SANDY SILT/SILTY SAND
SANDY SILT/SILT
BOTTOM OF BORING AT EL. 4342.2 SEE BORING LOG FOR DETAILS.
BOTTOM OF BORING AT EL. 4316.7'. SEE BORING LOG FOR DETAILS.
ELEVATION (FT)
DISTANCE (FT)
HORIZONTAL
VERTICAL
SCALE IN FEET
Figure 2.6-23
CANISTER TRANSFER BUILDING
FOUNDATION PROFILE 3-3'
LOOKING EAST
PRIVATE FUEL STORAGE FACILITY
SAFETY ANALYSIS REPORT
Revision 6

STONE & WEBSTER ENGINEERING CORPORATION

CALCULATION SHEET

5010.BS

CALCULATION IDENTIFICATION NUMBER				
J.O. OR W.O. NO. 05996.02	DIVISION & GROUP G(B)	CALCULATION NO. 05-2	OPTIONAL TASK CODE	PAGE 25A

TABLE 2 - Sheet 1 of 4
Laboratory Test Results on Clays and Silts in the Pad Emplacement Area

Boring No.	Sample	Z_{avg}	Natural Water Content	Liquid Limit	Plastic Limit	Plastic Index	Liquidity Index	Wet Density (pcf)	Dry Density (pcf)	Void Ratio	Saturation	Consolidation Tests: σ_{app} (ksf)	CR	RR	Triaxial Tests: UU σ_3 (ksf)	UU s_u (ksf)	UU ε_a (%)	CU σ_c (ksf)	CU s_u (ksf)	CU ε_a (%)
A-1	S 2	5.8	34.7	54.8	30.9	23.9	0.16													
A-1	S 3	10.8	19.8	28.8	25.8	3.0	-2.00													
A-1	S 4	15.8	22.3	30.2	27.6	2.6	-2.04													
A-1	S 5	20.8	55.4	58.6	43.0	15.6	0.79													
A-2	S 1	0.8	15.6	28.9	23.3	5.6	-1.38													
A-2	U 2B	5.6	40.1					85.9	61.3	1.70	0.64									
A-2	U 2C	6.2	52.8	70.2	42.9	27.3	0.36	70.7	46.2	2.58	0.56									
A-2	U 2D	6.7	48.8					80.4	54.1	2.06	0.64									
A-2	U 2E	7.0	45.4	61.8	36.7	25.1	0.35													
A-2	S 3	10.8	18.4	27.0	24.5	2.5	-2.44													
A-2	S 4	15.8	29.7	36.5	26.5	10.0	0.32													
A-2	S 5	20.8	28.2	38.0	26.8	11.2	0.13													
A-2	S 6	25.8	27.9	41.4	30.4	11.0	-0.23													
A-3	S 2	5.8	36.0	49.8	23.3	26.5	0.48													
A-3	S 3	10.8	43.3	60.1	35.1	25.0	0.33													
A-3	S 4	15.8	25.9	35.8	27.7	8.1	-0.22													
A-4	S 2	5.8	44.2	69.0	42.4	26.6	0.07													
A-4	S 3	10.8	10.8	Nonplastic																
A-4	S 4	15.8	19.3	29.9	22.4	7.5	-0.41													
A-4	S 5	20.8	37.8	56.5	41.6	14.9	-0.26													
A-4	S 6	25.8	15.2	29.1	19.8	9.3	-0.49													
B-1	U 2B	5.3	52.9	80.6	40.9	39.7	0.30	70.8	46.3	2.67	0.54							1	2.21	6.0
B-1	U 2C	5.9	47.1	66.1	33.4	32.7	0.42	79.3	53.9	2.15	0.60				0	2.03	1.7			
B-1	U 2D	6.5	45.2	59.8	34.7	25.1	0.42	76.7	52.8	2.22	0.55							2.1	3.26	15.0
B-1	S 3	10.8	23.0	39.4	29.0	10.4	-0.58													
B-1	S 4	15.8	23.0	35.2	25.9	9.3	-0.31													
B-1	S 5	20.8	45.9	50.3	35.8	14.5	0.70													
B-2	S 2	5.8	32.0	47.4	25.6	21.8	0.29													
B-2	U 1A	8.0	45.7																	
B-2	U 1F	10.0	45.1																	

[groot]\-5996\calc\G(B)\05-2\table_2.xls on 6/15/2000

STONE & WEBSTER ENGINEERING CORPORATION

CALCULATION SHEET

5010.65

CALCULATION IDENTIFICATION NUMBER			
J.O. OR W.O. NO. 05996.02	DIVISION & GROUP G(B)	CALCULATION NO. 05-2	OPTIONAL TASK CODE

PAGE 25 B

TABLE 2 - Sheet 2 of 4
Laboratory Test Results on Clays and Silts in the Pad Emplacement Area

Boring No.	Sample	z_{avg}	Natural Water Content	Liquid Limit	Plastic Limit	Plastic Index	Liquidity Index	Wet Density (pcf)	Dry Density (pcf)	Void Ratio	Saturation	Consolidation Tests: σ_{app} (ksf)	CR	ER	Triaxial Tests UU: σ_c (ksf)	UU: s_u (ksf)	UU: ε_a (%)	CU: σ_c (ksf)	CU: s_u (ksf)	CU: ε_a (%)
B-2	S 3	10.8	18.9	29.8	25.8	4.0	-1.73													
B-2	S 4	15.8	12.6		Nonplastic															
B-2	S 5	20.8	43.9	55.1	46.2	8.9	-0.26													
B-2	S 6	25.8	20.1	31.8	20.0	11.8	0.01													
B-3	S 1	9.8	8.9	26.6	19.7	6.9	-1.57													
B-3	U 1E	5.5	33.5	52.4	25.2	27.2	0.31	90.7	67.9	1.50	0.61				2.1	3.55	8.0			
B-3	U 1D	6.5	47.2																	
B-3	U 1E	6.7	45.7																	
B-3	U 1F	6.9	45.6																	
B-3	U 2D	10.5	15.2																	
B-3	U 2H	11.6	18.1																	
B-3	U 2J	12.0	22.2																	
B-3	S 3	20.8	44.6	54.3	41.6	12.7	0.24													
B-4	S 2	5.8	48.4	56.5	27.8	28.7	0.72													
B-4	U 3D	10.7	27.4	42.5	24.7	17.8	0.15	85.5	67.1	1.531	0.49				1.3	2.18	4.0			
B-4	U 3J	12.1	14.0																	
B-4	S 4	15.8	19.9	30.7	24.6	6.1	-0.77													
B-4	S 5	20.8	24.2	35.4	29.9	5.5	-1.04													
B-4	S 6	25.8	24.5	32.6	24.3	8.3	0.02													
C-1	S 2	5.8	53.0	67.4	39.3	28.1	0.49													
C-1	U 3B	10.9	30.3	33.0	28.1	4.9	0.45	84.3	64.7	1.63	0.51	7.2	0.252	0.011						
C-1	U 3C	11.1	38.9	47.8	34.6	13.2	0.33	77.5	55.8	2.04	0.52	5.6	0.310	0.008						
C-1	U 3D	11.5	46.7	61.1	44.1	17.0	0.15	75.8	51.7	2.29	0.56	6.0	0.339	0.017						
C-1	U 3E	11.7	43.2																	
C-1	U 3F	11.9	32.1																	
C-1	S 4	15.8	27.4	34.2	24.4	9.8	0.31													
C-1	S 5	20.8	42.7	49.7	38.7	11.0	0.36													
C-2	U 1A1	5.1	39.0																	
C-2	U 1A2	5.3	37.8																	
C-2	U 1C	6.0		76.9	39.1	37.8	-1.03													

[geol]\-5996\calc\G(B)\05-2\table_2.xls on 6/15/2000

STONE & WEBSTER ENGINEERING CORPORATION

CALCULATION SHEET

5010.65

CALCULATION IDENTIFICATION NUMBER				PAGE 25C
J.O. OR W.O. NO.	DIVISION & GROUP	CALCULATION NO.	OPTIONAL TASK CODE	
05996.02	G(B)	05-2		

TABLE 2 - Sheet 3 of 4

Laboratory Test Results on Clays and Silts in the Pad Emplacement Area

Boring No.	Sample	Z_{avg}	Natural Water Content	Liquid Limit	Plastic Limit	Plastic Index	Liquidity Index	Wet Density (pcf)	Dry Density (pcf)	Void Ratio	Saturation	Consolidation Tests: σ'_{app} (ksf)	CR	RR	Triaxial Tests: UU σ_c (ksf)	UU S_u (ksf)	UU ε_a (%)	CU σ_c (ksf)	CU S_u (ksf)	CU ε_a (%)
C-2	U 1C1	5.8	55.7					69.4	44.5	2.81	0.54									
C-2	U 1C2	6.0	58.2					63.7	40.2	3.22	0.49									
C-2	U 1C3	6.1	52.7					75.1	49.2	2.45	0.59									
C-2	U 1D	6.5	50.5	70.3	41.3	29.0	0.32	74.5	49.5	2.43	0.57							2.1	3.03	12.0
C-2	U 1E	6.9	47.9																	
C-2	U 2B	10.8	14.3					81.6	71.4	1.378	0.28									
C-2	U 2C	11.0	27.6	34.6	26.9	7.7	0.09	82.8	64.9	1.62	0.46	6.0	0.273	0.010						
C-2	U 2D	11.4	35.6					78.5	57.9	1.933	0.50				1.3	2.39	11.0			
C-2	U 2E	11.8	39.7	41.2	28.5	12.7	0.88	80.3	57.5	1.95	0.55									
C-2	U 2F	12.0	34.1																	
C-2	S 2	15.8	30.3	40.0	24.4	15.6	0.38													
C-2	S 3	20.8	41.8	48.8	37.2	11.6	0.40													
C-3	S 2	5.8	26.8	43.1	22.4	20.7	0.21													
C-3	S 3	10.8	32.6	48.8	29.4	19.4	0.16													
C-3	S 4	15.8	27.9	32.9	23.1	9.8	0.49													
C-3	S 5	20.8	39.5	50.8	35.8	15.0	0.25													
C-3	S 6	25.8	18.1	26.2	19.5	6.7	-0.21													
C-4	S 2A	5.2	28.6	46.1	22.9	23.2	0.25													
C-4	S 2B	6.0	50.6	69.5	44.2	25.3	0.25													
C-4	S 3	10.8	18.2	26.5	26.0	0.5	-15.6													
C-4	S 4	15.8	26.5	36.6	26.9	9.7	-0.04													
C-4	S 5	20.8	40.7	52.5	41.5	11.0	-0.07													
C-4	S 6	25.8	18.7	29.2	20.1	9.1	-0.15													
D-1	S 2	5.8	36.3	54.6	29.4	25.2	0.27													
D-1	S 3	10.8	28.6	40.5	25.2	15.3	0.22													
D-1	S 4	15.8	32.2	47.3	33.1	14.2	-0.06													
D-1	S 5	20.8	20.7	30.0	19.5	10.5	0.11													
D-2	S 2	5.8	36.9	46.4	31.1	15.3	0.38													
D-2	S 3	10.8	34.2	54.0	28.6	25.4	0.22													
D-2	S 4	15.8	22.6	44.3	29.9	14.4	-0.51													
D-2	S 5	20.8	12.2	37.7	31.6	6.1	-3.18													

[geol]\-5996\calc\G(B)\05-2\table_2.xls on 6/15/2000

STONE & WEBSTER ENGINEERING CORPORATION

CALCULATION SHEET

5010.65

CALCULATION IDENTIFICATION NUMBER				
J.O. OR W.O. NO. 05996.02	DIVISION & GROUP G(B)	CALCULATION NO. 05-2	OPTIONAL TASK CODE	PAGE 25D

TABLE 2 - Sheet 4 of 4
Laboratory Test Results on Clays and Silts in the Pad Emplacement Area

Boring No.	Sample	z_{avg}	Natural Water Content	Liquid Limit	Plastic Limit	Plastic Index	Liquidity Index	Wet Density (pcf)	Dry Density (pcf)	Void Ratio	Saturation	Consolidation Tests: σ_{max} (ksf)	CR	RR	Triaxial Tests UU: σ_c (ksf)	UU: s_u (ksf)	UU: ε_a (%)	CU: σ_c (ksf)	CU: s_u (ksf)	CU: ε_a (%)
D-2	S 6	25.8	13.9	31.4	19.5	11.9	-0.47													
D-3	S 2	5.8	23.5	43.4	27.3	16.1	-0.24													
D-3	S 3	10.8	25.0		Nonplastic															
D-3	S 4	15.8	36.8	40.6	28.0	12.6	0.70													
D-3	S 5	20.8	42.0	47.7	34.2	13.5	0.58													
D-4	S 2	5.8	38.0	49.3	27.7	21.6	0.48													
D-4	S 3A	10.3	16.8	24.7	23.3	1.4	-4.64													
D-4	S 4A	15.4	8.3		Nonplastic															
D-4	S 4B	16.2	32.8	42.8	25.7	17.1	0.42													
D-4	S 5	20.8	43.4	56.8	41.2	15.6	0.14													
D-4	S 6	25.8	18.0	27.0	21.6	5.4	-0.67													
Count		192	101	76	76	76	76	19	19	19	19	4	4	4	3	3	3	4	4	4
Max		25.8	58.2	80.6	46.2	39.7	0.88	90.7	71.4	3.22	0.64	7.2	0.339	0.017	1.3	2.39	11.0	2.1	3.55	15.0
Min		0.8	8.3	24.7	19.5	0.5	-15.6	63.7	40.2	1.38	0.28	5.6	0.252	0.008	0.0	2.03	1.7	1.0	2.21	6.0
Avg		12.5	32.6	45.0	30.0	15.0	-0.35	78.1	55.6	2.11	0.54	6.2	0.294	0.012	0.9	2.20	5.6	1.8	3.01	10.3
Mean		10.9	32.6	43.3	27.9	13.0	0.16	78.5	64.1	2.06	0.55	6.0	0.292	0.011	1.3	2.18	4.0	2.1	3.15	10.0

[got\\~5996\calc\G(B)\05-2\table_2.xls on 6/15/2000

STONE & WEBSTER ENGINEERING CORPORATION

5010.65

CALCULATION SHEET

CALCULATION IDENTIFICATION NUMBER				
J.O. OR W.O. NO.	DIVISION & GROUP	CALCULATION NO.	OPTIONAL TASK CODE	PAGE 25E
05996.02	G(B)	05-1 2		

TABLE 3

CTB Borings - Laboratory Test Results on Silts And Clays in Upper Layer

Boring	Sample	Average Depth (ft)	Elevation (ft)	Water Content (%)	Atterberg Limits LL	Atterberg Limits PL	Atterberg Limits PI	Saturation	% Fines	Specific Gravity	Wet Density (pcf)	Dry Density (pcf)	Void Ratio	Consolidation Test σ_{app} (ksf)	Consolidation Test CR	Consolidation Test RR	Consolidation Test C_v	Consolidation Test C_r	CU Triaxial Test σ_o (ksf)	CU Triaxial Test S_u (ksf)	CU Triaxial Test ε_a (%)
CTB-1	S-1	1.0	4471.4	25.3																	
CTB-1	S-2 (top)	5.1	4467.3	30.1	40.1	22.3	17.8														
CTB-1	S-2 (bot)	6.1	4466.3	65.6																	
CTB-1	U-3C	8.1	4464.3	50.6	56.0	28.9	27.1	0.70			86.4	57.4	1.96								
CTB-1	U-3D	8.7	4463.7	47.9				0.75			91.9	62.1	1.73						1.7	2.84	5.0
CTB-1	U-3E	9.1	4463.3	48.8																	
CTB-1	S-4 (top)	9.5	4462.9	37.4	41.2	23.2	18.0														
CTB-1	S-6	16.0	4456.4	10.7					56.8												
CTB-1	U-7C	21.1	4451.3	51.9	56.5	42.4	14.1	0.68			83.8	55.2	2.08								
CTB-1	U-7D	21.7	4450.7	45.1				0.72			91.2	62.9	1.70						1.7	2.73	5.0
CTB-1	U-7E	22.1	4450.3	43.0																	
CTB-1	S-8	26.0	4446.4	20.9																	
CTB-2	S-2 (bot)	6.3	4467.7	29.4	40.8	21.1	19.7														
CTB-2	S-3	8.0	4466.0	60.1																	
CTB-2	S-4	10.0	4464.0	45.8	56.2	29.9	26.3														
CTB-2	S-5	12.0	4462.0	26.0																	
CTB-2	S-6	16.0	4458.0	27.8	34.3	21.9	12.4														
CTB-2	S-7	21.0	4453.0	28.6																	
CTB-2	S-8	26.0	4448.0	30.0																	
CTB-2	S-9 (top)	30.1	4443.9	26.8																	
CTB-3	S-1	1.0	4471.9	18.7																	
CTB-3	S-2	6.0	4466.9	55.2	58.7	32.3	26.4														
CTB-3	S-3	8.0	4464.9	53.7																	
CTB-3	S-5	12.0	4460.9	39.5																	
CTB-3	S-6 (bot)	16.4	4456.5	24.0																	
CTB-3	S-7 (bot)	21.2	4451.7	53.1																	
CTB-3	S-8	26.0	4446.9	28.3	32.0	22.1	9.9														
CTB-4	S-2 (top)	2.2	4472.8	22.6																	
CTB-4	S-2 (bot)	3.2	4471.8	41.1																	
CTB-4	S-3	5.0	4470.0	27.9	39.9	22.4	17.5														
CTB-4	U-1A	6.0	4469.0	28.9																	

Page 1 of 4

STONE & WEBSTER ENGINEERING CORPORATION

CALCULATION SHEET

5010.65

CALCULATION IDENTIFICATION NUMBER			
J.O. OR W.O. NO. 05996.02	DIVISION & GROUP G(B)	CALCULATION NO. 05-X-2	OPTIONAL TASK CODE

PAGE 25F

TABLE 3 CONTINUED

CTB Borings - Laboratory Test Results on Silts And Clays in Upper Layer

Boring	Sample	Average Depth (ft)	Elevation (ft)	Water Content (%)	Atterberg Limits LL	Atterberg Limits PL	Atterberg Limits PI	Saturation	% Fines	Specific Gravity	Wet Density (pcf)	Dry Density (pcf)	Void Ratio	Consolidation Test σ_{app} (ksf)	Consolidation Test CR	Consolidation Test RR	Consolidation Test C_v	Consolidation Test C_r	CU Triaxial Test σ_3 (ksf)	CU Triaxial Test S_u (ksf)	CU Triaxial Test ε_a (%)
CTB-4	U-1C	7.0	4468.0	34.5				0.68	97.6		95.7	71.2	1.38								
CTB-4	U-1D	7.5	4467.5	60.3	67.9	39.3	28.6	0.62		2.73	74.9	46.7	2.65								
CTB-4	U-1E	7.9	4467.1	64.2																	
CTB-4	U-2D	9.5	4465.5	45.2				0.68			87.7	60.4	1.81						1.7	3.11	6.0
CTB-4	U-2E	9.9	4465.1	48.9	58.1	28.6	29.5	0.79			94.1	63.2	1.69	12.6	0.35	0.020	0.93	0.05			
CTB-4	U-2F	10.1	4464.9	53.0																	
CTB-4	S-6	11.0	4464.0	28.5	34.3	24.8	9.5														
CTB-4	U-7D	13.0	4462.0	22.6				0.60	69.2		101.3	82.7	1.03								
CTB-4	S-8 (top)	14.3	4460.7	20.4																	
CTB-4	S-10	19.0	4456.0	32.7	41.4	24.1	17.3												1.7	3.15	8.0
CTB-4	U-11D	21.2	4453.8	31.5	37.2	33.5	3.7	0.58	97.2		89.8	68.4	1.48								
CTB-4	U-11E	21.6	4453.4	25.0																	
CTB-4	S-12	23.0	4452.0	52.0	57.8	48.1	9.7														
CTB-4	U-13D	25.2	4449.8	37.4	43.2	26.7	16.5	0.78		2.72	101.4	73.8	1.30								
CTB-4	U-13E	25.5	4449.5	40.3																	
CTB-4	S-14	27.0	4448.0	14.8	28.3	18.5	9.8														
CTB-4	U-15C	28.0	4447.0	18.3				0.69			115.5	97.6	0.721								
CTB-4	U-15D	29.2	4445.8	14.4																	
CTB-5	S-2	3.0	4471.8	32.7																	
CTB-5	S-3	5.0	4469.8	72.6	75.3	43.5	31.8														
CTB-5	S-4 (bot)	7.2	4467.6	51.2																	
CTB-5	S-5	9.0	4465.8	48.8	51.5	27.3	24.2														
CTB-5	U-6A	10.0	4464.8	31.7																	
CTB-5	U-6C	10.8	4464.0	12.7				0.40			101.8	90.3	0.860								
CTB-5	U-6D	11.1	4463.7	18.6				0.64			111.3	93.8	0.790								
CTB-5	U-6E	11.3	4463.5	20.0				0.77	79.8		118.0	98.3	0.708								
CTB-5	U-6F	11.5	4463.3	16.4																	
CTB-5	S-9	17.0	4457.8	12.2					63.3												
CTB-5	U-10D	19.4	4455.4	27.7				0.58			94.5	74.0	1.29						1.7	2.93	8.0
CTB-5	U-10E	19.8	4455.0	33.3																	
CTB-5	S-11	21.0	4453.8	47.6	51.5	47.2	4.3														

Page 2 of 4

STONE & WEBSTER ENGINEERING CORPORATION

CALCULATION SHEET

5010.65

CALCULATION IDENTIFICATION NUMBER			
J.O. OR W.O. NO.	DIVISION & GROUP	CALCULATION NO.	OPTIONAL TASK CODE
05996.02	G(B)	05-Y 2	

PAGE 25 G

TABLE 3 CONTINUED

CTB Borings - Laboratory Test Results on Silts And Clays in Upper Layer

Boring	Sample	Average Depth (ft)	Elevation (ft)	Water Content (%)	Atterberg Limits LL	Atterberg Limits PL	Atterberg Limits PI	Saturation	% Fines	Specific Gravity	Wet Density (pcf)	Dry Density (pcf)	Void Ratio	Consolidation Test σ_{app} (ksf)	Consolidation Test CR	Consolidation Test RR	Consolidation Test C_a	Consolidation Test C_r	CU Triaxial Test σ_c (ksf)	CU Triaxial Test S_u (ksf)	CU Triaxial Test ε_a (%)
CTB-5	U-12B	23.2	4451.6	42.3				0.73			93.6	65.8	1.58								
CTB-5	U-12C	23.6	4451.2	52.4	51.5	32.8	18.7	0.85			96.4	63.3	1.68	12.3	0.33	0.014	0.89	0.04			
CTB-5	U-12D	23.9	4450.9	45.1				0.75			93.7	64.6	1.63								
CTB-5	U-12E	24.1	4450.7	50.8																	
CTB-5	S-13	25.0	4449.8	33.6	39.8	24.2	15.6														
CTB-5	U-14D	27.0	4447.8	30.5				0.88			113.9	87.2	0.947						1.7	1.66	12.0
CTB-5	U-14E	27.4	4447.4	26.2	30.0	19.5	10.5	0.82			114.7	90.9	0.868	25.5	0.13	0.014	0.25	0.03			
CTB-5	U-14F	27.6	4447.2	27.1																	
CTB-5	S-15 (top)	28.2	4446.6	17.6																	
CTB-5	S-15 (bot)	29.2	4445.6	9.0																	
CTB-6	S-1	1.0	4475.2	20.3																	
CTB-6	S-2	6.0	4470.2	31.0	42.9	21.5	21.4														
CTB-6	U-3A	7.1	4469.1	61.4																	
CTB-6	U-3B	7.6	4468.6	61.1	65.3	32.5	32.8	0.70			81.2	50.4	2.36								
CTB-6	U-3C	7.9	4468.3	56.6				0.77			88.5	56.4	2.01								
CTB-6	U-3D	8.3	4467.9	52.7				0.71			85.7	56.2	2.02						1.7	2.70	7.0
CTB-6	U-3E	8.7	4467.5	55.5																	
CTB-6	S-4 (top)	10.5	4465.7	52.9	56.9	27.9	29.0														
CTB-6	S-4 (bot)	11.5	4464.7	42.1																	
CTB-6	S-5 (top)	15.2	4461.0	10.2																	
CTB-6	S-6	21.0	4455.2	30.7																	
CTB-6	S-7	26.0	4450.2	37.8	41.5	33.9	7.6														
CTB-7	S-1	1.0	4472.1	21.1																	
CTB-7	S-2	6.0	4467.1	52.8	58.1	29.9	28.2														
CTB-7	S-5 (top)	15.2	4457.9	7.4																	
CTB-7	S-5 (bot)	16.2	4456.9	33.6																	
CTB-7	S-6	21.0	4452.1	46.9	51.6	33.5	18.1														
CTB-7	S-7	26.0	4447.1	20.9																	
CTB-8	S-1 (bot)	1.1	4472.8	31.8																	
CTB-8	S-2	6.0	4467.9	53.3	55.3	28.5	26.8														
CTB-8	S-3	8.0	4465.9	24.1																	

Page 3 of 4

STONE & WEBSTER ENGINEERING CORPORATION

CALCULATION SHEET

5010.65

CALCULATION IDENTIFICATION NUMBER			
J.O. OR W.O. NO.	DIVISION & GROUP	CALCULATION NO.	OPTIONAL TASK CODE
05996.02	G(B)	05-X 2	

PAGE 25H

TABLE 3 CONTINUED

CTB Borings - Laboratory Test Results on Silts And Clays in Upper Layer

Boring	Sample	Average Depth (ft)	Elevation (ft)	Water Content (%)	Atterberg Limits LL	PL	PI	% Saturation	% Fines	Specific Gravity	Wet Density (pcf)	Dry Density (pcf)	Void Ratio	Consolidation Test σ'_{app} (ksf)	CR	RR	C_v	C_r	CU Triaxial Test σ_c (ksf)	S_u (ksf)	ε_a (%)
CTB-S	S-7 (bot)	21.1	4452.8	57.0																	
CTB-S	S-8	26.0	4447.9	26.7	30.5	18.3	12.2														
CTB-N	U-1A	5.1	4469.0	30.6	38.4	23.1	15.3														
CTB-N	U-1B	5.7	4468.4	30.1	41.3	22.5	18.8	0.68			100.6	77.3	1.20						1.7	3.00	8.0
CTB-N	U-1D	6.7	4467.4	46.6	50.8	23.1	27.7														
CTB-N	U-1E	6.9	4467.2	67.7																	
CTB-N	U-2A	7.1	4467.0	69.0	74.2	45.4	28.8														
CTB-N	U-2B	7.7	4466.4	65.4				0.64			74.6	45.1	2.76						1.7	2.41	13.0
CTB-N	U-2C	8.3	4465.8	52.6				0.71			86.3	56.5	2.01								
CTB-N	U-2D	8.7	4465.4	63.0	60.6	36.8	23.8	0.68			78.8	48.4	2.51	6.1	0.37	0.020	1.31	0.07			
CTB-N	U-2E	8.8	4465.3	52.1																	
CTB-N	U-3A	9.0	4465.1	53.7																	
CTB-N	U-3C	9.6	4464.2	47.1				0.67			86.1	58.5	1.90								
CTB-N	U-3D	10.5	4463.6	52.2	61.1	30.8	30.3	0.72		2.71	86.3	56.7	1.98						1.7	2.73	7.0
CTB-N	U-3E	10.9	4463.2	53.1																	
CTB-S	U-1A	5.1	4469.4	85.5																	
CTB-S	U-1AA	5.3	4469.2	84.1	82.7	44.8	37.9	0.70			73.2	39.8	3.28								
CTB-S	U-1B	5.8	4468.7	73.6	66.2	40.9	25.3	0.72			78.0	44.9	2.78						1.7	2.05	12.0
CTB-S	U-1D	6.6	4467.9	60.7				0.74			84.8	52.8	2.22								
CTB-S	U-1E	6.9	4467.6	56.4																	
CTB-S	U-2D	8.4	4466.1	54.6	57.9	28.9	29.0	0.77			90.0	58.2	1.92						1.7	2.40	5.0
CTB-S	U-2E	8.8	4465.7	56.7																	
CTB-S	U-3C	10.1	4464.4	72.2	66.0	37.8	28.2	0.87	99.2	2.72	89.5	51.9	2.27	8.4	0.36	0.020	1.17	0.07			
CTB-S	U-3F	10.9	4463.6	31.2																	
		117	count	117	42	42	42	35		4	35	35	35	5	5	5	5	5	12	12	12
		30.1	max	85.5	82.7	48.1	37.9	0.88		2.73	118.0	98.3	3.28	25.5	0.37	0.020	1.31	0.07	1.7	3.15	13.0
		1.0	min	7.4	28.3	18.3	3.7	0.40		2.71	73.2	39.8	0.71	6.1	0.13	0.014	0.25	0.03	1.7	1.66	5.0
		13.4	avg	40.1	50.6	30.1	20.5	0.71		2.72	92.4	65.2	1.75	13.0	0.31	0.018	0.91	0.05	1.7	2.64	8.0
		10.1	mean	39.5	51.5	28.8	19.3	0.71		2.72	90.0	62.1	1.73	12.3	0.35	0.020	0.93	0.05	1.7	2.73	7.5

Page4 of 4

STONE & WEBSTER ENGINEERING CORPORATION

5010.65

CALCULATION SHEET

CALCULATION IDENTIFICATION NUMBER				PAGE 25 I
J.O. OR W.O. NO.	DIVISION & GROUP	CALCULATION NO.	OPTIONAL TASK CODE	
05996.02	G(B)	05-1 2		

TABLE 4

CTB Borings - Laboratory Test Results on Sands in 8 - 20 ft Depth

Boring	Sample	Average Depth (ft)	Elevation (ft)	Water Content (%)	Saturation	USC Code	% Fines	Specific Gravity	Wet Density (pcf)	Dry Density (pcf)	Void Ratio
CTB-1	S-6	16.0	4456.4	10.7		ML					
CTB-3	S-6 (top)	15.4	4457.5	14.6		SM					
CTB-4	U-7E	13.2	4461.8	10.2		SP					
CTB-4	S-8 (bot)	15.4	4459.6	5.4		SM	37.5				
CTB-4	U-9A	16.0	4459.0	4.6		ML					
CTB-4	U-9D	16.7	4458.3	4.5		SM		2.69			
CTB-4	U-9E	16.9	4458.1	5.2	0.18	SM	16.7		98.4	93.5	0.80
CTB-4	U-9F	17.1	4457.9	9.7	0.32	SM	34.2		101.0	92.1	0.82
CTB-4	U-9H	17.5	4457.5	6.6		SM					
CTB-5	S-7	13.0	4461.8	4.1		SM	21.6				
CTB-5	U-8A	14.0	4460.8	3.7		SM					
CTB-5	U-8D	15.4	4459.4	3.4	0.14	SM			105.8	102.4	0.64
CTB-5	U-8E	15.6	4459.2	6.5		SM					
CTB-6	S-5 (bot)	16.2	4460.0	5.6		SM					
CTB-7	U-3D	8.3	4464.8	2.7	0.11	SP	8.7	2.69	102.3	99.6	0.69
CTB-7	U-3E	8.5	4464.6	2.6		SP					
CTB-7	S-4	11.0	4462.1	6.4		SM					
CTB-7	S-5 (top)	15.2	4457.9	7.4		ML					
CTB-8	S-4	10.0	4463.9	3.6		SM	14.8				
CTB-8	S-5	12.0	4461.9	3.0		SM					
CTB-8	S-6	16.0	4457.9	5.5		SM	34.8				
CTB-8	U-3D	10.4	4464.1	10.0	0.23	SM	18.9		84.7	77.0	1.18
		22	count	22	5		8	2	5	5	5
		17.5	max	14.6	0.32		37.5	2.69	105.8	102.4	1.18
		8.3	min	2.6	0.11		8.7	2.69	84.7	77.0	0.64
		14.1	avg	6.2	0.19		23.4	2.69	98.4	92.9	0.83
		15.4	mean	5.5	0.18		20.3	2.69	101.0	93.5	0.80

CONETEC

Seismic Wave Velocity Calculations

Job No.: 99-315
Client: Stone & Webster
Location Private Fuel Storage Facility
Date: 4/24/99
CPT No.: CPT-1

Geophone Offset (m): 0.20
Source Offset (m): 0.56

Test Depth (m)	Ray Path (m)	Incremental Distance (m)	Interval Depth (m)	Vs Interval Time (ms)	Vs Interval Velocity (m/s)	Vp Interval Time (ms)	Vp Interval Velocity (m/s)
0.90	0.90						
1.90	1.79	0.89	1.2	4.92	181.6	2.56	349.0
2.90	2.76	0.97	2.2	7.02	137.8	3.00	322.5
3.90	3.74	0.98	3.2	5.44	181.0	2.97	331.5
4.90	4.73	0.99	4.2	3.79	261.5	2.18	454.6
5.90	5.73	0.99	5.2	4.10	242.5	2.08	478.0
6.90	6.72	1.00	6.2	3.62	276.1	2.51	396.8
7.90	7.72	1.00	7.2	3.83	260.3	2.56	389.4
8.90	8.72	1.00	8.2	2.87	347.6	1.82	548.2

Interval Depth (ft)	Vs Interval Velocity (ft/s)	Vp Interval Velocity (ft/s)	Y Parameter
3.9	596	1145	180
7.2	452	1058	134
10.5	594	1087	154
13.8	858	1491	195
17.1	795	1568	175
20.3	902	1301	207
23.6	854	1277	191
26.9	1140	1798	188

CONETEC

Seismic Wave Velocity Calculations

Job No.: 99-315
Client: Stone & Webster
Location Private Fuel Storage Facility
Date: 4/24/99
CPT No.: CPT-3

Geophone Offset (m): 0.20
Source Offset (m): 0.63

Test Depth (m)	Ray Path (m)	Incremental Distance (m)	Interval Depth (m)	Vs Interval Time (ms)	Vs Interval Velocity (m/s)	Vp Interval Time (ms)	Vp Interval Velocity (m/s)
0.75	0.84						
1.75	1.67	0.84	1.05	4.26	196.4	2.16	387.4
2.75	2.63	0.95	2.05	6.85	139.2	2.97	321.1
3.75	3.61	0.98	3.05	4.96	197.3	3.00	326.3
4.75	4.59	0.99	4.05	4.59	215.2	2.59	381.4
5.75	5.59	0.99	5.05	3.77	263.2	1.87	530.6
6.75	6.58	0.99	6.05	3.64	273.2	2.71	367.0
7.75	7.58	1.00	7.05	3.23	308.4	2.15	463.3
8.75	8.57	1.00	8.05	3.04	327.9	1.74	573.0

Interval Depth (ft)	Vs Interval Velocity (ft/s)	Vp Interval Velocity (ft/s)	Y Parameter
3.4	644	1271	209
6.7	457	1053	136
10.0	647	1070	171
13.3	706	1251	152
16.6	863	1740	169
19.8	896	1204	201
23.1	1011	1519	206
26.4	1076	1879	156

CONETEC

Seismic Wave Velocity Calculations

Job No.: 99-315
Client: Stone & Webster
Location Private Fuel Storage Facility
Date: 4/24/99
CPT No.: CPT-6

Geophone Offset (m): 0.20
Source Offset (m): 0.63

Test Depth (m)	Ray Path (m)	Incremental Distance (m)	Interval Depth (m)	Vs Interval Time (ms)	Vs Interval Velocity (m/s)	Vp Interval Time (ms)	Vp Interval Velocity (m/s)
0.75	0.84						
1.75	1.67	0.84	1.05	5.04	166.0	2.61	320.6
2.75	2.63	0.95	2.05	5.48	174.0	2.53	376.9
3.75	3.61	0.98	3.05	4.07	240.5	2.60	376.5
4.75	4.59	0.99	4.05	4.63	213.4	2.50	395.2
5.75	5.59	0.99	5.05	3.88	255.7	2.45	405.0
6.75	6.58	0.99	6.05	3.72	267.4	1.55	641.7

Interval Depth (ft)	Vs Interval Velocity (ft/s)	Vp Interval Velocity (ft/s)	Y Parameter
3.4	545	1052	186
6.7	571	1236	163
10.0	789	1235	194
13.3	700	1296	166
16.6	839	1328	204
19.8	877	2105	210

CONETEC

Seismic Wave Velocity Calculations

Job No.: 99-315
Client: Stone & Webster
Location Private Fuel Storage Facility
Date: 4/27/99
CPT No.: CPT-13

Geophone Offset (m): 0.20
Source Offset (m): 0.74

Test Depth (m)	Ray Path (m)	Incremental Distance (m)	Interval Depth (m)	Vs Interval Time (ms)	Vs Interval Velocity (m/s)	Vp Interval Time (ms)	Vp Interval Velocity (m/s)
0.75	0.92						
1.75	1.72	0.80	1.05	4.41	180.4	2.54	313.2
2.75	2.66	0.94	2.05	5.76	162.8	3.03	309.4
3.75	3.63	0.97	3.05	4.88	199.0	2.50	388.4
4.75	4.61	0.98	4.05	3.60	273.2	2.17	453.2
5.75	5.60	0.99	5.05	3.55	278.7	2.25	439.7
6.75	6.59	0.99	6.05	3.70	268.3	2.25	441.1
7.75	7.59	0.99	7.05	3.68	270.2	2.44	407.6

Interval Depth (ft)	Vs Interval Velocity (ft/s)	Vp Interval Velocity (ft/s)	Y Parameter
3.4	592	1027	194
6.7	534	1015	155
10.0	653	1274	165
13.3	896	1487	183
16.6	914	1442	195
19.8	880	1447	193
23.1	886	1337	189

CONETEC

Seismic Wave Velocity Calculations

Job No.: 99-315
Client: Stone & Webster
Location Private Fuel Storage Facility
Date: 4/27/99
CPT No.: CPT-15

Geophone Offset (m): 0.20
Source Offset (m): 0.56

Test Depth (m)	Ray Path (m)	Incremental Distance (m)	Interval Depth (m)	Vs Interval Time (ms)	Vs Interval Velocity (m/s)	Vp Interval Time (ms)	Vp Interval Velocity (m/s)
0.85	0.86						
1.85	1.74	0.88	1.15	5.85	151.2	2.13	415.2
2.85	2.71	0.97	2.15	5.81	166.3	2.40	402.5
3.85	3.69	0.98	3.15	5.74	171.5	2.78	354.0
4.85	4.68	0.99	4.15	3.48	284.7	2.26	438.4
5.85	5.68	0.99	5.15	3.93	252.9	2.24	443.8
6.85	6.67	1.00	6.15	3.63	274.3	2.40	414.9
7.85	7.67	1.00	7.15	3.75	265.8	2.29	435.3

Interval Depth (ft)	Vs Interval Velocity (ft/s)	Vp Interval Velocity (ft/s)	Y Parameter
3.8	496	1362	184
7.1	545	1320	171
10.3	562	1161	156
13.6	934	1438	206
16.9	830	1456	189
20.2	900	1361	202
23.5	872	1428	196

CONETEC

Seismic Wave Velocity Calculations

Job No.: 99-315
Client: Stone & Webster
Location: Private Fuel Storage Facility
Date: 4/27/99
CPT No.: CPT-18

Geophone Offset (m): 0.20
Source Offset (m): 0.61

Test Depth (m)	Ray Path (m)	Incremental Distance (m)	Interval Depth (m)	Vs Interval Time (ms)	Vs Interval Velocity (m/s)	Vp Interval Time (ms)	Vp Interval Velocity (m/s)
0.80	0.86						
1.80	1.71	0.86	1.1	5.63	152.2	2.50	342.7
2.80	2.67	0.96	2.1	6.63	144.5	2.76	347.2
3.80	3.65	0.98	3.1	4.95	198.1	2.12	462.6
4.80	4.64	0.99	4.1	4.15	238.3	2.47	400.4
5.80	5.63	0.99	5.1	4.39	226.2	2.15	461.8
6.80	6.63	1.00	6.1	3.72	267.5	1.93	515.5
7.80	7.62	1.00	7.1	3.79	262.9	2.34	425.8

Interval Depth (ft)	Vs Interval Velocity (ft/s)	Vp Interval Velocity (ft/s)	Y Parameter
3.6	499	1124	177
6.9	474	1139	155
10.2	650	1517	180
13.4	782	1313	187
16.7	742	1515	171
20.0	877	1691	212
23.3	862	1397	193

CONETEC

Seismic Wave Velocity Calculations

Job No.: 99-315
Client: Stone & Webster
Location Private Fuel Storage Facility
Date: 4/28/99
CPT No.: CPT-20

Geophone Offset (m): 0.20
Source Offset (m): 0.71

Test Depth (m)	Ray Path (m)	Incremental Distance (m)	Interval Depth (m)	Vs Interval Time (ms)	Vs Interval Velocity (m/s)	Vp Interval Time (ms)	Vp Interval Velocity (m/s)
0.80	0.93						
1.80	1.75	0.82	1.1	5.13	160.0	3.31	248.0
2.80	2.70	0.94	2.1	6.31	149.7	2.19	431.4
3.80	3.67	0.97	3.1	4.05	240.5	2.10	463.9
4.80	4.65	0.99	4.1	3.16	311.7	1.97	500.1
5.80	5.64	0.99	5.1	3.68	269.1	2.27	436.3
6.80	6.64	0.99	6.1	3.71	267.7	2.35	422.7
7.80	7.63	1.00	7.1	3.55	280.3	2.16	460.7

Interval Depth (ft)	Vs Interval Velocity (ft/s)	Vp Interval Velocity (ft/s)	Y Parameter
3.6	525	813	171
6.9	491	1415	148
10.2	789	1522	194
13.4	1023	1640	212
16.7	883	1431	194
20.0	878	1386	187
23.3	919	1511	201

CONETEC

Seismic Wave Velocity Calculations

Job No.: 99-315
Client: Stone & Webster
Location Private Fuel Storage Facility
Date: 4/28/99
CPT No.: CPT-21

Geophone Offset (m): 0.20
Source Offset (m): 0.41

Test Depth (m)	Ray Path (m)	Incremental Distance (m)	Interval Depth (m)	Vs Interval Time (ms)	Vs Interval Velocity (m/s)	Vp Interval Time (ms)	Vp Interval Velocity (m/s)
0.85	0.77						
1.85	1.70	0.93	1.15	4.89	190.5	2.71	343.8
2.85	2.68	0.98	2.15	7.42	132.3	2.90	338.4
3.85	3.67	0.99	3.15	4.63	214.1	2.78	356.6
4.85	4.67	1.00	4.15	3.61	275.6	2.14	465.0
5.85	5.66	1.00	5.15	4.02	248.0	1.99	500.9
6.85	6.66	1.00	6.15	3.66	272.6	2.36	422.8
7.85	7.66	1.00	7.15	3.92	254.7	2.29	436.0
8.85	8.66	1.00	8.15	3.21	311.1	1.67	598.0

Interval Depth (ft)	Vs Interval Velocity (ft/s)	Vp Interval Velocity (ft/s)	Y Parameter
3.8	625	1128	230
7.1	434	1110	138
10.3	702	1170	167
13.6	904	1525	205
16.9	813	1643	177
20.2	894	1387	199
23.5	835	1430	189
26.7	1021	1962	176

CONETEC

Seismic Wave Velocity Calculations

Job No.: 99-315
Client: Stone & Webster
Location Private Fuel Storage Facility
Date: 4/28/99
CPT No.: CPT-22

Geophone Offset (m): 0.20
Source Offset (m): 0.69

Test Depth (m)	Ray Path (m)	Incremental Distance (m)	Interval Depth (m)	Vs Interval Time (ms)	Vs Interval Velocity (m/s)	Vp Interval Time (ms)	Vp Interval Velocity (m/s)
0.85	0.95						
1.85	1.79	0.84	1.15	4.58	184.3	2.15	390.9
2.85	2.74	0.95	2.15	6.01	158.1	2.26	420.3
3.85	3.71	0.98	3.15	4.22	231.3	2.79	349.9
4.85	4.70	0.99	4.15	4.02	245.3	2.37	416.1
5.85	5.69	0.99	5.15	3.31	299.4	2.20	450.5
6.85	6.69	0.99	6.15	4.00	248.4	2.60	382.2
7.85	7.68	1.00	7.15	4.05	245.8	2.39	416.5

Interval Depth (ft)	Vs Interval Velocity (ft/s)	Vp Interval Velocity (ft/s)	Y Parameter
3.8	605	1282	191
7.1	518	1379	154
10.3	759	1148	184
13.6	805	1365	183
16.9	982	1478	189
20.2	815	1254	165
23.5	806	1366	167

CONETEC

Seismic Wave Velocity Calculations

Job No.: 99-315
Client: Stone & Webster
Location Private Fuel Storage Facility
Date: 4/29/99
CPT No.: CPT-31

Geophone Offset (m): 0.20
Source Offset (m): 0.41

Test Depth (m)	Ray Path (m)	Incremental Distance (m)	Interval Depth (m)	Vs Interval Time (ms)	Vs Interval Velocity (m/s)	Vp Interval Time (ms)	Vp Interval Velocity (m/s)
0.80	0.73						
1.80	1.65	0.92	1.1	5.43	170.3	3.56	259.8
2.80	2.63	0.98	2.1	6.11	160.5	2.82	347.7
3.80	3.62	0.99	3.1	3.59	276.1	2.54	390.2
4.80	4.62	0.99	4.1	3.69	269.6	1.97	505.1
5.80	5.61	1.00	5.1	3.47	287.2	1.90	524.6
6.80	6.61	1.00	6.1	3.63	274.9	2.13	468.4
7.80	7.61	1.00	7.1	3.63	275.0	1.90	525.4

Interval Depth (ft)	Vs Interval Velocity (ft/s)	Vp Interval Velocity (ft/s)	Y Parameter
3.6	559	852	208
6.9	526	1140	161
10.2	906	1280	212
13.4	884	1657	188
16.7	942	1721	203
20.0	902	1536	193
23.3	902	1723	186

CONETEC

Seismic Wave Velocity Calculations

Job No.: 99-315
Client: Stone & Webster
Location Private Fuel Storage Facility
Date: 4/29/99
CPT No.: CPT-33

Geophone Offset (m): 0.20
Source Offset (m): 0.79

Test Depth (m)	Ray Path (m)	Incremental Distance (m)	Interval Depth (m)	Vs Interval Time (ms)	Vs Interval Velocity (m/s)	Vp Interval Time (ms)	Vp Interval Velocity (m/s)
0.90	1.06						
1.90	1.87	0.82	1.2	5.29	154.8	2.54	322.5
2.90	2.81	0.94	2.2	5.51	170.3	3.01	311.8
3.90	3.78	0.97	3.2	3.66	265.1	2.38	407.6
4.90	4.77	0.98	4.2	3.57	275.2	1.93	509.1
5.90	5.75	0.99	5.2	3.59	275.4	2.20	449.3
6.90	6.75	0.99	6.2	3.74	265.2	2.40	413.3
7.90	7.74	0.99	7.2	3.65	272.3	2.71	366.8
8.90	8.74	1.00	8.2	3.31	300.7	2.05	485.5

Interval Depth (ft)	Vs Interval Velocity (ft/s)	Vp Interval Velocity (ft/s)	Y Parameter
3.9	508	1058	172
7.2	559	1023	168
10.5	869	1337	209
13.8	903	1670	185
17.1	903	1474	190
20.3	870	1356	193
23.6	893	1203	200
26.9	986	1593	180

CONETEC

Seismic Wave Velocity Calculations

Job No.: 99-315
Client: Stone & Webster
Location Private Fuel Storage Facility
Date: 4/29/99
CPT No.: CPT-34

Geophone Offset (m): 0.20
Source Offset (m): 0.86

Test Depth (m)	Ray Path (m)	Incremental Distance (m)	Interval Depth (m)	Vs Interval Time (ms)	Vs Interval Velocity (m/s)	Vp Interval Time (ms)	Vp Interval Velocity (m/s)
0.80	1.05						
1.80	1.82	0.77	1.1	5.68	135.2	2.51	305.9
2.80	2.74	0.92	2.1	6.73	137.0	2.89	319.1
3.80	3.70	0.96	3.1	4.65	207.0	2.62	367.5
4.80	4.68	0.98	4.1	3.55	275.6	2.51	389.8
5.80	5.67	0.99	5.1	3.62	272.4	1.77	557.0
6.80	6.66	0.99	6.1	3.84	257.8	2.45	404.1
7.80	7.65	0.98	7.1	3.61	275.0	2.48	400.3

Interval Depth (ft)	Vs Interval Velocity (ft/s)	Vp Interval Velocity (ft/s)	Y Parameter
3.6	443	1003	161
6.9	449	1046	153
10.2	679	1205	170
13.4	904	1279	192
16.7	893	1827	184
20.0	846	1326	188
23.3	902	1313	206

CONETEC

Seismic Wave Velocity Calculations

Job No.: 99-315
Client: Stone & Webster
Location Private Fuel Storage Facility
Date: 4/29/99
CPT No.: CPT-36

Geophone Offset (m): 0.20
Source Offset (m): 0.58

Test Depth (m)	Ray Path (m)	Incremental Distance (m)	Interval Depth (m)	Vs Interval Time (ms)	Vs Interval Velocity (m/s)	Vp Interval Time (ms)	Vp Interval Velocity (m/s)
0.80	0.83						
1.80	1.70	0.87	1.1	4.65	186.5	2.08	417.0
2.80	2.66	0.96	2.1	4.51	213.3	3.29	292.4
3.80	3.65	0.98	3.1	4.41	222.8	2.34	419.9
4.80	4.64	0.99	4.1	4.06	243.8	2.46	402.4
5.80	5.63	0.99	5.1	3.25	305.7	2.14	464.3
6.80	6.63	1.00	6.1	4.12	241.6	2.33	427.2
7.80	7.62	1.00	7.1	3.89	256.2	2.21	451.0

Interval Depth (ft)	Vs Interval Velocity (ft/s)	Vp Interval Velocity (ft/s)	Y Parameter
3.6	612	1368	196
6.9	700	959	197
10.2	731	1377	171
13.4	800	1320	175
16.7	1003	1523	200
20.0	793	1401	165
23.3	840	1479	179

CONETEC

Seismic Wave Velocity Calculations

Job No.: 99-315
Client: Stone & Webster
Location Private Fuel Storage Facility
Date: 4/29/99
CPT No.: CPT-37

Geophone Offset (m): 0.20
Source Offset (m): 0.58

Test Depth (m)	Ray Path (m)	Incremental Distance (m)	Interval Depth (m)	Vs Interval Time (ms)	Vs Interval Velocity (m/s)	Vp Interval Time (ms)	Vp Interval Velocity (m/s)
1.35	1.29						
2.35	2.23	0.94	1.65	5.57	168.6	2.87	327.1
3.35	3.20	0.98	2.65	5.24	186.3	2.93	333.1
4.35	4.19	0.99	3.65	4.37	225.9	2.74	360.4
5.35	5.18	0.99	4.65	3.88	255.7	2.48	400.1
6.35	6.18	0.99	5.65	3.81	261.1	2.25	442.1
7.35	7.17	1.00	6.65	3.72	267.8	2.51	396.9
8.35	8.17	1.00	7.65	4.31	231.4	2.70	369.3
9.35	9.17	1.00	8.65	3.59	277.9	2.24	445.4

Interval Depth (ft)	Vs Interval Velocity (ft/s)	Vp Interval Velocity (ft/s)	Y Parameter
5.4	553	1073	171
8.7	611	1093	184
12.0	741	1182	215
15.3	839	1312	204
18.5	856	1450	156
21.8	878	1302	201
25.1	759	1211	182
28.4	912	1461	198

CONETEC

Seismic Wave Velocity Calculations

Job No.: 99-315
Client: Stone & Webster
Location Private Fuel Storage Facility
Date: 4/29/99
CPT No.: CPT-38

Geophone Offset (m): 0.20
Source Offset (m): 0.53

Test Depth (m)	Ray Path (m)	Incremental Distance (m)	Interval Depth (m)	Vs Interval Time (ms)	Vs Interval Velocity (m/s)	Vp Interval Time (ms)	Vp Interval Velocity (m/s)
1.30	1.22						
2.30	2.17	0.94	1.6	6.63	142.5	2.45	385.8
3.30	3.14	0.98	2.6	5.99	163.5	2.96	330.8
4.30	4.13	0.99	3.6	4.04	244.8	2.44	405.4
5.30	5.13	0.99	4.6	4.03	246.5	2.12	468.6
6.30	6.12	1.00	5.6	3.62	275.0	2.34	425.4
7.30	7.12	1.00	6.6	4.03	247.3	2.16	461.5
8.30	8.12	1.00	7.6	3.69	270.3	2.79	357.6
9.30	9.12	1.00	8.6	3.42	291.8	2.13	468.6

Interval Depth (ft)	Vs Interval Velocity (ft/s)	Vp Interval Velocity (ft/s)	Y Parameter
5.2	467	1265	151
8.5	536	1085	180
11.8	803	1330	220
15.1	808	1537	152
18.4	902	1395	161
21.6	811	1514	182
24.9	887	1173	211
28.2	957	1537	203

Table 5

DIFFERENTIAL SHEAR-WAVE VELOCITY
(5' Interval Velocity Averaged Over 2.5' Intervals)

Boring CTB-5(OW)
PRIVATE FUEL STORAGE FACILITY

Interval Depth (feet bgs)	S-wave Velocity (feet / sec)
0.8 - 3.3	584
3.3 - 5.8	569
5.8 - 8.3	595
8.3 - 10.8	694
10.8 - 13.3	787
13.3 - 15.8	822
15.8 - 18.3	847
18.3 - 20.8	847
20.8 - 23.3	817
23.3 - 25.8	867
25.8 - 28.3	999
28.3 - 30.8	1068
30.8 - 33.3	1051
33.3 - 35.8	1081
35.8 - 38.3	1129
38.3 - 40.8	1215
40.8 - 43.3	1238
43.3 - 45.8	1123
45.8 - 48.3	1159
48.3 - 50.8	1257

Table 6

DIFFERENTIAL SHEAR-WAVE VELOCITY
(5' Interval Velocity Averaged Over 2.5' Intervals)

Boring CTB-5A

PRIVATE FUEL STORAGE FACILITY

Interval Depth (feet bgs)	S-wave Velocity (feet / sec)
44.0 - 46.5	1423
46.5 - 49.0	1356
49.0 - 51.5	1387
51.5 - 54.0	1677
54.0 - 56.5	1667
56.5 - 59.0	1427
59.0 - 61.5	1611
61.5 - 64.0	1950
64.0 - 66.5	1933
66.5 - 69.0	1724
69.0 - 71.5	1686
71.5 - 74.0	1900
74.0 - 76.5	1985
76.5 - 79.0	1622
79.0 - 81.5	1539
81.5 - 84.0	1855
84.0 - 86.5	1822
86.5 - 89.0	1753
89.0 - 91.5	1663
91.5 - 94.0	1586
94.0 - 96.5	2565
96.5 - 99.0	3794
99.0 - 101.5	3243
101.5 - 104.0	2278
104.0 - 106.5	2221

Table 7

AVERAGE COMPRESSION-WAVE VELOCITY

Boring CTB-5(OW)

PRIVATE FUEL STORAGE FACILITY

Interval Depth (feet bgs)	P-wave Velocity (feet / sec)
0.8 - 5.8	735
5.8 - 10.8	1165
10.8 - 35.8	1490
35.8 - 50.8	2100

Subject Skull Valley PFS

Project No. 4790

By R Youngs

Checked By

Task No.

File No.

Date 1/14/99

Date

Sheet 1 of 1

Message from Ivan Wong who is leading NEHRP hazard microzonation study in Salt Lake Valley.

Data they have for Salt Lake group indicates V_S in range of 1 - 1.75 km/sec

GEOMATRIX CONSULTANTS

Bob Youngs

From: James C. Pechmann [pechmann@seis.utah.edu]
Sent: Monday, January 25, 1999 1:45 PM
To: bycungs@geomatrix.com
Cc: arabasz@uuss.seis.utah.edu; pechmann@uuss.seis.utah.edu
Subject: Velocity Model

Bob,

The best velocity model for your purposes is probably the velocity model that we routinely use for locating earthquakes in the Wasatch Front region. This model is given in the first three columns below:

P Velocity (km/sec)	S Velocity (km/sec)	Depth to Top (km)	S Velocity from Keller et al. (1975 (km/sec)
3.40	1.95	0.0	3.4
5.90	3.39	1.4	3.5
6.40	3.68	15.5	3.2
7.50	4.31	25.4	4.0
7.90	4.54	42.0	

The P-wave model was modified from model B of Keller et al. (1975, JGR 80, 1093-1098) by adding the 7.9 km/sec layer at the bottom based on the work of Loeb and Pechmann (1986, Earthquake Notes 57 (1), 10). The S-wave model was calculated from the P-wave model using an empirically-determined P/S velocity ration of 1.74.

The Keller et al. P-wave model is from an unreversed vertical component refraction profile extending due south from the Bingham Canyon Copper Mine. Keller et al. (1974) also derived an S-wave model from transverse-component refraction data (velocities at right, above). However, their S-wave data were not very good (probably because the sources they used were quarry blasts), and they don't sound very confident about the S-wave model in their paper.

—Jim Pechmann

Salt Lake City Airport East (EAP)

DEPTH (m)	LITHOLOGY	Vs (m/sec)	ρ (g/cm^3)
→	Soft Clay	129	1.78
8.0	Soft Clay	175	1.78
14.0	Stiff Clay	223	2.00
22.0	Stiff Clay	223	2.00
34.0	Stiff Clay	304	2.00
52.0	Stiff Clay	571	2.00
58.0*	Unconsolidated Sediments	620	2.10
200	Unconsolidated Sediments	668	2.10
400	Unconsolidated Sediments	820	2.15
590	Semi-Consolidated Sediments	1310	2.20
1050	Consolidated Sediments	2890	2.65
2500	Bedrock	3460	2.75

Laird Park (LAI)

DEPTH (m)	LITHOLOGY	Vs (m/sec)	ρ (g/cm^3)
8	Interbedded Sand and Gravel	336	2.00
18	Tufa - Cemented Gravel	944	2.15
24	Stiff Clay, Sand or Gravel	536	2.00
28	Semi-Consolidated Sediments	992	2.15
56	Semi-Consolidated Sediments	1634	2.30
59*	Semi-Consolidated Sediments	1750	2.30
70	Weathered Limestone	2600	2.50
	Limestone	3000	2.75

City and County Building (CCH)

DEPTH (m)	LITHOLOGY	Vs (m/sec)	ρ (g/cm^3)
28	Clay	242	2.00
68*	Clay with some Gravel	384	2.00
83	Stiff Clay	820	2.15
270	Semi-Consolidated Sediments	1310	2.20
	Shale	3000	2.75

* Bottom of borehole
- - - Proposed layer boundaries
→ Top of water table

Figure 5. GEOLOGIC AND SHEAR-WAVE VELOCITY PROFILES

from Wong & Silva (1993

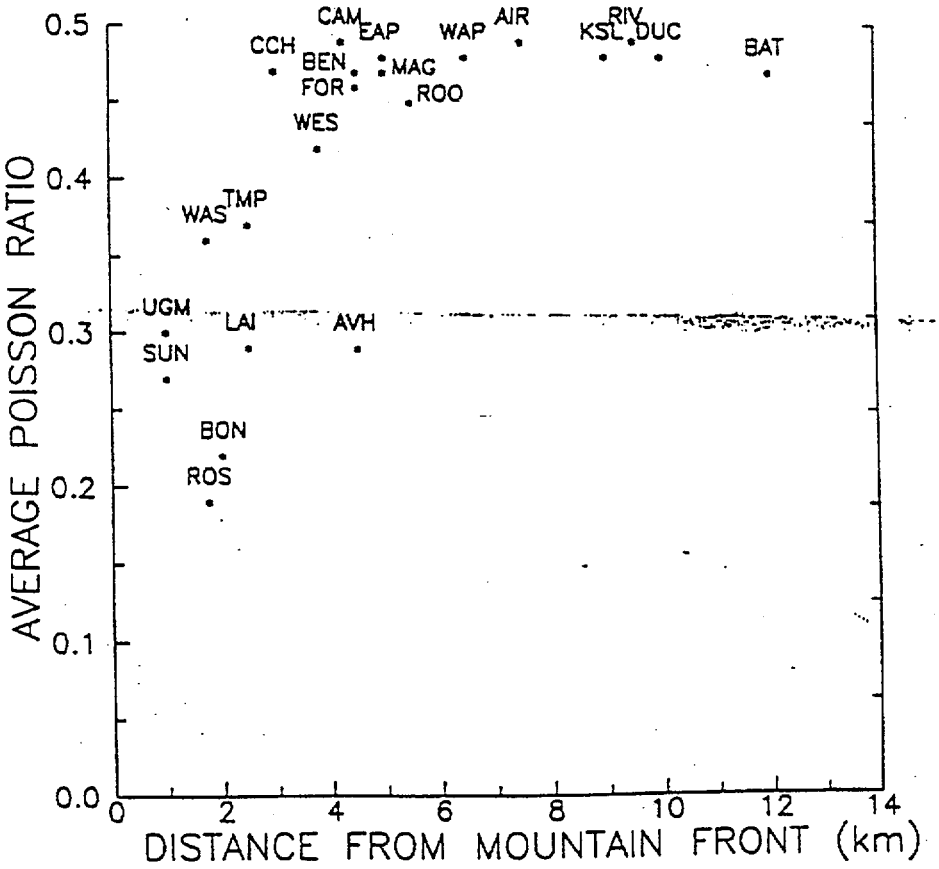

FIG. 11. Weighted average Poisson ratio (derived from borehole measurements) for each borehole as a function of distance from the Wasatch Mountains. More Poisson ratio variation and, generally, a lower value is apparent among boreholes located less than 5 km from the mountains. Boreholes are identified on the graph by their site name annotated above the data point.

Site Response Versus Shear Wave Velocity (V_s)

The similar areal distribution of borehole average V_s and site response variations described in the previous section led us to compare site response and V_s directly. As shown in the four graphs of Figure 13, a good nonlinear inverse relationship exists between V_s and site response with V_s decreasing as site response increases. Because a theoretical power-law relationship exists between seismic wave amplitude and impedance (e.g., Carter *et al.*, 1984), this type of relation was used to regress known site response against the V_s shown in Table 2. The goodness of fit for these regressions was measured by the correlation coefficient r. Using a power curve fit to the data, the highest degree of correlation ($r = 0.92$) occurs in the 1.0- to 2.0-sec period band, and the lowest ($r = 0.70$) occurs in 2.0- to 3.3-sec band. Three notable outlying values in the upper two graphs of Figure 13 are the data from sites 11, 8, and 1, which correspond to sites KSL, DUC, and AIR, respectively. These stations are located in the northwest part of the valley and are coincident with the greatest accumulation of Cenozoic sediment in the Salt Lake Valley (Mattick, 1970). The

from Williams and others (1993)

From: thomas.chang@swec.com [mailto:thomas.chang@swec.com]
Sent: Friday, March 23, 2001 10:11 AM
To: Bob Youngs
Cc: Jerry.Cooper@swec.com; paul.trudeau@swec.com
Subject: Re: Needed references for SSI calc package

Bob,

This is to confirm that the 5 ft of soil cement at the Skull Valley site which will be designed to have a minimum unit weight 100 pcf and low strain shear wave velocity to exceed 1,500 fps. As Paul Trudeau's fax of January 22, 2001 to you indicated that the soil cement around the Canister Trnsfer Building and between and around Storage Pads will be designed to have minimum unconfined compressive strength of 250 psi and shear wave velocity approximately 2,700 fps. The 2 ft thick layer of soil cement below the storage pads will be designed to have the unconfined comprressive strength not to exceed 100 psi in order to meet the casks tipover analysis requirement with static modulus less than 75,000 psi. This 2 ft thick layer soil cement which uniform across the storage pad area will have shear wave velocity greater than 1,500 fps.
Your earlier e-mail listing the g/gmax reduction and damping curves for the top 25 ft shallow soils that you and Paul worked will be documented in our revised Geotechnical Design Criteria Calc.

Tom Chang

From: thomas.chang@swec.com [mailto:thomas.chang@swec.com]
Sent: Thursday, March 22, 2001 1:46 PM
To: Bob Youngs
Cc: Jerry.Cooper@swec.com
Subject: Re: FW: G/Gmax and damping curves

Bob,

I have checked the g/gmax and damping values you used in Appendix F and the SSI properties calc. and confirmed that they are the same as those that will appear in our revised geotech design criteria calc. I hope this statement will satisfy your requirement for the completion of your calc.

Regards

Tom Chang

Bob Youngs <BYoungs@geomatrix.com> on 03/20/2001 12:44:14 PM

To: Thomas Chang/Transportation/SWEC@SWEC

cc: Jerry Cooper/Mechanical/SWEC@SWEC

Subject: FW: G/Gmax and damping curves

Tom:

This is a message I sent to Paul last Friday listing the final G/Gmax and damping curves we worked out for the 9 and 20 ft samples. Paul indicated that he was placing them in the revised geotech calc so that I could reference them in my calc.

> -----Original Message-----
> From: Bob Youngs
> Sent: Friday, March 16, 2001 1:16 PM
> To: 'Paul Trudeau'
> Subject: G/Gmax and damping curves
>

> Paul:
>
> listed below are the g/gmax and damping values I used in Appendix F and
> the SSI properties Calc. Would you make sure that they are the same as
> those that will appear in your revised geotech calc
>
> Thanks
>
> Bob Y.
>

```
>12     Skull Valley RC test results                          : 0 - 12 FT
>    0.0001  0.000316     0.001   0.00316     0.010    0.0316     0.100     0.316
>     1.000     3.160     10.00     31.60
>     1.000     1.000     1.000     0.990     0.950     0.800     0.550     0.300
>     0.120     0.060     0.040     0.03
>   12     Skull Valley RC test tesults                         : 0 - 12 ft
>    0.0001  0.000316     0.001   0.00316     0.010    0.0316     0.100     0.316
>     1.000     3.160     10.00     31.60
>     0.900     0.900     0.900     1.000     1.500     2.900     5.500     9.300
>     15.00     22.50     26.50     28.00
>   12     Skull Valley RC test results                         :18 - 25 FT
>    0.0001  0.000316     0.001   0.00316     0.010    0.0316     0.100     0.316
>     1.000     3.160     10.00     31.60
>     1.000     1.000     1.000     0.990     0.960     0.820     0.610     0.350
>     0.150     0.070     0.050     0.030
>   12     Skull Valley RC test tesults                         :18 - 25 ft
>    0.0001  0.000316     0.001   0.00316     0.010    0.0316     0.100     0.316
>     1.000     3.160     10.00     31.60
>     0.800     0.800     0.800     0.900     1.100     2.400     4.600     8.200
>     14.20     21.70     26.00     27.50
```

Calculation 05996.02-G(PO18)-2, Rev. 1
Attachment B
Analysis of Site Velocity Data

This attachment contains the listing of the computer programs, input, and output files for the statistical analysis of the velocity data at the Skull Valley site. The programs are VSSTATH for shear wave velocities and VPSTATH for compression wave velocities. The programs together with the input and output files are located in directory \CONESTAT on the accompanying disk.

The programs read in the layer designation then loop over the individual velocity profiles. For each profile the harmonic mean of all velocity measurements in a layer is computed and stored. The programs then compute the mean velocity in each layer and the covariance matrix.

```
  **** File: VSSTATH.FOR                                          ****
       program vsstath
 c.................layer averages for a profile computed as
harmonic mean
       parameter(mxl=40)
       character title*70,head*20,ofile*40,ifile*40
       real
dr(0:mxl),mvs(mxl),svs(mxl),cov(mxl,mxl),lvs(mxl,mxl),
      , err(mxl,mxl)
       integer npl(mxl),ndl(mxl,mxl)
 c
 99    print*,' enter ofile (q to quit): '
       read(5,'(a)') ofile
       if(ofile.eq.'q'.or.ofile.eq.'Q') STOP
       print*,' enter title :'
       read(5,'(a)') title
       print*,' enter np,nl, dr limits(0..nl): '
       read(5,*) np, nl, (dr(i),i=1,nl)
       dr(0)=0.0
       DO 10 i=1,nl
         mvs(i)=0.0
         svs(i)=0.0
         npl(i)=0
         DO 10 j=1,nl
           cov(i,j)=0.0
 10    CONTINUE
       DO 50 ip=1,np
         read(5,'(a)') ifile
         open(7,file=ifile)
         read(7,'(a)') head
         read(7,*) n
```

```
          DO 15 i=1,nl
            ndl(ip,i)=0
            lvs(ip,i)=0.0
15        CONTINUE
          DO 25 j=1,n
            read(7,*) kt,d,vs
            DO 20 i=1,nl
              IF(d.ge.dr(i-1).and.d.lt.dr(i)) then
                ndl(ip,i)=ndl(ip,i)+1
                lvs(ip,i)=lvs(ip,i)+1.0/vs
                go to 25
              ENDif
20          CONTINUE
25        CONTINUE
          close(7)
          DO 30 i=1,nl
c        print*,ndl(ip,i)
            IF(ndl(ip,i).gt.0) then
              npl(i)=npl(i)+1
              lvs(ip,i)=ndl(ip,i)/lvs(ip,i)
              mvs(i)=mvs(i)+lvs(ip,i)
              svs(i)=svs(i)+lvs(ip,i)**2
c        print'(2i5,f10.1)',ip,i,lvs(ip,i)
            ENDIF
30        CONTINUE
50      CONTINUE
c
        DO 60 i=1,nl
          write(18,'(25i6)') nint(dr(i-1)),nint(dr(i)),
     ,     (nint(lvs(ip,i)),ip=1,np)
          mvs(i)=mvs(i)/npl(i)
          IF(npl(i).gt.1) then
            varvs=(svs(i)-mvs(i)*mvs(i)*real(npl(i)))/real(npl(i)-
1)
           ELSE
            varvs=0.0
          ENDIF
          svs(i)=sqrt(max(varvs,0.0))
          DO 60 ip=1,np
            IF(ndl(ip,i).gt.0.0) then
              err(ip,i)=lvs(ip,i)-mvs(i)
             ELSE
              err(ip,i)=err(ip,i-1)
            ENDIF
60      CONTINUE
        DO 65 i=1,nl
          DO 65 j=1,nl
```

```
            DO 65 ip=1,np
 65            cov(i,j)=cov(i,j)+err(ip,i)*err(ip,j)
       DO 70 i=1,nl
         DO 70 j=1,i-1
 70        cov(i,j)=cov(i,j)/sqrt(cov(i,i)*cov(j,j))
       DO 75 i=1,nl
 75      cov(i,i)=1.0
       open(8,file=ofile)
       write(8,'(a)') title
       write(8,'('' Statistics of Layer Velocities'')')
       write(8,'('' Dmin Dmax    n  Avg Vs Sig Vs  90cimVs
COV'')')
       DO 80 i=1,nl
         sigmvs=svs(i)/sqrt(real(npl(i)))
         write(8,1) dr(i-
1),dr(i),npl(i),mvs(i),svs(i),1.645*sigmvs,
      ,   (cov(i,j),j=1,i)
 80    CONTINUE
       close(8)
       go to 99
 1     format(2f5.1,i5,3f8.1,12f8.3)
       END
```

```
 **** File: vs7l-all.in                                          ****
vs7l-all.out
Skull Valley layer statistics, all profiles
17 7 5 9.9 12.1 18.1 26.1 35  55
CPT01
CPT03
CPT06
CPT13
CPT15
CPT16
CPT18
CPT20
CPT21
CPT22
CPT31
CPT33
CPT34
CPT36
CPT37
CPT38
CTB05
q
```

```
 **** File: CPT01                                                ****
```

CPT 1
8

1	3.9	596	1145	0.314
1	7.2	452	1058	0.388
1	10.5	594	1087	0.287
1	13.8	858	1491	0.252
1	17.1	795	1568	0.327
1	20.3	902	1301	0.037
1	23.6	854	1277	0.095
1	26.9	1140	1798	0.164

**** File: CPT03 ****
CPT 3
8

3	3.4	644	1271	0.327
3	6.7	457	1053	0.384
3	10	647	1070	0.212
3	13.3	706	1251	0.266
3	16.6	863	1740	0.337
3	19.8	896	1204	-0.121
3	23.1	1011	1519	0.102
3	26.4	1078	1879	0.255

**** File: CPT06 ****
CTP 6
6

6	3.4	545	1052	0.317
6	6.7	571	1236	0.364
6	10	789	1235	0.155
6	13.3	700	1296	0.294
6	16.6	839	1328	0.168
6	19.8	877	2105	0.395

**** File: CPT13 ****
CPT13
7

13	3.4	592	1027	0.251
13	6.7	534	1015	0.309
13	10	653	1274	0.322
13	13.3	896	1487	0.215
13	16.6	914	1442	0.164
13	19.8	880	1447	0.207
13	23.1	886	1337	0.109

**** File: CPT15 ****
CPT 15
7

```
      15       3.8       496       1362      0.424
      15       7.1       545       1320      0.397
      15      10.3       562       1161      0.347
      15      13.6       934       1438      0.135
      15      16.9       830       1456      0.259
      15      20.2       900       1361      0.111
      15      23.5       872       1428      0.203

 **** File: CPT16                                                  ****
CPT16
7
      16       3.6       588       1272      0.364
      16       6.9       543       1094      0.337
      16      10.2       623       1083      0.253
      16      13.4       867       1446      0.219
      16      16.7       830       1398      0.228
      16        20       808       1391      0.245
      16      23.3       874       1305      0.093

 **** File: CPT18                                                  ****
CPT 18
6
      18       3.6       499       1124      0.377
      18       6.9       474       1139      0.395
      18      10.2       650       1517      0.388
      18      13.4       782       1313      0.225
      18      16.7       742       1515      0.342
      18        20       877       1691      0.316

 **** File: CPT20                                                  ****
CPT20
7
      20       3.6       525        813      0.142
      20       6.9       491       1415      0.432
      20      10.2       789       1522      0.316
      20      13.4      1023       1640      0.182
      20      16.7       883       1431      0.193
      20        20       878       1386      0.165
      20      23.3       919       1511      0.206

 **** File: CPT21                                                  ****
CPT 21
8
      21       3.8       625       1128      0.278
      21       7.1       434       1110      0.410
      21      10.3       702       1170      0.219
      21      13.6       904       1525      0.229
```

```
      21      16.9      813      1643     0.338
      21      20.2      894      1387     0.145
      21      23.5      835      1430     0.241
      21      26.7     1021      1962     0.314

 **** File: CPT22                                                  ****
CPT 22
7
      22       3.8      605      1282     0.357
      22       7.1      518      1379     0.418
      22      10.3      759      1148     0.112
      22      13.6      805      1365     0.233
      22      16.9      982      1478     0.105
      22      20.2      815      1254     0.134
      22      23.5      806      1366     0.233

 **** File: CPT31                                                  ****
CPT 31
7
      31       3.6      559       852     0.122
      31       6.9      526      1140     0.365
      31      10.2      906      1280    -0.002
      31      13.4      884      1657     0.301
      31      16.7      942      1721     0.286
      31        20      902      1536     0.237
      31      23.3      902      1723     0.311

 **** File: CPT33                                                  ****
CPT33
8
      33       3.9      508      1058     0.350
      33       7.2      559      1023     0.287
      33      10.5      869      1337     0.134
      33      13.8      903      1670     0.293
      33      17.1      903      1474     0.200
      33      20.3      870      1356     0.150
      33      23.6      893      1203    -0.114
      33      26.9      986      1593     0.189

 **** File: CPT34                                                  ****
CPT34
7
      34       3.6      443      1003     0.379
      34       6.9      449      1046     0.387
      34      10.2      679      1205     0.267
      34      13.4      904      1279     0.001
      34      16.7      893      1827     0.343
```

```
      34        20       846      1326     0.157
      34      23.3       902      1313     0.053

 **** File: CPT36                                          ****
CPT36
7
      36       3.6       612      1368     0.375
      36       6.9       700       959    -0.070
      36      10.2       731      1377     0.304
      36      13.4       800      1320     0.210
      36      16.7      1003      1523     0.117
      36        20       893      1401     0.158
      36      23.3       840      1479     0.262

 **** File: CPT37                                          ****
CPT37
8
      37       5.4       553      1073     0.319
      37       8.7       611      1093     0.273
      37        12       741      1182     0.176
      37      15.3       839      1312     0.154
      37      18.5       856      1450     0.233
      37      21.8       878      1302     0.083
      37      25.1       759      1211     0.177
      37      28.4       912      1461     0.181

 **** File: CPT38                                          ****
CPT38
8
      38       5.2       467      1265     0.421
      38       8.5       536      1085     0.339
      38      11.8       803      1330     0.213
      38      15.1       808      1537     0.309
      38      18.4       902      1395     0.141
      38      21.6       811      1514     0.299
      38      24.9       887      1173    -0.168
      38      28.2       957      1537     0.183

 **** File: CTB05                                          ****
CTB05
20
       5         2       680       990     0.053
       5       4.5       513       990     0.316
       5         7       603       990     0.205
       5       9.5       673       990     0.070
       5        12       853      1440     0.230
       5      14.5       791      1440     0.284
```

```
         5        17       858      1440     0.225
         5      19.5       885      1440     0.197
         5        22       768      1440     0.301
         5      24.5       862      1440     0.221
         5        27       992      1440     0.048
         5      29.5      1176      1440    -0.501
         5        32       965      1440     0.092
         5      34.5      1134      1440    -0.316
         5        37      1106      2085     0.304
         5      39.5      1173      2085     0.268
         5        42      1438      2085     0.046
         5      44.5      1007      2085     0.348
         5        47      1121      2085     0.297
         5      49.5      1429      2085     0.057
```

```
  **** File: vs71-all.out                                        ****
 Skull Valley layer statistics, all profiles
  Statistics of Layer Velocities
  Dmin Dmax    n  Avg Vs Sig Vs  90cimVs  COV
   0.0  5.0   15   561.5    56.9    24.2   1.000
   5.0  9.9   17   527.6    70.0    27.9   0.126   1.000
   9.9 12.1   17   726.5    99.8    39.8  -0.039   0.342   1.000
  12.1 18.1   17   854.2    55.3    22.1  -0.196   0.109   0.212
1.000
  18.1 26.1   17   871.3    32.1    12.8  -0.046  -0.356  -0.119
-0.046   1.000
  26.1 35.0    7  1021.9    77.5    48.2   0.122  -0.269  -0.266
-0.079   0.582   1.000
  35.0 55.0    1  1191.2     0.0     0.0   0.104  -0.345  -0.329
-0.054   0.643   0.984   1.000
```

```
  **** File: VPSTATH.FOR                                         ****
       program vpstath
 c.................layer averages for a profile computed as
harmonic mean
       parameter(mxl=40)
       character title*70,head*20,ofile*40,ifile*40
       real
dr(0:mxl),mvp(mxl),svp(mxl),cov(mxl,mxl),lvp(mxl,mxl),
      , err(mxl,mxl)
       integer npl(mxl),ndl(mxl,mxl)
 c
 99    print*,' enter ofile (q to quit): '
       read(5,'(a)') ofile
       if(ofile.eq.'q'.or.ofile.eq.'Q') STOP
       print*,' enter title :'
       read(5,'(a)') title
```

```
      print*,' enter np,nl, dr limits(1..6): '
      read(5,*) np, nl, (dr(i),i=1,nl)
      dr(0)=0.0
      DO 10 i=1,nl
        mvp(i)=0.0
        svp(i)=0.0
        npl(i)=0
        DO 10 j=1,nl
          cov(i,j)=0.0
10    CONTINUE
      DO 50 ip=1,np
        read(5,'(a)') ifile
        open(7,file=ifile)
        read(7,'(a)') head
        read(7,*) n
        DO 15 i=1,nl
          ndl(ip,i)=0
          lvp(ip,i)=0.0
15      CONTINUE
        DO 25 j=1,n
          read(7,*) kt,d,vs,vp
          DO 20 i=1,nl
            IF(d.ge.dr(i-1).and.d.lt.dr(i)) then
              ndl(ip,i)=ndl(ip,i)+1
              lvp(ip,i)=lvp(ip,i)+1.0/vp
              go to 25
            ENDif
20        CONTINUE
25      CONTINUE
        close(7)
        DO 30 i=1,nl
c      print*,ndl(ip,i)
          IF(ndl(ip,i).gt.0) then
            npl(i)=npl(i)+1
            lvp(ip,i)=ndl(ip,i)/lvp(ip,i)
            mvp(i)=mvp(i)+lvp(ip,i)
            svp(i)=svp(i)+lvp(ip,i)**2
c      print'(2i5,f10.1)',ip,i,lvp(ip,i)
          ENDIF
30      CONTINUE
50    CONTINUE
c
      DO 60 i=1,nl
        write(19,'(25i6)') nint(dr(i-1)),nint(dr(i)),
     ,    (nint(lvp(ip,i)),ip=1,np)
        mvp(i)=mvp(i)/npl(i)
        IF(npl(i).gt.1) then
```

```
            varvp=(svp(i)-mvp(i)*mvp(i)*real(npl(i)))/real(npl(i)-
1)
           ELSE
            varvp=0.0
          ENDIF
          svp(i)=sqrt(max(varvp,0.0))
          DO 60 ip=1,np
            IF(ndl(ip,i).gt.0.0) then
              err(ip,i)=lvp(ip,i)-mvp(i)
             ELSE
              err(ip,i)=err(ip,i-1)
            ENDIF
 60     CONTINUE
        DO 65 i=1,nl
          DO 65 j=1,nl
            DO 65 ip=1,np
 65           cov(i,j)=cov(i,j)+err(ip,i)*err(ip,j)
        DO 70 i=1,nl
          DO 70 j=1,i-1
 70         cov(i,j)=cov(i,j)/sqrt(cov(i,i)*cov(j,j))
        DO 75 i=1,nl
 75       cov(i,i)=1.0
        open(8,file=ofile)
        write(8,'(a)') title
        write(8,'('' Statistics of Layer Velocities'')')
        write(8,'('' Dmin Dmax    n  Avg vp Sig vp  90cimvp
COV'')')
        DO 80 i=1,nl
          sigmvp=svp(i)/sqrt(real(npl(i)))
          write(8,1) dr(i-
1),dr(i),npl(i),mvp(i),svp(i),1.645*sigmvp,
       ,   (cov(i,j),j=1,i)
 80     CONTINUE
        close(8)
        go to 99
 1      format(2f5.1,i5,3f8.1,12f8.3)
        END
```

```
 **** File: vp7l-all.in                                          ****
vp7l-all.out
Skull Valley layer statistics, all profiles
17 7 5 9.9 12.1 18.1 26.1 35  55
CPT01
CPT03
CPT06
CPT13
CPT15
```

```
CPT16
CPT18
CPT20
CPT21
CPT22
CPT31
CPT33
CPT34
CPT36
CPT37
CPT38
CTB05
q

 **** File: vp7l-all.out                                    ****
Skull Valley layer statistics, all profiles
 Statistics of Layer Velocities
 Dmin Dmax    n  Avg vp Sig vp  90cimvp  COV
  0.0  5.0   15  1116.5   170.4    72.4   1.000
  5.0  9.9   17  1131.1   134.1    53.5  -0.079   1.000
  9.9 12.1   17  1259.9   143.6    57.3  -0.491   0.062   1.000
 12.1 18.1   17  1472.2    95.4    38.0  -0.435  -0.039   0.077
1.000
 18.1 26.1   17  1439.8   204.6    81.6  -0.252   0.212   0.282
-0.273   1.000
 26.1 35.0    7  1667.1   210.3   130.8  -0.082   0.134  -0.064
-0.035   0.776   1.000
 35.0 55.0    1  2085.0     0.0     0.0  -0.135   0.071   0.013
-0.058   0.801   0.969   1.000
```

Calculation 05996.02-G(PO18)-2 Rev 1
Attachment C
Site Response Analyses

This attachment summarizes the site response analyses. The input (*.in), output (*.out), and final properties (*.pun) files are contained in the self-extracting zip file SITERESP.EXE located on the accompanying disk in directory \SITERESP. The files are designated by xx-Fy.*, where y refers to the input motion (N = 2,000-year fault-normal and P = 2,000-year fault-parallel), and xx refers to the velocity profile (HV = high range, MV = best estimate constant Tertiary velocity, MG = best estimate increasing Tertiary velocity, and LV = low range).

The results were then processed in the following manner.

Computer routine REWRTP.FOR was used to reformat the *.pun files for plotting. The input file REW.IN, and output files, *SCP, are listed below and are located on the accompanying disk in directory \RESULTS. Then computer routine PSTAT.FOR was used to compute the geometric mean shear modulus and average damping for each layer for the high range, best estimate, and low range velocity profiles. This routine and the input and output files are listed below and are located on the accompanying disk in directory \RESULTS. These values are the used in the spreadsheet SV-SSI-FEB01.XLS described in Attachment D.

```
  **** File: REWRTP.FOR                                          ****
       program REWRTp
       character ifile*40
 c
 99    read(5,'(a)') ifile
       IF(ifile.eq.'q'.or.ifile.eq.'Q') STOP
       open(7,file='..\siteresp\'//ifile(1:5)//'.pun')
       open(8,file=ifile(1:5)//'.scp')
       write(8,'(a)') ifile
       read(7,*) k,nl
       write(8,'(i5,''     Depth     Vsmax      Vs     Damping
G''
      ,  )') nl-1
       d=0.0
       DO 20 i=1,nl-1
         read(7,*) k,j,j,h,g,damp,uw,gmax
         v=sqrt(g*32.2/uw)
         vmax=sqrt(gmax*32.2/uw)
         dmp=d+h/2.0
         d=d+h
         write(8,'(i5,f10.2,2f10.3,f10.4,f10.2)')
i,dmp,vmax,v,damp,g
 20    CONTINUE
```

```
      close(7)
      close(8)
      print'('' completed '',a8)',ifile
      go to 99
      END
```

**** File: REW.IN ****

```
HV-FN
HV-FP
LV-FN
LV-FP
MV-FN
MV-FP
mg-FN
mg-FP
q
```

**** File: HV-FN.SCP ****

HV-FN

41	Depth	Vsmax	Vs	Damping	G
1	1.25	2121.000	2121.005	0.0090	13971.00
2	3.75	2121.000	2118.802	0.0092	13942.00
3	6.25	647.000	573.097	0.0306	816.00
4	8.75	647.000	545.388	0.0383	739.00
5	11.00	890.000	809.985	0.0264	1630.00
6	13.50	1046.000	993.443	0.0164	3065.00
7	16.50	1046.000	978.420	0.0189	2973.00
8	20.00	1068.000	983.724	0.0214	2825.00
9	24.00	1068.000	971.460	0.0233	2755.00
10	27.50	1250.000	1072.753	0.0469	4110.00
11	30.50	1250.000	1056.049	0.0501	3983.00
12	33.50	1250.000	1041.902	0.0528	3877.00
13	37.50	1683.000	1505.244	0.0379	8092.00
14	42.50	1683.000	1483.321	0.0412	7858.00
15	47.50	1683.000	1464.322	0.0440	7658.00
16	52.50	2546.000	2496.513	0.0109	23227.00
17	57.50	2546.000	2492.641	0.0112	23155.00
18	62.50	2546.000	2488.924	0.0115	23086.00
19	67.50	2546.000	2485.526	0.0117	23023.00
20	72.50	2546.000	2482.339	0.0119	22964.00
21	77.50	2546.000	2476.170	0.0126	22850.00
22	82.50	2546.000	2469.170	0.0132	22721.00
23	87.50	2546.000	2462.805	0.0139	22604.00
24	95.83	4101.000	4100.998	0.0428	70511.00
25	107.50	4101.000	4100.998	0.0428	70511.00
26	119.17	4101.000	4100.998	0.0428	70511.00
27	134.73	4101.000	4100.997	0.0428	75734.00

28	154.17	4101.000	4100.997	0.0428	75734.00
29	173.61	4101.000	4100.997	0.0428	75734.00
30	193.05	4101.000	4100.997	0.0428	75734.00
31	212.49	4101.000	4100.997	0.0428	75734.00
32	231.93	4101.000	4100.997	0.0428	75734.00
33	251.37	4101.000	4100.997	0.0428	75734.00
34	270.81	4101.000	4100.997	0.0428	75734.00
35	290.25	4101.000	4100.997	0.0428	75734.00
36	324.97	5657.000	5657.004	0.0310	144107.00
37	374.97	5657.000	5657.004	0.0310	144107.00
38	424.97	5657.000	5657.004	0.0310	144107.00
39	474.97	5657.000	5657.004	0.0310	144107.00
40	549.97	6398.000	6398.001	0.0253	184332.00
41	649.97	6398.000	6398.001	0.0253	184332.00

**** File: HV-FP.SCP ****

HV-FP

41	Depth	Vsmax	Vs	Damping	G
1	1.25	2121.000	2121.005	0.0090	13971.00
2	3.75	2121.000	2119.031	0.0092	13945.00
3	6.25	647.000	572.746	0.0307	815.00
4	8.75	647.000	540.197	0.0397	725.00
5	11.00	890.000	804.500	0.0274	1608.00
6	13.50	1046.000	987.429	0.0174	3028.00
7	16.50	1046.000	972.313	0.0199	2936.00
8	20.00	1068.000	976.033	0.0226	2781.00
9	24.00	1068.000	960.645	0.0251	2694.00
10	27.50	1250.000	1058.962	0.0496	4005.00
11	30.50	1250.000	1047.397	0.0518	3918.00
12	33.50	1250.000	1038.942	0.0534	3855.00
13	37.50	1683.000	1513.037	0.0367	8176.00
14	42.50	1683.000	1493.198	0.0397	7963.00
15	47.50	1683.000	1470.714	0.0431	7725.00
16	52.50	2546.000	2496.675	0.0109	23230.00
17	57.50	2546.000	2492.318	0.0112	23149.00
18	62.50	2546.000	2488.493	0.0115	23078.00
19	67.50	2546.000	2484.986	0.0117	23013.00
20	72.50	2546.000	2481.744	0.0120	22953.00
21	77.50	2546.000	2474.598	0.0127	22821.00
22	82.50	2546.000	2468.192	0.0133	22703.00
23	87.50	2546.000	2462.750	0.0139	22603.00
24	95.83	4101.000	4100.998	0.0428	70511.00
25	107.50	4101.000	4100.998	0.0428	70511.00
26	119.17	4101.000	4100.998	0.0428	70511.00
27	134.73	4101.000	4100.997	0.0428	75734.00
28	154.17	4101.000	4100.997	0.0428	75734.00
29	173.61	4101.000	4100.997	0.0428	75734.00

30	193.05	4101.000	4100.997	0.0428	75734.00
31	212.49	4101.000	4100.997	0.0428	75734.00
32	231.93	4101.000	4100.997	0.0428	75734.00
33	251.37	4101.000	4100.997	0.0428	75734.00
34	270.81	4101.000	4100.997	0.0428	75734.00
35	290.25	4101.000	4100.997	0.0428	75734.00
36	324.97	5657.000	5657.004	0.0310	144107.00
37	374.97	5657.000	5657.004	0.0310	144107.00
38	424.97	5657.000	5657.004	0.0310	144107.00
39	474.97	5657.000	5657.004	0.0310	144107.00
40	549.97	6398.000	6398.001	0.0253	184332.00
41	649.97	6398.000	6398.001	0.0253	184332.00

**** File: LV-FN.SCP ****

LV-FN

41	Depth	Vsmax	Vs	Damping	G
1	1.25	1061.000	1058.565	0.0095	3480.00
2	3.75	1061.000	1046.635	0.0121	3402.00
3	6.25	431.000	315.305	0.0573	247.00
4	8.75	431.000	292.801	0.0685	213.00
5	11.00	594.000	475.187	0.0457	561.00
6	13.50	697.000	620.833	0.0268	1197.00
7	16.50	697.000	599.728	0.0323	1117.00
8	20.00	712.000	594.859	0.0367	1033.00
9	24.00	712.000	584.109	0.0394	996.00
10	27.50	834.000	624.532	0.0774	1393.00
11	30.50	834.000	607.947	0.0829	1320.00
12	33.50	834.000	592.554	0.0879	1254.00
13	37.50	841.000	582.786	0.0925	1213.00
14	42.50	841.000	565.473	0.0978	1142.00
15	47.50	841.000	551.688	0.1020	1087.00
16	52.50	1273.000	1198.718	0.0204	5355.00
17	57.50	1273.000	1196.926	0.0208	5339.00
18	62.50	1273.000	1196.478	0.0208	5335.00
19	67.50	1273.000	1197.374	0.0207	5343.00
20	72.50	1273.000	1198.158	0.0205	5350.00
21	77.50	1273.000	1194.907	0.0211	5321.00
22	82.50	1273.000	1191.083	0.0219	5287.00
23	87.50	1273.000	1188.376	0.0224	5263.00
24	95.83	2051.000	2050.979	0.0397	17636.00
25	107.50	2051.000	2050.979	0.0397	17636.00
26	119.17	2051.000	2050.979	0.0397	17636.00
27	134.73	2051.000	2051.013	0.0397	18943.00
28	154.17	2051.000	2051.013	0.0397	18943.00
29	173.61	2051.000	2051.013	0.0397	18943.00
30	193.05	2051.000	2051.013	0.0397	18943.00
31	212.49	2051.000	2051.013	0.0397	18943.00

32	231.93	2051.000	2051.013	0.0397	18943.00
33	251.37	2051.000	2051.013	0.0397	18943.00
34	270.81	2051.000	2051.013	0.0397	18943.00
35	290.25	2051.000	2051.013	0.0397	18943.00
36	324.97	2051.000	2051.013	0.0397	18943.00
37	374.97	2051.000	2051.013	0.0397	18943.00
38	424.97	2051.000	2051.013	0.0397	18943.00
39	474.97	2051.000	2051.013	0.0397	18943.00
40	549.97	2051.000	2051.013	0.0397	18943.00
41	649.97	2051.000	2051.013	0.0397	18943.00

**** File: LV-FP.SCP ****

LV-FP

41	Depth	Vsmax	Vs	Damping	G
1	1.25	1061.000	1058.717	0.0094	3481.00
2	3.75	1061.000	1046.942	0.0120	3404.00
3	6.25	431.000	308.204	0.0608	236.00
4	8.75	431.000	276.541	0.0759	190.00
5	11.00	594.000	461.435	0.0495	529.00
6	13.50	697.000	614.054	0.0286	1171.00
7	16.50	697.000	604.541	0.0311	1135.00
8	20.00	712.000	602.014	0.0350	1058.00
9	24.00	712.000	590.814	0.0378	1019.00
10	27.50	834.000	633.656	0.0742	1434.00
11	30.50	834.000	617.544	0.0797	1362.00
12	33.50	834.000	607.487	0.0830	1318.00
13	37.50	841.000	593.262	0.0893	1257.00
14	42.50	841.000	558.999	0.0997	1116.00
15	47.50	841.000	539.110	0.1077	1038.00
16	52.50	1273.000	1190.632	0.0220	5283.00
17	57.50	1273.000	1185.890	0.0229	5241.00
18	62.50	1273.000	1183.398	0.0234	5219.00
19	67.50	1273.000	1183.512	0.0234	5220.00
20	72.50	1273.000	1185.551	0.0230	5238.00
21	77.50	1273.000	1188.602	0.0224	5265.00
22	82.50	1273.000	1192.546	0.0216	5300.00
23	87.50	1273.000	1191.421	0.0218	5290.00
24	95.83	2051.000	2050.979	0.0397	17636.00
25	107.50	2051.000	2050.979	0.0397	17636.00
26	119.17	2051.000	2050.979	0.0397	17636.00
27	134.73	2051.000	2051.013	0.0397	18943.00
28	154.17	2051.000	2051.013	0.0397	18943.00
29	173.61	2051.000	2051.013	0.0397	18943.00
30	193.05	2051.000	2051.013	0.0397	18943.00
31	212.49	2051.000	2051.013	0.0397	18943.00
32	231.93	2051.000	2051.013	0.0397	18943.00
33	251.37	2051.000	2051.013	0.0397	18943.00

34	270.81	2051.000	2051.013	0.0397	18943.00
35	290.25	2051.000	2051.013	0.0397	18943.00
36	324.97	2051.000	2051.013	0.0397	18943.00
37	374.97	2051.000	2051.013	0.0397	18943.00
38	424.97	2051.000	2051.013	0.0397	18943.00
39	474.97	2051.000	2051.013	0.0397	18943.00
40	549.97	2051.000	2051.013	0.0397	18943.00
41	649.97	2051.000	2051.013	0.0397	18943.00

**** File: MG-FN.SCP ****

mg-FN

41	Depth	Vsmax	Vs	Damping	G
1	1.25	1500.000	1500.045	0.0090	6988.00
2	3.75	1500.000	1493.915	0.0098	6931.00
3	6.25	528.000	430.758	0.0430	461.00
4	8.75	528.000	406.728	0.0504	411.00
5	11.00	727.000	628.373	0.0345	981.00
6	13.50	854.000	788.327	0.0210	1930.00
7	16.50	854.000	777.428	0.0232	1877.00
8	20.00	871.000	771.150	0.0278	1736.00
9	24.00	871.000	753.399	0.0315	1657.00
10	27.50	1022.000	829.940	0.0588	2460.00
11	30.50	1022.000	814.445	0.0634	2369.00
12	33.50	1022.000	799.175	0.0678	2281.00
13	37.50	1190.000	978.713	0.0556	3421.00
14	42.50	1190.000	953.792	0.0620	3249.00
15	47.50	1190.000	931.966	0.0675	3102.00
16	52.50	1800.000	1733.977	0.0149	11205.00
17	57.50	1800.000	1727.154	0.0159	11117.00
18	62.50	1800.000	1721.240	0.0167	11041.00
19	67.50	1800.000	1716.323	0.0174	10978.00
20	72.50	1800.000	1712.096	0.0180	10924.00
21	77.50	1800.000	1708.095	0.0186	10873.00
22	82.50	1800.000	1704.006	0.0191	10821.00
23	87.50	1800.000	1699.749	0.0197	10767.00
24	95.83	2900.000	2899.987	0.0470	35259.00
25	107.50	2900.000	2899.987	0.0470	35259.00
26	119.17	2900.000	2899.987	0.0470	35259.00
27	134.73	2900.000	2899.996	0.0470	37871.00
28	154.17	2900.000	2899.996	0.0470	37871.00
29	173.61	2900.000	2899.996	0.0470	37871.00
30	193.05	2900.000	2899.996	0.0470	37871.00
31	212.49	2900.000	2899.996	0.0470	37871.00
32	231.93	2900.000	2899.996	0.0470	37871.00
33	251.37	2900.000	2899.996	0.0470	37871.00
34	270.81	2900.000	2899.996	0.0470	37871.00
35	290.25	2900.000	2899.996	0.0470	37871.00

36	324.97	4000.000	4000.009	0.0340	72050.00
37	374.97	4000.000	4000.009	0.0340	72050.00
38	424.97	4000.000	4000.009	0.0340	72050.00
39	474.97	4000.000	4000.009	0.0340	72050.00
40	549.97	5000.000	5000.008	0.0272	112578.00
41	649.97	5000.000	5000.008	0.0272	112578.00

**** File: MG-FP.SCP ****

mg-FP

41	Depth	Vsmax	Vs	Damping	G
1	1.25	1500.000	1500.045	0.0090	6988.00
2	3.75	1500.000	1494.023	0.0098	6932.00
3	6.25	528.000	427.475	0.0441	454.00
4	8.75	528.000	396.201	0.0536	390.00
5	11.00	727.000	616.409	0.0374	944.00
6	13.50	854.000	782.176	0.0222	1900.00
7	16.50	854.000	767.633	0.0253	1830.00
8	20.00	871.000	763.337	0.0295	1701.00
9	24.00	871.000	753.172	0.0316	1656.00
10	27.50	1022.000	842.995	0.0548	2538.00
11	30.50	1022.000	824.184	0.0605	2426.00
12	33.50	1022.000	800.924	0.0673	2291.00
13	37.50	1190.000	978.857	0.0555	3422.00
14	42.50	1190.000	957.455	0.0611	3274.00
15	47.50	1190.000	936.312	0.0664	3131.00
16	52.50	1800.000	1735.910	0.0147	11230.00
17	57.50	1800.000	1732.970	0.0151	11192.00
18	62.50	1800.000	1727.465	0.0158	11121.00
19	67.50	1800.000	1720.383	0.0169	11030.00
20	72.50	1800.000	1714.446	0.0177	10954.00
21	77.50	1800.000	1708.488	0.0185	10878.00
22	82.50	1800.000	1702.036	0.0194	10796.00
23	87.50	1800.000	1696.035	0.0202	10720.00
24	95.83	2900.000	2899.987	0.0470	35259.00
25	107.50	2900.000	2899.987	0.0470	35259.00
26	119.17	2900.000	2899.987	0.0470	35259.00
27	134.73	2900.000	2899.996	0.0470	37871.00
28	154.17	2900.000	2899.996	0.0470	37871.00
29	173.61	2900.000	2899.996	0.0470	37871.00
30	193.05	2900.000	2899.996	0.0470	37871.00
31	212.49	2900.000	2899.996	0.0470	37871.00
32	231.93	2900.000	2899.996	0.0470	37871.00
33	251.37	2900.000	2899.996	0.0470	37871.00
34	270.81	2900.000	2899.996	0.0470	37871.00
35	290.25	2900.000	2899.996	0.0470	37871.00
36	324.97	4000.000	4000.009	0.0340	72050.00
37	374.97	4000.000	4000.009	0.0340	72050.00

38	424.97	4000.000	4000.009	0.0340	72050.00
39	474.97	4000.000	4000.009	0.0340	72050.00
40	549.97	5000.000	5000.008	0.0272	112578.00
41	649.97	5000.000	5000.008	0.0272	112578.00

**** File: MV-FN.SCP ****

MV-FN

41	Depth	Vsmax	Vs	Damping	G
1	1.25	1500.000	1500.045	0.0090	6988.00
2	3.75	1500.000	1493.915	0.0098	6931.00
3	6.25	528.000	430.758	0.0430	461.00
4	8.75	528.000	406.728	0.0504	411.00
5	11.00	727.000	628.373	0.0345	981.00
6	13.50	854.000	788.327	0.0210	1930.00
7	16.50	854.000	777.428	0.0232	1877.00
8	20.00	871.000	771.150	0.0278	1736.00
9	24.00	871.000	753.399	0.0315	1657.00
10	27.50	1022.000	829.940	0.0588	2460.00
11	30.50	1022.000	814.445	0.0634	2369.00
12	33.50	1022.000	799.175	0.0678	2281.00
13	37.50	1190.000	978.713	0.0556	3421.00
14	42.50	1190.000	953.792	0.0620	3249.00
15	47.50	1190.000	931.966	0.0675	3102.00
16	52.50	1800.000	1733.977	0.0149	11205.00
17	57.50	1800.000	1727.154	0.0159	11117.00
18	62.50	1800.000	1721.240	0.0167	11041.00
19	67.50	1800.000	1716.323	0.0174	10978.00
20	72.50	1800.000	1712.096	0.0180	10924.00
21	77.50	1800.000	1708.095	0.0186	10873.00
22	82.50	1800.000	1704.006	0.0191	10821.00
23	87.50	1800.000	1699.749	0.0197	10767.00
24	95.83	2900.000	2899.987	0.0394	35259.00
25	107.50	2900.000	2899.987	0.0394	35259.00
26	119.17	2900.000	2899.987	0.0394	35259.00
27	134.73	2900.000	2899.996	0.0394	37871.00
28	154.17	2900.000	2899.996	0.0394	37871.00
29	173.61	2900.000	2899.996	0.0394	37871.00
30	193.05	2900.000	2899.996	0.0394	37871.00
31	212.49	2900.000	2899.996	0.0394	37871.00
32	231.93	2900.000	2899.996	0.0394	37871.00
33	251.37	2900.000	2899.996	0.0394	37871.00
34	270.81	2900.000	2899.996	0.0394	37871.00
35	290.25	2900.000	2899.996	0.0394	37871.00
36	324.97	2900.000	2899.996	0.0394	37871.00
37	374.97	2900.000	2899.996	0.0394	37871.00
38	424.97	2900.000	2899.996	0.0394	37871.00
39	474.97	2900.000	2899.996	0.0394	37871.00

40	549.97	2900.000	2899.996	0.0394	37871.00
41	649.97	2900.000	2899.996	0.0394	37871.00

**** File: MV-FP.SCP ****

MV-FP

41	Depth	Vsmax	Vs	Damping	G
1	1.25	1500.000	1500.045	0.0090	6988.00
2	3.75	1500.000	1494.023	0.0098	6932.00
3	6.25	528.000	427.475	0.0441	454.00
4	8.75	528.000	396.201	0.0536	390.00
5	11.00	727.000	616.409	0.0374	944.00
6	13.50	854.000	782.176	0.0222	1900.00
7	16.50	854.000	767.633	0.0253	1830.00
8	20.00	871.000	763.337	0.0295	1701.00
9	24.00	871.000	753.172	0.0316	1656.00
10	27.50	1022.000	842.995	0.0548	2538.00
11	30.50	1022.000	824.184	0.0605	2426.00
12	33.50	1022.000	800.924	0.0673	2291.00
13	37.50	1190.000	978.857	0.0555	3422.00
14	42.50	1190.000	957.455	0.0611	3274.00
15	47.50	1190.000	936.312	0.0664	3131.00
16	52.50	1800.000	1735.910	0.0147	11230.00
17	57.50	1800.000	1732.970	0.0151	11192.00
18	62.50	1800.000	1727.465	0.0158	11121.00
19	67.50	1800.000	1720.383	0.0169	11030.00
20	72.50	1800.000	1714.446	0.0177	10954.00
21	77.50	1800.000	1708.488	0.0185	10878.00
22	82.50	1800.000	1702.036	0.0194	10796.00
23	87.50	1800.000	1696.035	0.0202	10720.00
24	95.83	2900.000	2899.987	0.0394	35259.00
25	107.50	2900.000	2899.987	0.0394	35259.00
26	119.17	2900.000	2899.987	0.0394	35259.00
27	134.73	2900.000	2899.996	0.0394	37871.00
28	154.17	2900.000	2899.996	0.0394	37871.00
29	173.61	2900.000	2899.996	0.0394	37871.00
30	193.05	2900.000	2899.996	0.0394	37871.00
31	212.49	2900.000	2899.996	0.0394	37871.00
32	231.93	2900.000	2899.996	0.0394	37871.00
33	251.37	2900.000	2899.996	0.0394	37871.00
34	270.81	2900.000	2899.996	0.0394	37871.00
35	290.25	2900.000	2899.996	0.0394	37871.00
36	324.97	2900.000	2899.996	0.0394	37871.00
37	374.97	2900.000	2899.996	0.0394	37871.00
38	424.97	2900.000	2899.996	0.0394	37871.00
39	474.97	2900.000	2899.996	0.0394	37871.00
40	549.97	2900.000	2899.996	0.0394	37871.00
41	649.97	2900.000	2899.996	0.0394	37871.00

```
 **** File: PSTAT.FOR                                          ****
      program PSTAT2
      character ifile*40,ofile*40,title*70
      real mlg(100),md(100),dmp(100),uw(100)
C
99    print*,' enter ifile: '
      read(5,'(a)') ifile
      IF(ifile.eq.'q'.or.ifile.eq.'Q') STOP
      open(7,file=ifile)
      read(7,'(a)') ofile
      open(9,file=ofile)
      read(7,'(a)') title
      write(9,'(a)') title
      DO 10 i=1,100
        mlg(i)=0.0
        md(i)=0.0
10    CONTINUE
      read(7,*) nout
      DO 30 iout=1,nout
        read(7,'(a)') ifile
        open(8,file='..\siteresp\'//ifile(1:5)//'.pun')
        read(8,*) k,nl
        d=0.0
        DO 20 i=1,nl-1
          read(8,*) k,j,j,h,g,damp,uw(i),gmax
          mlg(i)=mlg(i)+log(g)
          md(i)=md(i)+damp
          dmp(i)=d+h/2.0
          d=d+h
20      CONTINUE
        close(8)
        print'('' completed '',a8)',ifile
30    CONTINUE
      close(7)
      write(9,'(i5,t12,''H      MPD      Vs          UW
Damping'',
     , ''      G'')') nl-1
      db=0.0
      DO 40 i=1,nl-1
        h=2.0*(dmp(i)-db)
        db=db+h
        g=exp(mlg(i)/real(nout))
        damp=md(i)/real(nout)
        v=sqrt(g*32.2/uw(i))
        write(9,'(i5,2f8.2,f10.3,2f10.4,f10.2)') i,h,dmp(i),v,
     ,   uw(i),damp,g
```

```
40     CONTINUE
       close(9)
       go to 99
       END

 **** File: STAT-HVS.IN                                          ****
stat-hvs.out
Statistics High Vs
2
hV-FN
hV-FP
q

 **** File: STAT-HVS.OUT                                         ****
Statistics High Vs
   41       H        MPD        Vs          UW       Damping        G
    1     2.50      1.25    2121.005      0.1000     0.0090    13971.00
    2     2.50      3.75    2118.916      0.1000     0.0092    13943.50
    3     2.50      6.25     572.921      0.0800     0.0306      815.50
    4     2.50      8.75     542.786      0.0800     0.0390      731.97
    5     2.00     11.00     807.237      0.0800     0.0269     1618.96
    6     3.00     13.50     990.432      0.1000     0.0169     3046.44
    7     3.00     16.50     975.362      0.1000     0.0194     2954.44
    8     4.00     20.00     979.871      0.0940     0.0220     2802.91
    9     4.00     24.00     966.037      0.0940     0.0242     2724.33
   10     3.00     27.50    1065.836      0.1150     0.0482     4057.16
   11     3.00     30.50    1051.714      0.1150     0.0509     3950.37
   12     3.00     33.50    1040.421      0.1150     0.0531     3865.98
   13     5.00     37.50    1509.135      0.1150     0.0373     8133.89
   14     5.00     42.50    1488.251      0.1150     0.0405     7910.33
   15     5.00     47.50    1467.515      0.1150     0.0435     7691.43
   16     5.00     52.50    2496.595      0.1200     0.0109    23228.51
   17     5.00     57.50    2492.479      0.1200     0.0112    23151.99
   18     5.00     62.50    2488.708      0.1200     0.0115    23082.00
   19     5.00     67.50    2485.255      0.1200     0.0117    23017.98
   20     5.00     72.50    2482.042      0.1200     0.0120    22958.51
   21     5.00     77.50    2475.383      0.1200     0.0126    22835.48
   22     5.00     82.50    2468.681      0.1200     0.0133    22711.99
   23     5.00     87.50    2462.777      0.1200     0.0139    22603.50
   24    11.67     95.83    4100.997      0.1350     0.0428    70510.98
   25    11.67    107.50    4100.997      0.1350     0.0428    70510.98
   26    11.67    119.17    4100.997      0.1350     0.0428    70510.98
   27    19.44    134.73    4100.997      0.1450     0.0428    75734.00
   28    19.44    154.17    4100.997      0.1450     0.0428    75734.00
   29    19.44    173.61    4100.997      0.1450     0.0428    75734.00
   30    19.44    193.05    4100.997      0.1450     0.0428    75734.00
   31    19.44    212.49    4100.997      0.1450     0.0428    75734.00
```

32	19.44	231.93	4100.997	0.1450	0.0428	75734.00
33	19.44	251.37	4100.997	0.1450	0.0428	75734.00
34	19.44	270.81	4100.997	0.1450	0.0428	75734.00
35	19.44	290.25	4100.997	0.1450	0.0428	75734.00
36	50.00	324.97	5657.003	0.1450	0.0310	144106.97
37	50.00	374.97	5657.003	0.1450	0.0310	144106.97
38	50.00	424.97	5657.003	0.1450	0.0310	144106.97
39	50.00	474.97	5657.003	0.1450	0.0310	144106.97
40	100.00	549.97	6398.000	0.1450	0.0253	184331.97
41	100.00	649.97	6398.000	0.1450	0.0253	184331.97

**** File: STAT-LVS.IN ****

```
stat-lvs.out
Statistics Low Vs
2
LV-FN
LV-FP
q
```

**** File: STAT-LVS.OUT ****

Statistics Low Vs

41	H	MPD	Vs	UW	Damping	G
1	2.50	1.25	1058.641	0.1000	0.0094	3480.50
2	2.50	3.75	1046.789	0.1000	0.0121	3403.00
3	2.50	6.25	311.735	0.0800	0.0591	241.44
4	2.50	8.75	284.555	0.0800	0.0722	201.17
5	2.00	11.00	468.261	0.0800	0.0476	544.77
6	3.00	13.50	617.434	0.1000	0.0277	1183.93
7	3.00	16.50	602.130	0.1000	0.0317	1125.96
8	4.00	20.00	598.426	0.0940	0.0359	1045.43
9	4.00	24.00	587.452	0.0940	0.0386	1007.43
10	3.00	27.50	629.077	0.1150	0.0758	1413.35
11	3.00	30.50	612.727	0.1150	0.0813	1340.84
12	3.00	33.50	599.974	0.1150	0.0855	1285.60
13	5.00	37.50	588.001	0.1150	0.0909	1234.80
14	5.00	42.50	562.227	0.1150	0.0988	1128.93
15	5.00	47.50	545.363	0.1150	0.1049	1062.22
16	5.00	52.50	1194.668	0.1200	0.0212	5318.88
17	5.00	57.50	1191.395	0.1200	0.0218	5289.77
18	5.00	62.50	1189.920	0.1200	0.0221	5276.68
19	5.00	67.50	1190.423	0.1200	0.0220	5281.14
20	5.00	72.50	1191.838	0.1200	0.0217	5293.71
21	5.00	77.50	1191.750	0.1200	0.0218	5292.92
22	5.00	82.50	1191.814	0.1200	0.0217	5293.50
23	5.00	87.50	1189.898	0.1200	0.0221	5276.48
24	11.67	95.83	2050.979	0.1350	0.0397	17636.00
25	11.67	107.50	2050.979	0.1350	0.0397	17636.00

26	11.67	119.17	2050.979	0.1350	0.0397	17636.00
27	19.44	134.73	2051.013	0.1450	0.0397	18943.00
28	19.44	154.17	2051.013	0.1450	0.0397	18943.00
29	19.44	173.61	2051.013	0.1450	0.0397	18943.00
30	19.44	193.05	2051.013	0.1450	0.0397	18943.00
31	19.44	212.49	2051.013	0.1450	0.0397	18943.00
32	19.44	231.93	2051.013	0.1450	0.0397	18943.00
33	19.44	251.37	2051.013	0.1450	0.0397	18943.00
34	19.44	270.81	2051.013	0.1450	0.0397	18943.00
35	19.44	290.25	2051.013	0.1450	0.0397	18943.00
36	50.00	324.97	2051.013	0.1450	0.0397	18943.00
37	50.00	374.97	2051.013	0.1450	0.0397	18943.00
38	50.00	424.97	2051.013	0.1450	0.0397	18943.00
39	50.00	474.97	2051.013	0.1450	0.0397	18943.00
40	100.00	549.97	2051.013	0.1450	0.0397	18943.00
41	100.00	649.97	2051.013	0.1450	0.0397	18943.00

**** File: STAT-MVS.IN ****

```
stat-mvs.out
Statistics Mean Vs
4
mV-FN
mV-FP
mg-FN
mg-FP
q
```

**** File: STAT-MVS.OUT ****

Statistics Mean Vs

41	H	MPD	Vs	UW	Damping	G
1	2.50	1.25	1500.045	0.1000	0.0090	6988.00
2	2.50	3.75	1493.969	0.1000	0.0098	6931.50
3	2.50	6.25	429.113	0.0800	0.0435	457.49
4	2.50	8.75	401.430	0.0800	0.0520	400.36
5	2.00	11.00	622.362	0.0800	0.0360	962.32
6	3.00	13.50	785.246	0.1000	0.0216	1914.94
7	3.00	16.50	772.515	0.1000	0.0242	1853.35
8	4.00	20.00	767.233	0.0940	0.0286	1718.41
9	4.00	24.00	753.286	0.0940	0.0315	1656.50
10	3.00	27.50	836.442	0.1150	0.0568	2498.70
11	3.00	30.50	819.300	0.1150	0.0619	2397.33
12	3.00	33.50	800.049	0.1150	0.0676	2286.00
13	5.00	37.50	978.785	0.1150	0.0555	3421.50
14	5.00	42.50	955.622	0.1150	0.0615	3261.48
15	5.00	47.50	934.136	0.1150	0.0669	3116.47
16	5.00	52.50	1734.943	0.1200	0.0148	11217.49
17	5.00	57.50	1730.060	0.1200	0.0155	11154.44

18	5.00	62.50	1724.350	0.1200	0.0163	11080.93
19	5.00	67.50	1718.351	0.1200	0.0171	11003.97
20	5.00	72.50	1713.271	0.1200	0.0178	10938.99
21	5.00	77.50	1708.291	0.1200	0.0185	10875.50
22	5.00	82.50	1703.020	0.1200	0.0193	10808.49
23	5.00	87.50	1697.891	0.1200	0.0200	10743.48
24	11.67	95.83	2899.987	0.1350	0.0432	35259.00
25	11.67	107.50	2899.987	0.1350	0.0432	35259.00
26	11.67	119.17	2899.987	0.1350	0.0432	35259.00
27	19.44	134.73	2899.995	0.1450	0.0432	37870.99
28	19.44	154.17	2899.995	0.1450	0.0432	37870.99
29	19.44	173.61	2899.995	0.1450	0.0432	37870.99
30	19.44	193.05	2899.995	0.1450	0.0432	37870.99
31	19.44	212.49	2899.995	0.1450	0.0432	37870.99
32	19.44	231.93	2899.995	0.1450	0.0432	37870.99
33	19.44	251.37	2899.995	0.1450	0.0432	37870.99
34	19.44	270.81	2899.995	0.1450	0.0432	37870.99
35	19.44	290.25	2899.995	0.1450	0.0432	37870.99
36	50.00	324.97	3405.878	0.1450	0.0367	52236.05
37	50.00	374.97	3405.878	0.1450	0.0367	52236.05
38	50.00	424.97	3405.878	0.1450	0.0367	52236.05
39	50.00	474.97	3405.878	0.1450	0.0367	52236.05
40	100.00	549.97	3807.886	0.1450	0.0333	65295.01
41	100.00	649.97	3807.886	0.1450	0.0333	65295.01

Calculation 05996.02-G(PO18)-2, Rev. 01
Attachment D
Development of Dynamic Soil Properties

This attachment contains a printout of EXCEL spreadsheet SV-SSI-FEB01.XLS in which the results of the site response analyses are used to compute the dynamic soil properties for the SASSI model and the spring-dashpot-lumped mass model. The spreadsheet is located on the accompanying disk in directory \RESULTS. The spreadsheet contains five sheets.

SHEETS 1, 2, and 3

Sheets 1, 2, and 3 contain the results of averaging the SHAKE output files for the high range, best estimate, and low range velocity models, respectively. Columns A through G contain the average results of the SHAKE analyses as calculated in Attachment C. Column H contains the low-strain compression wave velocities from Tables 1, 5a, and 5b. The weighted average velocities, unit weight, and damping within the top 30 feet are computed on these sheets in cells J1:O23. Column J computes the depth-weighting factor using the equation

$$fac(d) = (30 + ped - d)/30$$

where d is the depth of the layer midpoint from Column C and *ped* is a factor to account for the storage pad embedment depth. On average, the pads are to be embedded approximately 3 feet, leaving 2 feet of soil cement beneath them. Thus for the best estimate case, *ped* was set to 3 feet. For the high range profile, it was assumed that the soil cement would have a maximum thickness of about 7 feet, resulting in 4 feet of soil cement beneath the pad. To account for this effect, *ped* was set to 1 foot, so that 4 feet of the soil cement properties would be included in the depth-averaged results, maximizing the soil stiffness. For the low range profile, it was assumed that the soil cement would have the minimum thickness beneath the pad of 1 foot. To account for this effect, *ped* was set to 4 foot, so that 1 feet of the soil cement properties would be included in the depth-averaged results, minimizing the soil stiffness.

Column K computes the depth factor, Equation **(D-1)** times the layer thickness from Column B (note that the layer thickness for the first two layers in Columns B and C have been adjusted from the results in Attachment C to account for the variability in soil cement thickness discussed above). These are the weighting factors for the properties in each layer. Columns L, M, N, and O list the layer values for shear modulus, damping, unit weight, and compression wave velocity from columns G, F, E, and H multiplied by the weighting factors in column K. The compression wave velocities are squared to approximate bulk modulus. Cells L21:O21 list the sums of the values in the corresponding columns divided by the sum of the weighting factors in cell K21. These are the depth-weighted average values for each parameter. Cell M23 computes the equivalent shear wave velocity from the average shear modulus G in Cell M21 and the average unit weight γ in cell N21 using the equation:

$$V_S = \sqrt{\frac{G}{\gamma/32.2\text{ft/sec}^2}}$$

Cell O23 computes the average compression wave velocity as the square root of the depth-weighted average of the layer velocities squared.

SHEET 4

Sheet four contains the simplified SASSI profiles derived from the SHAKE output files. Column A indicates the SHAKE analysis layers on sheets 1, 2, or 3 that are combined to form a single layer in the SASSI model profile. Column B takes the depth to the lop of each layer group from bottom depth of the higher layer in Column C, and column C sums the layer thicknesses from the appropriate results on Sheets 1, 2, or 3, and adds them to the top depth to get the bottom depth. Column D computes the unit weight as the average values for the appropriate layers on sheets 1, 2, or 3. Columns E and F compute the wave velocities as the harmonic mean of the values for the appropriate layers on sheets 1, 2, or 3. Column G computes the Poisson's ratio using the relationship:

$$\mu = \frac{\left(V_P/V_S\right)^2 - 2}{2\left[\left(V_P/V_S\right)^2 - 1\right]}$$

Sheet 5

Sheet 5 contains the calculation of the spring, dashpot, and lumped mass parameters following the procedure used in calculation 05996.01 G(PO5)-1. A copy of the previous calculation is attached to provide the basis for the calculations in the spreadsheet. The values in cells B5:D12 are taken from cells L21:O23 on sheets 1, 2, or 3. The values in cells A18:D37 are computed using Equations **(4)**, **(5)**, and **(6)**. Interpolation of the required constants is performed in cells A39:D53 using values taken from the tables attached to calculation 05996.01 G(PO5)-1.

Subject SKULL VALLEY NSF

By Chin Man Mak Checked By C.C. Chin

Date 2/26/97 Date 2/26/97

ESTIMATION OF DYNAMIC PARAMETERS

1. Vertical d.o.f

Analysis is based on equations published by Newmark() and Rosenblueth (1971). Copies of the equations are attached on Page 10/11 in this section 1.5

$h = 0.27\sqrt{A}$

$A = 30 \times 64 = 1920\ ft^2$

$h = 0.27\sqrt{1920} = 11.83$

$M = Ah\rho$

$m = \frac{M}{A} = h\rho = 81 \times \frac{11.83}{32.2}$ $psf/ft/s^2$

$= 30\ \frac{lb\text{-}sec^2}{ft^3}$ or $0.03\ kcf\text{-}sec^2$. *

$K_v = \frac{E\sqrt{A}\,C_s}{1-\nu^2}$

$C_s = 1.1$ for $\frac{L}{B} = 2.13$

$\therefore k_v = \frac{K_v}{A} = \frac{E}{\sqrt{A}}\frac{C_s}{1-\nu^2} = \frac{1915 \times 1.1}{\sqrt{1920}\,(1-0.433^2)} = 59\ kcf.$ *

$C = 5.42\sqrt{K_v \rho h^3}$

$c = \frac{C}{A} = \frac{5.42}{A}\sqrt{k_v A \rho h^3}$ *

$= \frac{5.42}{1920}\sqrt{59 \times 1920 \times \frac{0.081}{32.2} \times 11.83^3}$

$= 1.94\ kcf\text{-}sec.$

* Superseded by Table 2 on p. 9 of 17 in Att. D

Subject SKULL VALLEY NSF

By Chin Man Mok Checked By C. C. Chen

Date 2/26/97 Date 2/26/97

2. Horizontal dof

$h = 0.05\sqrt{A}$

$= 0.05\sqrt{1920} = 2.191$ ft.

$M = Ah\rho$

$m = \frac{M}{A} = h\rho = \frac{0.081 \times 2.191}{32.2} = 0.0055$ kcf-sec^2 *

or 5.51 pcf-sec^2

$K_h = \frac{E\sqrt{A}\,k_T}{1-\nu^2}$

$k_T = 0.75$ for $\nu = 0.433$

$\therefore k_h = \frac{K_h}{A} = \frac{1915 \times 0.75}{\sqrt{1920}\,(1-0.433^2)} = 40.3$ kcf

$C = 41.1\sqrt{K\rho h^3}$

$c = \frac{C}{A} = \frac{41.1}{A}\sqrt{k_h A \rho h^3}$ *

$= \frac{41.1}{1920}\sqrt{40.3 \times 1920 \times \frac{0.081}{32.2} \times 2.191^3}$

$= 0.969$ kcf-sec.

* Superseded by Table 2 on p. 9 of 17 in attachment D.

By Chin Man Moic Checked By C.C. CHIN

Date 2/26/97 Date 2/26/97

3. Rocking d.o.f.

$h = 0.25\sqrt{A}$

$= 0.35\sqrt{1920} = 15.34$ ft.

$M = Ah\rho$

$m = \frac{M}{A} = h\rho = \frac{0.081 \times 15.34}{32.2} = 0.0386$ kcf-sec^2

≈ 38.6 pcf-sec^2 *

$K_r = \frac{EI\,k_\phi}{\sqrt{A}(1-\nu^2)} = \frac{ELB^3 k_\phi}{12\sqrt{BL}(1-\nu^2)} = \frac{1915 \times 64 \times 30^3 \times 2.57}{12\sqrt{1920}(1-0.433^2)}$

≈ 19906560 kip-ft/rad

$(= 19906024)$

$k_\phi = 2.57$

$\text{Moment} = \int_{-\frac{B}{2}}^{\frac{B}{2}} k_r L x^2 \phi\, dx = \frac{k_r L \phi}{3}(x^3)\Big|_{-\frac{B}{2}}^{\frac{B}{2}}$

$= \frac{k_r L \phi}{3}\frac{2B^3}{8} = \frac{k_r LB^3}{12}\phi$ plus *

$\therefore k_r \frac{LB^3}{12} = \frac{ELB^3 \times 2.57}{12\sqrt{BL}(1-\nu^2)}$

$= \frac{2.57E}{\sqrt{BL}(1-\nu^2)} = \frac{1915 \times 2.57}{\sqrt{1920}(1-0.433^2)} = 138.24$ kcf. *

$C = 0.97\sqrt{K\rho h^5}$

$C = 0.97\sqrt{19906560 \times \frac{0.081}{32.2} \times 15.34^5}$

$= 200054.3$ k-sec-ft/rad

$c = \frac{C}{I} = \frac{200054.3 \times 12}{64 \times 30^3} = 1.39$ kcf-sec

↳ (ref. moment $= \int_{-\frac{B}{2}}^{\frac{B}{2}} c L x^2 \dot{\phi}\, dx = c \cdot I\dot{\phi}$ where $I = \frac{LB^3}{12}$)

* Superseded by Table 2 on p. 9 of 17 in Attachment D

velocity of Love waves lies between these two shear velocities and is a function of the frequency. Using primes to denote the stratum, the velocity of Love waves v_l can be found from

$$\mu\left(1 - \frac{v_l^2}{v_s^2}\right)^{1/2} - \mu'\left(\frac{v_l^2}{v_s'^2} - 1\right)^{1/2} \tan \kappa H\left(\frac{v_l^2}{v_s'^2} - 1\right)^{1/2} = 0 \qquad (3.57)$$

where $\kappa = \omega/v_l$. We see that as $\kappa \to 0$, or when we deal with long waves, $v_l \to v_s$, and as $\kappa \to \infty$, for short waves, $v_l \to v_s'$.

Solutions are available for Rayleigh, Love, and other types of waves under a variety of stratification conditions. In many such solutions the velocity of wave propagation is a function of the wave frequency. When this happens, unless we are dealing with sinusoidal, steady-state conditions, we find that the shape of a disturbance changes as it travels along the medium in question. Sharp disturbances become trains of waves, each train containing oscillations of essentially equal frequency. Further, the velocity of a group of waves under these conditions differs from the velocity of an individual wave. This type of dispersion does not necessarily combine in additive manner with the dispersion due to internal damping[5] and accounts partly for the increase in duration of earthquake motions with focal distance.

3.14 *Group Velocity*

We have seen that in viscoelastic materials, wave velocities are functions of the frequency of the waves. Even in a perfectly elastic solid, Love waves, among others, travel with a velocity that depends on the frequency and hence, ordinarily, on wavelength. The phenomenon, known as dispersion, gives rise to reinforcement and interference of waves having nearly the same velocities. This causes the appearance of clusters of waves of essentially equal wavelengths. The location of these clusters in space moves with a velocity, called *group velocity*, that differs from the velocities of the waves.

Some idea of the effect of dispersion in this context may be gleaned from the study of the combination of two one-dimensional waves of the same amplitude but slightly different frequencies and velocities. Let us consider, then, the combined wave

$$x = a \sin \kappa(X - vt) + \sin (\kappa + \Delta\kappa)[X - (v + \Delta v)t]$$

where $\kappa v = \omega$, the circular frequency. This we can write in the form

$$x = 2a \sin\left(\frac{2\kappa + \Delta\kappa}{2} X - \frac{2\omega + \Delta\omega}{2} t\right) \cos\left(\frac{\Delta\kappa}{2} X - \frac{\Delta\omega}{2} t\right)$$

The sine function in this expression represents a wave with a frequency and a length equal to the averages of the original waves. The cosine function is a

[5] This remark is proved for waves traveling along a linearly damped cylindrical rod (Hunter, 1960).

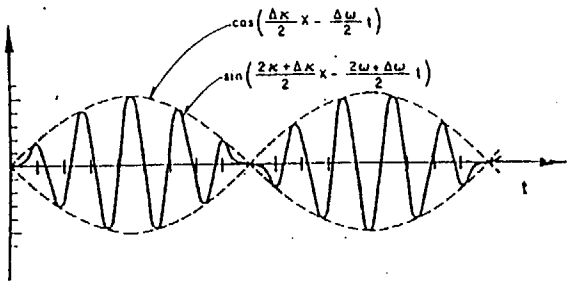

Figure 3.15. Combined wave.

very long wave that envelops the motions corresponding to the first factor, as shown by the dashed line in Fig. 3.15. This envelope moves in the direction of the waves with a velocity equal to $(\Delta\omega/2)/(\Delta\kappa/2)$ or $\Delta\omega/\Delta\kappa$. In the limit, when there is a continuous spectrum of wave frequencies, we may write for the group velocity

$$v_g = \frac{d\omega}{d\kappa} = v + \kappa \frac{dv}{d\kappa}$$

or, introducing the symbol $\Lambda = 2\pi/\kappa$ for wavelength,

$$v_g = v - \Lambda \frac{dv}{d\Lambda}$$

Only when v does not depend on the wavelength does the group velocity coincide with the wave velocity, and no clusters develop.

It can be shown that, when dispersed waves undergo reflection and refraction at an interface, the angles that the corresponding paths form with the interface are functions of the individual wave velocities as for nondispersed waves, while the velocities of transmission of energy follow the law of the group velocities.[6]

3.15 *Soil-Foundation Interaction*

The same contact stresses between soil and foundation that may be held responsible for earthquake effects on structures also cause deformations in the soil, especially in the vicinity of every structural foundation. The phenomenon constitutes one form of dynamic soil-structure interaction. It is also known in the literature as "energy feedback to the ground," "foundation yielding," and "foundation compliance." It has received considerable attention with a

[6] A more thorough explanation of the matter of group velocity, based on a Fourier integral representation of dispersed waves, is found in Bullen (1953), pp. 58-66, 93-95, and 107-108.

view to application both to seismic problems and to the study of vibrations of machine foundations. Yet no entirely satisfactory solution is available for cases other than circular foundations, even under the assumption of perfectly elastic soil behavior.

A rigid body resting on soil has six degrees of freedom: for example, an up-and-down motion, torsion about a vertical axis, two degrees in rocking, and two degrees of horizontal translation. Suppose that the responses in all modes were known for a massless body subjected either to an instantaneous pulse or to a harmonic, steady-state disturbance along each component. Then appropriate use of either convolution integrals, Laplace (Sandi, 1960), or Fourier (Monge and Rosenberg, 1964) transforms would permit calculation of the responses of any structure of linear behavior resting on a rigid foundation supported in turn by a soil of linear behavior.

Most of the solutions available concern a rigid plate, either circular or rectangular, resting on an isotropic, homogeneous, linearly elastic halfspace, under steady-state vibration and have been obtained assuming that the distribution of contact stresses is the same as under static loading, independently of the frequency of vibration. Actually the distribution of contact stresses depends on the frequency. Lysmer (1965) has succeeded in solving the problem of a rigid plate under steady-state vertical oscillation taking into account the proper distribution of contact stresses. To this end he has taken the solution for a flexible plate that applies a vibratory uniform pressure on the ground (Sung, 1953). By subtracting the effects of a smaller concentric plate he has obtained the responses to a ring that applies uniformly distributed vibratory pressures; by replacing the rigid plate with a set of 20 concentric rings and equating their vertical displacements at every instant he has obtained a numerical solution.

Using a somewhat similar approach, Elorduy (1967) has developed a method applicable to the vibrations of a rigid plate of arbitrary shape resting on an elastic halfspace. He makes use of the known solution for the free-field effects of a vertical (Pekeris, 1955) or a horizontal (Chao, 1960) concentrated pulse applied at a point of the free surface of the elastic halfspace. He then solves two sets of simultaneous equations to satisfy the boundary condition at the base of the plate. Elorduy's application to rectangular plates is beset with the simplifying assumption that the phase lag between force and displacement is the same at all points of contact between the plate and the halfspace. Nevertheless, his solution for the oscillations of a square plate agrees well with the solution due to Kobori (1962), which was obtained by a different procedure.

Elorduy's approach, after removing the simplifying assumption and incorporating an explicit consideration of coupling between vertical and horizontal displacements, can give results as accurate as desired for plates of arbitrary shape. However, as in Lysmer's treatment, the method gives rise to sets of very ill-conditioned equations in some range of the variables. This difficulty was obviated by Robertson (1966) through a transformation of the integral equation from which these sets of equations are derived. He was thus able to arrive at the exact solution for the vertical oscillations of a rigid circular plate on an

elastic halfspace. His method can be adapted to the analysis of the rocking, torsional, and translational oscillations of rigid circular plates and to the vibrations of infinitely long rigid band plates. However, it is not applicable in any form to finite square or rectangular plates.

Tajimi (1969) has been able to solve the problem of rocking and translational oscillations of a rigid, circular, cylindrical pier embedded in an elastic stratum when both the stratum and the pier rest on an elastic halfspace.

A comparison of the exact solution for a rigid circular plate on an elastic halfspace with the solution based on the same distribution as under static conditions shows that the latter is satisfactory up to and somewhat beyond the resonant frequency, but not much beyond. For very high frequencies the solution obtained by assuming a static pressure distribution even predicts an equivalent negative damping, which makes it unacceptable. In the study of the vibration of machine foundations, such high frequencies are often of interest; in problems of earthquake-resistant design this is not necessarily the case. Since many problems have been solved only under the simplifying assumption in question, we shall retain it in the presentation of some solutions.

Our lack of concern with very high frequencies stems from the following consideration. It is well known that soil-foundation interaction may affect the fundamental mode and period of vibration appreciably but that its effects are small on the second mode and period and negligible on the higher harmonics. As an illustration consider a flexural two-mass system. Let the flexibilities be concentrated at the base and at the first mass, the masses be equal to each other, the flexibilities also be equal to each other, and the masses be equally spaced. If we introduce a spring at the foundation to simulate rocking, with the same flexibility as the spring elements at the joints, the fundamental period will increase 36 percent while the second natural period increases 8 percent. Indeed, it follows from the orthogonality of natural modes that if the fundamental mode of vibration of a building is a straight line, there can be no base overturning moment in any of the higher modes (Bielak, 1969) and hence these are not affected by the possibility of interaction with rocking motion of the base. Since the fundamental mode is almost always approximately straight, interaction can rarely have an important effect on the higher modes and periods. [This conclusion is apparently contradicted in papers by Parmelee (1967 and 1969), but the corresponding solutions fail to take into account vibration in other natural modes when analyzing the response in any given mode.]

Now, the fundamental period of the soil-structure system is not smaller than that of an infinitely rigid structure resting on the same soil and having the same masses and geometry as the structure in question. Because the second natural period in buildings is of the order of one half to one third of the fundamental (except when soil-foundation interaction is such as to make the fundamental mode much more significant than the harmonics), we are not interested in an accurate evaluation of the phenomenon of foundation compliance much beyond a frequency equal to about twice the first resonant frequency associated with a rigid block resting on soil, and usually not much beyond the first resonant frequency.

In principle, once the solutions were available for instantaneous pulses or steady-state disturbances, integral transforms would solve every problem of interest. The approach would be impractical, however, and would preclude analyzing nonlinear structures. A more attractive even if only approximate treatment replaces the soil with a virtual mass fixed to the foundation, a massless spring, and a massless dashpot in parallel with the spring. The three parameters must be defined for every degree of freedom and may be so placed as to include correctly coupling between the various degrees. In this manner we have no difficulty in applying the standard methods of analysis for multidegree systems to a new system, whose degrees of freedom include those of the structure proper plus six of the foundation, and we may even deal with nonlinear structural behavior.

A rigorous treatment of this sort would require having two of the parameters in every degree of freedom vary with the frequency of vibration because we would have to adjust for two quantities at each frequency: the amplitude of response and its phase shift with respect to a harmonic excitation. If, as proposed, we take the parameters as independent of frequency, we must fulfill certain conditions. In a simple system, as we saw in Chapter 1, the response at low frequency is essentially sensitive to the spring constant. Hence, if our model is to cover a range of low frequencies, the spring stiffnesses must coincide with the values derived from static loading. (In a real soil this is to be interpreted as a rapid, quasistatic loading in which consolidation and creep are not given the opportunity to occur to an appreciable extent.) In the ranges of the resonant frequencies the dynamic magnifications of responses are sensitive only to the percentages of damping; these ranges will fix the dashpot constants. For high frequencies, only the masses are significant. Lysmer points out that, as the frequency of excitation tends to infinity, the wavelengths of the disturbances emanating from the foundation tend to zero; hence the virtual masses must also tend to zero, and if we wish our solution to hold for all possible frequencies, we must take the virtual mass in every natural mode as zero.

Reasoning along these lines and adjusting to the exact solution we mentioned earlier for the vertical oscillations of a circular plate, so as to minimize the error in the amplitude of the responses to a harmonic force applied at the center of the plate, Lysmer proposes the following parameters for this degree of freedom

$$K = \frac{4}{1-\nu}\mu r \tag{3.58}$$

$$C = \frac{0.85Kr}{v_s} \tag{3.59}$$

where K is the spring constant, ν and μ are Poisson's ratio and modulus of rigidity, r is the radius of the plate, C the dashpot constant, and v_s the velocity of shear waves in the soil ($\sqrt{\mu/\rho}$). The spring constant in Eq. 3.58 is that for static loading. The dashpot constant in Eq. 3.59 is chosen such that in the entire range of possible Poisson ratios, $0 \leq \nu \leq 0.5$ and forcing frequencies $0 \leq \omega \leq \infty$, the computed amplitude of the response does not differ from the exact

solution by more than about 30 percent; in the range of greatest interest, it differs by less than 20 percent. The phase change between the force and the response is automatically approximated also in a rough manner.

The model described is the simplest that replaces the soil with a small number of elements having parameters independent of the frequency and yet gives the correct order of magnitude of the responses. But the condition that the model be acceptable for very high frequencies causes a loss of accuracy in the lower frequency range, and this loss is unnecessary in the analysis of responses to earthquakes. By introducing a virtual mass of soil we have one additional parameter that permits a better adjustment over a limited range of frequencies. When we do this, the computed responses will be smaller than in the absence of the virtual mass if we retain the dashpot constant as given by Eq. 3.59. Hence we must compensate by adopting a smaller dashpot constant. The following constants (Nieto, Rosenblueth, and Rascón, 1965) give response amplitudes that check with the "exact" solution [which assumes the same contact stress distribution as under static loading (Sezawa, 1927a; Reissner, 1936; Arnold, Bycroft, and Warburton, 1955; Richart, 1962)] within a few percent at least up to forcing frequencies equal to twice that of resonance: K as in Eq. 3.58, the virtual mass equal to that of a cylindrical body of soil having the same base as the plate and a height h equal to 0.27 times the square root of the base area A (Fig. 3.16), and a dashpot constant

$$C = \frac{0.64Kr}{v_s}$$

The latter can be put in the more convenient form

$$C = \frac{1.35Kh}{v_s} \tag{3.60}$$

A comparison with the "exact" solution is shown in Fig. 3.17.

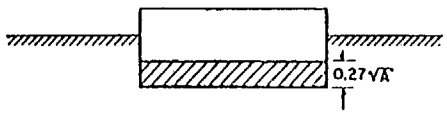

Figure 3.16. Virtual mass in vertical oscillations of circular plate.

Using a similar type of adjustment together with available information on spring constants and solutions for circular and rectangular rigid plates, Table 3.1 has been constructed (Nieto, Rosenblueth, and Rascón, 1965; Barkan, 1962). It is a partial list of stiffnesses, virtual masses, and dashpot constants for various degrees of freedom of plates of these shapes.

The positions of the springs and dashpots are important to reflect the proper coupling between various degrees of freedom. Owing to symmetry, in circular and rectangular plates with uniformly distributed mass, there is coupling only between the rocking and transverse-displacement degrees. In plates of other

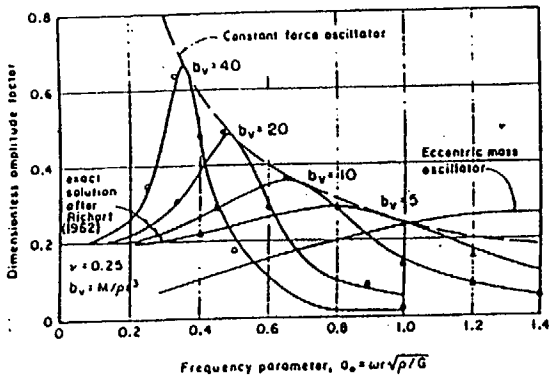

Figure 3.17. Comparison of responses of circular plates to vertical excitation.

TABLE 3.1. STIFFNESSES, VIRTUAL MASSES, AND DASHPOT CONSTANTS

Degree of freedom	Height of soil prism	Dashpot constant	Stiffness	
			Circular base	Rectangular base*
Vertical	$0.27\sqrt{A}$	$5.42\sqrt{K\rho h^3}$	$4\mu r/(1-\nu)$	$E\sqrt{A}\,c_z/(1-\nu^2)$
Horizontal	$0.05\sqrt{A}$	$41.1\sqrt{K\rho h^3}$	$5.8\kappa\mu r(1-\nu^2)/(2-\nu)^2$	$E\sqrt{A}\,k_x/(1-\nu^2)$
Rocking†	$0.35\sqrt{A}$	$0.97\sqrt{K\rho h^3}$	$2.7\mu r^3(\nu=0)$	$Elk_\phi/\sqrt{A}(1-\nu^2)$
Torsion	$0.25\sqrt{A}$	$3.76\sqrt{K\rho h^3}$	$16\mu r^3/3$	$1.5EJk_x/\sqrt{A}(1-\nu^2)$

Aspect ratio	c_z	k_x					k_ϕ‡
		$\nu = 0.1$	0.2	0.3	0.4	0.5	
1	1.06	1.00	0.938	0.868	0.792	0.704	1.984
1.5	1.07	1.01	0.942	0.864	0.770	0.692	2.254
2.0	1.09	1.02	0.945	0.870	0.784	0.686	2.510
3.0	1.13	1.05	0.975	0.906	0.806	0.700	2.955
5.0	1.22	1.15	1.050	0.950	0.850	0.732	3.700
10.0	1.41	1.25	1.160	1.040	0.940	0.940	4.981

*Coefficients c_z, k_x, and k_ϕ tabulated in subsequent columns.
†Take moments of inertia with respect to axis at soil-foundation interface.
‡Rocking parallel to long side.

shapes or with other mass distributions, there may be coupling with other degrees of freedom or among all six of them. The same situation sometimes stems from asymmetric distribution of stiffnesses in the superstructure.

Comparisons (Nieto, Rosenblueth, and Rascón, 1965) are shown in Figs. 3.18–3.20 between the response amplitudes obtained from the models described in Table 3.1 and the "exact" solutions for steady-state harmonic excitation (Sung, 1953; Richart, 1962). We notice that the agreement for horizontal vibrations is comparable to that for vertical oscillations in Fig. 3.17. Agreement is adequate for torsional and rocking motion throughout most of the range of excitation frequencies covered in the figures, except in the neighborhood of the

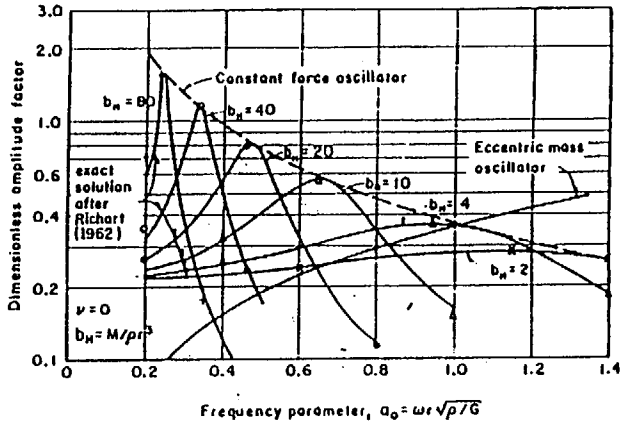

Figure 3.18. Comparison of responses of circular plates to horizontal excitation.

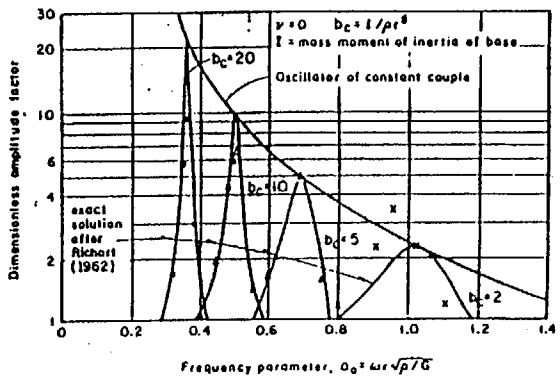

Figure 3.19. Comparison of responses of circular plates to rocking excitation.

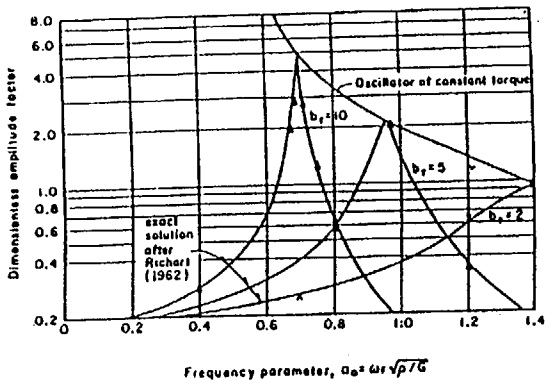

Figure 3.20. Comparison of responses of circular plates to torsional excitation.

resonant values when these are very small or very large. The discrepancy is important in these short intervals and should not be disregarded in the analysis of machine foundations or in the calculation of responses to earthquakes having well-defined, prevailing frequencies when these frequencies lie close to the rocking or torsional natural frequencies of the machine foundations. For most purposes in earthquake-resistant design, however, these discrepancies may well be overlooked because they affect only the contributions of short intervals in the entire range of significant frequencies of the motion.

Matters would improve if we varied one or two parameters in the models as a function of frequency. No doubt this should be done in the cases of narrow-band excitation that we quoted in the foregoing paragraph. Apparently, we could always proceed in this manner when using modal analysis. By trial and error or iteration we could find the values of parameters giving the best adjustment in the neighborhood of the natural frequencies of the soil-structure system and recompute these frequencies in terms of those parameters. But modal analysis does not apply strictly when we include soil-structure interaction because the combined system lacks classical natural modes. Hence, if we resort to modal analysis at all, great refinements are unwarranted. And if we wish to attain great accuracy there will be little advantage in adopting the simplified models proposed in this article, and we shall do well to return to the "exact" solutions. These allow us to compute the *transfer functions* of the system (its responses to instantaneous pulses), from which we can find the effects of various types of earthquakes on systems of linear behavior, as will be done in Chapters 9 and 10.

Ordinarily, analysis of pronouncedly nonlinear systems with soil-structure interaction will be formulated validly in terms of the models that Table 3.1 proposes, since nonlinearity will ensure that a vast range of frequencies will enter into play.

For other shapes of foundation the constants K for vertical oscillations are obtained readily by making reasonable assumptions about the contact pressure distribution, using charts (Newmark, 1947) to find the settlement of various points as though the foundation were flexible and to compute the foundation's average contact pressure and average settlement. Ordinarily the ratio of the two will give a satisfactory approximation to K. For example, under a circular plate subjected to a central vertical load the obviously wrong assumption that the contact pressure is uniform gives an error of only 5 percent (Timoshenko and Goodier, 1951). The spring constants that correspond to rocking oscillations can be obtained in similar fashion, while those for torsional and horizontal motions require integration of Cerrutti's equation for displacements at the ground surface. Once K has been obtained, the data in Table 3.1 can be used as a guide to estimate the dashpot constant and the virtual mass of soil. Studies are needed to allow reasonable estimates to be made of these parameters for deep, compensated foundations and for foundations on piles.

Numerical solutions have been obtained using high-speed computers for specific two-dimensional cases using lumped-parameter models and finite elements (Parmelee, 1969; Wilson, 1969). Some solutions correspond to surface foundations on a halfspace; others correspond to a foundation on a soil layer that in turn rests on a bedrock halfspace (Whitman, 1969), to partially compensated foundations (J. K. Minami and Sakurai, 1969), to a circular pier in a layered halfspace (Tajimi, 1969), and to foundations on point bearing piles (Penzien, Scheffey, and Parmelee, 1964; Kobori, Minai, and Inoue, 1969). Essentially the same remarks apply as the ones made on the problem of multiple wave reflection (Section 3.5) concerning "radiation damping" and the correct specification of boundary conditions where the soil or rock is assumed to terminate.

PROBLEMS[7]

3.1*. Compute the fundamental period of a cylindrical chimney stack of steel with circular cross section 6 ft in diameter, whose height is 90 ft, and whose thickness is $\frac{1}{4}$ in. (Fig. 3.21). Neglect shear deformations, rotary inertia, damping, gravity effects, and soil-foundation interaction.

Ans. 0.406 sec.

3.2. The unit weight and modulus of elasticity of a soil formation are 2.0 ton/m³ and 2×10^4 ton/m². Compute the velocities of dilatational, rotational, and Rayleigh waves in this material. Assume that Poisson's relation applies.

Ans. $v_p = 1085$ m/sec, $v_s = 626$ m/sec, $v_r = 576$ m/sec.

3.3*. A 30-m layer of the material specified in Problem 3.2 rests on what may be idealized as a semiinfinite rock formation having a unit weight of 2.8 ton/m³, a modulus of elasticity of 3×10^4 ton/m², and a Poisson's ratio of 0.25. Compute the

[7] Solution of problems marked with an asterisk is lengthy.

2,000-yr DB
Results for High Velocity

Layer	Thickness (ft)	Midpoint Depth (ft)	Vs (fps)	Unit Weight (kcf)	Damping Ratio	G	Vp (fps)
1	1	0.5	2121.005	0.1	0.009	13971	3380
2	4	3	2118.916	0.1	0.0092	13943.5	3380
3	2.5	6.25	572.921	0.08	0.0306	815.5	1385
4	2.5	8.75	542.786	0.08	0.039	731.97	1385
5	2	11	807.237	0.08	0.0269	1618.96	1543
6	3	13.5	990.432	0.1	0.0169	3046.44	1803
7	3	16.5	975.362	0.1	0.0194	2954.44	1803
8	4	20	979.871	0.094	0.022	2802.91	1764
9	4	24	966.037	0.094	0.0242	2724.33	1764
10	3	27.5	1065.836	0.115	0.0482	4057.16	2042
11	3	30.5	1051.714	0.115	0.0509	3950.37	2042
12	3	33.5	1040.421	0.115	0.0531	3865.98	2042
13	5	37.5	1509.135	0.115	0.0373	8133.89	2949
14	5	42.5	1488.251	0.115	0.0405	7910.33	2949
15	5	47.5	1467.515	0.115	0.0435	7691.43	2949
16	5	52.5	2496.595	0.12	0.0109	23228.51	4808
17	5	57.5	2492.479	0.12	0.0112	23151.99	4808
18	5	62.5	2488.708	0.12	0.0115	23082	4808
19	5	67.5	2485.255	0.12	0.0117	23017.98	4808
20	5	72.5	2482.042	0.12	0.012	22958.51	4808
21	5	77.5	2475.383	0.12	0.0126	22835.48	4808
22	5	82.5	2468.681	0.12	0.0133	22711.99	4808
23	5	87.5	2462.777	0.12	0.0139	22603.5	4808
24	11.67	95.83	4100.997	0.135	0.0428	70510.98	7104
25	11.67	107.5	4100.997	0.135	0.0428	70510.98	7104
26	11.67	119.17	4100.997	0.135	0.0428	70510.98	7104
27	19.44	134.73	4100.997	0.145	0.0428	75734	7104
28	19.44	154.17	4100.997	0.145	0.0428	75734	7104
29	19.44	173.61	4100.997	0.145	0.0428	75734	7104
30	19.44	193.05	4100.997	0.145	0.0428	75734	7104
31	19.44	212.49	4100.997	0.145	0.0428	75734	7104
32	19.44	231.93	4100.997	0.145	0.0428	75734	7104
33	19.44	251.37	4100.997	0.145	0.0428	75734	7104
34	19.44	270.81	4100.997	0.145	0.0428	75734	7104
35	19.44	290.25	4100.997	0.145	0.0428	75734	7104
36	50	324.97	5657.003	0.145	0.031	144106.97	9798
37	50	374.97	5657.003	0.145	0.031	144106.97	9798
38	50	424.97	5657.003	0.145	0.031	144106.97	9798
39	50	474.97	5657.003	0.145	0.031	144106.97	9798
40	100	549.97	6398	0.145	0.0253	184331.97	11155
41	100	649.97	6398	0.145	0.0253	184331.97	11155

Equivalent Properties for Top 30 Feet (minus top 1 ft) -High Range

Depth Factor (30-MPD)	Depth Factor x Thickness	G contrib. (ksf)	Damping contrib. (%)	Unit Wt. contrib. (kcf)	Vp^2 contrib. (fps^2)
0.9333	3.7333	52055.733	3.43	0.3733	42651093.3
0.8250	2.0625	1681.969	6.31	0.1650	3956339.06
0.7417	1.8542	1357.194	7.23	0.1483	3556708.85
0.6667	1.3333	2158.613	3.59	0.1067	3174465.33
0.5833	1.7500	5331.270	2.96	0.1750	5688915.75
0.4833	1.4500	4283.938	2.81	0.1450	4713673.05
0.3667	1.4667	4110.935	3.23	0.1379	4563820.8
0.2333	0.9333	2542.708	2.26	0.0877	2904249.6
0.1167	0.3500	1420.006	1.69	0.0403	1459417.4
0.0167	0.0500	197.519	0.25	0.0058	208488.2
	14.9833	5014.898	2.25	0.0924	4863882.41
		Equiv Vs	1321.75	**Avg Vp**	2205.42114

2,000-yr DB
Results for Best Estimate Velocity

Layer	Thickness (ft)	Midpoint Depth (ft)	Vs (fps)	Unit Weight (kcf)	Damping Ratio	G	Vp (fps)
1	3	1.5	1500.045	0.1	0.009	6988	2390
2	2	4	1493.969	0.1	0.0098	6931.5	2390
3	2.5	6.25	429.113	0.08	0.0435	457.49	1131
4	2.5	8.75	401.43	0.08	0.052	400.36	1131
5	2	11	622.362	0.08	0.036	962.32	1260
6	3	13.5	785.246	0.1	0.0216	1914.94	1472
7	3	16.5	772.515	0.1	0.0242	1853.35	1472
8	4	20	767.233	0.094	0.0286	1718.41	1440
9	4	24	753.286	0.094	0.0315	1656.5	1440
10	3	27.5	836.442	0.115	0.0568	2498.7	1667
11	3	30.5	819.3	0.115	0.0619	2397.33	1667
12	3	33.5	800.049	0.115	0.0676	2286	1667
13	5	37.5	978.785	0.115	0.0555	3421.5	2085
14	5	42.5	955.622	0.115	0.0615	3261.48	2085
15	5	47.5	934.136	0.115	0.0669	3116.47	2085
16	5	52.5	1734.943	0.12	0.0148	11217.49	3400
17	5	57.5	1730.06	0.12	0.0155	11154.44	3400
18	5	62.5	1724.35	0.12	0.0163	11080.93	3400
19	5	67.5	1718.351	0.12	0.0171	11003.97	3400
20	5	72.5	1713.271	0.12	0.0178	10938.99	3400
21	5	77.5	1708.291	0.12	0.0185	10875.5	3400
22	5	82.5	1703.02	0.12	0.0193	10808.49	3400
23	5	87.5	1697.891	0.12	0.02	10743.48	3400
24	11.67	95.83	2899.987	0.135	0.0432	35259	5023
25	11.67	107.5	2899.987	0.135	0.0432	35259	5023
26	11.67	119.17	2899.987	0.135	0.0432	35259	5023
27	19.44	134.73	2899.995	0.145	0.0432	37870.99	5023
28	19.44	154.17	2899.995	0.145	0.0432	37870.99	5023
29	19.44	173.61	2899.995	0.145	0.0432	37870.99	5023
30	19.44	193.05	2899.995	0.145	0.0432	37870.99	5023
31	19.44	212.49	2899.995	0.145	0.0432	37870.99	5023
32	19.44	231.93	2899.995	0.145	0.0432	37870.99	5023
33	19.44	251.37	2899.995	0.145	0.0432	37870.99	5023
34	19.44	270.81	2899.995	0.145	0.0432	37870.99	5023
35	19.44	290.25	2899.995	0.145	0.0432	37870.99	5023
36	50	324.97	3405.878	0.145	0.0367	52236.05	5975.5
37	50	374.97	3405.878	0.145	0.0367	52236.05	5975.5
38	50	424.97	3405.878	0.145	0.0367	52236.05	5975.5
39	50	474.97	3405.878	0.145	0.0367	52236.05	5975.5
40	100	549.97	3807.886	0.145	0.0333	65295.01	6841.5
41	100	649.97	3807.886	0.145	0.0333	65295.01	6841.5

Equivalent Properties for Top 30 Feet (minus top 3 ft) -Best Estimate

Depth Factor (33-MPD)	Depth Factor x Thickness	G contrib. (ksf)	Damping contrib. (%)	Unit Wt. contrib. (kcf)	Vp^2 contrib. (fps^2)
0.9667	1.9333	13400.900	1.89	0.1933	11043393.33
0.8917	2.2292	1019.821	9.70	0.1783	2851463.063
0.8083	2.0208	809.061	10.51	0.1617	2584971.188
0.7333	1.4667	1411.403	5.28	0.1173	2328480
0.6500	1.9500	3734.133	4.21	0.1950	4225228.8
0.5500	1.6500	3058.028	3.99	0.1650	3575193.6
0.4333	1.7333	2978.577	4.96	0.1629	3594240
0.3000	1.2000	1987.800	3.78	0.1128	2488320
0.1833	0.5500	1374.285	3.12	0.0633	1528388.95
0.0833	0.2500	599.333	1.55	0.0288	694722.25
	14.9833	2027.142	3.27	0.0920	2330215.874
		Equiv Vs	842.34	**Avg Vp**	1526.504463

2,000-yr DB
Results for Low Velocity

Layer	Thickness (ft)	Midpoint Depth (ft)	Vs (fps)	Unit Weight (kcf)	Damping Ratio	G	Vp (fps)
1	4	2	1058.641	0.1	0.0094	3480.5	1690
2	1	4.5	1046.789	0.1	0.0121	3403	1690
3	2.5	6.25	311.735	0.08	0.0591	241.44	923
4	2.5	8.75	284.555	0.08	0.0722	201.17	923
5	2	11	468.261	0.08	0.0476	544.77	1029
6	3	13.5	617.434	0.1	0.0277	1183.93	1202
7	3	16.5	602.13	0.1	0.0317	1125.96	1202
8	4	20	598.426	0.094	0.0359	1045.43	1176
9	4	24	587.452	0.094	0.0386	1007.43	1176
10	3	27.5	629.077	0.115	0.0758	1413.35	1361
11	3	30.5	612.727	0.115	0.0813	1340.84	1361
12	3	33.5	599.974	0.115	0.0855	1285.6	1361
13	5	37.5	588.001	0.115	0.0909	1234.8	1474
14	5	42.5	562.227	0.115	0.0988	1128.93	1474
15	5	47.5	545.363	0.115	0.1049	1062.22	1474
16	5	52.5	1194.668	0.12	0.0212	5318.88	2404
17	5	57.5	1191.395	0.12	0.0218	5289.77	2404
18	5	62.5	1189.92	0.12	0.0221	5276.68	2404
19	5	67.5	1190.423	0.12	0.022	5281.14	2404
20	5	72.5	1191.838	0.12	0.0217	5293.71	2404
21	5	77.5	1191.75	0.12	0.0218	5292.92	2404
22	5	82.5	1191.814	0.12	0.0217	5293.5	2404
23	5	87.5	1189.898	0.12	0.0221	5276.48	2404
24	11.67	95.83	2050.979	0.135	0.0397	17636	3552
25	11.67	107.5	2050.979	0.135	0.0397	17636	3552
26	11.67	119.17	2050.979	0.135	0.0397	17636	3552
27	19.44	134.73	2051.013	0.145	0.0397	18943	3552
28	19.44	154.17	2051.013	0.145	0.0397	18943	3552
29	19.44	173.61	2051.013	0.145	0.0397	18943	3552
30	19.44	193.05	2051.013	0.145	0.0397	18943	3552
31	19.44	212.49	2051.013	0.145	0.0397	18943	3552
32	19.44	231.93	2051.013	0.145	0.0397	18943	3552
33	19.44	251.37	2051.013	0.145	0.0397	18943	3552
34	19.44	270.81	2051.013	0.145	0.0397	18943	3552
35	19.44	290.25	2051.013	0.145	0.0397	18943	3552
36	50	324.97	2051.013	0.145	0.0397	18943	3552
37	50	374.97	2051.013	0.145	0.0397	18943	3552
38	50	424.97	2051.013	0.145	0.0397	18943	3552
39	50	474.97	2051.013	0.145	0.0397	18943	3552
40	100	549.97	2051.013	0.145	0.0397	18943	3552
41	100	649.97	2051.013	0.145	0.0397	18943	3552

Equivalent Properties for Top 30 Feet (minus top 4 ft) - Low Range

Depth Factor (34-MPD)	Depth Factor x Thickness	G contrib. (ksf)	Damping contrib. (%)	Unit Wt. contrib. (kcf)	Vp^2 contrib. (fps^2)
0.9833	0.9833	3346.283	1.19	0.0983	2808449.167
0.9250	2.3125	558.330	13.67	0.1850	1970085.813
0.8417	2.1042	423.295	15.19	0.1683	1792600.604
0.7667	1.5333	835.314	7.30	0.1227	1622880
0.6833	2.0500	2427.057	5.68	0.2050	2961848.2
0.5833	1.7500	1970.430	5.55	0.1750	2528407
0.4667	1.8667	1951.469	6.70	0.1755	2581555.2
0.3333	1.3333	1343.240	5.15	0.1253	1843968
0.2167	0.6500	918.678	4.93	0.0748	1204008.65
0.1167	0.3500	469.294	2.85	0.0403	648312.35
0.0167	0.0500	64.280	0.43	0.0058	92616.05
	14.9833	954.906	4.58	0.0918	1338469.257
		Equiv Vs	578.66	**Avg Vp**	1156.922321

Table 6
Dynamic Soil Properties for SASSI Model
High Range Properties

Shake Layers	Depth Top (ft)	Depth Bottom (ft)	Density (pcf)	Wave Velocity Vs (fps)	Wave Velocity Vp (fps)	Damping Ratio Shear (%)	Damping Ratio Compression (%)	Poisson's Ratio
1-2	0	5	100	2120	3380	0.91	0.91	0.176
3-4	5	10	80	557	1385	3.48	3.48	0.403
5	10	12	80	807	1543	2.69	2.69	0.312
6-7	12	18	100	983	1803	1.82	1.82	0.289
8-9	18	26	94	973	1764	2.31	2.31	0.281
10-12	26	35	115	1053	2042	5.07	5.07	0.319
13-15	35	50	115	1488	2949	4.04	4.04	0.329
16-23	50	90	120	2481	4808	1.21	1.21	0.318
24-26	90	125	135	4101	7104	4.28	4.28	0.250
27-35	125	300	145	4101	7104	4.28	4.28	0.250
36-39	300	500	145	5657	9798	3.10	3.10	0.250
40-41	500	700	145	6398	11155	2.53	2.53	0.255
	700		170	6398	11155	2.16	1.00	0.255

Best Estimate Properties

Shake Layers	Depth Top (ft)	Depth Bottom (ft)	Density (pcf)	Wave Velocity Vs (fps)	Wave Velocity Vp (fps)	Damping Ratio Shear (%)	Damping Ratio Compression (%)	Poisson's Ratio
1-2	0	5	100	1497	2390	0.94	0.94	0.177
3-4	5	10	80	415	1131	4.78	4.78	0.422
5	10	12	80	622	1260	3.60	3.60	0.339
6-7	12	18	100	779	1472	2.29	2.29	0.306
8-9	18	26	94	760	1440	3.01	3.01	0.307
10-12	26	35	115	818	1667	6.21	6.21	0.341
13-15	35	50	115	956	2085	6.13	6.13	0.367
16-23	50	90	120	1716	3400	1.74	1.74	0.329
24-26	90	125	135	2900	5023	4.32	4.32	0.250
27-35	125	300	145	2900	5023	4.32	4.32	0.250
36-39	300	500	145	3450	5976	3.67	3.67	0.250
40-41	500	700	145	3950	6842	3.33	3.33	0.250
	700		170	6398	11155	1.76	1.00	0.255

Low Range Properties

Shake Layers	Depth Top (ft)	Depth Bottom (ft)	Density (pcf)	Wave Velocity Vs (fps)	Wave Velocity Vp (fps)	Damping Ratio Shear (%)	Damping Ratio Compression (%)	Poisson's Ratio
1-2	0	5	100	1053	1690	1.08	1.08	0.183
3-4	5	10	80	298	923	6.57	6.57	0.442
5	10	12	80	622	1260	3.60	3.60	0.339
6-7	12	18	100	610	1202	2.97	2.97	0.327
8-9	18	26	94	593	1176	3.73	3.73	0.330
10-12	26	35	115	614	1361	8.09	8.09	0.372
13-15	35	50	115	565	1474	9.82	9.82	0.414
16-23	50	90	120	1191	2404	2.18	2.18	0.337
24-26	90	125	135	2051	3552	3.97	3.97	0.250
27-35	125	300	145	2051	3552	3.97	3.97	0.250
36-39	300	500	145	2051	3552	3.97	3.97	0.250
40-41	500	700	145	2051	3552	3.97	3.97	0.250
	700		170	6398	11155	2.16	1.00	0.255

Table 7

Dynamic Soil Properties for Spring-Dashpot-Mass Model

	Upper Range	Best Estimate	Lower Range	
Vp	2205	1527	1157	
Vs	1322	842	579	
G (ksf)	5015	2027	955	
beta S (%)	2.3	3.3	4.6	
E (ksf)	12234	5194	2546	
beta P (%)	2.3	3.3	4.6	
Poisson's Ratio	0.220	0.281	0.333	
Unit Wt. (pcf)	92.4	92.0	91.8	
A (30x67) sqft	2010	2010	2010	
Aspect Ratio	2.233	2.233	2.233	
Vertical Mode				
h	12.10	12.10	12.10	
m (pcf-sec^2)	**34.75**	**34.58**	**34.52**	mass/area (pcf-sec^2)
kv (kcf)	**315.20**	**138.29**	**70.23**	spring constant/area (kcf)
c (kcf-sec)	**4.84**	**3.20**	**2.28**	dashpot constant/area (kcf-sec)
Horizontal Mode				
h	2.24	2.24	2.24	
Kappa T	0.937	0.892	0.760	
m (pcf-sec^2)	**6.43**	**6.40**	**6.39**	mass/area (pcf-sec^2)
kh (kcf)	**268.79**	**112.24**	**48.52**	spring constant/area (kcf)
c (kcf-sec)	**2.70**	**1.74**	**1.14**	dashpot constant/area (kcf-sec)
Rocking Mode				
h	15.69	15.69	15.69	
Kr	112978035.57	49565892.37	25172167.30	
C	538785.878	356027.756	253487.104	
m (pcf-sec^2)	**45.04**	**44.83**	**44.75**	mass/area (pcf-sec^2)
kr (kcf)	**736.87**	**323.28**	**164.18**	spring constant/area (kcf)
c (kcf-sec)	**3.57**	**2.36**	**1.68**	dashpot constant/area (kcf-sec)

Interpolation of constants

Aspect Ratio	**Cs**	**Cs**	**Cs**
2.000	1.090	1.090	1.090
2.233	1.099	1.099	1.099
3.000	1.130	1.130	1.130

Aspect Ratio	**Kappa T**	**Kappa T**	**Kappa T**
2.000	0.930	0.884	0.755
2.233	0.937	0.892	0.760
3.000	0.961	0.919	0.773

Aspect Ratio	**kappa phi**	**kappa phi**	**kappa phi**
2.000	2.510	2.510	2.510
2.233	2.614	2.614	2.614
3.000	2.955	2.955	2.955

STONE & WEBSTER ENGINEERING CORPORATION

CALCULATION TITLE PAGE

*SEE INSTRUCTIONS ON REVERSE SIDE

▲ 5010.64 (FRONT)

CLIENT & PROJECT Private Fuel Storage Facility, LLC Private Fuel Storage Facility, Skull Valley, UT	**PAGE 1 OF** ~~34~~ 35
CALCULATION TITLE (Indicative of the Objective): Development of Time Histories for 2,000-Year Return Period Design Spectra	**QA CATEGORY (✓)** ☒ I – NUCLEAR SAFETY RELATED ☐ II ☐ III ☐ OTHER

CALCULATION IDENTIFICATION NUMBER				OPTIONAL WORK PACKAGE NO.
J.O. OR W.O. NO.	**DIVISION & GROUP**	**CURRENT CALC. NO.**	**OPTIONAL TASK CODE**	
05996.02	Geotechnical	G(PO18)-3	N/A	N/A

* APPROVALS – SIGNATURE & DATE			REV. NO. OR NEW CALC. NO.	SUPERSEDES * CALC. NO. OR REV. NO.	CONFIRMATION * REQUIRED (✓)	
PREPARER(S)/DATE(S)	**REVIEWER(S)/DATE(S)**	**INDEPENDENT REVIEWER(S)/DATE(S)**			**YES**	**NO**
Robert R. Youngs 8/24/99	Chin Man Mok 8/24/99	Chin Man Mok 8/24/99	0	N/A		X
Robert R. Youngs 3/21/01	Chin-Man Mok 3/21/01	Chin-Man Mok 3/21/01	1	05996.02 -G(PO18)-3 Rev 0		

DISTRIBUTION *

GROUP	NAME & LOCATION	COPY SENT (✓)	GROUP	NAME & LOCATION	COPY SENT (✓)
RECORDS MGT. FILES (OR FIRE FILE IF NONE)	Geomatrix Consultants, Inc. Oakland, California	original ☐ ☐			☐ ☐ ☐

CALCULATION SUMMARY

J.O./W.O./CALCULATION NO.	REVISION	PAGE 2 OF 35
05996.02	1	

▲ 5010.62

CLIENT / PROJECT	Private Fuel Storage Facility, LLC Private Fuel Storage Facility, Skull Valley, Utah	QA CATEGORY / CODE CLASS I

SUBJECT / TITLE

Development of Time Histories for 2,000-Year Return Period Design Spectra

OBJECTIVE OF CALCULATION

Develop a 3-component set of time histories that are compatible with the 2,000-year return period design response spectra and satisfy US NRC Standard Review Plan 3.7.1 (1989).

CALCULATION METHOD / ASSUMPTIONS

1. Select natural recordings consistent with controlling design event.
2. Scale motions to match design spectra at 5% damping and estimated spectra at 2% and 10% damping
3. Develop target PSD using standard Review Plan Appendix A and ratio of design spectra to REGGUIDE 1.60
4. Adjust time histories to meet envelop requirements for 5% response spectra and PSD of Standard Review Plan.

SOURCES OF DATA / EQUATIONS

See list of references on Page 11 of 34.

Computer Programs:
SPECTRA: A computer program to compute response spectra. Verification in project files

CONCLUSIONS

A 3-component set of time histories were developed for the 2,000-year Design spectra that satisfy requirements of US NRC Standard Review Plan 3.7.1 (1989). Time histories are on attached disk

REVIEWER (S) COMMENTS		
	PREPARER Robert R. Youngs	DATE 3/21/01
	REVIEWER / CHECKER Chin Man Mok	DATE 3/21/01
	INDEPENDENT REVIEWER Chin Man Mok	DATE 3/21/01

STONE & WEBSTER ENGINEERING CORPORATION

CALCULATION SHEET

CALCULATION IDENTIFICATION NUMBER				PAGE 3 OF 35
J.O. OR W.O. NO.	DIVISION & GROUP	CALCULATION NO.	OPTIONAL TASK CODE	
05996.02	Geotechnical	G(PO18)-3	N/A	

RECORD OF REVISIONS

Revision 0 - Original Issue

Revision 1 - The revision was performed to incorporate a new design ground motion level. The entire calculation was revised.

CALCULATION SHEET	J.O./W.O./CALCULATION NO. 05996.02-G(PO18)-3	REVISION 1	PAGE 4 OF 35
PREPARER/DATE Robert R. Youngs 3/21/01	REVIEWER/CHECKER/DATE Chin Man Mok 3/21/01	INDEPENDENT REVIEWER/DATE Chin Man Mok 3/21/01	
SUBJECT / TITLE Development of Time Histories for 2,000-Year Return Period Design Spectra		QA CATEGORY / CODE CLASS I	

TABLE OF CONTENTS AND HISTORIC DATA
(Revisions, Additions, Deletions, Etc.)

PRIVATE FUEL STORAGE FACILITY
SKULL VALLEY, UTAH

DEVELOPMENT OF TIME HISTORIES FOR 2,000-YEAR RETURN PERIOD DESIGN SPECTRA
Calculation 05996.02-G(PO18)-3 (Rev. 01)

1.0 INTRODUCTION

In this calculation a three-component set of artificial time histories were generated to match the 2,000-year return-period design response spectra for the Private Fuel Storage Facility located in Skull Valley, Utah. The time histories were generated by selecting an actual ground motion recording from an earthquake and site compatible with the design event defined in Geomatrix (2001). The time histories were then scaled to meet the requirements for a single artificial time history specified in Section 3.7.1.2 of the U.S. Nuclear Regulatory Commission's Standard Review Plan (US Nuclear Regulatory Commission, 1989). Scaling was performed using both frequency domain and time domain techniques. Rev 01 of this calculation differs from Rev 00 due to a change in the target design spectra.

2.0 SELECTED RECORDING

The design ground motions for the Skull Valley Private Fuel Storage Facility were developed from a probabilistic seismic hazard analysis. The 2,000-year return period equal-hazard response spectra represents earthquakes with a mean magnitude of **M** 6.4-6.5 and a mean (log) distance of 5 to 6 km. The controlling fault is the Stansbury fault located 9 km east of the site with a mean maximum magnitude of **M** 7.0. The site is located in the hanging wall block of the fault and is underlain be shallow stiff soils overlying tertiary semi-consolidated sediments. The design response spectra developed in Geomatrix (2001) include the near-fault effects of directivity and systematic fault-normal to fault-parallel differences at frequencies less than 2 Hz (spectral periods > 0.5 sec).

A strong motion recording that provides a good fit to these criteria is the Sturno recording of the November 23, 1980 **M** 6.9 Irpinia, Italy earthquake. The Sturno site is located approximately 11 km from the northwest end of the fault rupture in the hanging wall block. The processed time history was obtained from Pacific Engineering and Analysis from a set of time histories processed for the US Geological Survey for the Yucca Mountain project. The Sturno site is indicated to be a rock site (Spudich et al., 1997). However, the spectral scaling will adjust the

recording to achieve the desired frequency content. The original time histories were digitized at a time step of 0.00244 seconds. For this analysis they were interpolated to a time step of 0.005 seconds. The band width of the processed accelerograms is 0.13 to 30 Hz for the horizontal components and 0.13 to 33 Hz for the vertical component. The horizontal components of the recording are oriented at azimuths of 000 and 270, while the strike of the main rupture was northwest. Therefore the two horizontal recordings were used to compute a fault-normal component at an azimuth of 045 and a fault-parallel component at azimuth 315. The parameters of the recording motions and the interpolated and rotated motions are given in the following table.

Component	PGA (g)	PGV (cm/s)	PGD (cm)	V/A (cm/s/g)	D/A (cm/g)	AD/V^2	5%-75% Energy Duration (sec)	5%-95% Energy Duration (sec)
Original Processed Time Histories								
STU000	0.251	37.0	11.8	147.6	46.9	2.1	7.2	15.3
STU270	0.358	52.7	33.1	147.3	92.5	4.2	6.3	15.5
STUVRT	0.260	26.0	10.6	100.2	40.9	4.0	7.3	11.9
Interpolated and Rotated Time Histories								
STU-fn	0.234	43.1	23.7	184.4	101.4	2.9	7.9	16.9
STU-fp	0.302	46.5	23.4	154.0	77.4	3.2	6.1	12.3
STUvrt	0.254	26.0	10.6	102.3	41.5	3.9	7.3	11.9

Figure 1 shows the original accelerograms. Figure 2 shows the interpolated and rotated accelerograms, and Figures 3 and 4 show the integrated velocity and displacement time histories. Figure 5 compares the 5% damped response spectra for the interpolated and rotated accelerograms to the design ground motion response spectra from Geomatrix (2001).

3.0 SCALING TO DESIGN SPECTRA

The initial scaling of the accelerograms was performed using program RASCAL (Silva and Lee, 1987). This program operates in the frequency domain. The stochastic ground motion model (e.g. Boore, 1983, 1986) is used to generate a Fourier amplitude spectrum for the appropriate magnitude earthquake that is used as an initial estimate. Random vibration theory (RVT) is then used to compute a response spectrum from the Fourier amplitude spectrum. The RVT response spectrum is compared to the target response spectrum and the Fourier amplitude spectrum is adjusted iteratively to minimize the difference between the target response spectrum and the RVT response spectrum. A time history (TH) is then created using the adjusted Fourier amplitude spectrum and the phase from the selected accelerogram. The resulting time history is

used to compute a response spectrum. The TH response spectrum is compared to the target response spectrum and the Fourier amplitude spectrum for the TH is adjusted iteratively to minimize the difference between the target response spectrum and the TH response spectrum. Figure 6 shows the developed from the initial frequency domain scaling and Figure 7 compares the response spectra for these time histories to the design response spectra.

The final scaling was performed using the time-domain technique developed by Lilhanand and Tseng (1988). This approach scales the motion to match a target response spectrum by adjusting the time history in small increments in the vicinity of the time for the peak spectral response. Attachment A to Rev 00 of this calculation (Geomatrix 1999) contains a description of the technique and a computer program to implement it developed by Dr. Norm Abrahamson.

One advantage of the approach is that the response spectra for multiple damping levels can be used as the target spectra. Matching the response spectra for multiple damping levels helps prevent development of "holes" in the frequency content of the resulting time history. The design ground motion spectra developed in Geomatrix (2001) are specified for 5% damping only. Abrahamson and Silva (1996) developed adjustment factors to scale 5% damped response spectra to other damping levels from the analysis of a large number of empirical response spectra. Figure 8 shows the adjustment factors for 2% and 10% damping for horizontal and vertical motions for an **M** 6.5 earthquake. These factors were used to create 2% and 10% damping response spectra consistent with the 5% damping design response spectra. The 2% and 10% damping spectra were also used as target spectra to ensure that the resulting time histories are broad-banded. Figure 9 shows the developed from the time domain scaling. These time histories have been baseline corrected to remove displacement drift by subtracting a 6^{th} order polynomial fit to the integrated displacement time history. Figure 10 compares the response spectra for these time histories to the 5% design response spectra and the associated 2% and 10% spectra created using the factors on Figure 8.

The final steps in the processing were: shortening the total duration to 30 seconds by removing the long, low amplitude tail of the records; adjusting the PGA value to be more consistent with the design spectrum PGA; and scaling the time histories upward by a small factor to meet the response spectrum envelope criteria specified in Section 3.7.1.2 of the Standard Review Plan. The resulting time histories are shown on Figures 11, 12, and 13. The parameters of the design time histories are:

Component	PGA (g)	PGV (cm/s)	PGD (cm)	V/A (cm/s/g)	D/A (cm/g)	AD/V^2	5%-75% Energy Duration (sec)	5%-95% Energy Duration (sec)
fault-normal	0.728	43.9	23.7	60.3	32.5	8.8	10.1	20.9
fault-parallel	0.707	43.2	14.2	61.1	20.0	5.3	9.2	21.4
vertical	0.721	26.5	9.6	36.7	13.3	9.7	8.6	16.8

Figure 14 shows the time history of normalized cumulative energy $\left(\sum_{i=1}^{t} a(i)^2 \Big/ \sum_{i=1}^{T} a(i)^2\right)$.

4.0 COMPARISON WITH REGULATORY REQUIREMENTS

Envelop of Design Response Spectra

Section 3.7.1 of the Standard Review Plan specifies that response spectral values computed from a single artificial time history must envelop the target design spectrum such that no more that 5 points of the response spectrum obtained from the time history fall below the design spectrum, with none more than 10% below. Table 3.7.1-1 of the Standard Review Plan provides an acceptable set of frequencies for computation of the response spectrum. This table is reproduced below.

Frequency Range (Hz)	Frequency Increment (Hz)
0.2 – 3.0	0.1
3.0 – 3.6	0.15
3.6 – 5.0	0.2
5.0 – 8.0	0.25
8.0 – 15.0	0.5
15.0 – 18.0	1.0
18.0 – 22.0	2.0
22.0 – 34.0	3.0

The result is a set of 75 frequencies. Table 1 lists these frequencies together with the control points of the design response spectra defined in Geomatrix (2001). The bold entries in Table 1 indicate these control points. The design spectral values between the control points were obtained by linear interpolation of log(frequency) versus log(spectral acceleration). Also listed in Table 1 are the 5% damped spectral ordinates computed from the time histories. The spectral ordinates were computed using program **SPECTRA**. Verification of this program is in a separate report. The time histories and computed response spectra are located in directory **\FINALIZE** on the attached disk. The shaded entries in Table 1 indicate the points where the

time history response spectrum falls below the design response spectrum. For the fault-parallel time history, only two points fall below the 5%-damped design spectrum because the fit at other damping levels controlled the time history scaling. The time histories meet the requirements for enveloping the design response spectra.

Envelop of Target Power Spectral Density

Section 3.7.1 of the Standard Review Plan specifies that if a single time history is to be used, then it must have a power spectral density (PSD) that exceeds 80% of a target PSD. The one-sided PSD, $S_{0(\omega)}$, is related to the Fourier amplitude spectrum, $|F_{(\omega)}|$ by the relationship:

$$S_{0(\omega)} = \frac{2\left|\bar{F}_{\omega}\right|^2}{2\pi T_D} \tag{1}$$

where T_D is the duration of near maximum and near stationary power of an acceleration time history. Equation (2) in Appendix A of the Standard Review Plan Section 3.7.1 provides a target PSD for the Regulatory Guide 1.60 horizontal response spectrum anchored to 1.0 g PGA. The relationship is:

$$\begin{aligned}
&\text{For } f < 2.5 \text{ Hz} \\
S_{0(\omega)} &= 650 \text{ in}^2/\text{sec}^3 (f/2.5)^{0.2} \\
&\text{For } 2.5 \le f < 9 \text{ Hz} \\
S_{0(\omega)} &= 650 \text{ in}^2/\text{sec}^3 (2.5/f)^{1.8} \\
&\text{For } 9 \le f < 16 \text{ Hz} \\
S_{0(\omega)} &= 64.8 \text{ in}^2/\text{sec}^3 (9/f)^3 \\
&\text{For } f \ge 16 \text{ Hz} \\
S_{0(\omega)} &= 11.5 \text{ in}^2/\text{sec}^3 (16/f)^8
\end{aligned} \tag{2}$$

Appendix A of the Standard Review Plan Section 3.7.1 indicates that a target PSD for the Regulatory Guide 1.60 horizontal response spectrum anchored to an other PGA value can be obtained by multiplying Equation **(2)** by the square of the design PGA. A target PSD for the Skull Valley 2,000-year design response spectra was obtained by extending this approach. At each frequency f, the target PSD for the Skull Valley design response spectrum, $\{S_{0(\omega)}\}_{SV}$, is obtained by the expression:

$$\{S_{0(\omega)}\}_{SV} = \{S_{0(\omega)}\}_{RG1.60} \cdot [SA(f)_{SV} / SA(f)_{RG1.60}]^2 \quad (3)$$

where $SA(f)$ is the acceleration response spectral ordinate at frequency f, and the subscripts SV and RG1.60 refer to the Skull Valley design spectrum and the Regulatory Guide 1.60 horizontal response spectrum anchored to 1.0 g PGA, respectively. A small computer code, **TPSD**, located in directory **\TPSD** on the attached disk was used to scale Equation **(2)** using Equation **(3)**.

The PSD for the time histories shown on Figures 11, 12, and 13 were computed using a small computer code, **PSD**, located in directory **\PSD** on the attached disk. The program uses as input a Fourier spectrum of the time history. Each frequency in the Fourier spectrum, $S_{0(\omega)}$ is computed using Equation **(1)**. The appropriate duration for nearly constant power, T_D, was set equal to the 5%-75% cumulative energy duration of the final time histories listed above. The values for the three time histories are somewhat longer than the values obtained for the original time histories. The Fourier spectra were computed using program **FT** located in directory **\FT** on the attached disk. The program outputs columns containing the frequency, real, imaginary, and absolute amplitude Fourier components. Testing of the program indicates that the Fourier amplitude spectrum must be scaled by Δt to obtain units of g-seconds when the input time history is in g's. The Fourier amplitudes output from program **FT** were scaled by a factor of 1.9311 = 0.005*386.22 in/sec^2/g with program **PSD**. Program **PSD** then smoothes the PSD by computing the average value over a frequency window of ±20% of f, following the procedure described in Appendix A to Section 3.7.1 of the Standard Review Plan. Figures 19, 20, and 21 compare the PSD's computed for the time histories to 80% of the target PSDs shown on Figure 18. All of the target PSDs are enveloped at the 80% level.

Component-to-Component Cross-Correlation

ASCE Standard 4-86 (American Society of Civil Engineers, 1986) recommends that the cross-correlation between the three components of a time history set used in nuclear plant analysis be less that 0.3. EXCEL® spreadsheet **CC-R01.XLS** in directory **\FINALIZE** on the attached disk contains columns with the three time histories. The CORREL function was used to compute the zero-lag cross-correlation between the three time histories. The values are:

Fault-normal to fault-parallel	-0.06
Fault-normal to vertical	-0.02
Fault-parallel to vertical	0.06

These values indicate that the time histories are uncorrelated.

5.0 REFERENCES

American Society of Civil Engineers (1986), Seismic analysis of safety-related nuclear structures and commentary on standard for seismic analysis of safety-related nuclear structures: ASCE Standard 4-86.

Abrahamson, N.A., and Silva, W.J., 1996, Empirical ground motion models: *in* Silva, W.C., Abrahamson, N., Toro, G., and Costantino, C., 1998, Description and validation of the stochastic ground motion model: Report submitted to Brookhaven National Laboratory, Associated Universities, Inc., New York.

Boore, D.M., 1983, Stochastic simulation of high-frequency ground motions based on seismological models of the radiated spectra: Bulletin of the Seismological Society of America, v. 73, p. 1865-1894.

Boore, D.M., 1986, Short period P- and S-wave radiation from large earthquakes: Implications for spectral scaling relations: Bulletin of the Seismological Society of America, v. 76, p. 43-64.

Geomatrix Consultants, Inc., 2001, Development of design ground motions for the Private Fuel Storage Facility, Skull Valley, Utah – Rev 01: report prepared for Stone & Webster Engineering Corporation, March, 6 p.

Lilhanand, K., and Tseng, W.S, 1988, Development and application of realistic earthquake time histories compatible with multiple-damping response spectra: Ninth World Conference on Earthquake Engineering, Tokyo, Japan, v. II, 819-824.

Silva, W.J., and Lee, K., 1987, WES RASCAL code for synthesizing earthquake ground motions: State-of-the-art for assessing earthquake hazards in the United States: U.S. Army Waterways Experiment Station, Report 24, Miscellaneous Paper S-73-1, 120 p.

Spudich, P., Fletcher, J.B., Hellweg, M., Boatwright, J., Sullivan, C., Joyner, W.B., Hanks, T.C., Boore, D.M., McGarr, A., Baker, L.M., and Lindh, A.G., 1997, SEA96 – a new predictive relation for earthquake ground motions in extensional tectonic regimes: Seismological Research Letters, v. 68, p. 190-198.

U.S. Nuclear Regulatory Commission, 1989, Standard Review Plan; Office of Nuclear Reactor Regulation, Revision 2, Document NUREG-0800.

Table 1

Comparison of Time History and Design Response Spectra

	Period (sec)	Frequency (Hz)	5% Damping Design Basis (g)	Fault-normal Time History (g)	Mismatch (%)	5% Damping Design Basis (g)	Fault-parallel Time History (g)	Mismatch (%)	Vertical Design Basis (g)	Vertical Time History (g)	Mismatch (%)
	0.01	100.0	**0.711**			**0.711**			**0.695**		
	0.02	50.0							**0.695**		
1	**0.0294**	34.0	**0.711**	0.76927	8.2	**0.711**	0.78683	10.7	0.9025	0.99628	10.4
2	0.0323	31.0	0.7526	0.77982	3.6	0.7526	0.80991	7.6	0.9609	1.00017	4.1
3	0.0357	28.0	0.8010	0.84131	5.0	0.8010	0.86948	8.5	1.0293	1.04885	1.9
4	0.0400	25.0	0.8588	0.9047	5.3	0.8588	0.93079	8.4	1.1116	1.19269	7.3
5	0.0455	22.0	0.9291	0.98317	5.8	0.9291	1.02187	10.0	1.2122	1.35589	11.8
6	**0.0500**	20.0	**0.985**	1.03022	4.6	**0.985**	1.08005	9.6	**1.293**	1.44014	11.4
7	0.0556	18.0	1.0471	1.06662	1.9	1.0471	1.1203	7.0	1.3750	1.50653	9.6
8	0.0588	17.0	1.0823	1.12944	4.4	1.0823	1.18812	9.8	1.4215	1.51701	6.7
9	0.0625	16.0	1.1210	1.2124	8.2	1.1210	1.21054	8.0	1.4727	1.55963	5.9
10	0.0667	15.0	1.1638	1.29985	11.7	1.1638	1.23824	6.4	1.5293	1.61816	5.8
11	0.0690	14.5	1.1869	1.27762	7.6	1.1869	1.22454	3.2	1.5598	1.59245	2.1
12	0.0714	14.0	1.2113	1.27619	5.4	1.2113	1.2691	4.8	1.5921	1.70303	7.0
13	0.0741	13.5	1.2370	1.27427	3.0	1.2370	1.34037	8.4	1.6261	1.78858	10.0
	0.0750		**1.246**			**1.246**			**1.638**		
14	0.0769	13.0	1.2695	1.31321	3.4	1.2695	1.38925	9.4	1.6485	1.69913	3.1
15	0.0800	12.5	1.3068	1.36309	4.3	1.3068	1.36613	4.5	1.6648	1.86983	12.3
16	0.0833	12.0	1.3468	1.42453	5.8	1.3468	1.33278	-1.0	1.6820	1.81249	7.8
17	0.0870	11.5	1.3899	1.44809	4.2	1.3899	1.48302	6.7	1.7001	1.77089	4.2
18	0.0909	11.0	1.4363	1.44918	0.9	1.4363	1.56928	9.3	1.7193	1.84069	7.1
19	0.0952	10.5	1.4865	1.58465	6.6	1.4865	1.5737	5.9	1.7395	1.96952	13.2
20	**0.100**	10.0	**1.541**	1.58448	2.8	**1.541**	1.60646	4.2	**1.761**	2.00011	13.6
21	0.105	9.5	1.5812	1.69622	7.3	1.5812	1.72729	9.2	1.7445	1.74355	-0.1
22	0.111	9.0	1.6247	1.74391	7.3	1.6247	1.79984	10.8	1.7274	1.94131	12.4
23	0.118	8.5	1.6721	1.71854	2.8	1.6721	1.69923	1.6	1.7094	1.72835	1.1
24	0.125	8.0	1.7237	1.84728	7.2	1.7237	1.86824	8.4	1.6905	1.79545	6.2
25	0.129	7.8	1.7514	1.83035	4.5	1.7514	1.88174	7.4	1.6807	1.76637	5.1
26	0.133	7.5	1.7805	1.77161	-0.5	1.7805	1.90084	6.8	1.6707	1.79384	7.4
27	0.138	7.3	1.8111	1.80989	-0.1	1.8111	1.9507	7.7	1.6603	1.85589	11.8
28	0.143	7.0	1.8433	1.89042	2.6	1.8433	1.88747	2.4	1.6497	1.73188	5.0
29	0.148	6.7	1.8773	2.01524	7.3	1.8773	1.95493	4.1	1.6387	1.57356	-4.0
	0.150		**1.889**			**1.889**			**1.635**		
30	0.154	6.5	1.8994	1.9722	3.8	1.8994	1.89939	-0.0	1.6154	1.56433	-3.2
31	0.160	6.3	1.9157	2.04385	6.7	1.9157	2.05623	7.3	1.5856	1.79473	13.2
32	0.167	6.0	1.9328	2.08635	7.9	1.9328	2.10562	8.9	1.5551	1.61986	4.2

33	0.174	5.8	1.9508	2.0622	5.7	1.9508	1.99702	2.4	1.5240	1.71253	12.4
34	0.182	5.5	1.9697	2.11064	7.2	1.9697	1.9581	-0.6	1.4921	1.60323	7.4
35	0.190	5.2	1.9898	2.05929	3.5	1.9898	2.13389	7.2	1.4594	1.51181	3.6
36	**0.200**	5.0	**2.011**	2.14129	6.5	**2.011**	2.18846	8.8	**1.426**	1.47945	3.7
37	0.208	4.8	1.9772	2.1528	8.9	1.9772	2.07742	5.1	1.3702	1.55493	13.5
38	0.217	4.6	1.9425	2.11203	8.7	1.9425	2.09823	8.0	1.3143	1.38905	5.7
39	0.227	4.4	1.9069	2.01372	5.6	1.9069	2.08812	9.5	1.2584	1.38993	10.5
40	0.238	4.2	1.8704	2.04416	9.3	1.8704	1.95396	4.5	1.2023	1.31668	9.5
41	0.250	4.0	1.8328	1.83278	-0.0	1.8328	1.91029	4.2	1.1463	1.26114	10.0
42	0.263	3.8	1.7941	1.9148	6.7	1.7941	1.90854	6.4	1.0902	1.15981	6.4
43	0.278	3.6	1.7542	1.86855	6.5	1.7542	1.85945	6.0	1.0340	1.11098	7.4
44	0.290	3.4	1.7235	1.87361	8.7	1.7235	1.81318	5.2	0.9918	1.13626	14.6
	0.300		**1.699**			**1.699**			**0.959**		
45	0.303	3.3	1.6828	1.80503	7.3	1.6828	1.77131	5.3	0.9467	1.04903	10.8
46	0.317	3.2	1.6097	1.64734	2.3	1.6097	1.74337	8.3	0.8919	0.96341	8.0
47	0.333	3.0	1.5364	1.61059	4.8	1.5364	1.67163	8.8	0.8377	0.93903	12.1
48	0.345	2.9	1.4875	1.6184	8.8	1.4875	1.64246	10.4	0.8021	0.88341	10.1
49	0.357	2.8	1.4385	1.59768	11.1	1.4385	1.61483	12.3	0.7668	0.75297	-1.8
50	0.370	2.7	1.3894	1.53479	10.5	1.3894	1.56713	12.8	0.7318	0.80264	9.7
51	0.385	2.6	1.3402	1.43771	7.3	1.3402	1.47974	10.4	0.6972	0.80324	15.2
52	**0.400**	2.5	**1.291**	1.29745	0.5	**1.291**	1.33766	3.6	**0.663**	0.76616	15.6
53	0.417	2.4	1.2431	1.32383	6.5	1.2431	1.36554	9.8	0.6317	0.66191	4.8
54	0.435	2.3	1.1951	1.29492	8.4	1.1951	1.31723	10.2	0.6006	0.644	7.2
55	0.455	2.2	1.1469	1.17245	2.2	1.1469	1.29691	13.1	0.5698	0.60888	6.9
56	0.476	2.1	1.0985	1.14662	4.4	1.0985	1.24187	13.0	0.5393	0.59974	11.2
57	**0.500**	2.0	**1.050**	1.07825	2.7	**1.050**	1.17603	12.0	**0.509**	0.56712	11.4
58	0.526	1.9	0.9962	1.05154	5.6	0.9962	1.16298	16.7	0.4807	0.53385	11.1
59	0.556	1.8	0.9425	0.8856	-6.0	0.9425	1.12603	19.5	0.4526	0.47324	4.6
60	0.588	1.7	0.8889	0.9198	3.5	0.8889	1.03206	16.1	0.4247	0.45997	8.3
61	0.625	1.6	0.8354	0.88903	6.4	0.8354	0.92933	11.2	0.3970	0.42693	7.5
62	0.667	1.5	0.7819	0.73934	-5.4	0.7819	0.94301	20.6	0.3694	0.39032	5.7
63	0.714	1.4	0.7285	0.78578	7.9	0.7285	0.85834	17.8	0.3421	0.38997	14.0
	0.750		**0.693**			**0.693**			**0.324**		
64	0.769	1.3	0.6763	0.75236	11.3	0.6706	0.77482	15.5	0.3152	0.30952	-1.8
65	0.833	1.2	0.6260	0.64803	3.5	0.6044	0.71335	18.0	0.2889	0.33617	16.3
66	0.909	1.1	0.5756	0.5838	1.4	0.5398	0.63656	17.9	0.2629	0.28059	6.7
67	**1.00**	1.0	**0.525**	0.58508	11.4	**0.477**	0.56703	18.9	**0.237**	0.26506	11.8
68	1.11	0.9	0.4594	0.44851	-2.4	0.4074	0.50923	25.0	0.2086	0.23842	14.3
69	1.25	0.8	0.3956	0.4175	5.5	0.3416	0.44719	30.9	0.1808	0.20408	12.8
70	1.43	0.7	0.3340	0.3604	7.9	0.2797	0.3794	35.6	0.1538	0.18618	21.0
	1.50		**0.314**			**0.260**			**0.145**		
71	1.67	0.6	0.2770	0.30842	11.3	0.2244	0.28255	25.9	0.1284	0.14389	12.1
72	**2.00**	0.5	**0.223**	0.25	12.1	**0.174**	0.20892	20.1	**0.104**	0.12739	22.5
73	2.50	0.4	0.1773	0.20195	13.9	0.1281	0.14228	11.1	0.0815	0.09851	20.9
	3.00		**0.147**			**0.0997**			**0.0668**		

74	3.33	0.3	0.1290	0.14663	13.6	0.0848	0.09173	8.2	0.0586	0.07144	21.8
	4.00		**0.103**			**0.0640**			**0.0468**		
75	**5.00**	0.2	**0.0811**	0.08607	6.1	**0.0457**	0.05354	17.2	**0.0367**	0.04509	22.9
				Minimum	-6.0		**Minimum**	-1.0		**Minimum**	-4.0

Bold values indicate control points in design ground response spectrum, intermediate values obtained by log(period)-log(SA) interpolation

Shaded values indicate negative mismatch between time history spectrum and design response spectrum

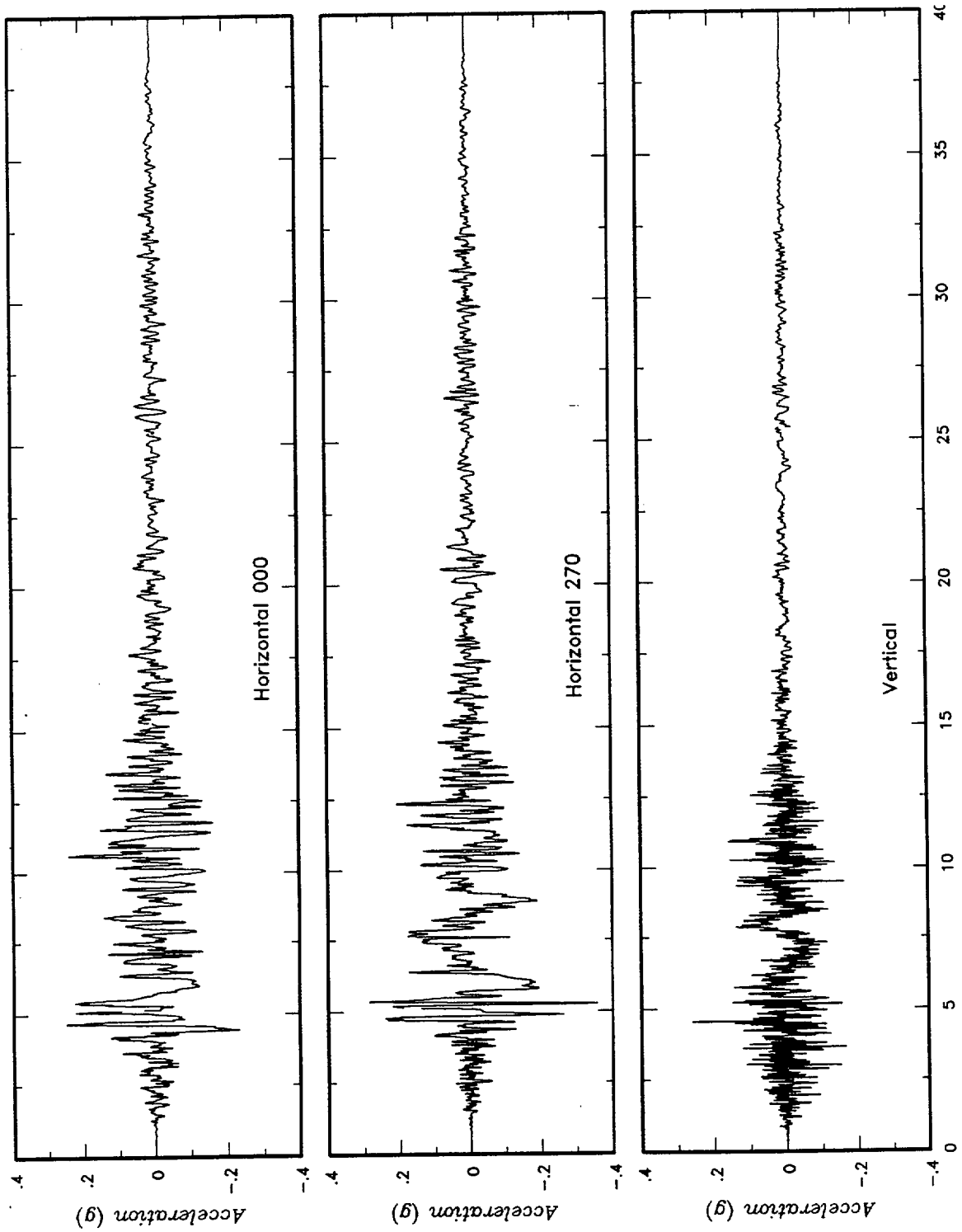

Figure 1 Irpinia, Italy 11/23/80 Main Shock – Sturno Site

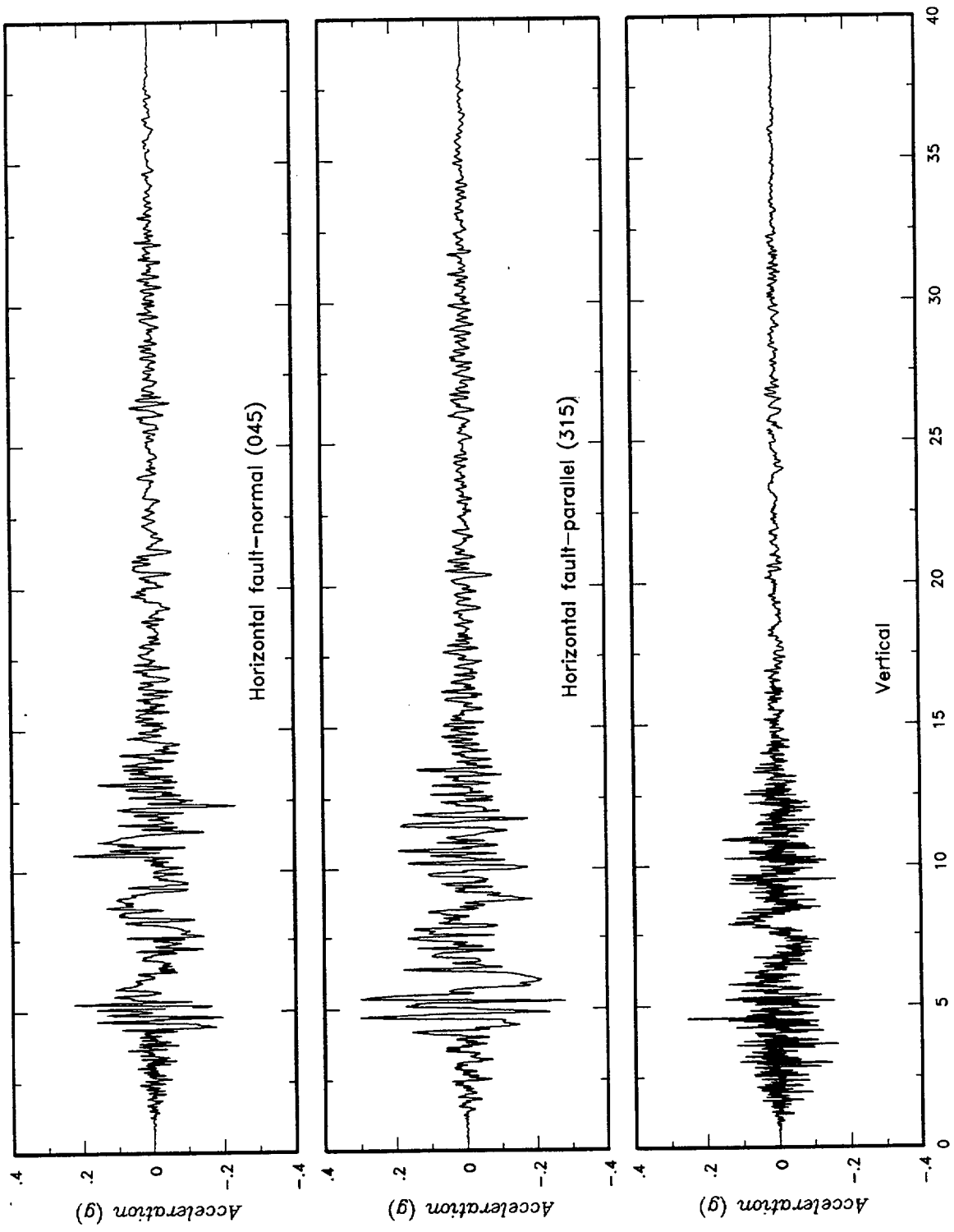

Figure 2 Irpinia, Italy 11/23/80 Main Shock – Sturno Site interpolated to 0.005 and rotated

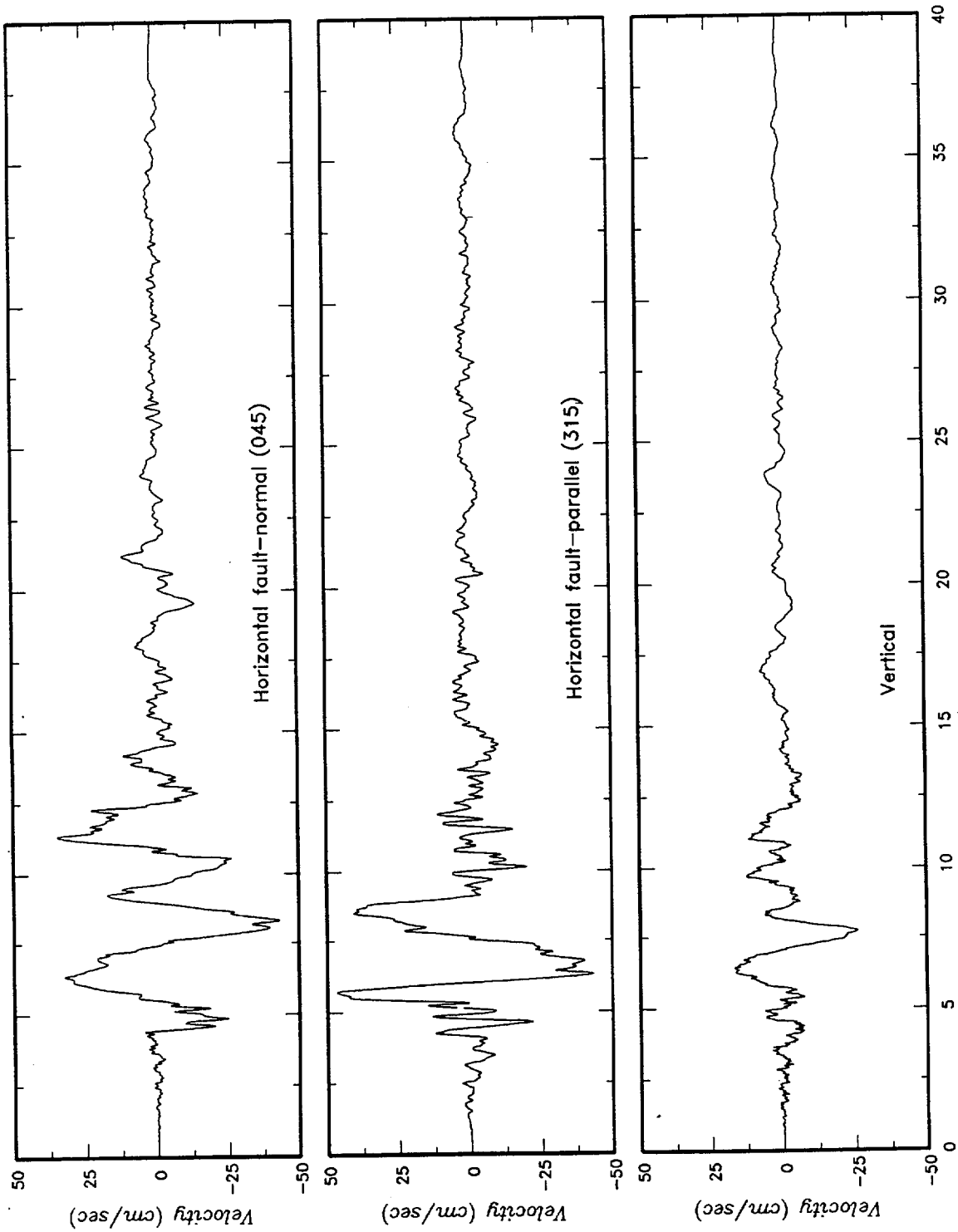

Figure 3 Irpinia, Italy 11/23/80 Main Shock – Sturno Site interpolated to 0.005 and rotated

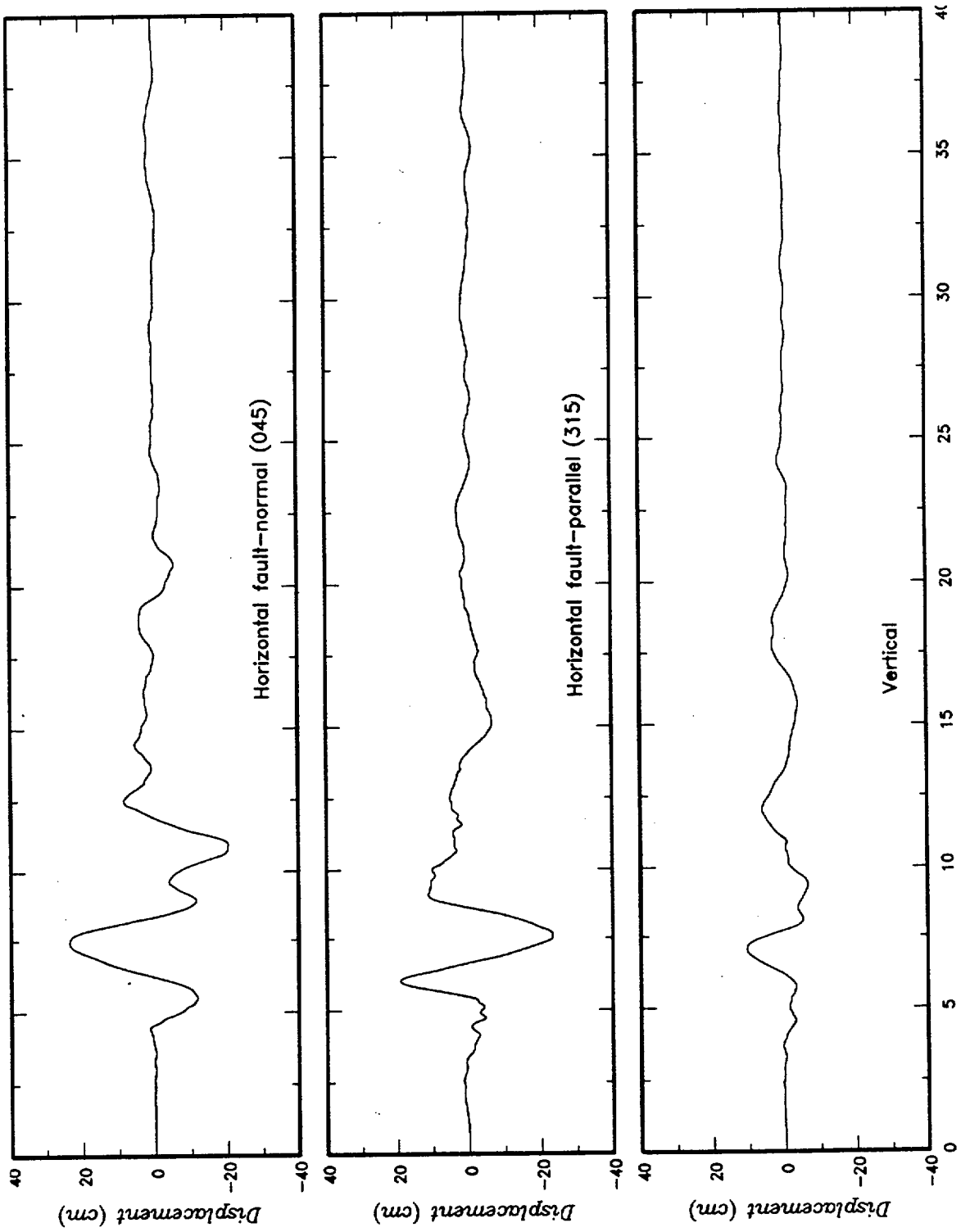

Figure 4 Irpinia, Italy 11/23/80 Main Shock – Sturno Site interpolated to 0.005 and rotated

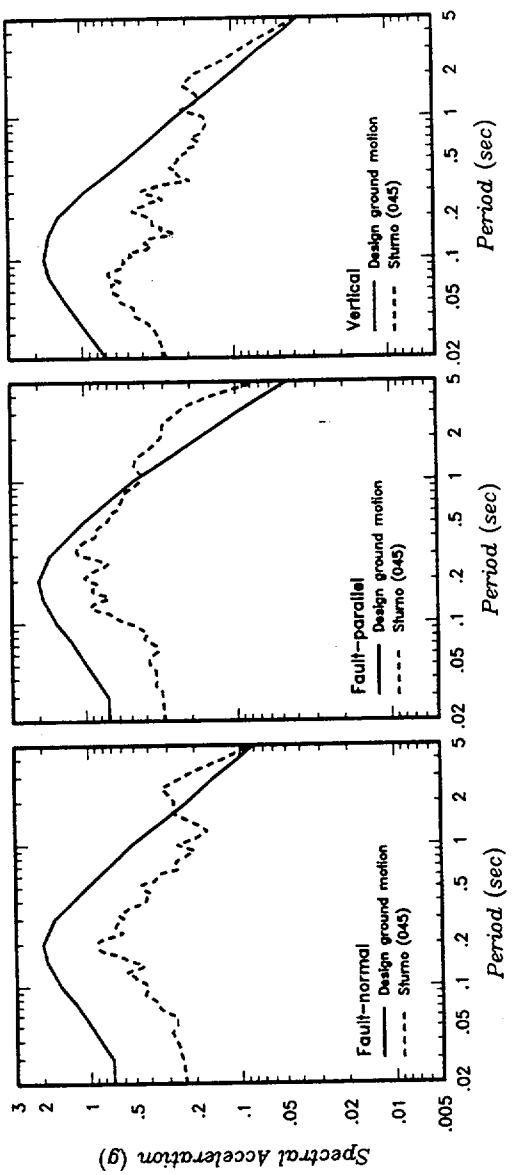

Figure 5 Irpinia Main Shock Compared to Design Spectra

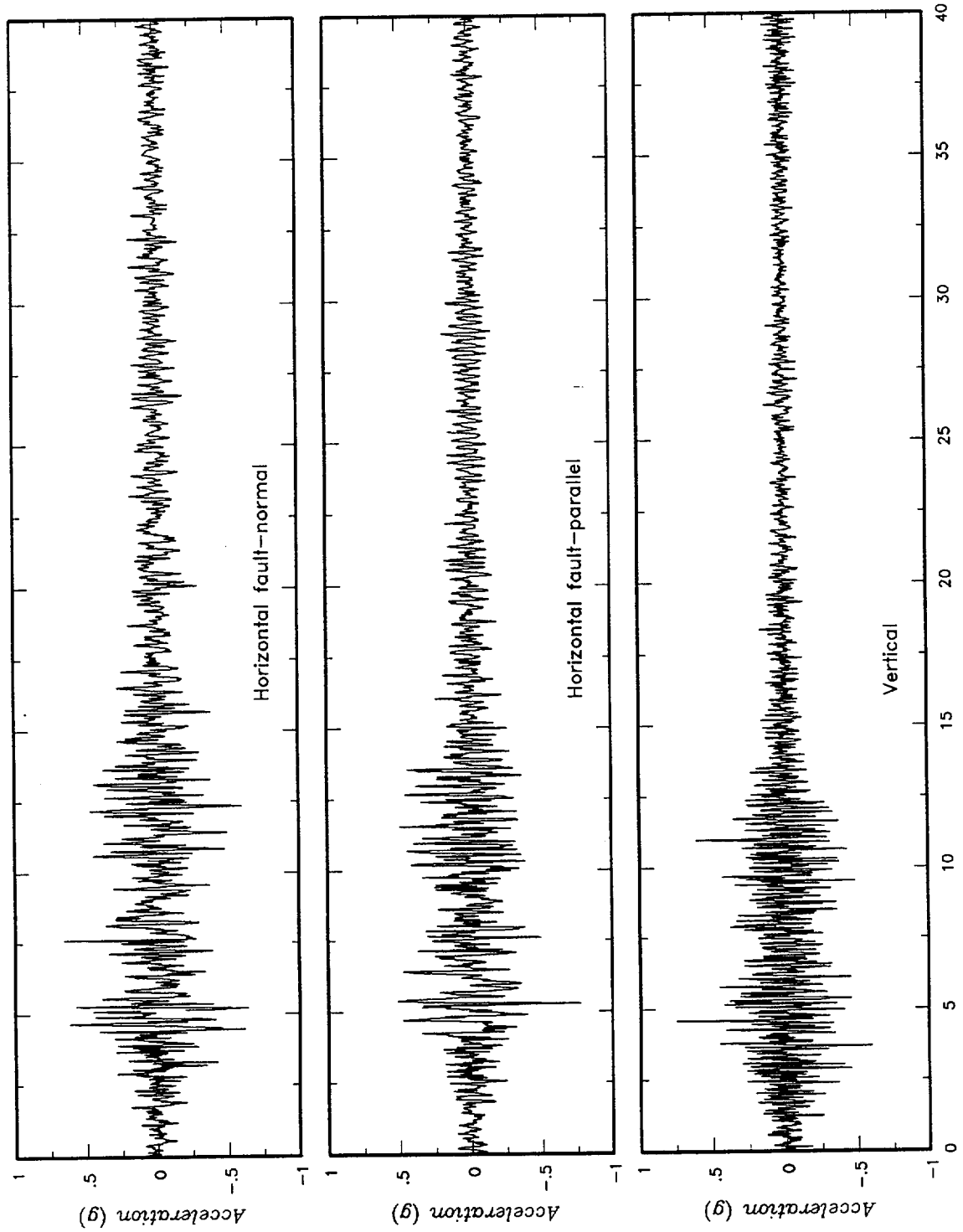

Figure 6 Time Histories from Initial Frequency–domain Scaling

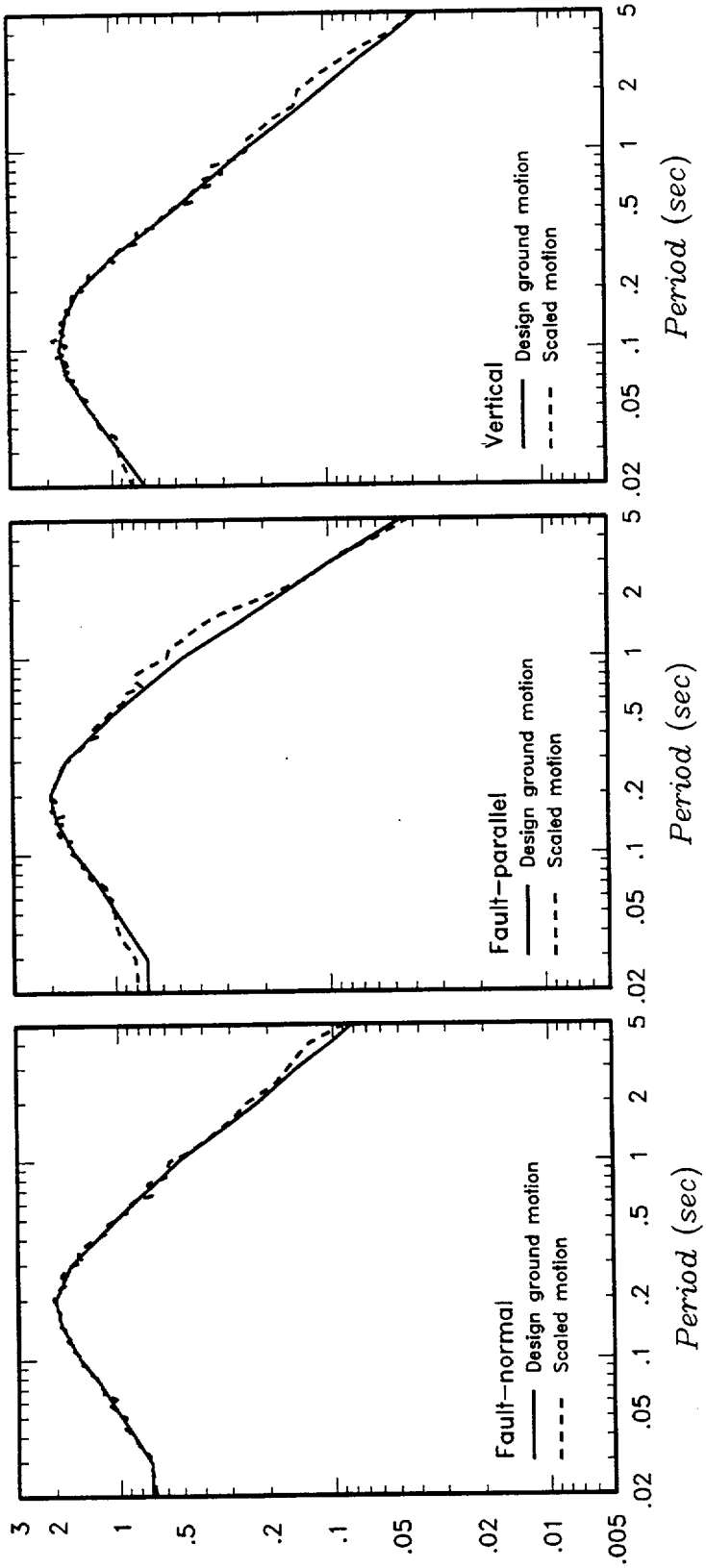

Figure 7 Spectra from Frequency–domain Scaling Compared to Design Spectra

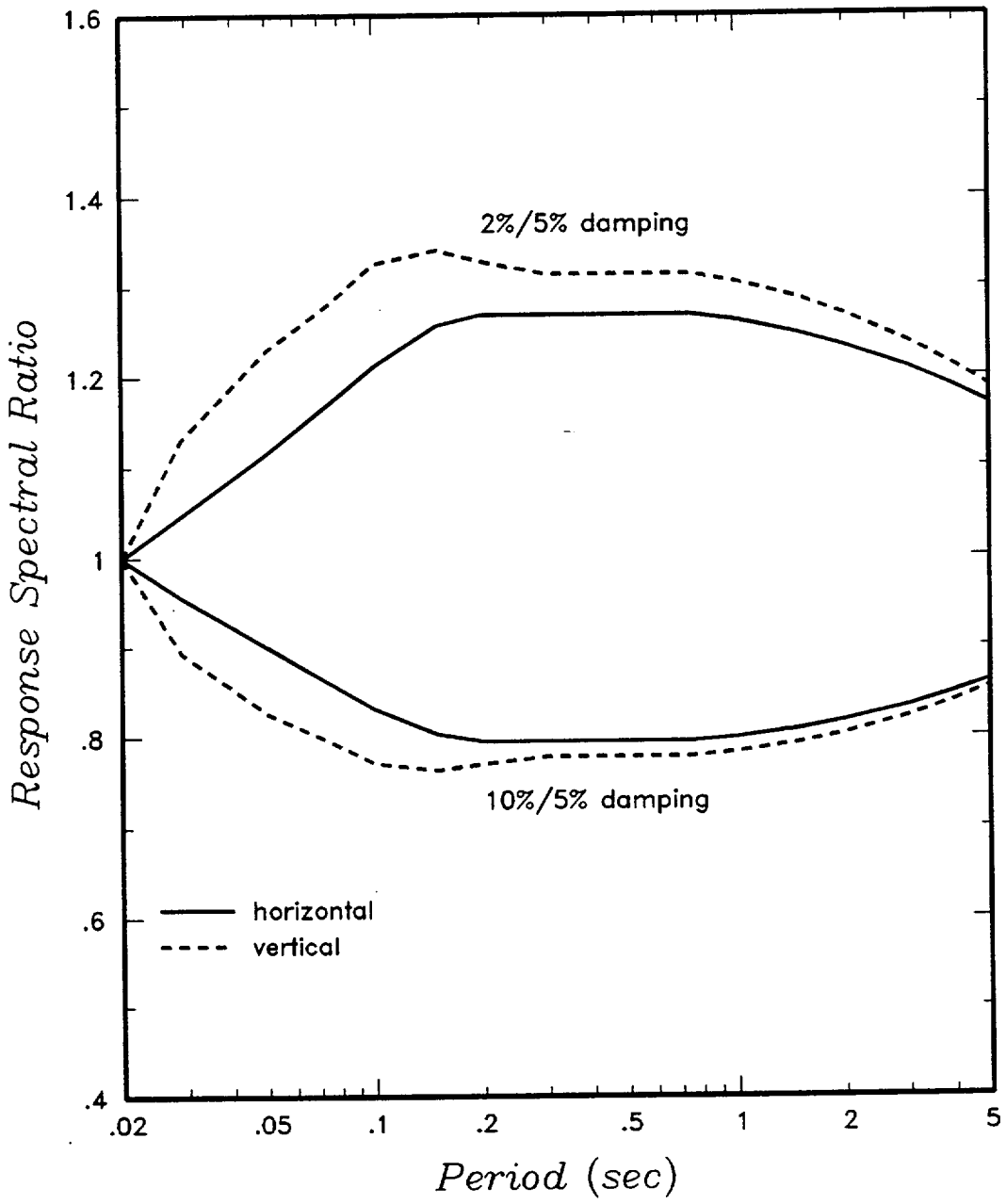

Figure 8 Response spectra damping adjustment factors from Abrahamson and Silva (1996)

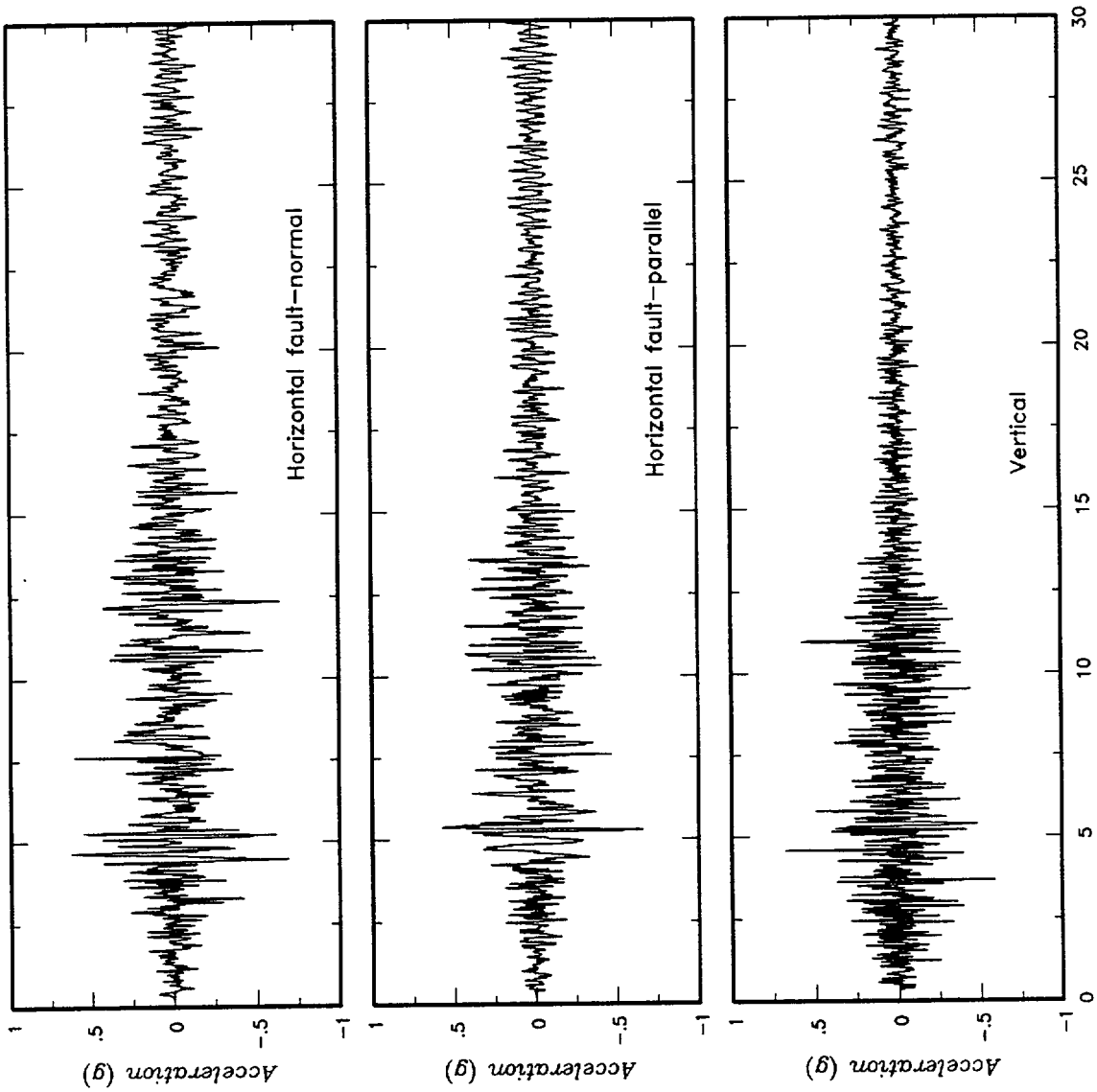

Figure 9 Time Histories from Time-domain Scaling

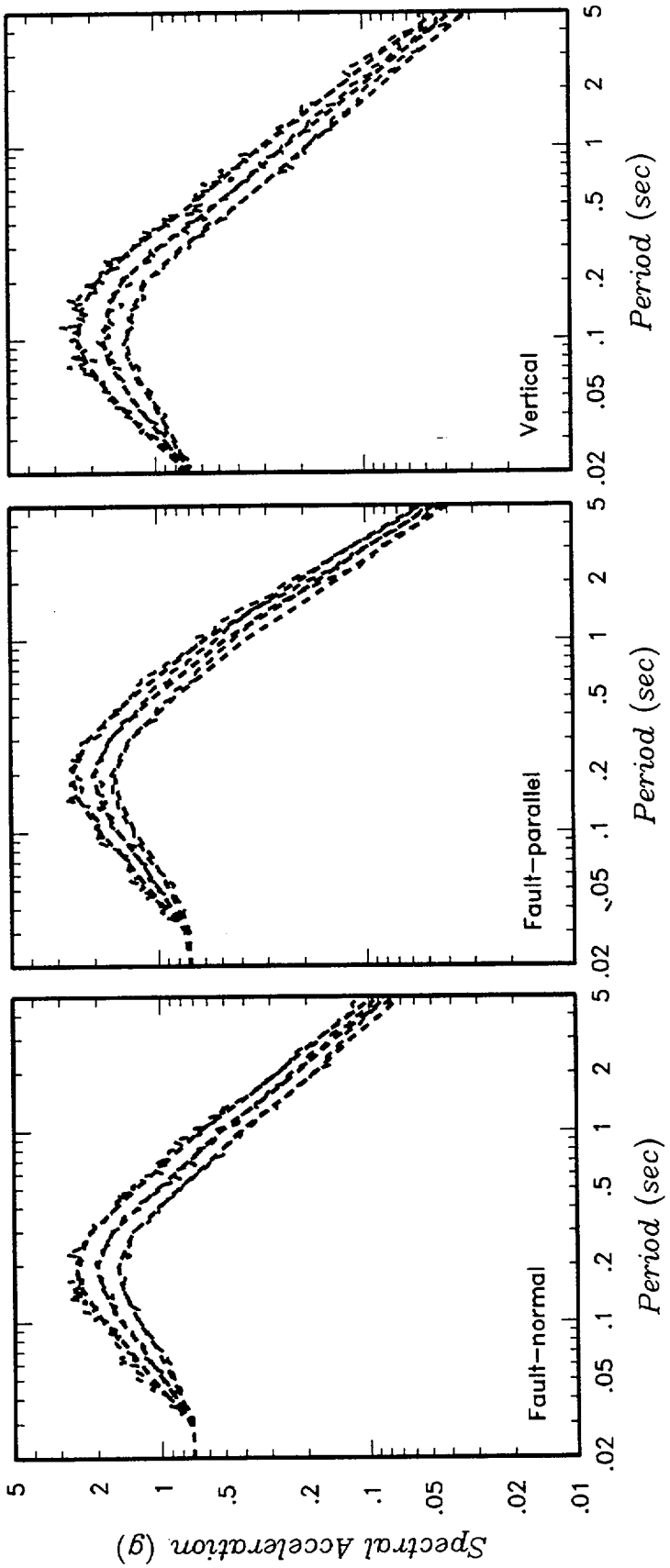

Figure 10 Spectra from Time-domain Scaling Compared to Design Spectra

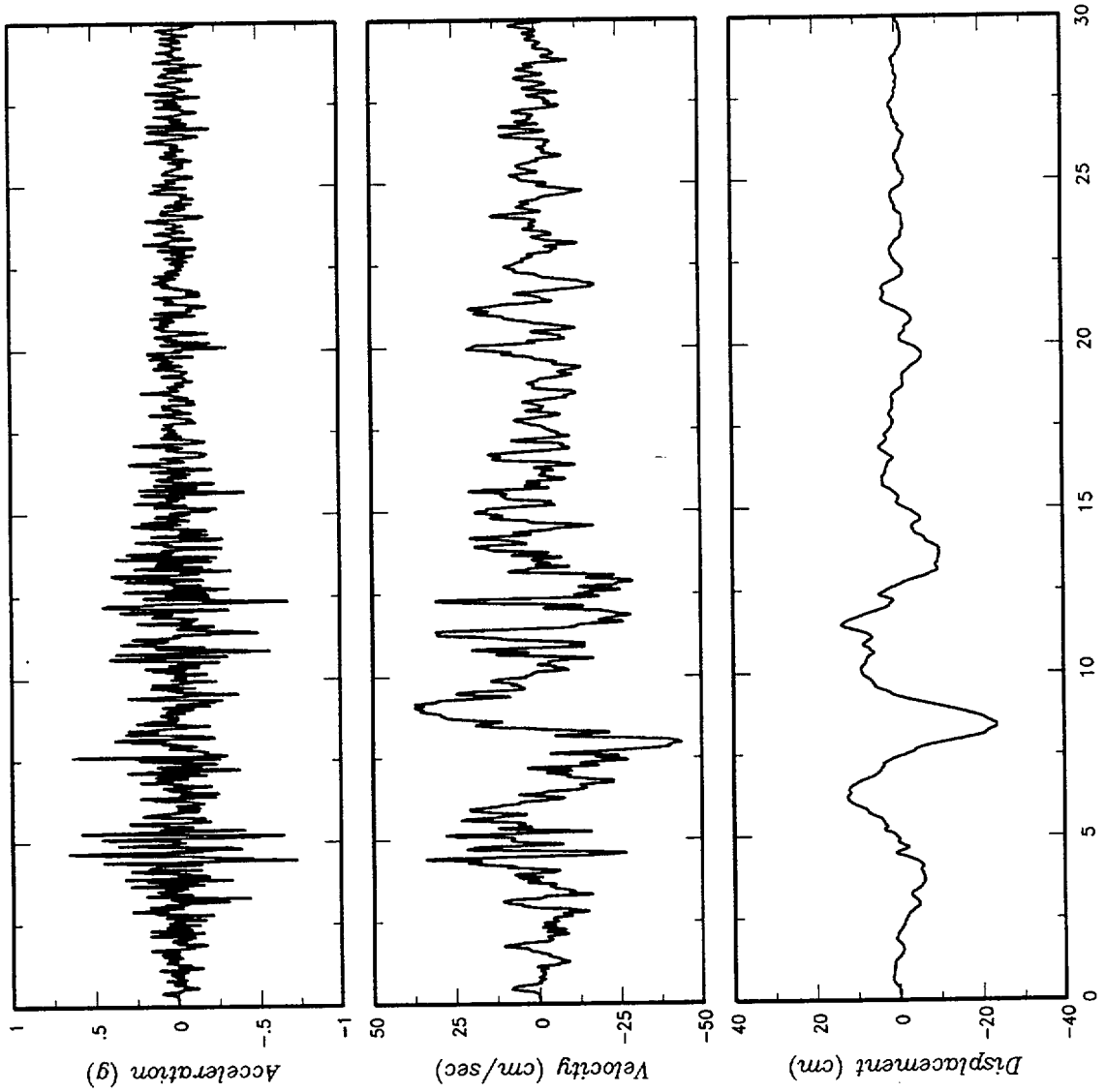

Figure 11 Final Fault–Normal (east–west) Time History

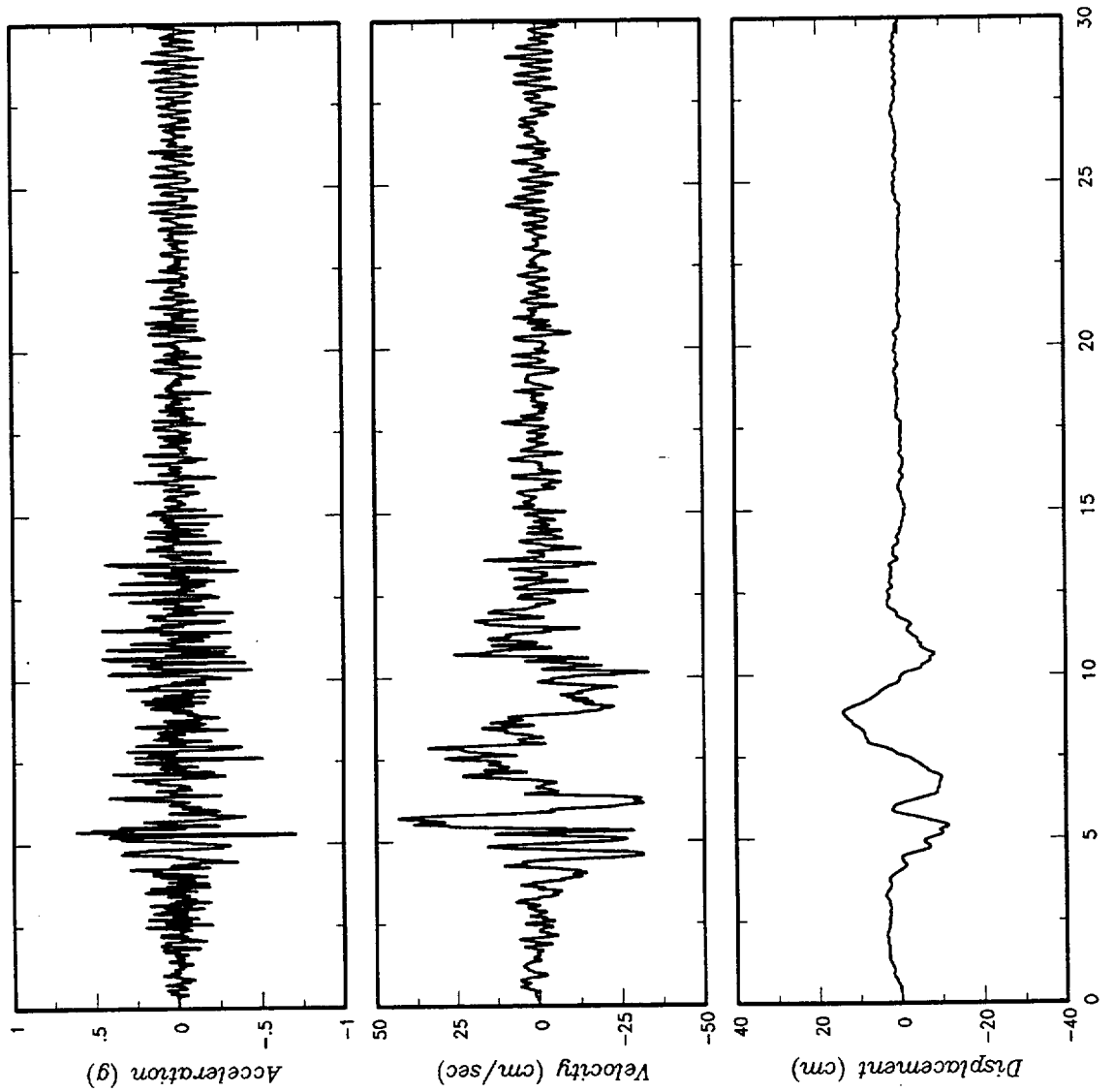

Figure 12 Final Fault-Parallel (north-south) Time History

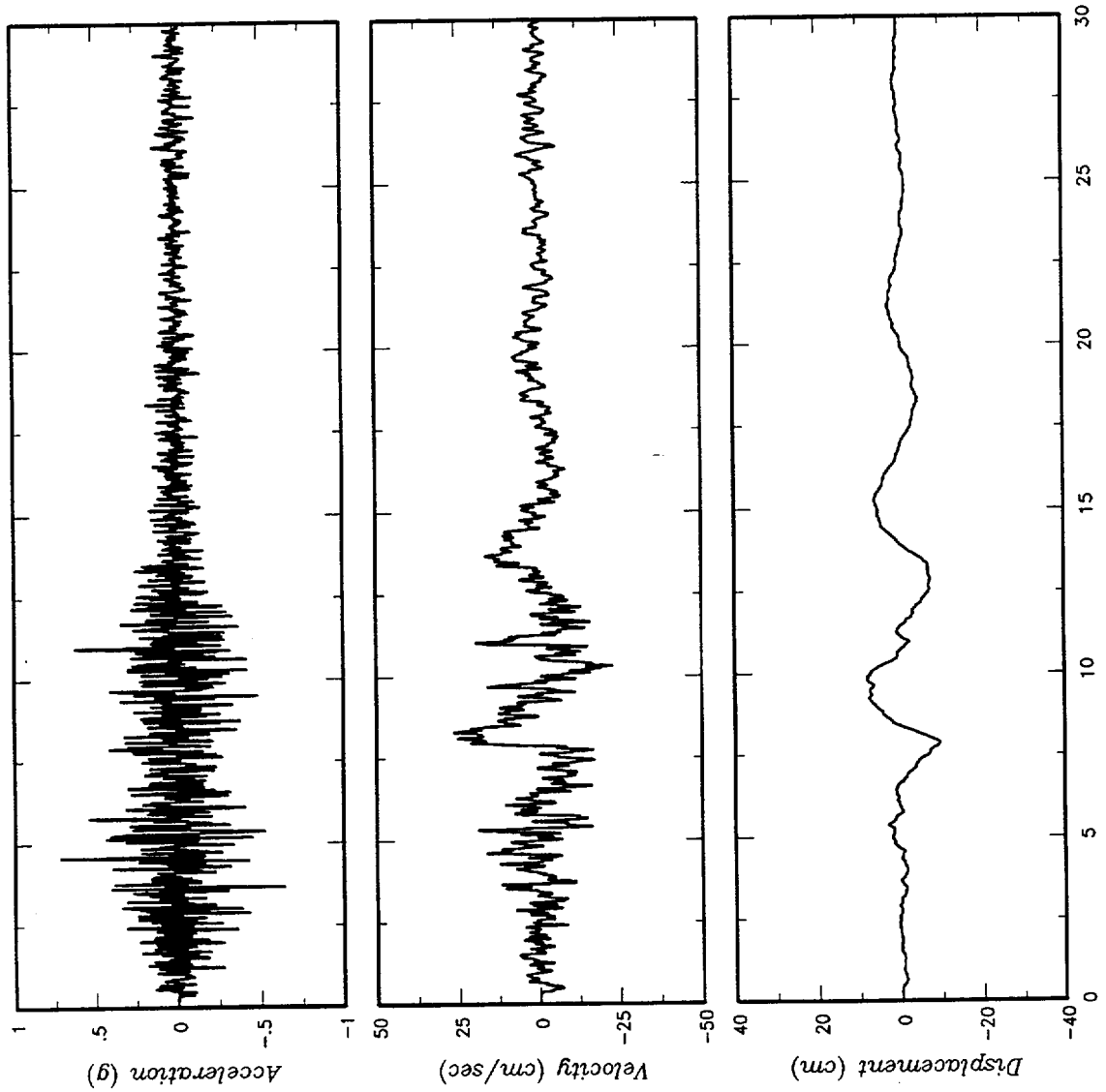

Figure 13 Final Vertical Time History

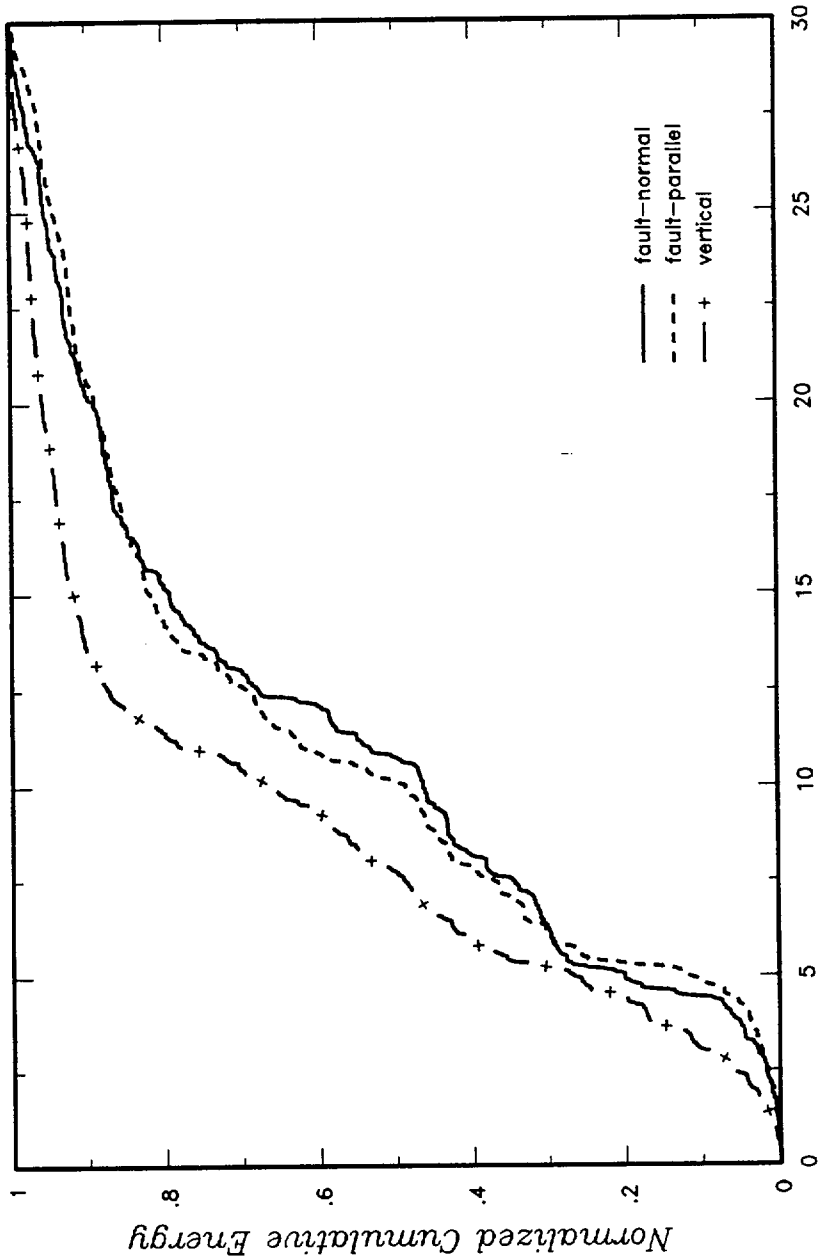

Figure 14 Normalized Cumulative Energy versus Time

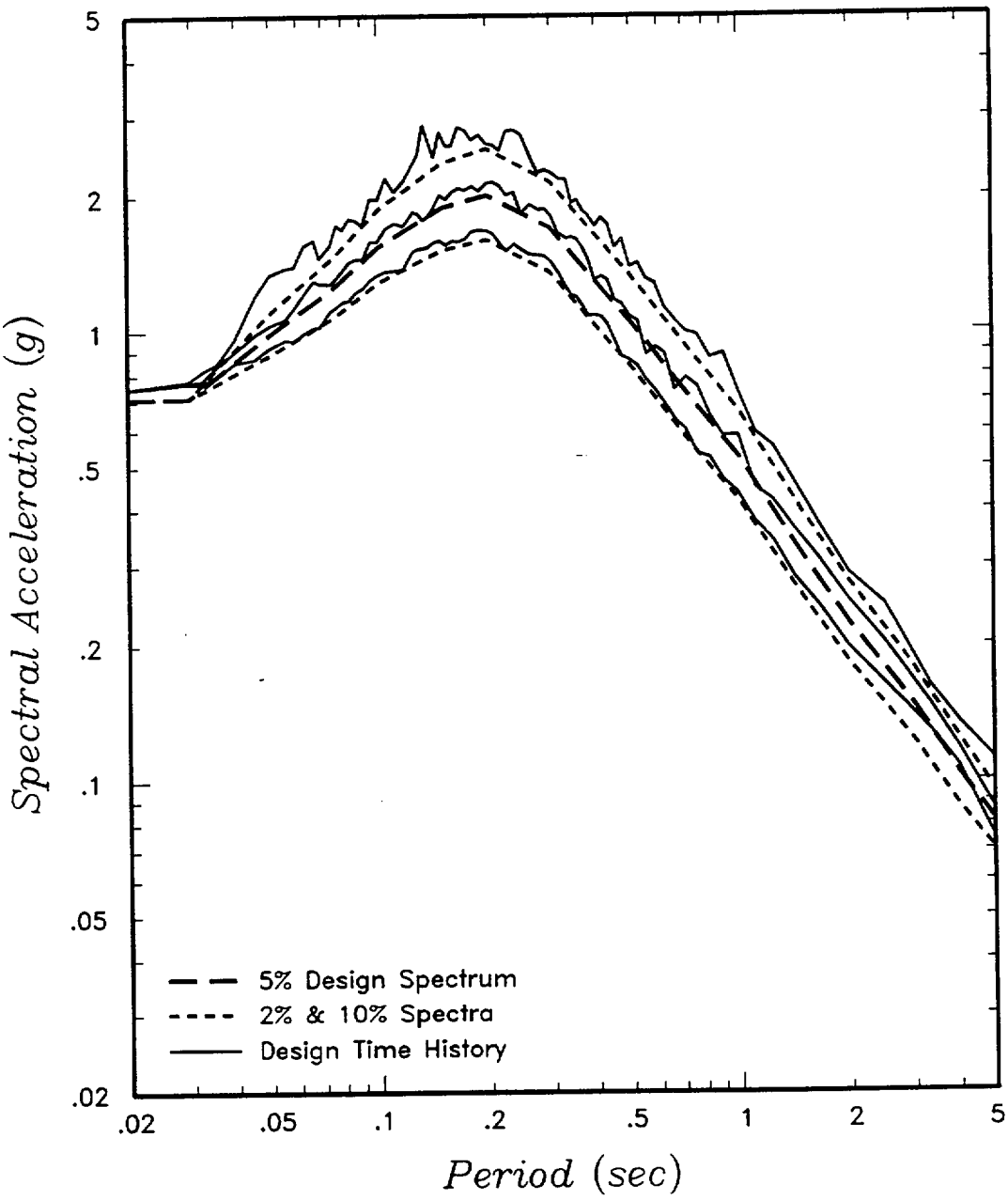

Figure 15 Comparison of Design and Time History Spectra for Fault–normal Component

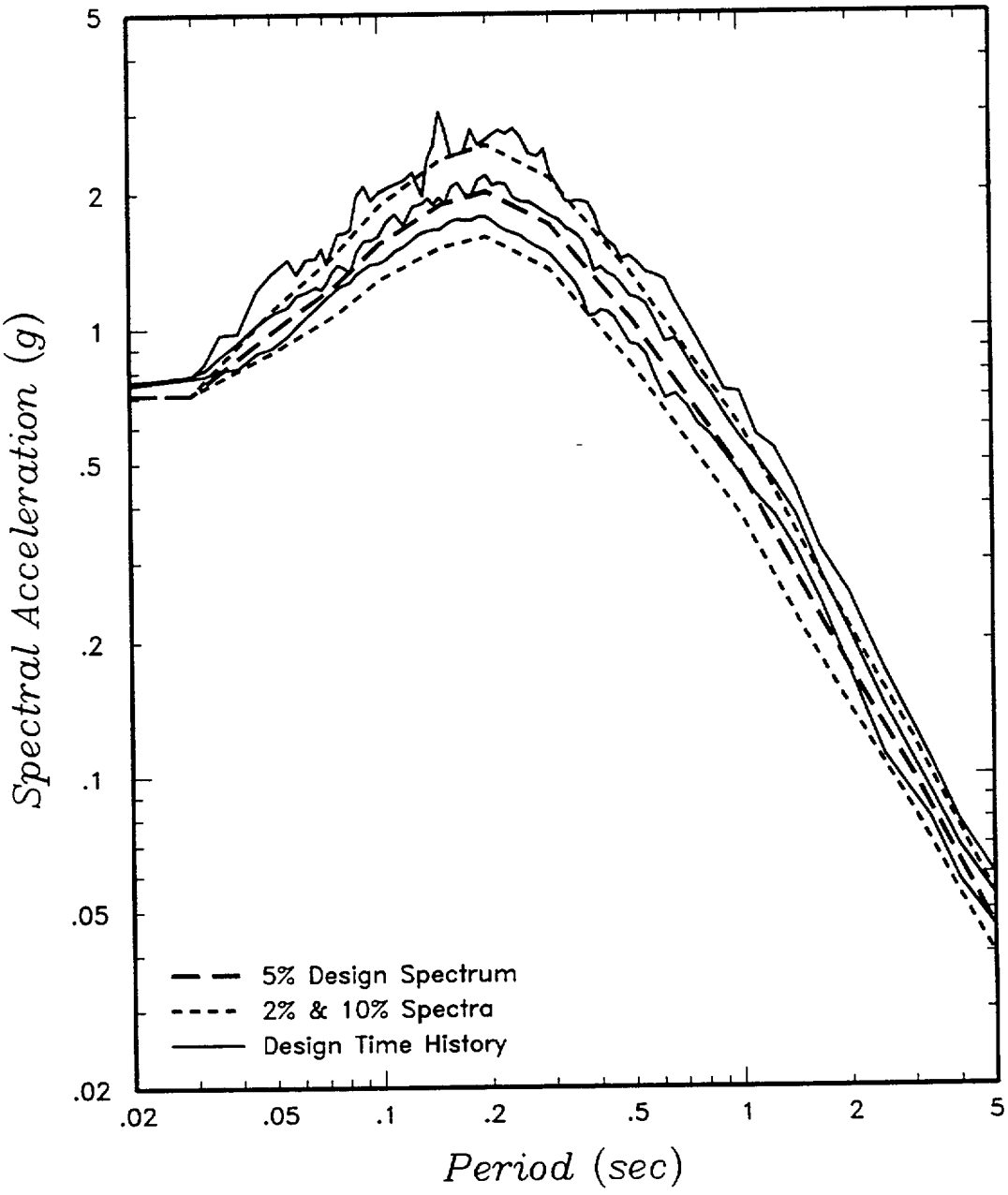

Figure 16 Comparison of Design and Time History Spectra for Fault-parallel Component

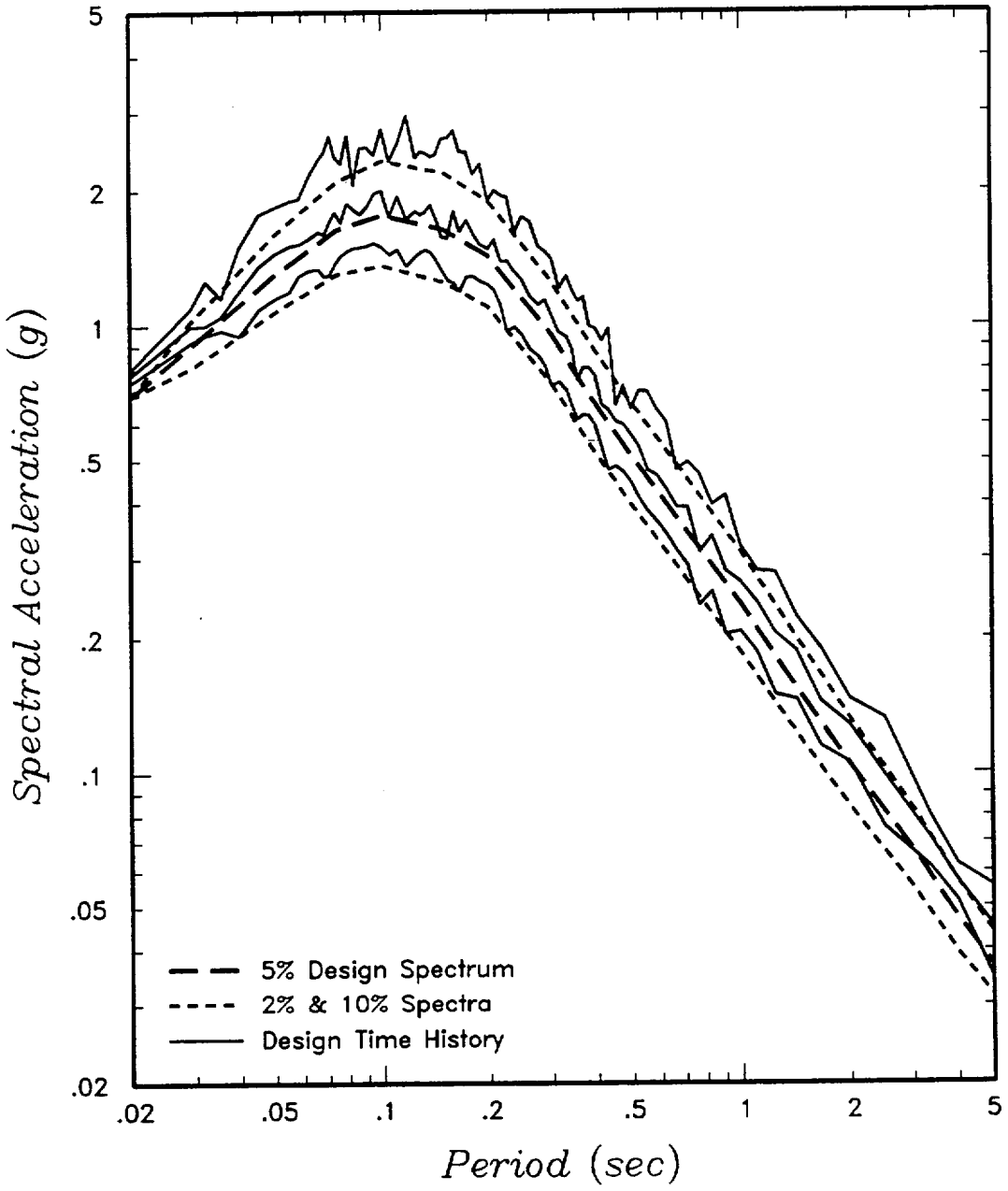

Figure 17 Comparison of Design and Time History Spectra for Vertical Component

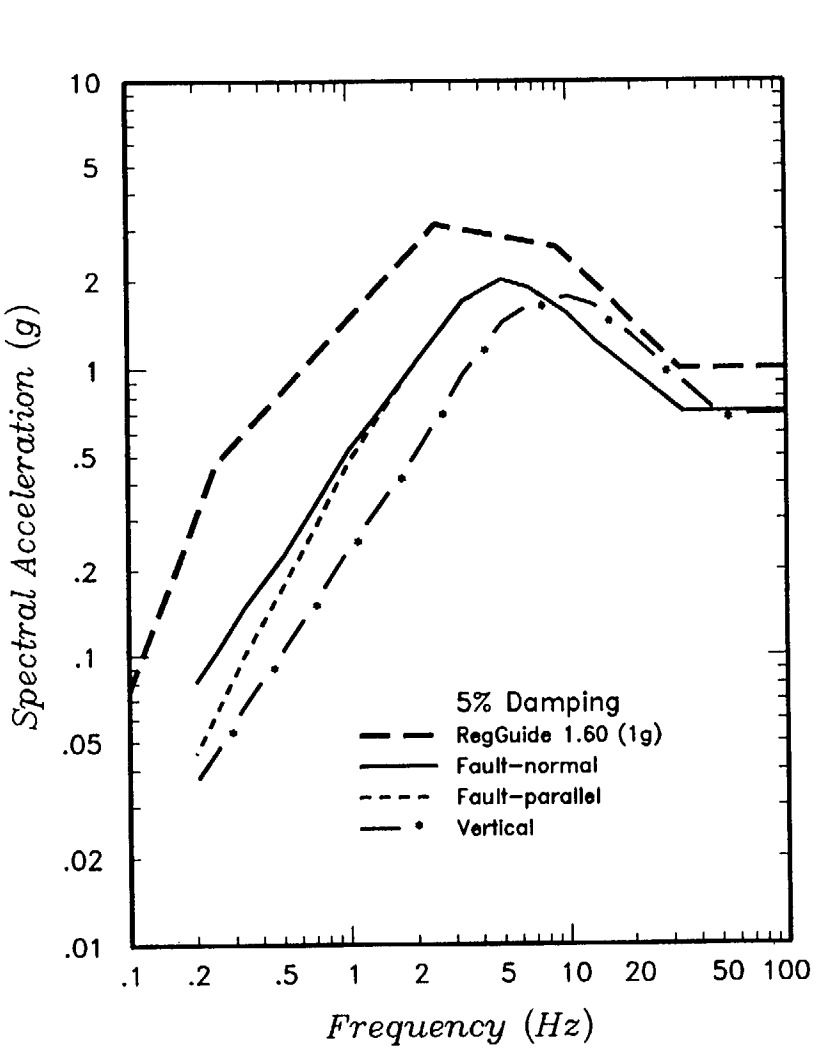

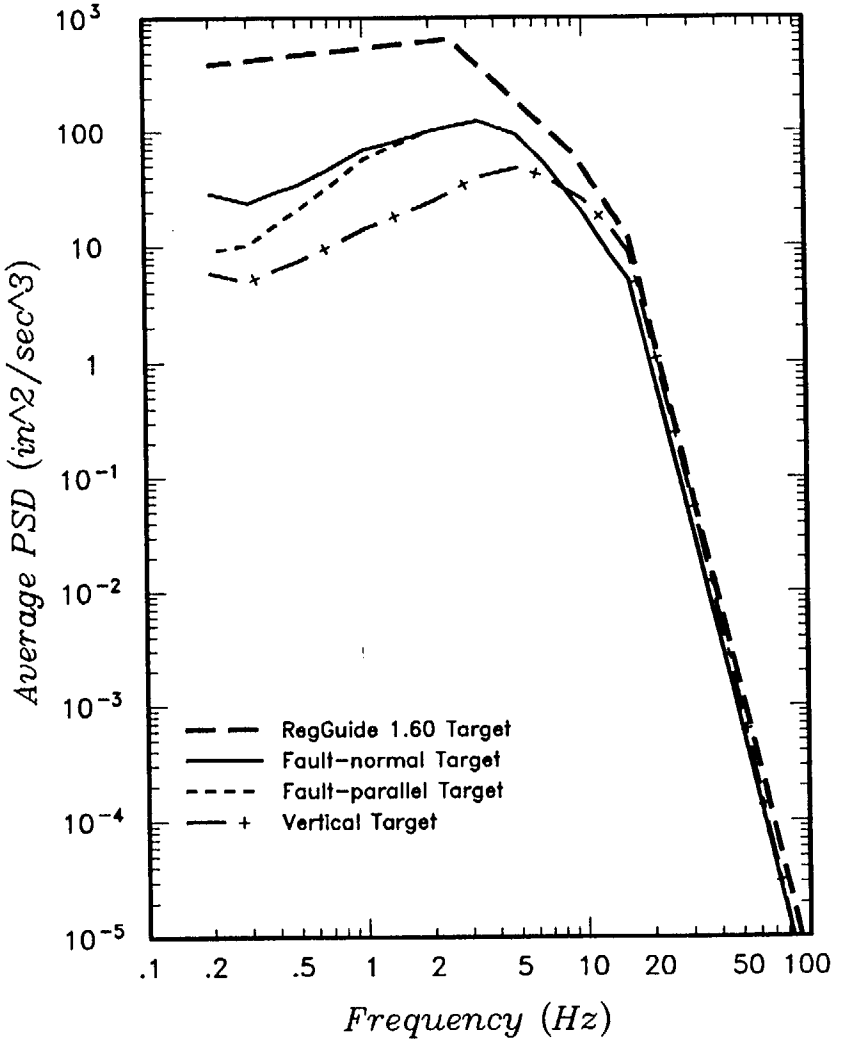

Figure 18 Target PSDs for Design Response Spectra

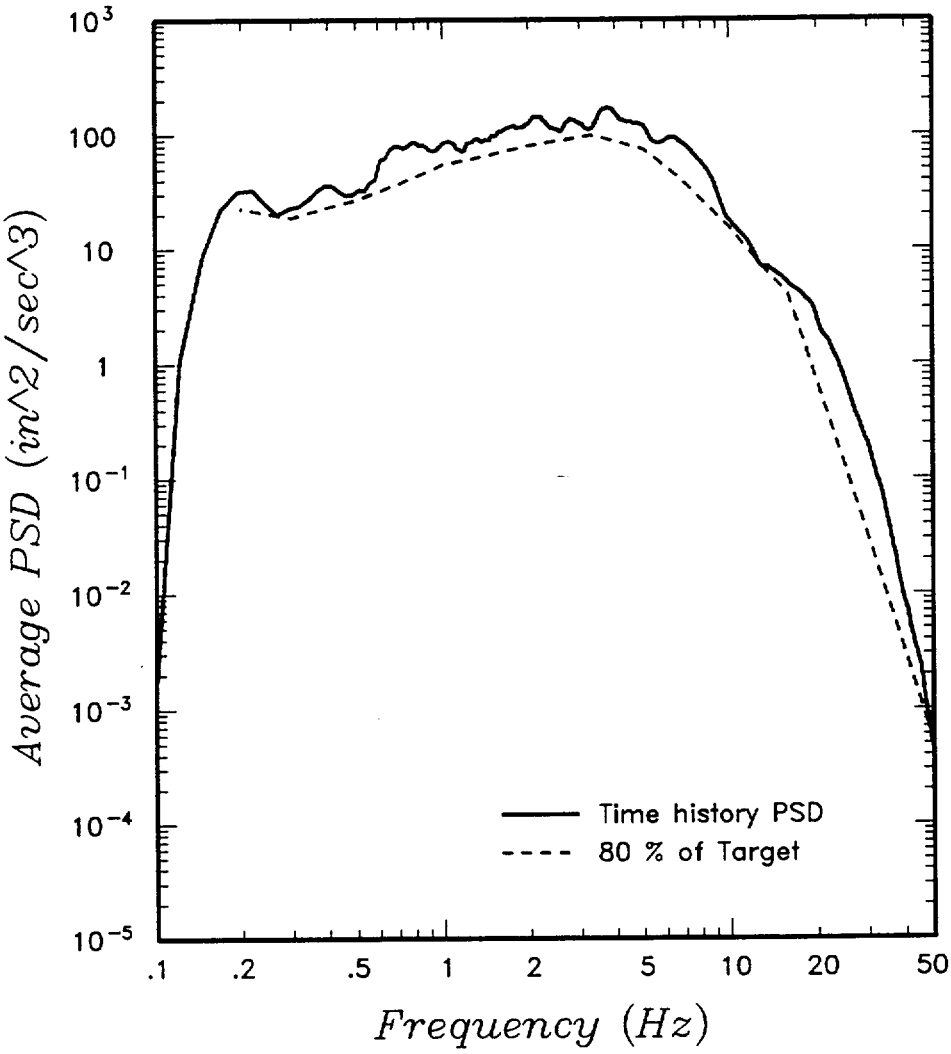

Figure 19 Comparison of Time History PSD to Target PSD for Fault–normal Component

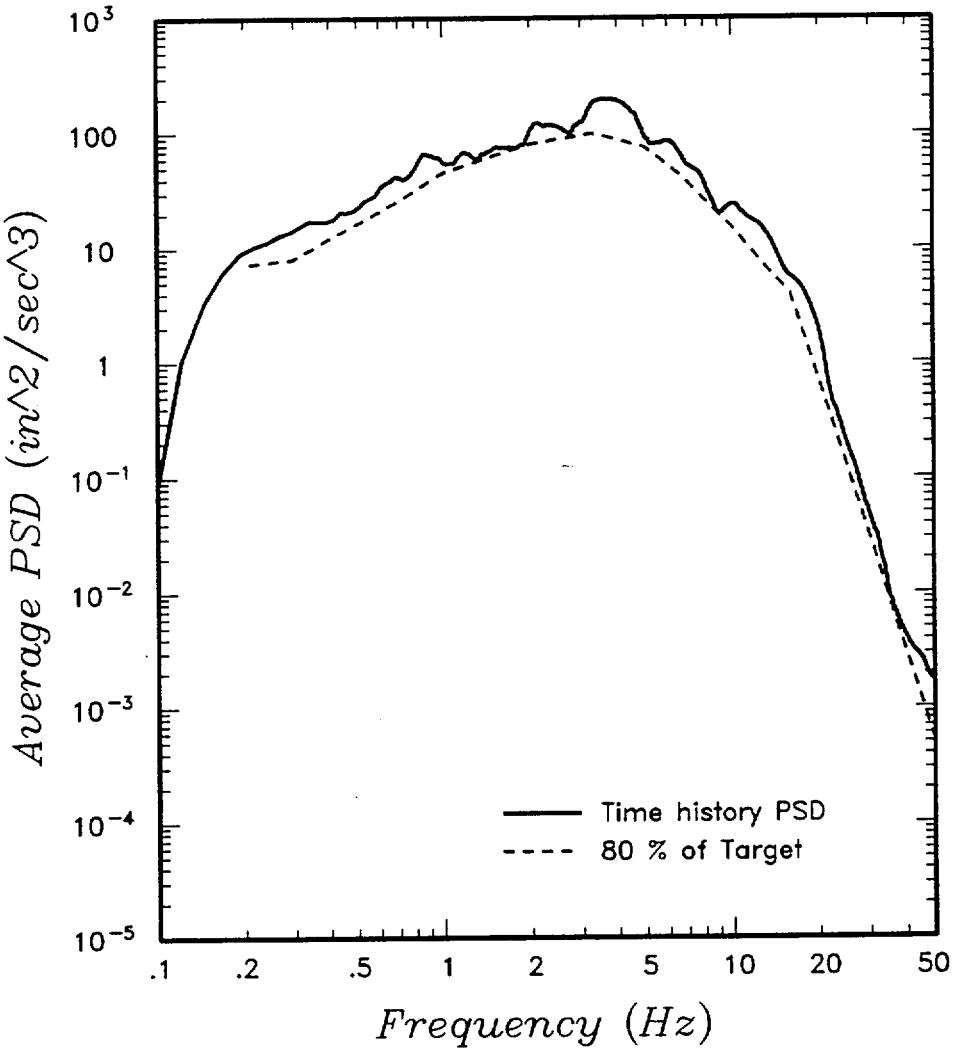

Figure 20 Comparison of Time History PSD to Target PSD for Fault-parallel Component

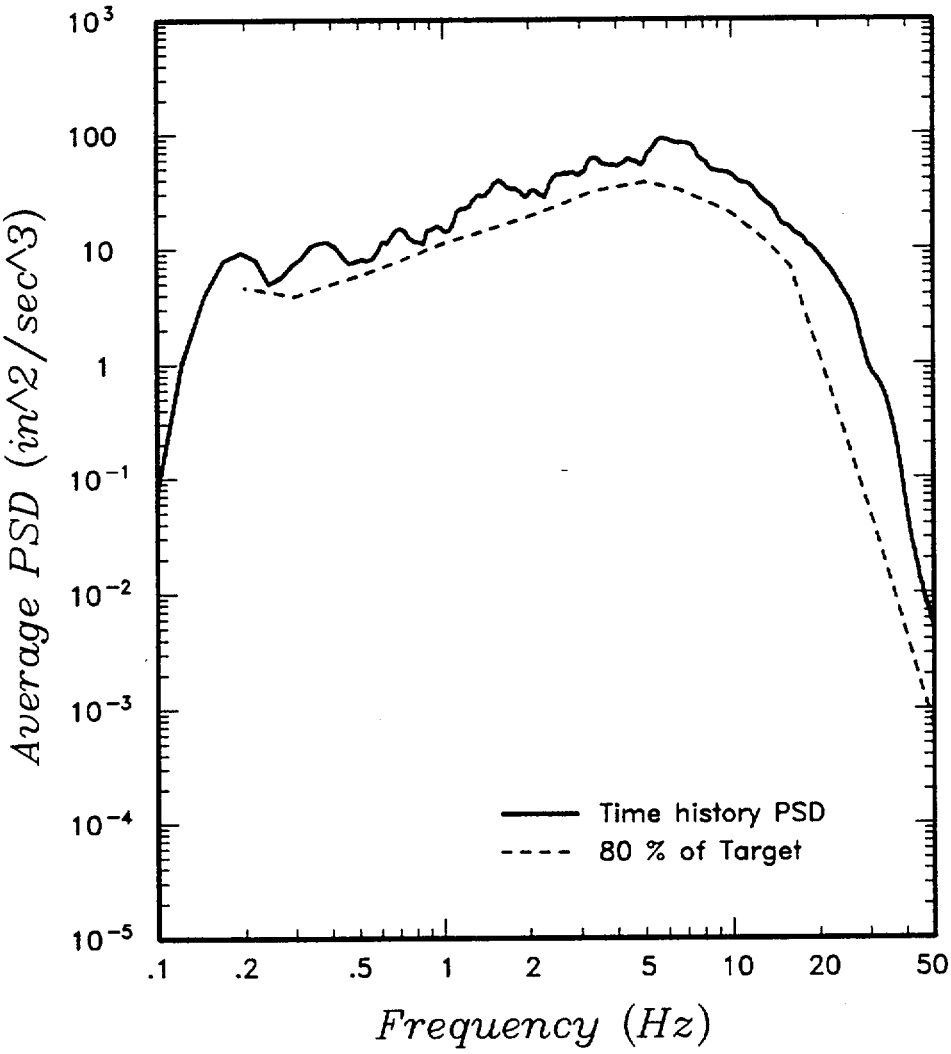

Figure 21 Comparison of Time History PSD to Target PSD for Vertical Component

FAULT EVALUATION STUDY AND SEISMIC HAZARD ASSESSMENT, REVISION 1

History of Revisions

Volume 1

- Revised cover page
  - Added "Revision 1" to title
  - Updated Geomatrix address
  - Updated report date to March 2001

- Section 6
  - Revised pages 88-93
  - Added Table 6-1: 2,000-year Return Period Equal-hazard Spectra
  - Revised Figures 6-8 through 6-24; replaced with Figure 6-8, Rev. 1 through 6-26, Rev. 1

Volume II

- Revised cover page
  - Added "Revision 1" to title
  - Updated Geomatrix address
  - Updated report date to March 2001

Volume III

- Revised cover page
  - Added "Revision 1" to title
  - Updated Geomatrix address
  - Updated report date to March 2001

- Appendix F
  - Revised all pages
  - Figures F-1 through F-17 replaced with Figures F-1. Rev. 1 through F-17, Rev. 1

FINAL REPORT – VOLUME I of III

Fault Evaluation Study and Seismic Hazard Assessment, Revision 1

Private Fuel Storage Facility

Skull Valley, Utah

Prepared for:

Stone & Webster Engineering Corporation
P.O. Box 5406
Denver, Colorado 80217-5406

Prepared by:

Geomatrix Consultants, Inc.
2101 Webster Street, 12th Floor
Oakland, California 94612
(510) 663-4100

March 2001

Project No. 4790.002

VOLUME II – APPENDIXES A – E

Fault Evaluation Study and Seismic Hazard Assessment, Revision 1

Private Fuel Storage Facility

Skull Valley, Utah

Prepared for:

Stone & Webster Engineering Corporation
P.O. Box 5406
Denver, Colorado 80217-5406

Prepared by:

Geomatrix Consultants, Inc.
2101 Webster Street, 12th Floor
Oakland, California 94612
(510) 663-4100

March 2001

Project No. 4790.002

VOLUME III – APPENDIX F

Fault Evaluation Study and Seismic Hazard Assessment, Revision 1

Private Fuel Storage Facility

Skull Valley, Utah

Prepared for:

Stone & Webster Engineering Corporation
P.O. Box 5406
Denver, Colorado 80217-5406

Prepared by:

Geomatrix Consultants, Inc.
2101 Webster Street, 12th Floor
Oakland, California 94612
(510) 663-4100

March 2001

Project No. 4790.002

TABLE OF CONTENTS

TABLE OF CONTENTS
(Continued)

TABLE OF CONTENTS
(Continued)

TABLES

FIGURES

TABLE OF CONTENTS
(Continued)

TABLE OF CONTENTS
(Continued)

PLATES

TABLE OF CONTENTS
(Continued)

APPENDIXES

The above periods of compete catalog reporting were used to estimate the recurrence parameters for each of the seismic source zones using the maximum likelihood technique (Weichart, 1980). Figure 6-8 shows the resulting recurrence relationships compared to the recorded seismicity within each source zone. The uncertainty in the recurrence relationship for each source zone was modeled by specifying a range of possible *b*-values and seismicity rates and computing the relative likelihood that each to the resulting recurrence relationships generated the observed earthquake catalog. These relative likelihoods were normalized into discrete probability distributions for the recurrence parameters (see Figure 6-3).

6.2.2.2 Maximum Magnitude

Most of the large earthquakes that have occurred in the Basin and Range province can be associated with specific faults. For this assessment, we assess the maximum size of an earthquake that might occur on an unrecognizable fault and use this to assign maximum magnitudes to the seismic source zones. Because the hypothesized fault is unrecognized from surface geologic studies, its maximum magnitude is considered to be the largest earthquake that can occur without rupturing the surface (termed the threshold of surface faulting). Wells and Coppersmith (1993) have studied the presence or absence of surface faulting as a function of magnitude. Their studies have shown that the magnitude at which there is a 50% probability of surface faulting is magnitude 6; at magnitude 5.5 the probability is about 20% and at magnitude 6.5 the probability is about 80%. Based on these analyses, we consider the maximum magnitude for an earthquake occurring in the seismic source zones to be uniformly distributed in the range of **M** 5.5 to 6.5, with a mean value of 6.0.

6.3 GROUND MOTION ATTENUATION MODELS

At present, strong motion data recorded in Utah are very limited. In the past, evaluations of seismic hazard, (e.g., Youngs and others, 1987) have typically concluded from examination of the limited strong and weak motion (i.e. seismographic network recordings) that strong ground motion attenuation relationships developed from analysis of California earthquake recordings can be used for Basin and Range sites. However, more recent studies have used examinations of world-wide normal faulting earthquake data together with a variety of modeling techniques to infer that there may be significant differences between strong ground motions in California and those from normal faulting earthquakes in extensional tectonic regimes, such as the Basin and Range region of north-central Utah. Much of this work was reviewed as part of the seismic hazard assessment for the proposed nuclear waste repository at Yucca Mountain, Nevada (CRWMS M&O, 1998). As part of that study, a panel of seven ground motion experts was assembled to provide assessments of the appropriate ground motion models for the Basin and

Range region of southern Nevada. In that study, two basic approaches were used to develop ground motion attenuation relationships, one based on modifications to empirical California strong motion attenuation relationships and one based on numerical modeling. For this study, we utilize results of the Yucca mountain study to adapt California empirical ground motions to the conditions at Skull Valley, Utah. The modifications to the empirical attenuation relationships account for the effects of the characteristics of the earthquake source, the crustal wave propagation path, and the local site geology. The results of the numerical modeling conducted for Yucca Mountain are site-specific to the conditions there and are not directly transferable to the Skull Valley site. Therefore, they were not used in this study.

Appendix F describes the selection and modification of the empirical attenuation models for this study. The Yucca Mountain Ground Motion Expert Panel selected seven empirical ground motion attenuation relationships for modeling rock site motions from normal faulting earthquakes. As discussed in Appendix F, six these were selected to assess horizontal ground motions at the Skull Valley site. These are: Abrahamson and Silva (1997), Boore and others (1997), Campbell (1997), Idriss (1997), Sadigh and others (1997), and Spudich and others (1997). The relationships developed by Abrahamson and Silva (1997), Campbell (1997), and Sadigh and others (1997) also provide assessments of vertical ground motions.

With the exception of the Spudich and others (1997) model, the selected empirical attenuation relationships were developed primarily from California strike-slip and reverse faulting earthquake data. The Yucca Mountain Ground Motion Expert Panel developed five alternative sets of scaling factors to adjust these relationships to normal faulting conditions. For this study we adopted these scaling factors, resulting in twenty alternative attenuation relationships for horizontal motions and eleven for vertical motions. We also adopted the averages of the relative weights assigned to these factors by the seven panel members (see Tables F-1 and F-2).

Following the approach used by the Yucca Mountain Ground Motion Expert Panel, we also adjust the selected attenuation relationships for the lower rate of ground motion attenuation (higher Q) in north-central Utah as compared to California, and for the expected difference in the response of the Skull Valley sediments compared to the California alluvial soils represented in the empirical data used to derive the attenuation relationships. These adjustments are described in Appendix F.

Two alternative site adjustment factors are developed in Appendix F to adjust the rock site attenuation relationships to the subsurface conditions at the Skull Valley site. The first is based on site response modeling. The response of the Skull Valley profile is compared to the response

of profiles appropriate to the rock site attenuation relationships. The second is based on comparing empirical strong motion data recorded on shallow soil sites (the conditions at Skull Valley) to ground motion levels predicted using the rock site attenuation relationships. As discussed in Appendix F, the site adjustment factors based on the site response model are given twice the weight assigned to the empirical site adjustment factors (0.67 versus 0.33 weight).

Figure 6-9 compares the resulting attenuation relationships for horizontal ground motions. Shown on the plots are the estimated ground motions for peak ground acceleration and 5%-damped spectral acceleration at a period of 1.0 second. Each of the six attenuation relationships is shown with the multiple scaling factors for seismic source effects and the two alternative site adjustment factors. Figure 6-10 presents similar comparisons for the vertical attenuation relationships.

6.4 PROBABILISTIC SEISMIC HAZARD RESULTS FOR GROUND SHAKING HAZARD

Seismic hazard calculations were made for peak ground acceleration and 5%-damped response spectral accelerations at periods of 0.075, 0.1, 0.2, 0.3, 0.5, 1.0, 2.0, and 4.0 seconds for horizontal and vertical motions. For hazard computations, the fault-specific sources were modeled as segmented planar surfaces. The areal source zones were modeled as a set of closely spaced parallel fault planes occupying the source regions outlined in Figure 6-7. The probability density function for distance to earthquake rupture for each source was computed assuming earthquake ruptures were uniformly distributed along the length of the fault plane. The depth distribution for earthquakes was based on the observed depth distribution for well-located earthquakes shown on Figure 6-4. The distance density functions were computed consistent with the distance measure used in each of the attenuation relationships. A rectangular rupture area for a given size earthquake is located at a random point on the fault plane. The closest distance to this rectangle was used as the distance measure in the Abrahamson and Silva (1997), Idriss (1997), and Sadigh and others (1997) models. The same distance was used in the Campbell (1997) model, except that the rupture was not allowed to come shallower than two km. For the Boore and others (1997) and Spudich and others (1997) relationships, the rectangular rupture area on the fault was projected vertically to the surface and the closest distance to this surface projection was used.

The rupture size of an event was specified by the relationship $\ln(\text{area}) = 2.095\mathbf{M} - 7.88$ developed from the results presented in Wells and Coppersmith (1994). The specified relationship gives the mean rupture area for a specific magnitude rather than the median (mean log) rupture area. Studies by Bender (1984) have shown that the use of mean estimates of rupture size in the computation of hazard yields results nearly equal to those obtained when the statistical uncertainty in the size of

individual ruptures is incorporated in the analysis. The hazard was computed with the distribution in peak ground motion above the median attenuation relationships truncated at three standard deviations.

Distributions for the annual frequency of exceeding various levels of peak ground acceleration and spectral acceleration were developed by performing hazard computations using Equation **(6-2)** with the input parameters defined by each end branch of the logic trees. The hazard was computed considering the contributions of earthquakes of magnitude **M** 5 and larger (m^0=5). At each ground motion level, the complete set of results forms a discrete distribution for frequency of exceedance, $\nu(z)$. The computed distributions were used to obtain the mean frequency of exceeding various levels of peak ground motion (mean hazard curve) as well as hazard curves representing various percentiles of the distributions. The logic trees represent our best judgement as to the uncertainty in defining the input parameters and thus the computed distributions represent our confidence in the estimated hazard.

6.4.1 Computed Hazard for Horizontal Ground Motions

Figure 6-11 presents the computed mean peak hazard and the 5th- to 95th-percentile hazard curves for peak horizontal acceleration and 5%-damped horizontal spectral acceleration at a period of 1.0 second at the CTB site. The uncertainty band is about ¾ of an order of magnitude in frequency of exceedance at low ground motion levels to an order of magnitude at large ground motion levels. The distribution in computed frequency of exceedance is somewhat skewed with the mean frequency of exceedance lying above the median.

Figure 6-12 shows the contributions of the various seismic sources to the total hazard. The dominating sources are the Stansbury and the East-Springline faults. The relative contribution of the Stansbury fault increases for long period ground motions because of the potential for the occurrence of larger earthquakes on this fault compared to the Skull Valley faults (see Figure 6-6).

Figure 6-13 shows the relative contribution of events in different magnitude intervals to the computed mean hazard. Each plot in the figure presents a histogram of the percent contributions of events in 0.25 magnitude unit-wide intervals separated by distance from the site. Histograms are presented for peak acceleration and spectral acceleration at a period of 1.0 seconds for mean annual frequencies of exceedance of 2×10^{-3}, 5×10^{-4}, and 10^{-4} (return periods of 500, 2,000 and 10,000 years, respectively). The hazard is dominated by ground motions from nearby **M** 6 to 7 events, consistent with the dominance of the Stansbury and East-Springline faults.

The distributions in the computed hazard shown on Figure 6-11 represent the cumulative effect of all levels of parameter uncertainty included in the hazard model logic trees. The relative contribution of various components of the model to the overall uncertainty can be readily identified from the logic tree formulation. This is accomplished by selecting the node for the parameter to be examined and then computing the hazard, giving each branch in succession a weight of unity and all other branches at that node zero weight. For example, the contribution of uncertainty in selecting the appropriate attenuation relationship can be obtained by computing the mean hazard assuming each of the five attenuation relationships is, in turn, the "correct" relationship, with weight of 1.0, and the other five have zero weight. The resulting hazard curves are shown on Figure 6-14. In the plots, the heavy solid curve corresponds to the mean hazard and the light solid curves the 5^{th}- and 95^{th}-percentiles of the distribution in exceedance frequency from Figure 6-11. The six labeled curves are the resulting conditional mean hazard for each of the attenuation relationships. These are then mean results over the alternative source scaling relationships applied to each attenuation relationship (see Appendix F, Table F-1). The difference between the conditional means represent the uncertainty in the computed hazard due to uncertainty in selecting the appropriate attenuation relationship. The results shown on Figure 6-14 indicate that the choice of attenuation relationship is a major contributor to uncertainty in the hazard.

Figures 6-15 and 6-16 show the effect of the alternative scaling factors applied to the empirical attenuation relationships on the computed hazard. Figure 6-15 shows the effect of the alternative source scaling factors on the hazard. It is expected that the "Q only" scaling would produce the highest hazard. However, for peak ground acceleration, the highest hazard results from the use of the Abrahamson and Silva (1997) attenuation relationship (Figure 6-14). The Yucca Mountain Ground Motion Expert Panel did not apply "Q only" scaling to this relationship. Thus the "Q only" scaling curves shown on Figure 6-15 are the weighted combination of the other five attenuation relationships with "Q only" scaling applied. If "Q only" scaling had been applied to the Abrahamson and Silva (1997) relationship, then the combined "Q only" scaling result would have been noticeably higher.

Figure 6-16 shows the effect of the alternative site adjustment factors on the computed hazard. There is a significant effect on the peak acceleration hazard reflecting the significant difference in the two site adjustment factors defined in Appendix F. A low frequencies the two approaches yield similar site adjustment factors, and thus similar hazard levels.

Figures 6-17, 6-18, and 6-19 show the effect of the alternative modeling of the Skull Valley faults (see Figure 6-5) on the hazard computed from these sources alone (the contribution from

the other sources shown on Figure 6-12 is not included). Figure 6-17 shows the effect of the alternative models for the geometry and extent of the West fault. As can be seen from the figure, the alternative models have little effect on the hazard. This is because the East fault dominates the hazard from the Skull Valley faults due to its higher assessed slip rate (see Figure 6-12) and the alternative models for the West fault have only a minor effect on the parameters for the East fault. Similarly, Figure 6-18 shows that consideration of the West fault as an independent source or as a secondary feature for the west fault has a minimal impact on the hazard. Figure 6-19 shows the effect of considering the East and Springline faults to be separate segments or to be linked into a single fault. Considering them to be combined into a single fault produces slightly higher hazard at low probabilities of exceedance and for longer period motions because of the potential for large magnitude earthquakes to occur on the combined source than when they are considered to be separate segments.

Figure 6-20 compares the computed hazard in the western portion of the site area to the hazard at the CTB building. The hazard at the two locations is nearly identical.

6.4.2 Computed Hazard for Vertical Ground Motions

Figure 6-21 presents the computed mean peak hazard and the 5^{th}- to 95^{th}-percentile hazard curves for peak vertical acceleration and 5%-damped vertical spectral acceleration at a period of 1.0 second at the CTB site. The uncertainty band for vertical peak acceleration hazard is similar to that obtained for horizontal peak acceleration, while the uncertainty for vertical spectral acceleration hazard at a period of 1.0 second is somewhat smaller that that obtained for horizontal spectral accelerations.

Figure 6-22 shows the contributions of the various seismic sources to the total hazard for vertical motions. As was the case for horizontal motions, the dominating sources are the Stansbury and the East-Springline faults.

Figure 6-23 shows the effect of the alternative attenuation relationships on the mean hazard for vertical motions. There is greater spread in the hazard results for peak vertical acceleration than for vertical spectral acceleration because the vertical spectral acceleration attenuation relationships produce more similar estimates than the vertical peak acceleration attenuation relationships at close distances (see Figure 6-10).

6.4.3 Contributions to Uncertainty

Figure 6-24 summarizes the contributions to the uncertainty in the total hazard at the CTB site. The plots present histograms showing the relative contribution of the various components of the uncertainty model (logic trees) to the uncertainty in the total hazard at ground motion levels corresponding to a return period of 2,000 years. The components are listed across the bottom and are in order: site adjustment factor (WUS rock to Skull Valley), empirical attenuation model, earthquake source scaling factor (California strike-slip to normal faulting), maximum seismogenic depth of faulting, alternative models for the West fault geometry, independence of the West fault, fault segmentation, fault activity, fault dip, maximum magnitude, seismic source recurrence rate, *b*-value of exponential portions of recurrence relationships, and magnitude distribution model. The major contributors to the uncertainty in the hazard are the selection of the alternative attenuation relationships, selection of the approach to the site adjustment factor, and assessment of maximum magnitude, recurrence rate and form of the magnitude distribution for the faults.

6.4.4 2,000-yr Equal-hazard Spectra

Figure 6-25 shows the mean hazard curves for peak ground acceleration and 5%-damped spectral acceleration at eight spectral periods for horizontal and vertical motions. These hazard curves were interpolated to obtain ground motions with a return period of 2,000 years (annual frequency of exceedance of 5×10^{-4}). Figure 6-26 compares the resulting equal-hazard spectra for horizontal and vertical motions. The spectral accelerations are listed in Table 6-4.

8.0 REFERENCES

Abrahamson, N.A., and Silva, W.J., 1997, Empirical response spectral attenuation relations for shallow crustal earthquakes: Seismological Research Letters, v. 68, p. 94-127.

Anderson, J.G., 1979, Estimating the seismicity from geological structure for seismic risk studies: Bulletin of the Seismological Society of America, v. 69, p. 135-158.

Anderson, J.G., and Hough, S.E., 1984, A model for the shape of the Fourier amplitude spectrum of acceleration at high frequencies: Bulletin of the Seismological Society of America, v. 74, p. 1969-1994.

Anderson, J.G., Wesnousky, S.G., and Stirling, M.W., 1996, Earthquake size as a function of fault slip rate, Bulletin of the Seismological Society of America, v. 86, 3, p 683-690.

Anderson, L.W., and Miller, D.G., 1979, Quaternary fault map of Utah: Long Beach, California, Fugro, Inc., 35 p., scale 1:500,000.

Anderson, N.A., and Silva, W.J., 1997, Empirical response spectral attenuation relations for shallow crustal earthquakes: Seismological Research Letters, v. 68, p. 94-127.

Arabasz, W.J., Pechmann, J.C., and Brown, E.D., 1989, Evaluation of seismicity relevant to the proposed siting of a Superconducting Supercollider (SSC) in Tooele County, Utah: Utah Geological and Mineral Survey Miscellaneous Publication 89-1, 107 p.

Arabasz, W.J., Nava, S.J., and Phelps, W.T., 1997, Mining seismicity in the Wasatch Plateau and Book Cliffs coal mining districts, Utah, USA, in Gibowicz, S.J., and Lasocki, S. (eds.), Rockbursts and Seismicity in Mines: Proceedings of the 4th International Symposium on Rockbursts and Seismicity in Mines/Krakow/Poland, August 11-14.

Barnhard, T.P., and Dodge, R.L., 1988, Map of fault scarps formed on unconsolidated sediments, Tooele 1° x 2° quadrangle, northwestern Utah: U. S. Geological Survey Miscellaneous Field Studies Map MF-1990, scale 1:250,000.

Bender, B., 1984, Seismic hazard estimation using a finite fault rupture model: Bulletin of the Seismological Society of America, v. 74, p. 1899-1923.

Birkeland, P.W., 1984, Soils and Geomorphology: Oxford University Press, New York, 372 p.

Bishop, K.M., 1997, Miocene rock-avalanche deposits, Halloran/Silurian Hills area, southeastern California: Environmental & Engineering Geoscience, v. III, no. 4, p. 501-512.

Bonilla, M.G., 1988, Minimum earthquake magnitude associated with coseismic surface faulting: Bulletin of the Association of Engineering Geologist, v. 25, p. 17-29.

Bonilla, M.G., Mark, R.K., and Lienkaemper, J.J., 1984, Statistical relations among earthquake magnitude, surface rupture length, and surface fault displacement: Bulletin of the Seismological Society of America, v. 74, no. 6, p. 2379-2411.

Boore, D.M., 1983, Stochastic simulation of high-frequency ground motions based on seismological models of the radiated spectra: Bulletin of the Seismological Society of America, v. 73, p. 1865-1894.

Boore, D.M., 1986, Short period P- and S-wave radiation from large earthquakes: Implications for spectral scaling relations: Bulletin of the Seismological Society of America, v. 76, p. 43-64.

Boore, D.M., Joyner, W.B., and Fumal, T.E., 1997, Equations for estimating horizontal response spectra and peak acceleration from western North American earthquakes–A summary of recent work: Seismological Research Letters, v. 68, p. 128-153.

Brimhall, W.H., and Merritt, L.B., 1981, The geology of Utah Lake, implications for resource management: Great Basin Naturalist Memoirs Number 5, p. 24-42, scale 1:250,000.

Bucknam, R.C., 1977, Map of suspected fault scarps in unconsolidated deposits, Tooele 1° x 2° sheet, Utah: U. S. Geological Survey Open-File Report 77-495.

Bucknam, R.C., and Anderson, R.E., 1979, Map of fault scarps on unconsolidated sediments, Delta 1° x 2° quadrangle, Utah: U.S. Geological Survey Open-File Report 79-366, 21 p., scale 1;250,000.

Campbell, K.W., 1997, Empirical near-source attenuation relationships for horizontal and vertical components of peak ground acceleration, peak ground velocity, and pseudo-absolute acceleration response spectra: Seismological Research Letters, v. 68, p. 154-179.

Civilian Radioactive Waste Management System Management and Operating Contractor (CRWMS M&O), 1998, Probabilistic seismic hazard analyses for fault displacement and vibratory ground motion at Yucca Mountain, Nevada: U.S. Department of Energy DE-AC04-94AL85000, Prepared for the U.S. Geological Survey, February 23.

Cook, K.L., Bankey, V., Mabey, D.R., and DePangher, M., 1989, Complete Bouguer gravity anomaly map of Utah: Utah Geological and Mineral Survey Map 122, scale 1:500,000.

Cook, K.L., Gray, E.F., Iverson, R.M., and Strohmeier, M.T., 1980, Bottom gravity meter regional survey of the Great Salt Lake, Utah: in Gwynn, J.W. (ed.), Great Salt Lake, a scientific, historical and economic overview: Utah Geological and Mineralogical Survey Bulletin 116, p. 125-143.

Cook, K.L., Montgomery, J.R., Smith, J.T., and Gray, E.F., 1975, Simple Bouguer gravity anomaly map of Utah: Utah Geological and Mineral Survey Map 37, scale 1:1,000,000.

Coppersmith, K.J., and Youngs, R.R., 1986, Capturing uncertainty in probabilistic seismic hazard assessment within intraplate tectonic environments, in Proceedings, Third U.S. National Conference on Earthquake Engineering: Earthquake Engineering Research Institute, v. 1, p. 301-312.

Cornell, C.A., 1968, Engineering seismic risk analysis: Bulletin of the Seismological Society of America, v. 58, p. 1583-1606.

Cornell, C.A., 1971, Probabilistic analysis of damage to structures under seismic loads, in D.A. Howells, Haigh, I.P., and Taylor, C. (eds.), Dynamic waves in civil engineering: John Wiley, London.

Crone, A.J., 1983, Amount of displacement and estimated age of a Holocene surface faulting event, eastern Great Basin, Millard County, Utah, in Gurgel, K.D., (ed.), Geologic excursion in neotectonics and engineering geology in Utah: Utah Geological and Mineral Survey Special Studies, v. 62, p. 49-55.

Currey, D.R., 1980, Coastal geomorphology of Great Salt Lake and vicinity, in Gwynn, J.W., (ed.), Great Salt Lake–A scientific, historical, and economic overview: Utah Geological and Mineral Survey Bulletin, v. 116, p. 69-82.

Currey, D.R., 1982, Lake Bonneville–selected features of relevance to neotectonic analysis: U. S. Geological Survey Open-File Report 82-1070.

Currey, D.R., Atwood, G., and D.R. Mabey, 1983, Major levels of Great Salt Lake and Lake Bonneville; Utah Geological Survey Map 73, 1:750,000-scale plate.

Currey, E.R., Oviatt, C.G., and Plyler, G.B., 1983, Lake Bonneville stratigraphy, geomorphology, and isostatic deformation in west-central Utah: Utah Geological and Mineral Survey Special Studies 62.

Dobrin, M.B., 1976, Introduction to Geophysical Prospecting (third edition): McGraw-Hill, Inc., New York, 630 p.

Dunne, G.C., 1977, Geology and structural evolution of Old Dad Mountain, Mojave Desert, California: Geological Society of America Bulletin, v. 88, p. 737-748.

Eardley, A.J., and Gvosdetsky, V., 1960, Analysis of Pleistocene core from Great Salt Lake, Utah: Geological Society of America Bulletin, v. 71, p. 1323-1344.

Eardley, A.J., Shuey, R.T., Gvosdetsky, V., Nash, W.P., Picard, M.D., Grey, D.C., and Kukla, G.J., 1973, Lake cycles in the Bonneville basin, Utah: Geological Society of America Bulletin, v. 84, p. 211-216.

Electric Power Research Institute (EPRI), 1988, Seismic hazard methodology for the Central and Eastern United States: NP-4726-A (revised), v. 1-10.

Electric Power Research Institute (EPRI), 1993, Guidelines for determining design basis ground motions: EPRI TR-102293, v. 1-5.

Everitt, B.L., and Kaliser, B.N., 1980, Geology for assessment of seismic risk in the Tooele and Rush Valleys, Tooele County, Utah: Utah Geological Survey Special Studies 51, 33 p.

Geosphere Midwest, 1997, Seismic survey of the Private Fuel Storage Facility, Skull Valley, Utah: report prepared for Stone & Webster Engineering Corporation.

Grose, L.T., 1959, Structure and petrology of the northeast part of the Soda Mountains, San Bernardino County, California: Geological Society of America Bulletin, v. 70, p. 1509-1547.

Gutenberg, B., and Richter, C.F., 1954, Seismicity of the earth and associated phenomena: Princeton, New Jersey, Princeton University Press, 310 p.

Hanks, T.C., 1979, *b* values and ω^{-2} seismic source models: Implications for tectonic stress variations along active crustal fault zones and the estimation of high-frequency strong ground motion: Journal of Geophysical Research, V. 84, p. 2235-2242.

Hanks, T.C., and McGuire, R.K., 1981, The character of high frequency strong ground motion: Bulletin of the Seismological Society of America, v. 71, p. 2071-2095.

Hanks, T.C., Buchnam, R.C., Jajoie, K.R., and Wallace, R.E., 1984, Modifications of wave-cut and faulting-controlled landforms: Journal of Geophysical Research, v. 89, no. B7, p. 5771-5790.

Hecker, S., 1993, Quaternary tectonics of Utah with emphasis on earthquake-hazard characterization: Utah Geological Survey Bulletin 127, 157 p., 2 plates.

Helm, J.M., 1995, Quaternary faulting in the Stansbury fault zone, Tooele County, Utah, in Lund, W.R., (ed.), Environmental and Engineering Geology of the Wasatch Front Region: Utah Geological Association Publication 24, p. 31-44.

Hintze, L.F., (*compiler*), 1988, Geologic map of Utah (scale 1:500,000): Utah Geological and Mineral Survey, Salt Lake City, Utah.

Hood, J.W., and Waddell, K.M., 1968, Hydrologic reconnaissance of Skull Valley, Tooele County, Utah: Utah Department of Natural Resources, Technical Publication No. 18, 57 p.

Jackson, M.E., 1991, Paleoseismology of Utah, volume 3 – the number and timing of Holocene Paleoseismic events on the Nephi and Levan segments, Wasatch fault zone, Utah: Utah Geological Survey Special Studies 78, 23 pp.

Johnson, J.B., and Cook, K.L., 1957, Regional gravity survey of parts of Tooele, Juab, and Millard Counties, Utah: Geophysics, v. 22, p. 48-61.

Hood, J. W., and Waddell, K.M., 1968, Hydrologic reconnaissance of Skull Valley, Tooele County, Utah: Utah Department of Natural Resources, Technical Publication No. 18, 57 p.

Idriss, I.M., 1997, Updated ground motion attenuation relationship for rock sites, published in CRWMS M&O (1998), Ground Motion Characterization Data Packages Volume 1, Section 4.1.3, 2 pg.

Keaton, J.R., Currey, D.R., and Olig, S.J., 1987, Paleoseismicity and earthquake hazards evaluation of the West Valley fault zone, Salt Lake City, Dames and Moore, Final Technical Report for U. S Geological Survey, Contract No. 14-08-0001-22048, 55 p.

Keefer, D.L., and Bodily, S.E., 1983, Three-point approximations for continuous random variables: Management Science, v. 29, p. 595-609.

Kimball, J.K., 1983, The use of site dependent spectra: Proceedings of Conference XXII, A Workshop on "Site-Specific Effects of Soil and Rock on Ground Motion and the Implications for Earthquake-Resistant Design," Santa Fe, New Mexico, July 25-27, U.S. Geological Survey Open File Report 83-845, p. 401-422.

Krinitzsky, E.L., 1989, Empirical earthquake ground motions for an engineering site with fault sources—Tooele Army Depot, Utah: Bulletin of the Association of Engineering Geologists, v. 26, no. 3, p. 283-308.

Kulkarni, R.B., Youngs, R.R., and Coppersmith, K.J., 1984, Assessment of confidence intervals for results of seismic hazard analysis: Proceedings of the Eighth World Conference on Earthquake Engineering, San Francisco, California, v. 1, p. 263-270.

Light, A., and Kaufman, D., 1997, Amino acid paleotemperature reconstruction and radiocarbon shoreline chronology of the Lake Bonneville Basin, USA: Geological Society of America Abstracts with Programs, v. 29, no. 6, p. A-253.

Ludwig, W.J., Nafe, J.E., and Drake, C.L., 1970, Part 1, Regional observations, in Maxwell, A.E., (ed.), New Concepts of Sea Floor Evolution: Wiley Interscience, New York, p. 53-84.

Machette, M.N., and Scott, W.E., 1988, Field trip introduction–A brief review of research on lake cycles and neotectonics of the eastern basin and range province: Utah Geological and Mineral Survey Miscellaneous Publication 88-1, p. 7-14.

Machette, M.N., 1989, Preliminary surficial geologic map of the Wasatch fault zone, eastern part of Utah Valley, Utah County, and parts of Salt Lake and Juab Counties, Utah: U.S. Geological Survey Miscellaneous Field Studies Map MF-2109, scale 1:50,000.

Machette, M.N., Personious, S.F., Nelson, A.R., Schwartz, D.P., and Lund, W.R., 1991, The Wasatch fault zone, Utah-segmentation and history of Holocene earthquakes: Journal of Structural Geology, v. 13, p. 137-149.

Mason, D.B., 1996, Earthquake magnitude potential of the Intermountain seismic belt, USA, from surface-parameter scaling of late Quaternary faults: Bulletin of the Seismological Society of America, v. 86, p. 1487-1506.

Maurer, R.E., 1970, Geology of the Cedar Mountains, Tooele County, Utah: Ph.D. dissertation, University of Utah, Salt Lake City, 184 p., plus maps.

McCalpin, J.P., and Nishenko, S.P., 1996, Holocene paleoseismicity, temporal clustering, and probabilities of future large (M>7) earthquakes on the Wasatch fault zone, Utah: Journal of Geophysical Research, v. 101, no. B3, p. 6233-6253.

Miller, A., and Rice, T., 1983, Discrete approximations to probability distributions: Management Science, v. 29, p. 352-362.

Mohapatra, G.K., and Johnson, R.A., 1998, Localization of listric faults at thrust fault ramps beneath the Great Salt Lake Basin, Utah – evidence from seismic imaging and finite element modeling: Journal of Geophysical Research, v. 103, p. 10,047-10,063.

Mohapatra, G., Petropoulos, G., and Johnson, R.A., 1993, Extension and structural evolution beneath the Great Salt Lake, Utah: Results from reflection seismic imaging (abs): EOS Transactions, v. 74, p. 412.

Moore, W.J., and Sorenson, M.L., 1979, Geologic map of the Tooele 1¡ by 2¡ Quadrangle, Utah: U.S. Geological Survey Miscellaneous Investigations Series Map I-1132, scale 1:100,000.

Morris, H.T., 1987, Preliminary geologic map of the Delta 2° quadrangle, Tooele, Juab, Millard, and Utah Counties, Utah: U.S. Geological Survey Open-File Report 87-185, 18 p., scale 1:250,000.

Mukulich, M., and Smith, R.B., 1974, Seismic reflection and aeromagnetic surveys of the Great Salt Lake, Utah: Geological Society of America Bulletin, v. 85, p. 991-1002.

National Research Council, 1988, Probabilistic seismic hazard analysis: National Academy Press, Washington, D.C., 97 p.

Olig, S.S., Youngs, R.R., and Wong, I., 1998, Preliminary probabilistic seismic hazard analysis for surface fault displacement at TA-3 Los Alamos National Laboratory: Prepared for Los Alamos National Laboratory, University of California, Los Alamos, NM.

Olig, S.S., Lund, W.R., and Black, B.D., 1994, Large mid-Holocene and late Pleistocene earthquakes on the Oquirrh fault zone, Utah: Geomorphology, v. 10, p. 285-315.

Oviatt, C.G., and Currey, D.R., 1987, Pre-Bonneville Quaternary lakes in the Bonneville basin, Utah, in Kopp, R.S., and Cohenour, R.E., (eds.), Cenozoic geology of western Utah–sites for precious metal and hydrocarbon accumulations: Utah Geological Association Publication 16, p. 257-263.

Oviatt, C.G., 1997, Lake Bonneville fluctuations and global climate change: Geology, v. 25, p. 155-158.

Oviatt, C.G., Currey, D.R., and Miller, D.M., 1990, Age and paleoclimatic significance of the Stansbury shoreline of Lake Bonneville, northeastern Great Basin: Quaternary Research, v. 33, p 291-305.

Oviatt, C.G., Currey, D.R., and Sack, D., 1992, Radiocarbon chronology of Lake Bonneville, eastern Great Basin, USA: Palaeogeography, Palaeoclimatology, Palaeoecology, v. 99, p. 225-241.

Oviatt, C.G., and Miller, D.M., 1997, New explorations along the northern shores of Lake Bonneville: Brigham Young University Geology Studies 1997, v. 42, Part II, p. 345-371.

Peacock, D.C.P., and Sanderson, D.J., 1991, Displacements, segment linkage, and relay ramps in normal fault zones: Journal of Structural Geology, v. 13, no. 6, p. 721-733.

Pechmann, J.C., Nash, W.P., Vivieros, J.J., and Smith, R.B., 1987, Slip rate and earthquake potential of the East Great Salt Lake faults, Utah (abs.): EOS Transaction, v. 68, p. 1369.

Perkins, M.E., Brown, F.H., Nash, W.P., McIntosh, W., and William, S.K., 1998, Sequence, age, and source of silicic fallout tuffs in middle to late Miocene basins of the northern basin and range province: Geological Society of America Bulletin, v. 110, no. 3, p. 344-360.

Personius, S.F., 1990, Surficial geologic map of the Brigham City segment and adjacent parts of the Weber and Collinston segments, Wasatch fault zone, Box Elder and Weber counties, Utah: Utah Geological Survey Miscellaneous Investigations Series Map I-1979, scale 1:50,000.

Pezzopane, S.K., and Dawson, T.E., 1996, Fault displacement hazard: A summary of issues and information, in Seismotectonic framework and characterization of faulting at Yucca Mountain, Nevada: U.S. Geological Survey Administrative Report prepared for the U.S. Department of Energy, Chapter 9, 160 p.

Pierce, K.L., and Colman, S.M., 1986, Effect of height and orientation (microclimate) on geomorphic degradation rates and processes, late-glacial terrace scarps in central Idaho: Geological Society of America Bulletin, v. 97, p. 869-885.

Rigby, J.K., 1958, Geology of the Stansbury Mountains, Toole County, Utah: Utah Geological Society Guidebook 13, 168 p.

Rigby, J.K., 1958, Geology of the Stansbury Mountains, Toole County, Utah, in Guidebook to the Geology of Utah: Utah Geological Society, no. 13, 175 p.

Sabetta, F., and Pugliese, A., 1996, Estimation of response spectra and simulation of nonstationary earthquake ground motions: Bulletin of the Seismological Society of America, v. 86, p. 337-352.

Sack, D., 1993, Quaternary geologic map of Skull Valley, Tooele County, Utah: Utah Geological Survey Map 150, Scale 1:100,000.

Sadigh, K., Chang, C.-Y., Egan, J.A., Makdisi, F., and Youngs, R.R., 1997, Attenuation relationships for shallow crustal earthquakes based on California strong motion data: Seismological Research Letters, v. 68, p. 180-189.

Schnabel, P.B., J. Lysmer, and H.B. Seed, 1972, SHAKE: a computer program for earthquake response analysis of horizontally layered sites: Earthquake Engineering Research Institute, University of California, Berkeley, Report EERC 72-12.

Schwartz, D.P., 1987, Earthquakes of the Holocene: Reviews of Geophysics, v. 25, p. 1197-1202.

Senior Seismic Hazard Analysis Committee (SSHAC), 1997, Recommendations for probabilistic seismic hazard analysis – Guidance on uncertainty and use of experts: U.S. Nuclear Regulatory Commission (NRC) NUREG/CR-6372, Washington, D.C.

Shackleton, N.J., and Opdyke, N.D., 1973, Oxygen isotope and paleomagnetic stratigraphy of equatorial Pacific core V28-238–Oxygen isotope temperatures and ice volumes on a 10^5 year and 10^6 year scale: Quaternary Research, v. 3, p. 39-55.

Silva, W., 1986, Soil response to earthquake ground motion: Report prepared for the Electric Power Research Institute, Research Project RP2556-07, September.

Silva, W.J. and R.B. Darragh, 1996, Engineering characterization of strong ground motion recorded at rock sites: Report submitted to the Electric Power Research Institute, EPRI RP 2556-48.

Silva, W.C., Abrahamson, N., Toro, G., and Costantino, C., 1998, Description and validation of the stochastic ground motion model: Report submitted to Brookhaven National Laboratory, Associated Universities, Inc., New York.

Singh, S., and Herrmann, R.B., 1983, Regionalization of crustal coda Q in the continental U.S.: Journal of Geophysical Research, v. 88, p. 527-538.

Smith, R.B., and Arabasz, W.J., 1991, Seismicity in the Intermountain Seismic Belt, in Slemmons, D.B., Engdahl, E.R., Zoback, M.D., and Blackwell, D.D., (eds.), Neotectonics of North America: Geological Society of America, Decade Map Volume 1, Boulder, Colorado, p. 185-228.

Smith, R.B., and Bruhn, R.L., 1984, Intraplate extensional tectonics of the eastern Basin-Range; inferences on structural style from seismic reflection data, regional tectonics,

and thermal-mechanical models of brittle/ductile deformation: Journal of Geophysical Research, v. 89, p. 5733-5762.

Smith, R.B., Richins, W.D., and Doser, D.I., 1985, The 1983 Borah Peak, Idaho earthquake - regional seismicity, kinematics of faulting, and tectonic mechanism: Proceedings of Workshop XXVIII on the Borah Peak, Idaho, Earthquake, v. A, U.S. Geological Survey Open-File Report 85-290, p. 236-263.

Solomon, B.J., 1993, Quaternary geologic maps of Tooele Valley and the West Desert Hazardous Industry Area, Tooele County, Utah: Utah Geological Survey Open-File Report 296, 48 p. 1:24,000 scale.

Spudich, P., Fletcher, J.B., Hellweg, M., Boatwright, J., Sullivan, C., Joyner, W.B., Hanks, T.C., Boore, D.M., McGarr, A., Baker, L.M., and Lindh, A.G., 1997, SEA96 – a new predictive relation for earthquake ground motions in extensional tectonic regimes: Seismological Research Letters, v. 68, p. 190-198.

Stepp, J.C., 1972, Analysis of completeness of the earthquake sample in the Puget Sound area an its effect on statistical estimates of earthquake hazard: Proceedings of the International Conference on Microzonation, v. 2, p. 897-910.

Stone & Webster Engineering Corporation (SWEC), 1997, SAR Chapter 2 – Site characteristics (with Appendices); submitted to Nuclear Regulatory Commission, June 25, 1997.

Suppe, J., 1983, Geometry and kinematics of fault-bend folding: American Journal of Science, v. 283, p. 684-721.

Swan, F.H., III, Schwartz, D.P., and Cluff, L.S., 1980, Recurrence of moderate to large magnitude earthquakes produced by surface faulting on the Wasatch Fault Zone, Utah: Bulletin of the Seismological Society of America, v. 70, no. 5, p. 1431-1462.

Teichert, J.A., 1959, Geology of the southern Stansbury range, Tooele County, Utah: Utah Geological and Mineral Society, Bulletin 65, May.

Tinsley, J.C., King, K.W., Trumm, D.A., Carver, D.L., and Williams, R., 1991, Geologic aspects of shear-wave velocity and relative ground response in the Salt Lake Valley, Utah: Proceedings of the 27th Symposium on Engineering Geology and Geotechnical Engineering, p. 25-1-9.

Tocher, D., 1958, Earthquake energy and ground breakage: Bulletin of the Seismological Society of America, v. 48, no. 2, p. 147-153.

Todd, V.R., 1983, Late Miocene displacement of Pre-Tertiary and Tertiary rocks in the Matline Mountains, northwestern Utah: Geological Society of America Memoir 157, p. 239.

Tooker, E.W., and Roberts, R.J., 1971, Structures related to thrust faults in the Stansbury Mountains, Utah: U.S. Geological Survey Professional Paper 750-B, p. B1-B12.

Topping, D.J., 1993, Paleogeographic reconstruction of the Death Valley extended region–Evidence from Miocene large rock-avalanche deposits in the Amargosa Chaos Basin, California: Geological Society of America Bulletin, v. 105, p. 1190-1213.

U.S. Department of Energy (USDOE), 1997, Topical report YMP/TR-002-NP – Methodology to assess fault displacement and vibratory ground motion hazards at Yucca Mountain, Revision 1: Civilian Radioactive Waste Management System Management and Operating Contractor.

Viveiros, J.J., 1986, Cenozoic tectonics of the Great Salt Lake from seismic reflection data: M.S. thesis, University of Utah, Salt Lake City, Utah, 81 p.

Weichert, D.H., 1980, Estimation of the earthquake recurrence parameters for unequal observation periods for different magnitudes: Bulletin of the Seismological Society of America, v. 70, p. 1337-1346.

Wells, D.L., and Coppersmith, K.J., 1993, Likelihood of surface rupture as a function of magnitude (abs.): Seismological Research Letters, v. 64, no. 1 p. 54.

Wells, D.W., and Coppersmith, K.J., 1994, New empirical relationships among magnitude, rupture length, rupture width, rupture area, and surface displacement, Bulletin of the Seismological Society of America, v. 84, p. 974-1002.

Wesnousky, S.G., 1986, Earthquakes, Quaternary faults, and seismic hazards in California: Journal of Geophysical Research, v. 91, no. B12, p. 12,587-12,631.

Williams, R.A., King, K.W., and Tinsley, J.C., 1993, Site response estimates in Salt Lake Valley, Utah, from borehole seismic velocities: Bulletin of the Seismological Society of America, v. 83, p. 862-889.

Wong, I., and Silva, W.J., 1993, Site-specific strong ground motion estimates for the Salt Lake Valley, Utah: Utah Geological Survey Miscellaneous Publication 93-9, 34 p.

Wong, I., Olig, S., Green, R., Moriwaki, Y., Abrahamson, N., Baures, D., Silva, W., Somerville, P., Davidson, D., Pilz, J., and Dunne, B., 1995, Seismic hazard evaluation of the Magna tailings impoundment: Environmental and Engineering Geology of the Wasatch Front Region, Utah Geological Association Publication 24, p. 95-110.

Woodward, N.B., Boyer, S.B., and Suppe, J., 1989, Balanced geological cross-sections: an essential technique in geological research and exploration: American Geophysical Union Short Course in Geology, v. 6, 132 p.

Youngs, R.R., and Coppersmith, K.J., 1985, Implications of fault slip rates and earthquake recurrence models for probabilistic seismic hazard estimates: Bulletin of the Seismological Society of America, v. 75, p. 939-964.

Youngs, R.R., Swan, F.H., III, Power, M.P., Schwartz, D. P., and Green, R.K., 1987, Analysis of earthquake ground shaking hazard along the Wasatch Front, Utah: in Gori, P.L., and

Hays, W.W. (eds.), Assessment of regional earthquake hazards and risk along the Wasatch Front, Utah, volume II: U.S. Geological Survey Open-File Report 87-585, p. M-1-110.

Zoback, M.L., 1983, Structure and cenozoic tectonism along the Wasatch fault zone, Utah; in Miller D.M., Todd, V.R., and Howard, K.A., (eds.), Tectonic and Stratigraphic Studies in the Eastern Great Basin: Geological Society of America Memoir 157, p. 3-37.

TABLE 6-4

2,000-YEAR RETURN PERIOD EQUAL-HAZARD SPECTRA

Private Fuel Storage Facility
Skull Valley, Utah

Period (sec)	Spectral Acceleration (g)	
	Horizontal	Vertical
PGA	0.707	0.695
0.075	1.246	1.628
0.1	1.541	1.752
0.2	1.983	1.426
0.3	1.677	0.959
0.4	1.278	0.663
0.5	1.045	0.509
1.0	0.475	0.223
2.0	0.164	0.0878
4.0	0.0667	0.0368

Non-GDS

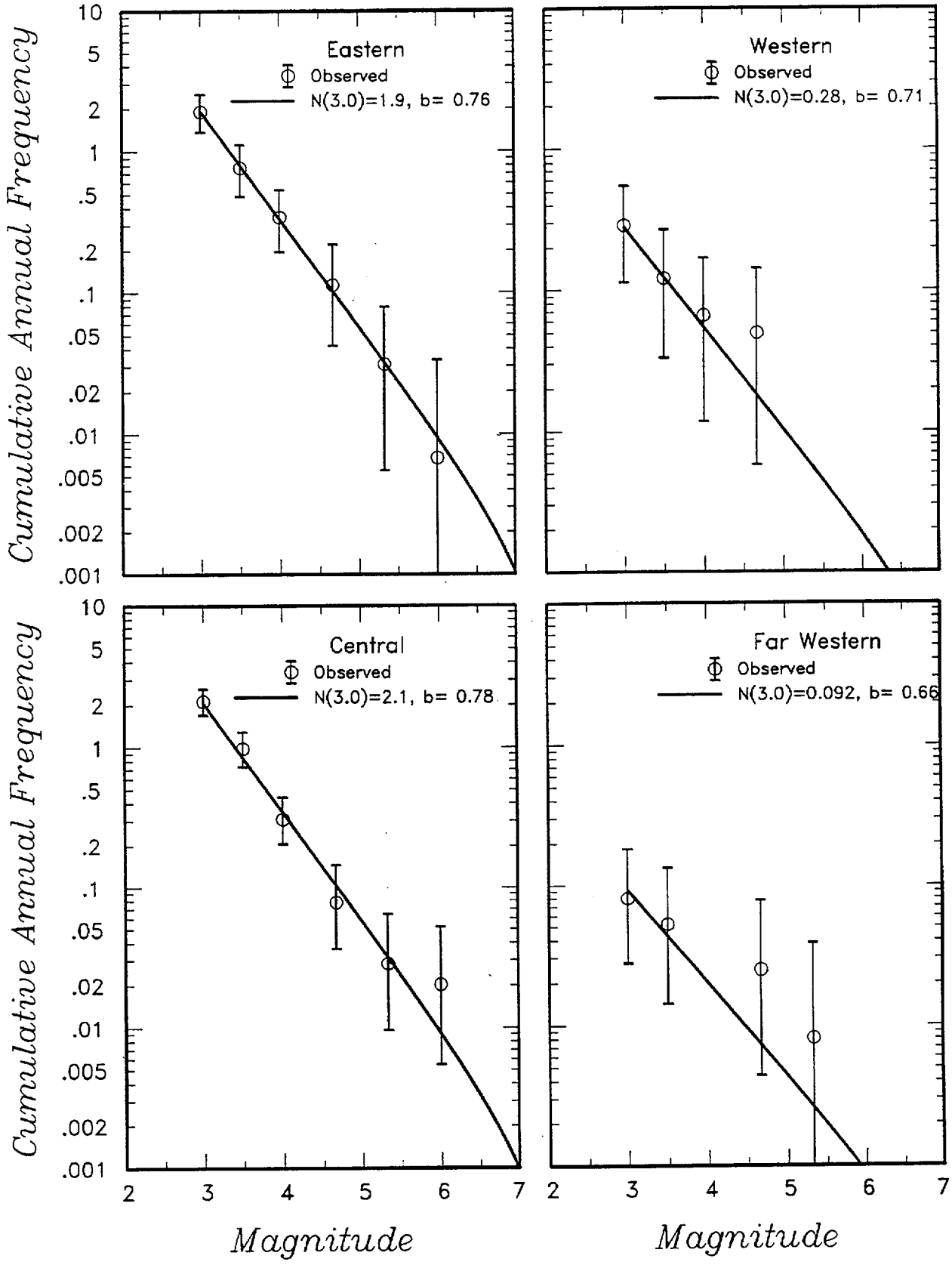

FIG6-8-REV1.DOC

GEOMATRIX

EARTHQUAKE RECURRENCE PARAMETERS FOR THE SEISMIC SOURCE ZONES
Private Fuel Storage Facility
Skull Valley, Utah

Project No. 4790.002

Figure **6-8**

FIG6-9A-REV1.DOC

Non-GDS

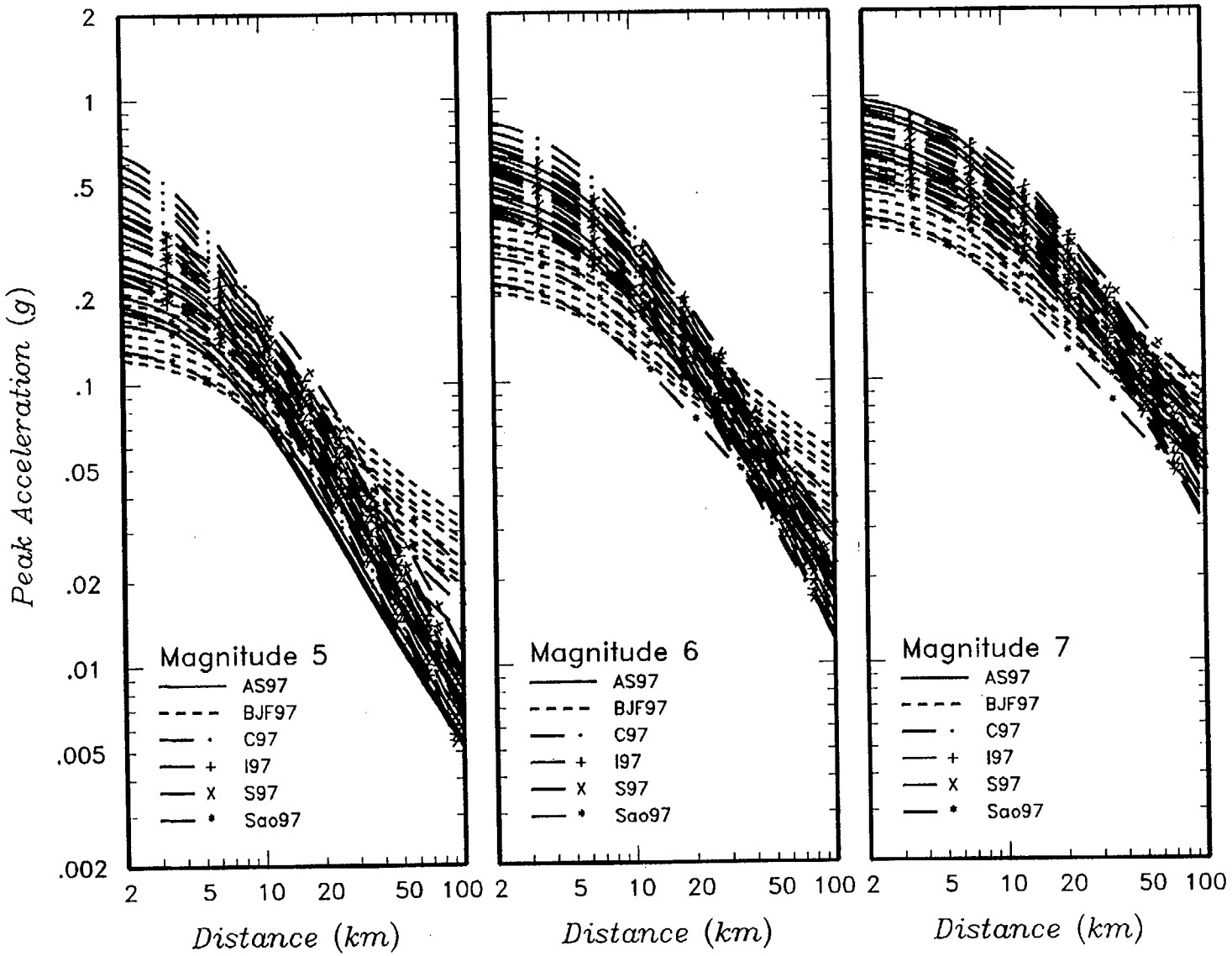

GEOMATRIX

COMPARISON OF HORIZONTAL MOTION ATTENUATION RELATIONSHIPS USED IN THE HAZARD ANALYSIS.
Private Fuel Storage Facility
Skull Valley, Utah
(Page 1 of 2)

Project No.
4790.002

Figure
6-9a

FIG6-9B-REV1.DOC

Non-GDS

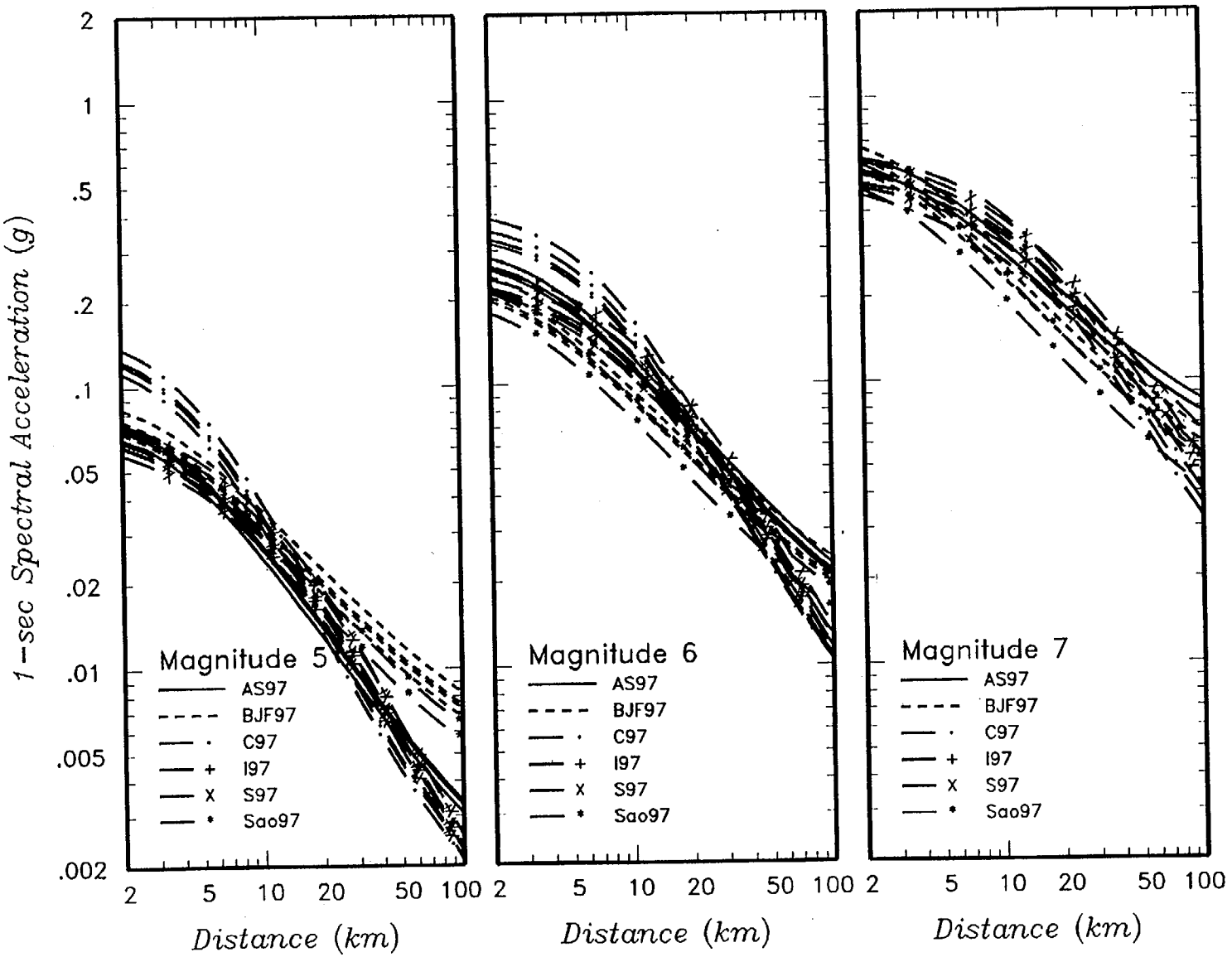

GEOMATRIX

COMPARISON OF HORIZONTAL MOTION ATTENUATION RELATIONSHIPS USED IN THE HAZARD ANALYSIS.
Private Fuel Storage Facility
Skull Valley, Utah
(Page 2 of 2)

Project No.
4790.002

Figure
6-9b

FIG6-10A-REV1.DOC

Non-GDS

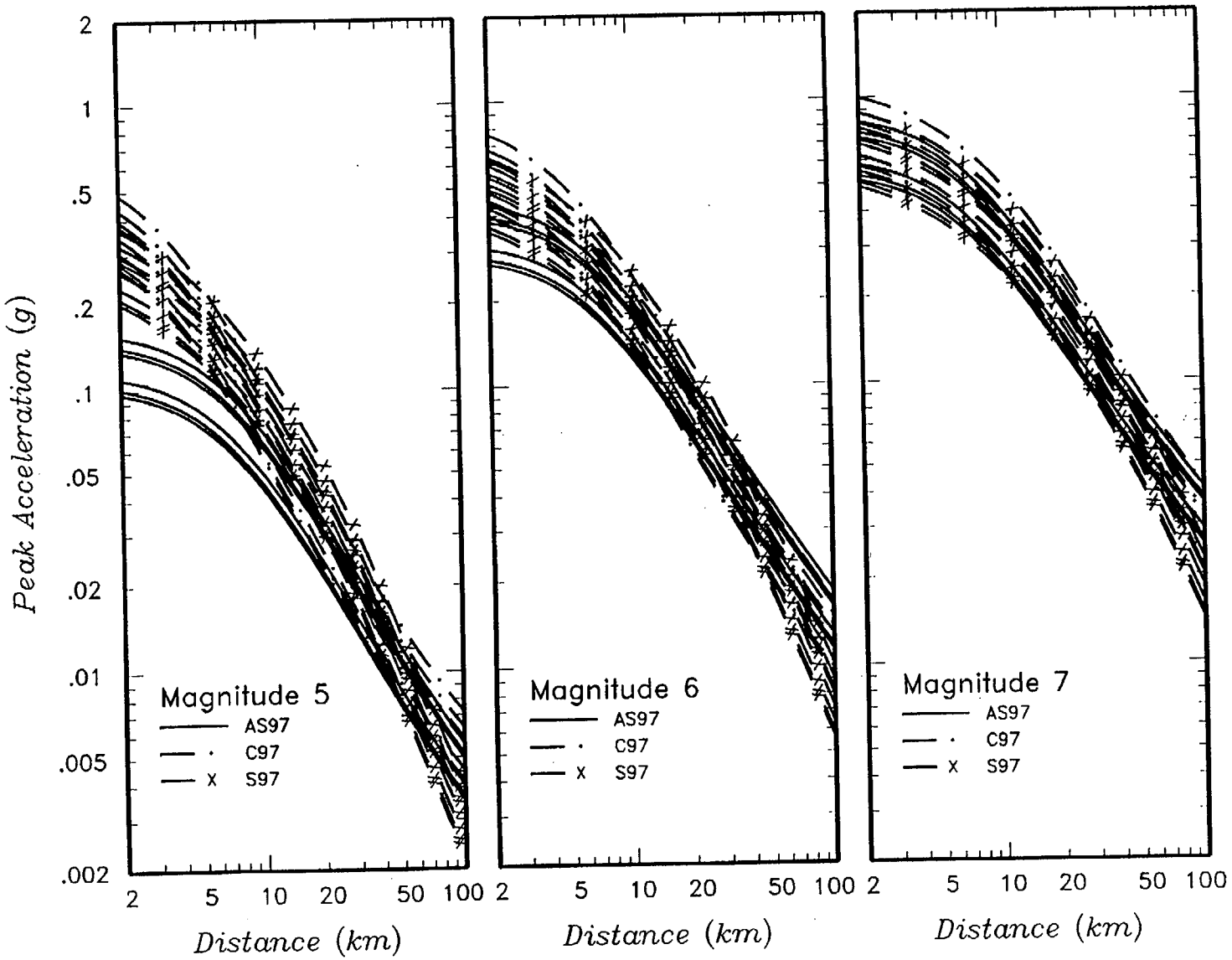

GEOMATRIX

COMPARISON OF VERTICAL MOTION ATTENUATION RELATIONSHIPS USED IN THE HAZARD ANALYSIS.
Private Fuel Storage Facility
Skull Valley, Utah
(Page 1 of 2)

Project No.
4790.002

Figure
6-10a

FIG6-10B-REV1.DOC

Non-GDS

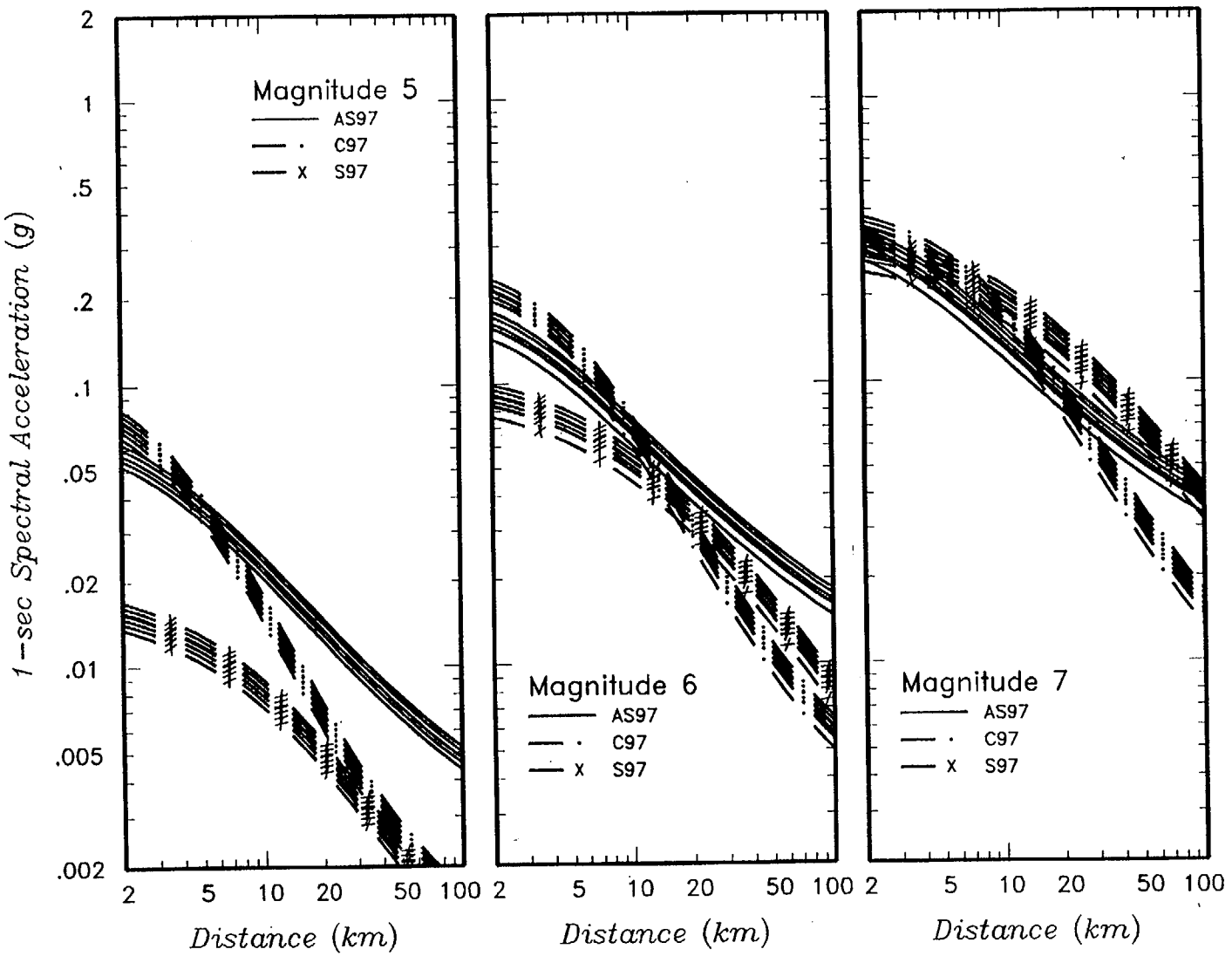

GEOMATRIX

COMPARISON OF VERTICAL MOTION ATTENUATION RELATIONSHIPS USED IN THE HAZARD ANALYSIS.
Private Fuel Storage Facility
Skull Valley, Utah
(Page 2 of 2)

Project No.
4790.002

Figure
6-10b

FIG6-11-REV1.DOC

Non-GDS

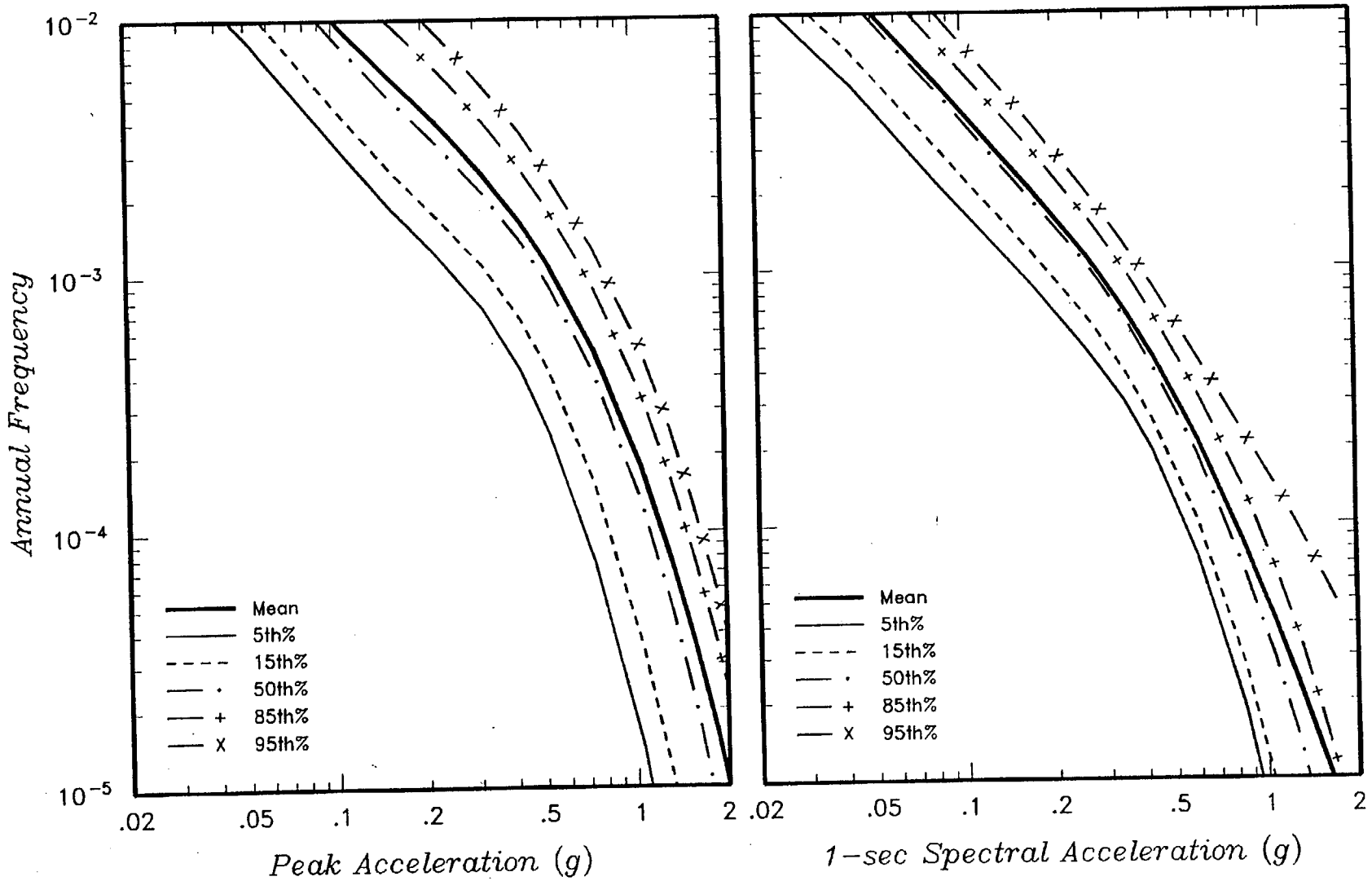

GEOMATRIX

COMPUTED TOTAL MEAN AND 5TH- TO 95TH-PERCENTILE
HORIZONTAL MOTION HAZARD CURVES FOR THE CTB SITE.
Private Fuel Storage Facility
Skull Valley, Utah

Project No.
4790.002

Figure
6-11

FIG6-12-REV1.DOC

Non-GDS

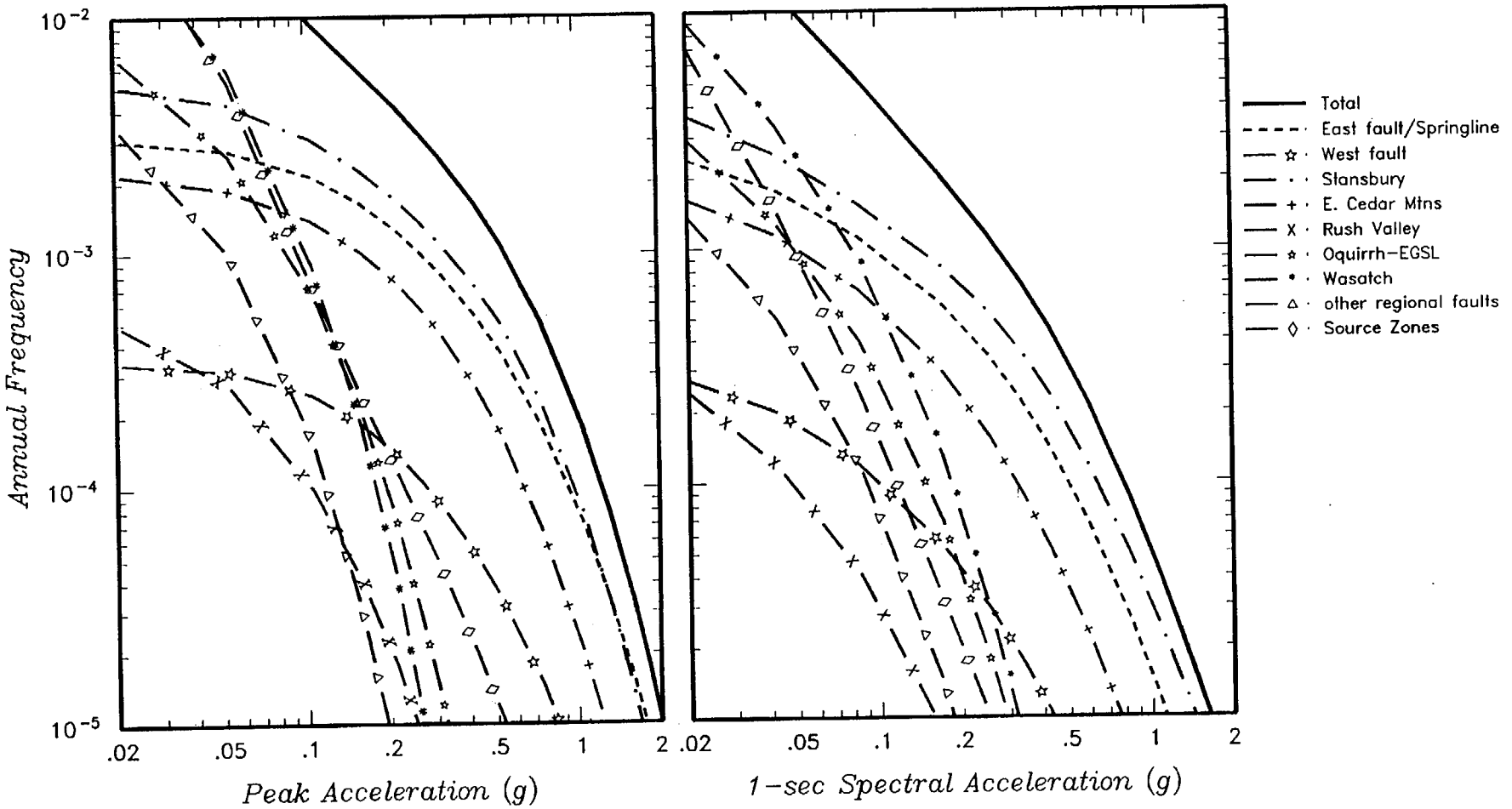

GEOMATRIX

CONTRIBUTIONS OF INDIVIDUAL SOURCES TO TOTAL MEAN HAZARD FOR HORIZONTAL MOTION AT THE CTB SITE.
Private Fuel Storage Facility
Skull Valley, Utah

Project No. 4790.002

Figure **6-12**

Non-GDS

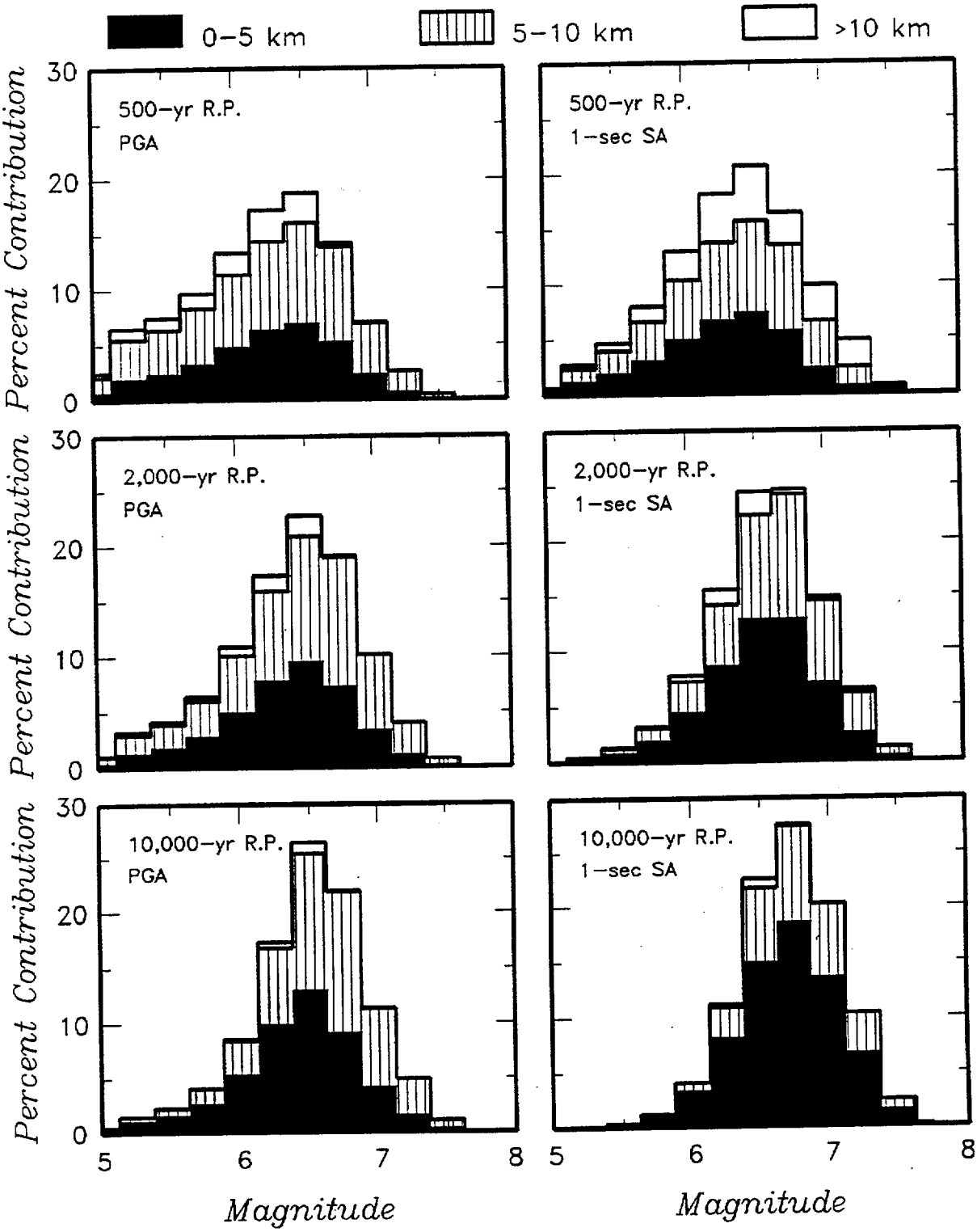

FIG6-13-REV1.DOC

GEOMATRIX

RELATIVE CONTRIBUTION OF EVENTS IN VARIOUS MAGNITUDE INTERVALS SEPARATED BY DISTANCE TO TOTAL MEAN HAZARD FOR HORIZONTAL MOTION AT THE CTB SITE.
Private Fuel Storage Facility
Skull Valley, Utah

Project No.
4790.002

Figure
6-13

FIG6-14-REV1.DOC

Non-GDS

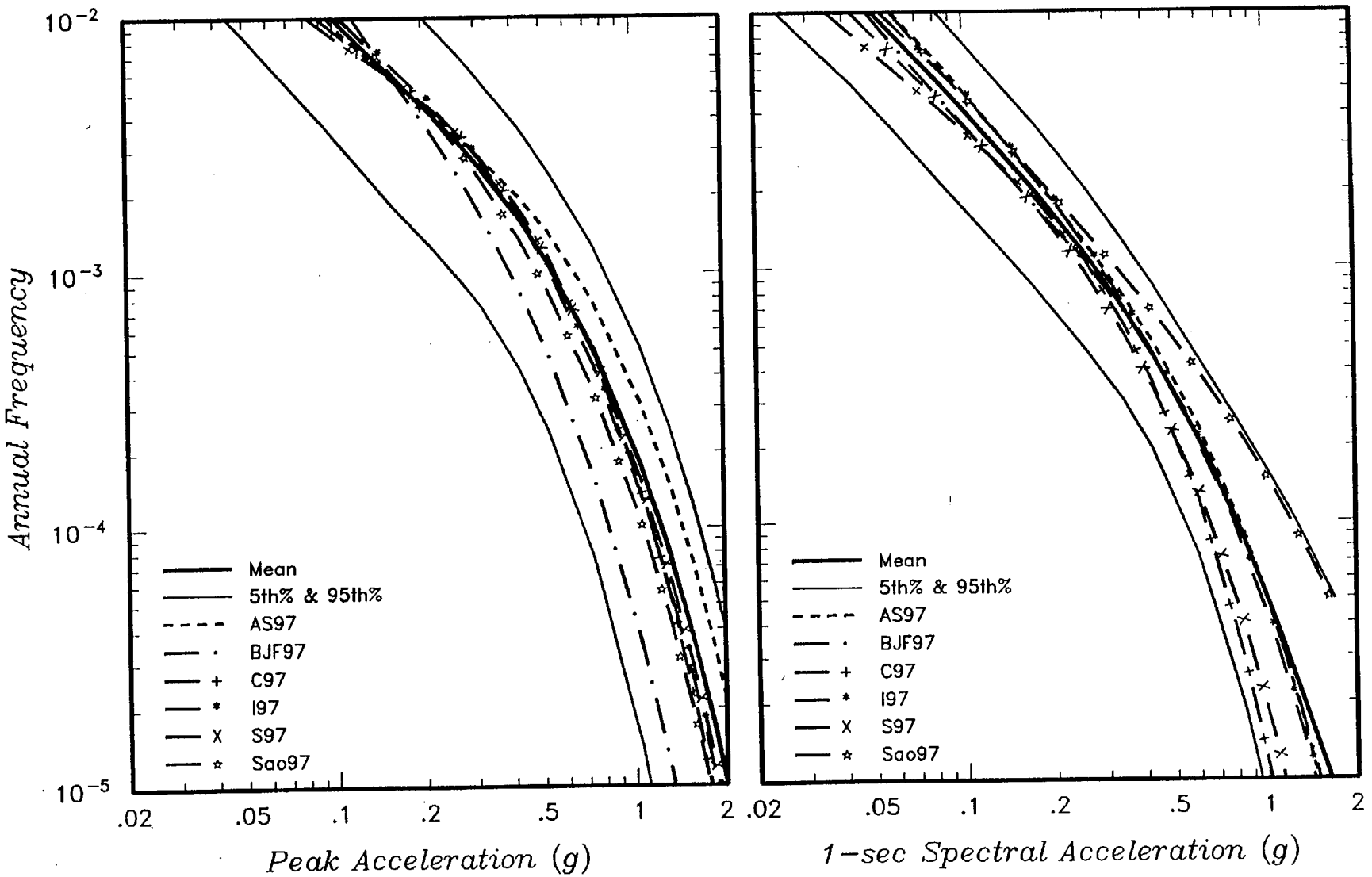

GEOMATRIX

EFFECT OF CHOICE OF ATTENUATION RELATIONSHIP ON MEAN HAZARD FOR HORIZONTAL MOTION AT THE CTB SITE.
Private Fuel Storage Facility
Skull Valley, Utah

Project No. 4790.002

Figure **6-14**

FIG6-15-REV1.DOC

Non-GDS

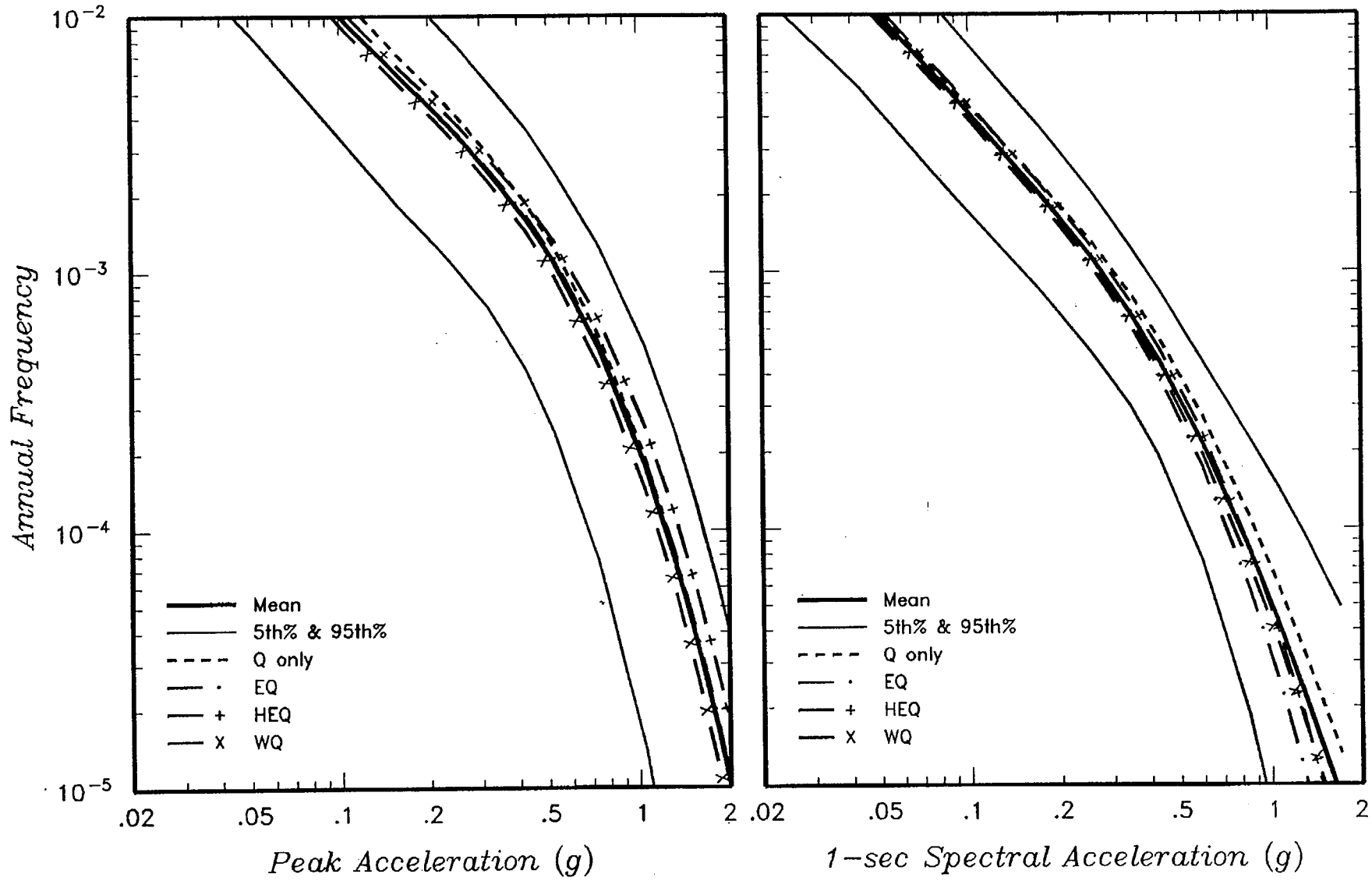

GEOMATRIX

EFFECT OF ALTERNATIVE SOURCE SCALING APPROACHES ON HAZARD
Private Fuel Storage Facility
Skull Valley, Utah

Project No.
4790.002

Figure
6-15

FIG6-16-REV1.DOC

Non-GDS

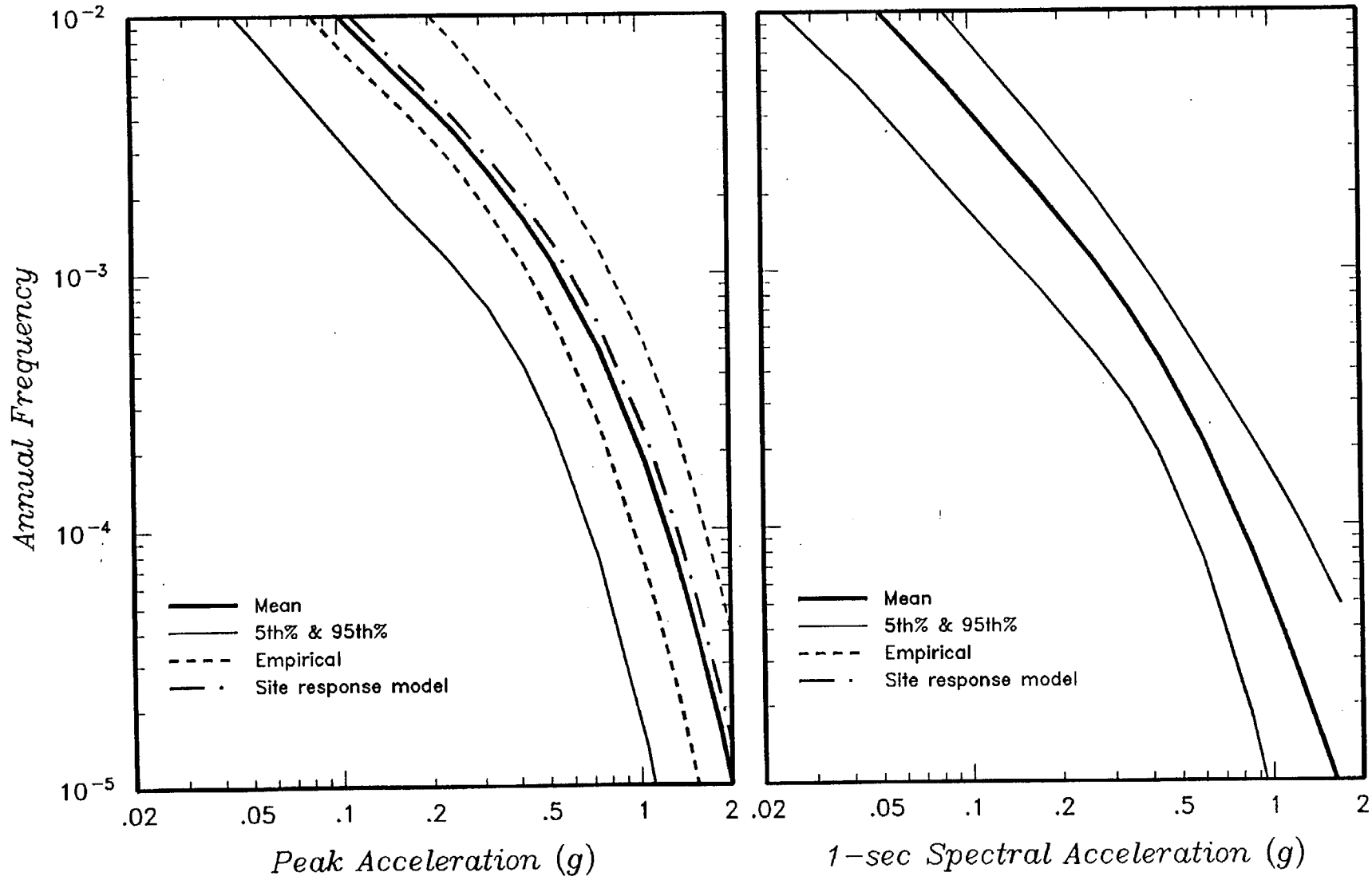

GEOMATRIX

EFFECT PF ALTERNATIVE SITE ADJUSTMENT FACTORS ON HAZARD
Private Fuel Storage Facility
Skull Valley, Utah

Project No.
4790.002

Figure
6-16

FIG6-17-REV1.DOC

Non-GDS

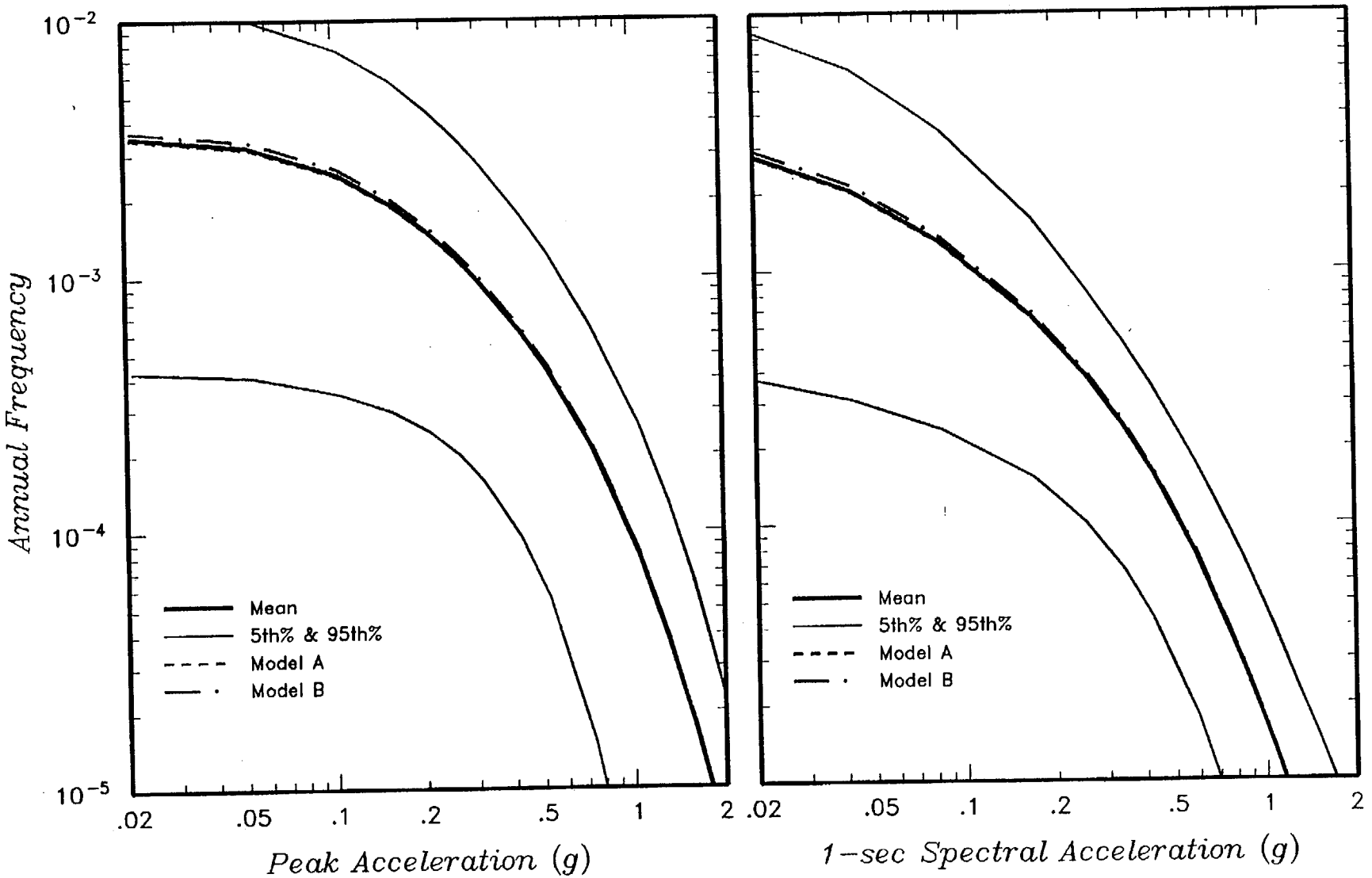

GEOMATRIX

EFFECT OF ALTERNATIVE MODELS FOR THE SKULL VALLEY FAULTS ON MEAN HAZARD FOR HORIZONTAL MOTION FROM THESE FAULTS AT THE CTB SITE.
Private Fuel Storage Facility
Skull Valley, Utah

Project No.
4790.002

Figure
6-17

FIG6-18-REV1.DOC

Non-GDS

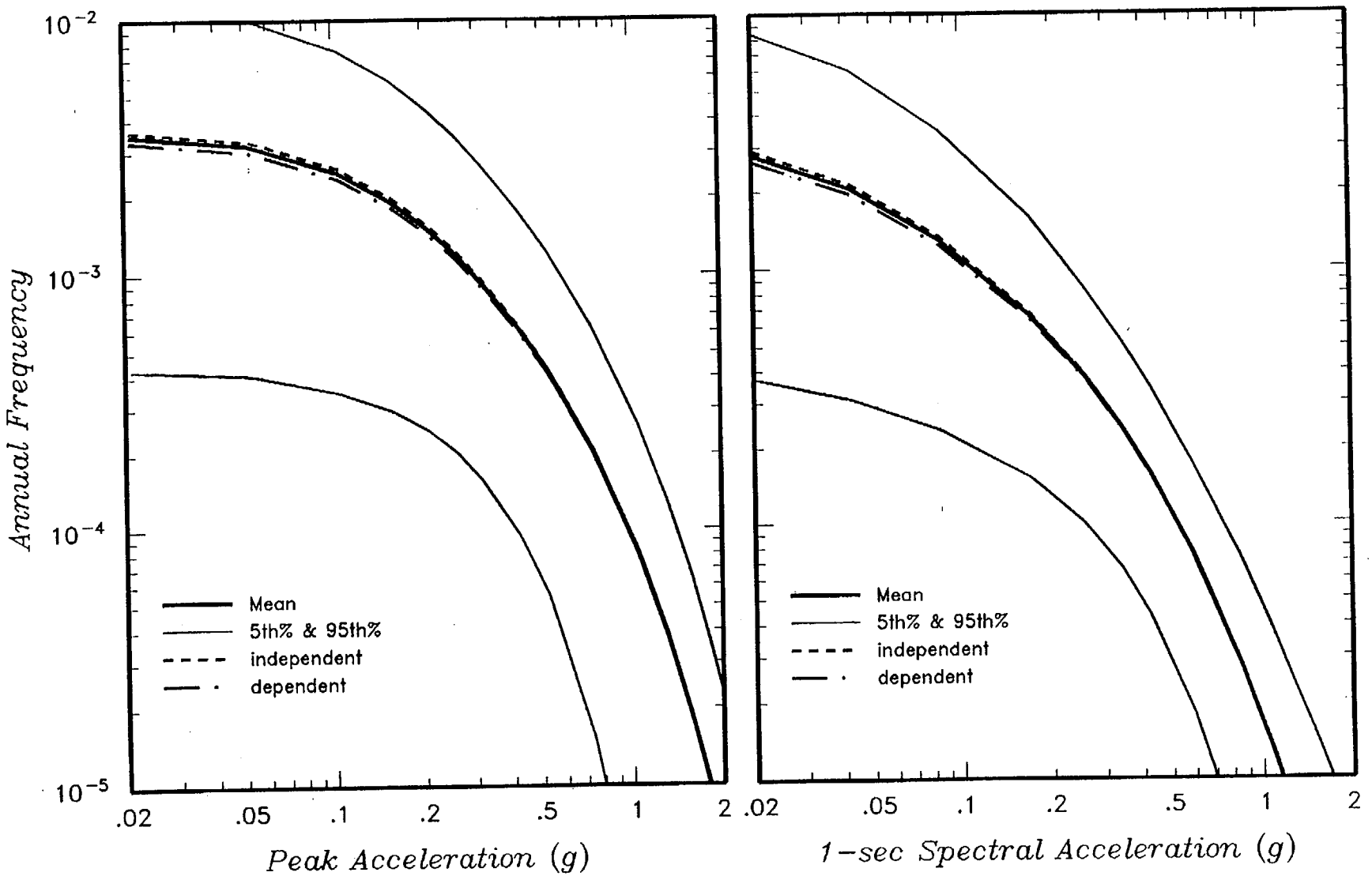

GEOMATRIX

EFFECT OF INDEPENDENCE ON THE WEST FAULT ON MEAN HAZARD FOR HORIZONTAL MOTION FROM THE SKULL VALLEY FAULTS AT THE CTB SITE.
Private Fuel Storage Facility
Skull Valley, Utah

Project No.
4790.002

Figure
6-18

FIG6-19-REV1.DOC

Non-GDS

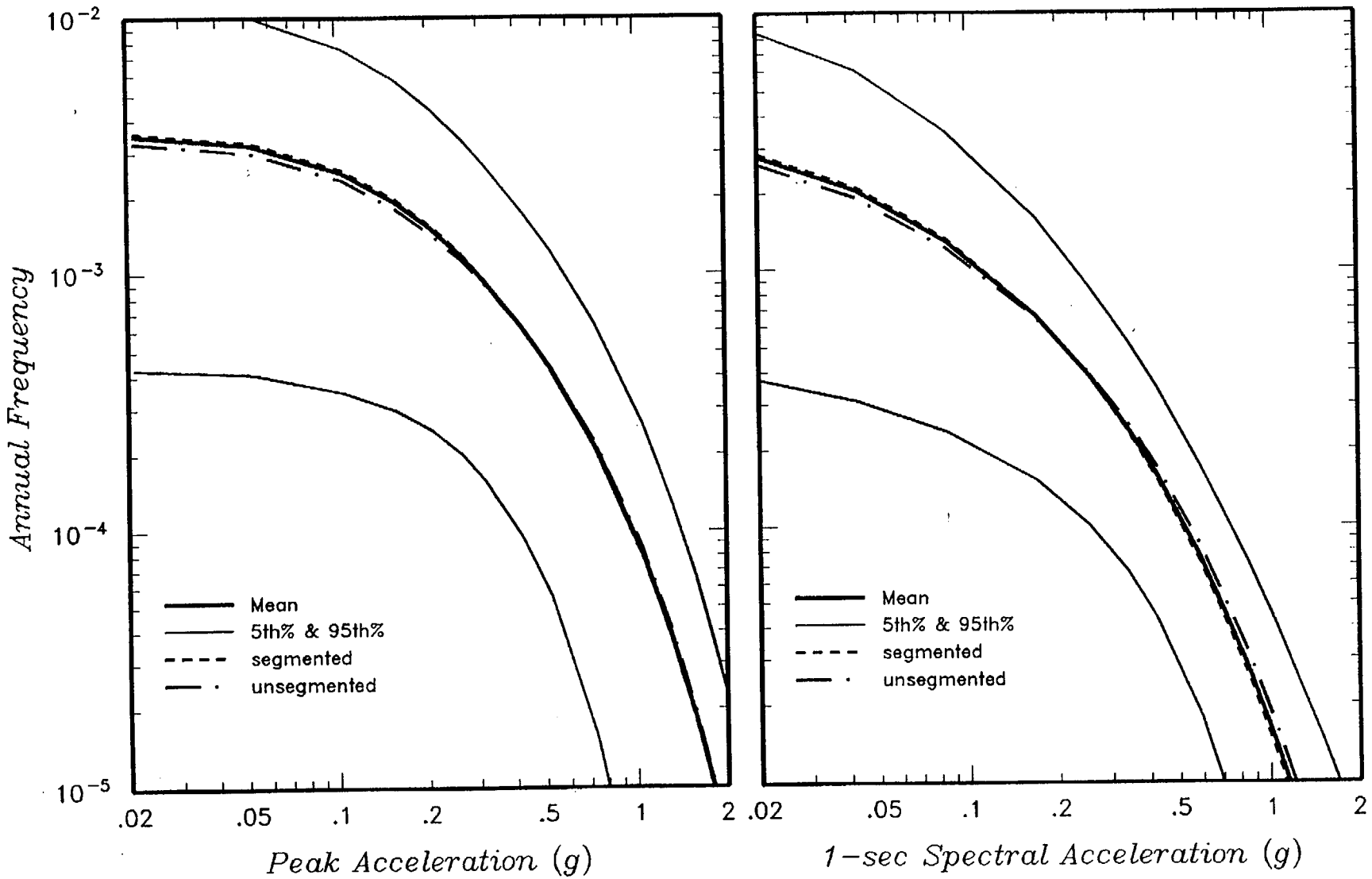

GEOMATRIX

EFFECT OF SEGMENTATION MODELS FOR THE EAST/SPRINGLINE FAULTS ON MEAN HAZARD FOR HORIZONTAL MOTION FROM THE SKULL VALLEY FAULTS AT THE CTB SITE.
Private Fuel Storage Facility
Skull Valley, Utah

Project No.
4790.002

Figure
6-19

FIG6-20-REV1.DOC

Non-GDS

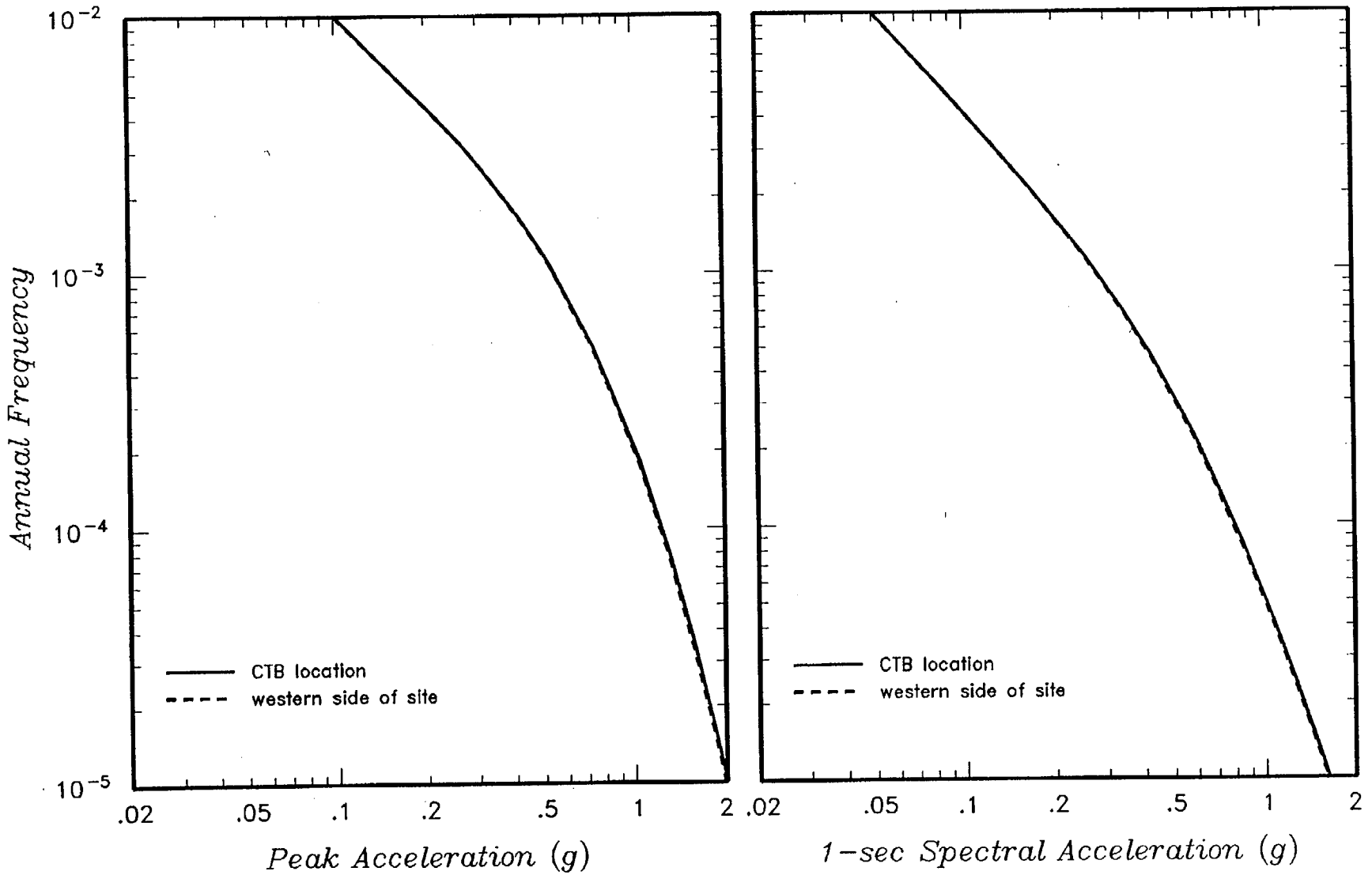

GEOMATRIX

COMPARISON OF TOTAL MEAN HAZARD FOR HORIZONTAL MOTION AT THE CTB LOCATION AND WESTERN SIDE OF SITE AREA.
Private Fuel Storage Facility
Skull Valley, Utah

Project No.
4790.002

Figure
6-20

FIG6-21-REV1.DOC

Non-GDS

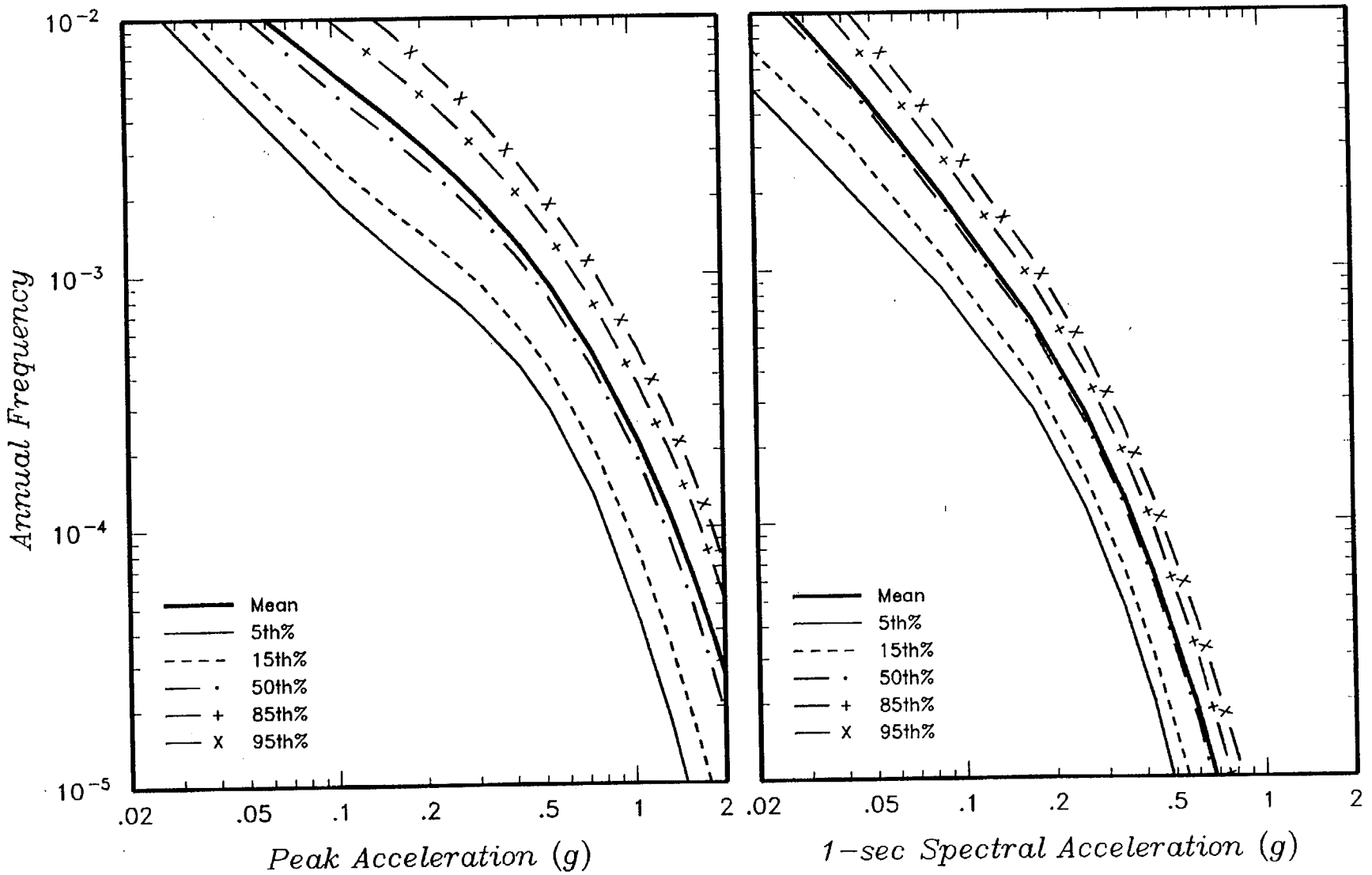

GEOMATRIX

COMPUTED TOTAL MEAN AND 5[IH]- TO 95[IH]-PERCENTILE VERTICAL MOTION HAZARD CURVES FOR THE CTB SITE.
Private Fuel Storage Facility
Skull Valley, Utah

Project No. 4790.002

Figure **6-21**

FIG6-22-REV1.DOC

Non-GDS

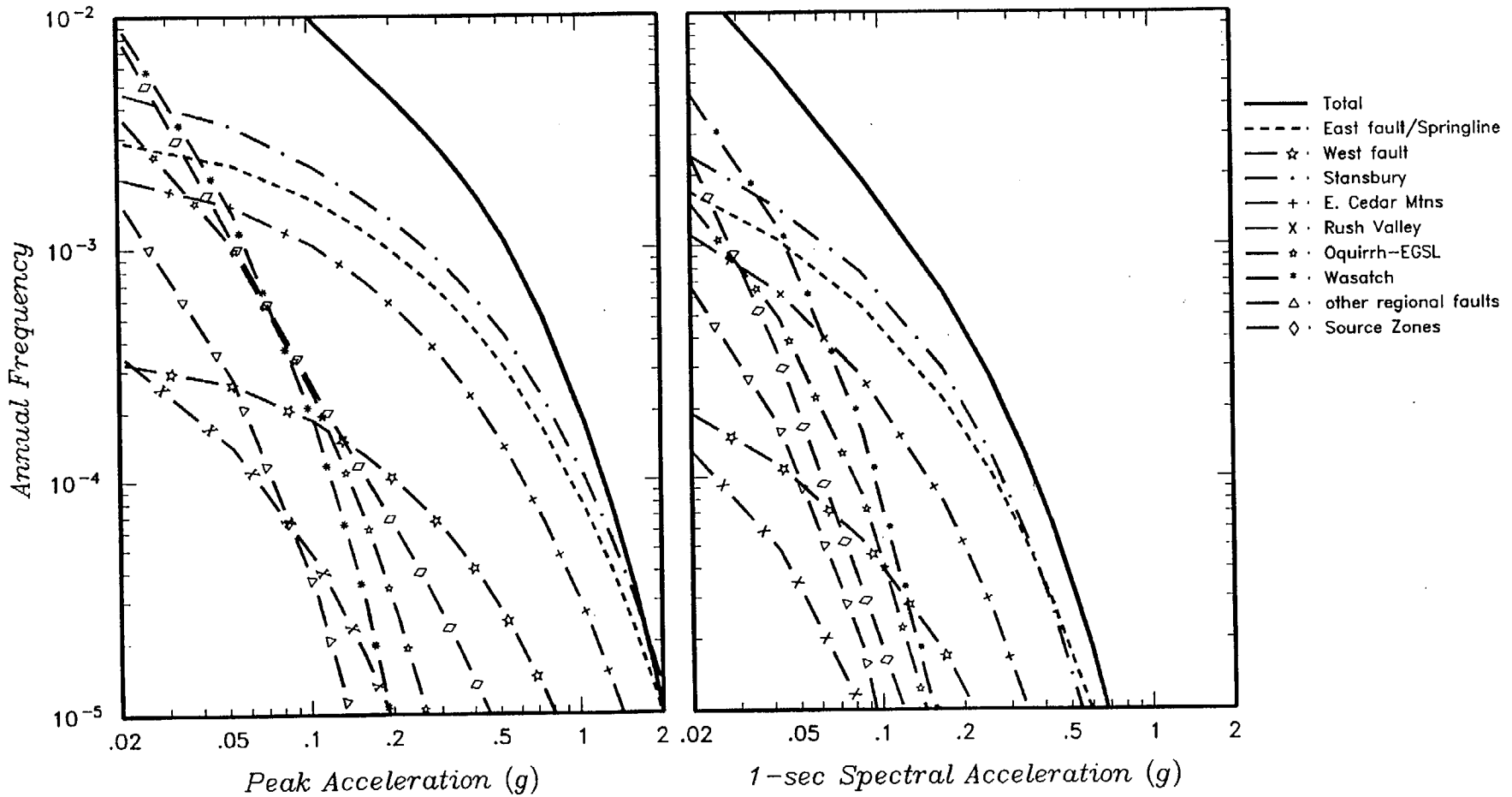

GEOMATRIX

CONTRIBUTIONS OF INDIVIDUAL SOURCES TO TOTAL MEAN HAZARD FOR VERTICAL MOTION AT THE CTB SITE.
Private Fuel Storage Facility
Skull Valley, Utah

Project No. 4790.002

Figure **6-22**

FIG6-23-REV1.DOC

Non-GDS

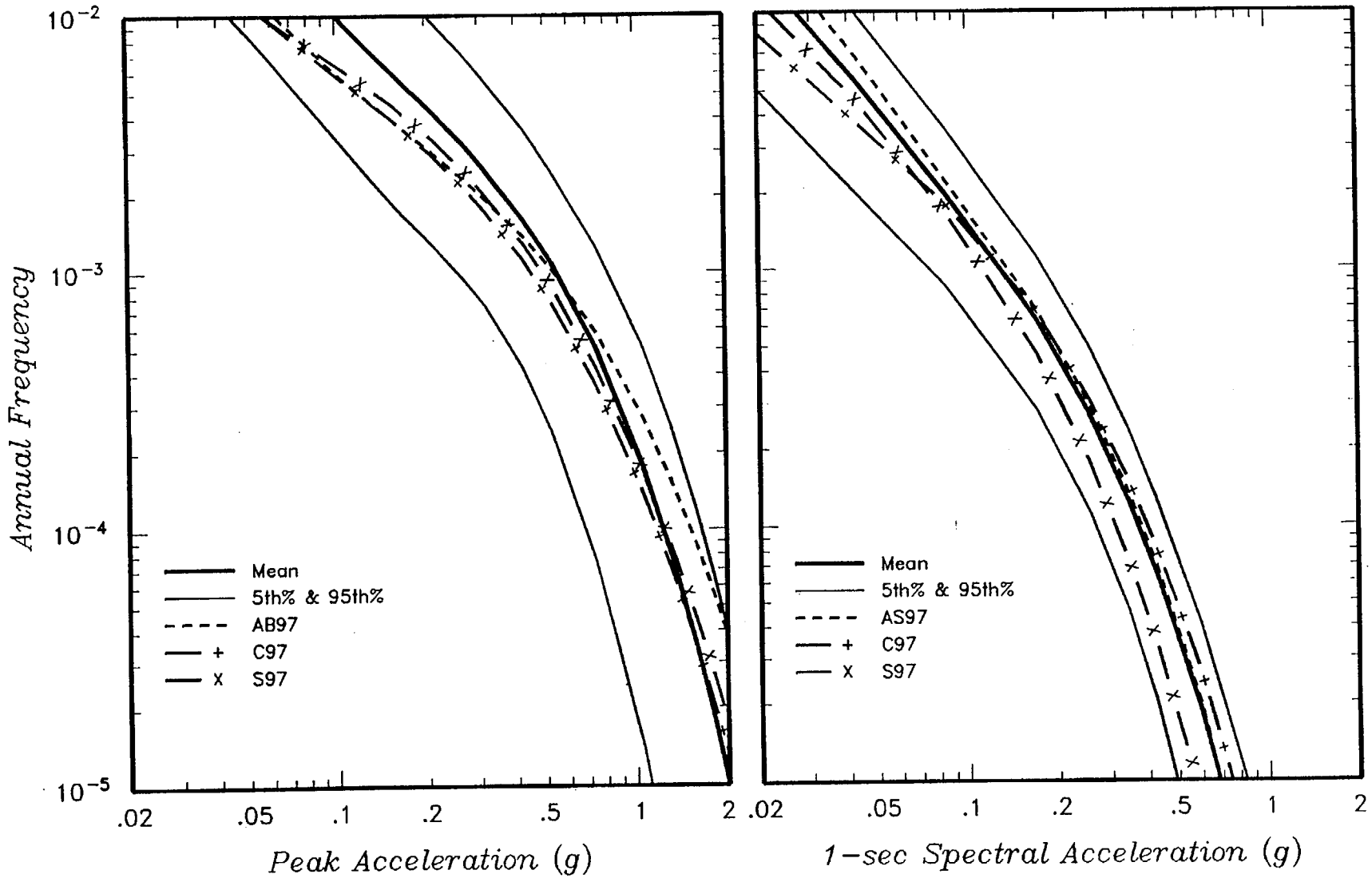

GEOMATRIX

EFFECT OF CHOICE OF ATTENUATION RELATIONSHIP ON MEAN HAZARD FOR VERTICAL MOTION AT THE CTB SITE.
Private Fuel Storage Facility
Skull Valley, Utah

Project No. 4790.002

Figure **6-23**

Non-GDS

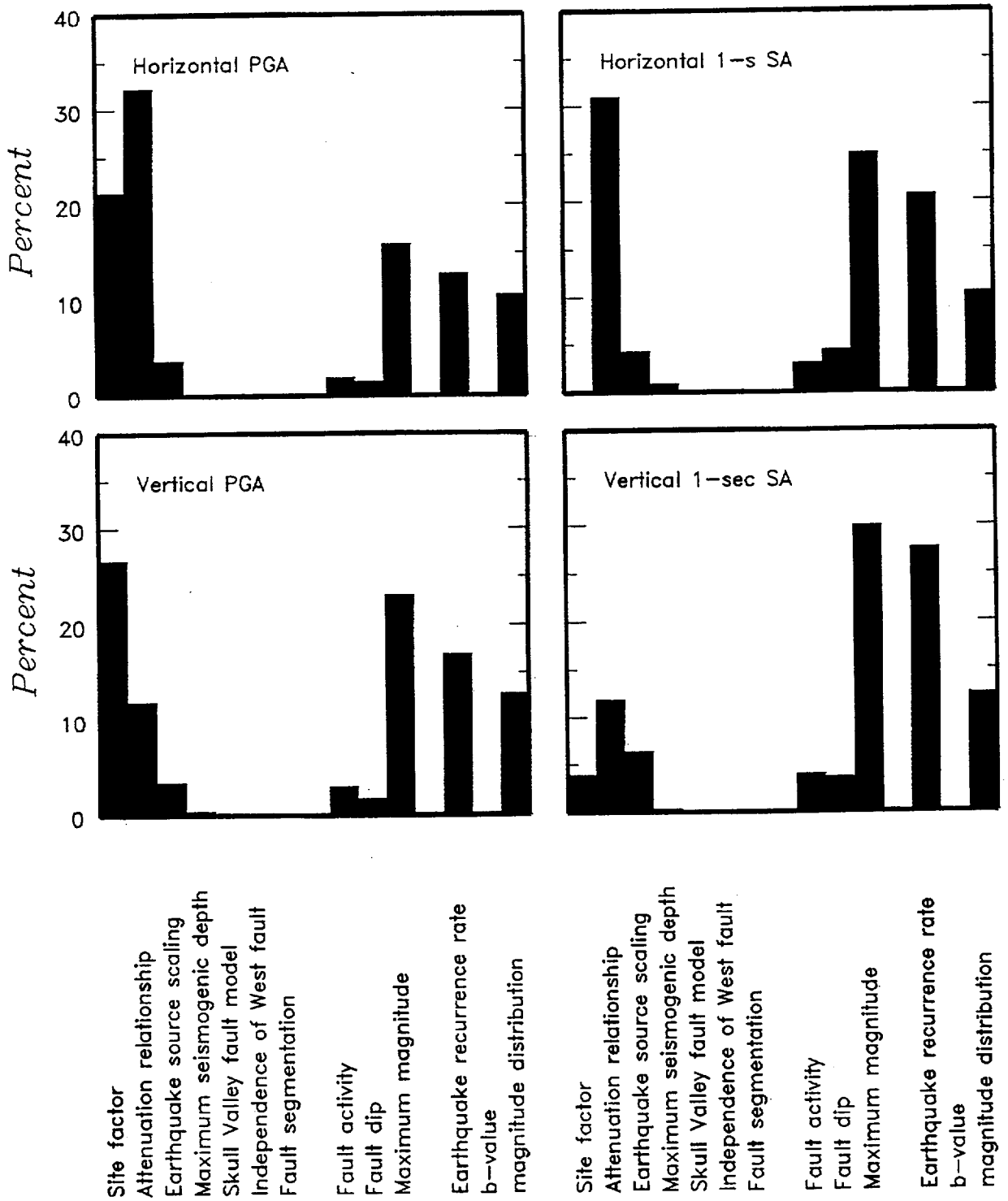

FIG6-24-REV1.DOC

GEOMATRIX

RELATIVE CONTRIBUTION OF THE UNCERTAINTY IN THE COMPONENTS OF THE SEISMIC HAZARD MODEL TO THE TOTAL UNCERTAINTY IN THE HAZARD AT THE CTB SITE.
Private Fuel Storage Facility
Skull Valley, Utah

Project No. 4790.002

Figure 6-24

FIG6-25-REV1.DOC

Non-GDS

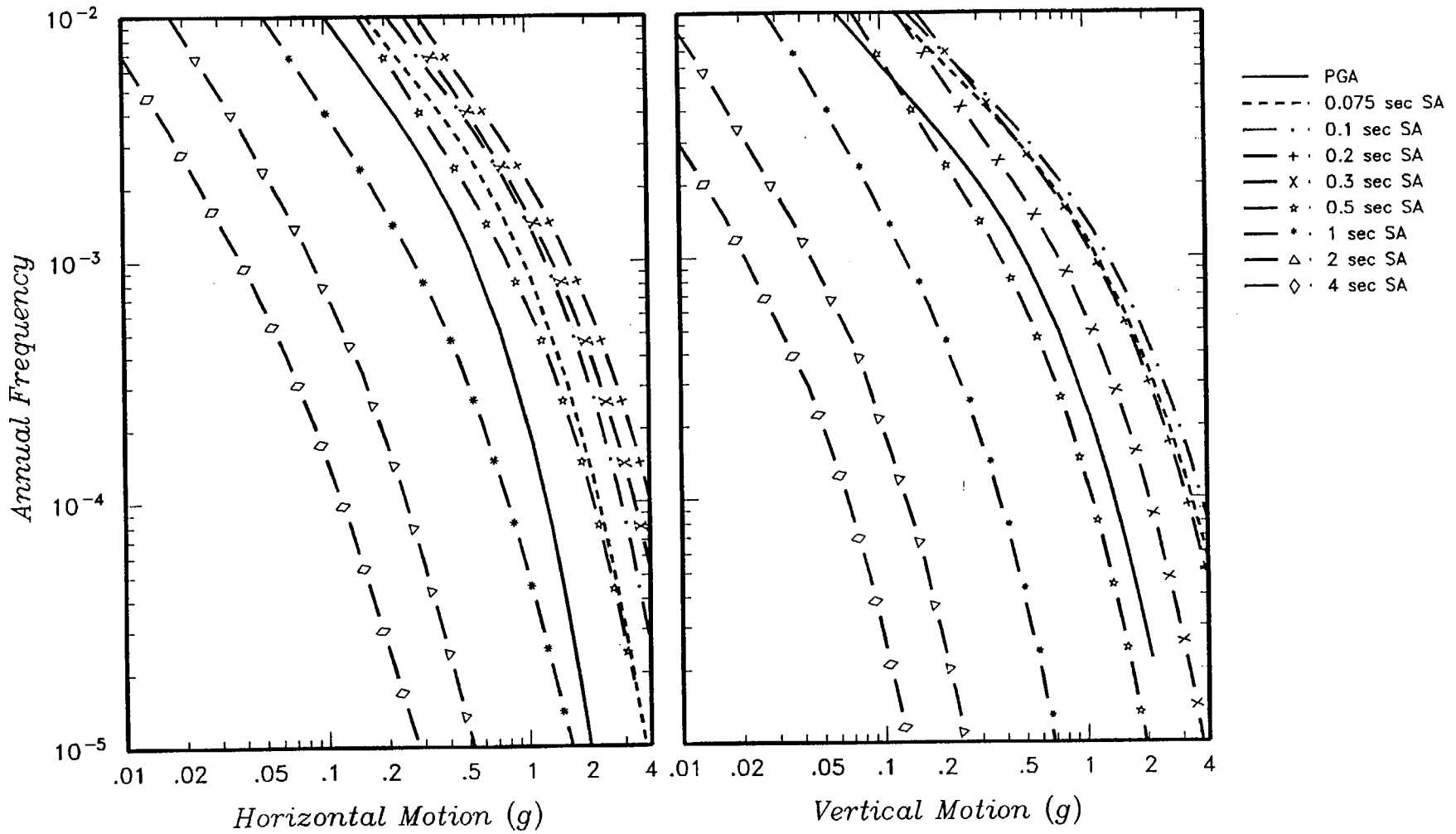

GEOMATRIX

MEAN SEISMIC HAZARD CURVES FOR HORIZONTAL AND VERTICAL MOTIONS FOR THE CTB SITE.
Private Fuel Storage Facility
Skull Valley, Utah

Project No.
4790.002

Figure
6-25

Non-GDS

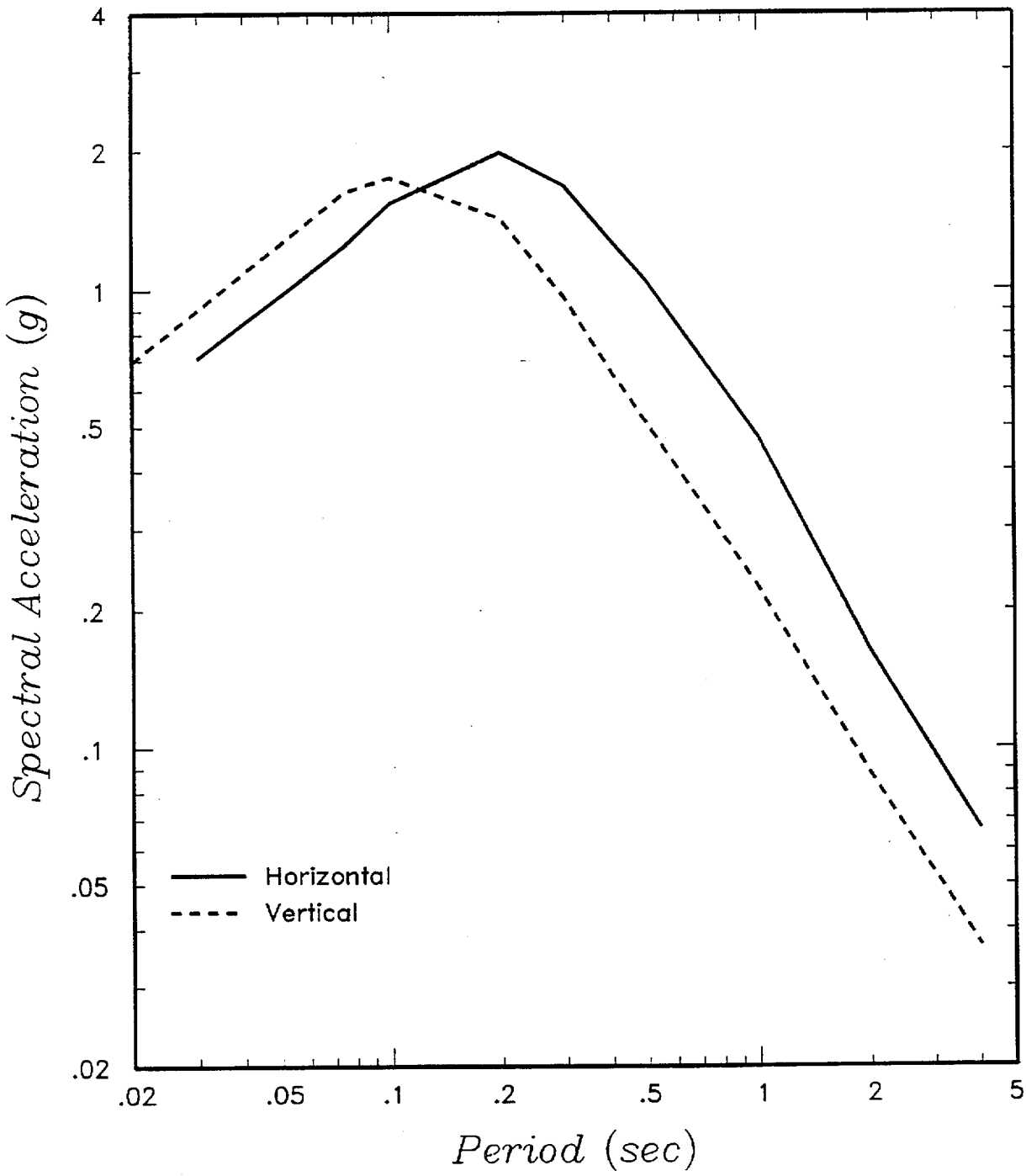

FIG6-26-REV1.DOC

GEOMATRIX

2,000-YEAR RETURN PERIOD EQUAL-HAZARD SPECTRA
Private Fuel Storage Facility
Skull Valley, Utah

Project No.
4790.002

Figure
6-26

APPENDIX F, REV. 1

ASSESSMENT OF APPROPRIATE GROUND MOTION ATTENUATION RELATIONSHIPS

March 2001

APPENDIX F
ASSESSMENT OF APPROPRIATE GROUND MOTION ATTENUATION RELATIONSHIPS

INTRODUCTION

At present, strong motion data recorded in Utah are very limited. In the past, evaluations of seismic hazard, (e.g. Youngs and others, 1987) have typically concluded from examination of the limited strong and weak motion (i.e. seismographic network recordings) that strong ground motion attenuation relationships developed from analysis of California earthquake recordings can be used for Basin and Range sites. However, more recent studies have used examinations of world-wide normal faulting earthquake data together with a variety of modeling techniques to infer that there may be significant differences between strong ground motions in California and those from normal faulting earthquakes in extensional tectonic regimes, such as the Basin and Range region of north-central Utah. Much of this work was reviewed as part of the seismic hazard assessment for the proposed nuclear waste repository at Yucca Mountain, Nevada (CRWMS M&O, 1998). As part of that study, a panel of seven ground motion experts was assembled to provide assessments of the appropriate ground motion models for the Basin and Range region of southern Nevada. In that study, two basic approaches were used to develop ground motion attenuation relationships, one based on modifications to empirical California strong motion attenuation relationships and one based on numerical modeling. For this study, we utilize the approaches developed in the Yucca Mountain study and the applicable results of that study to modify California empirical ground motions to the conditions at Skull Valley, Utah. These modified attenuation relationships account for the effects of the characteristics of the earthquake source, the crustal wave propagation path, and the local site geology.

MODIFICATIONS FOR EARTHQUAKE SOURCE EFFECTS

The ground motion expert panel for the Yucca Mountain study selected seven alternative empirical attenuation relationships for use in estimating strong ground motions from normal faulting earthquakes. These relationships are listed in Table F-1. Five alternative scaling factors were developed for the project to scale the California attenuation relationships for the difference between the earthquake sources of California strike-slip earthquakes and normal faulting earthquakes (see column 2 of Table F-1). The first is the assumption that there is no significant difference (no scaling). The second scaling method is a set of empirical adjustment factors derived by Dr. N. Abrahamson to adjust the Abrahamson and Silva (1997) attenuation relationships from strike-slip to normal faulting (designated A-E in Table F-1). The third

scaling method used by the expert panel is one-half of the empirical adjustment factors developed by Dr. N. Abrahamson (designated 1/2A-E in Table F-1). The fourth and fifth scaling factors were developed by Drs. K. Campbell and W. Silva, respectively, using the point source stochastic ground motion model and the difference in stress drop between California strike-slip and extensional normal faulting earthquakes (designated KCSC and WSSC, respectively in Table F-1).

The amount of scaling as a function of earthquake magnitude and spectral period is shown on Figure F-1. The empirical scaling relationship developed by Dr. Abrahamson was only defined for the period range of PGA to 2.0 seconds. For this study we assume that the scaling factor he obtained for 2.0 second spectral acceleration also applies to longer periods.

The third column of Table F-1 lists the relative weights applied to each of the scaled empirical attenuation relationships. These weights are an average of the weights assigned by the seven ground motion panel experts. We adopt these average weights and scaling factors as the appropriate scaled empirical attenuation relationships for normal faulting earthquakes in Utah. The assessments for the Yucca Mountain project were for rock site conditions, while the Skull Valley site is located on alluvial soils. However, as is discussed later in this Appendix, the shear wave velocity profile at the Skull valley site is not greatly dissimilar to that at many of the strong motion recording stations represented in the California "rock" strong motion data base. Therefore, the six empirical rock site attenuation relationships based primarily on California strong motion data can appropriately be used to assess the hazard at the Skull Valley site. The relationship developed by Sabetta and Pugliese (1996) was not included because it was given a low weight by only one expert, resulting in a combined average relative weight of less than one percent. Also, as indicated on Figure F-1, the scaling factors developed by Drs. Campbell (KCSC) and Silva (WSSC) are very similar. Therefore, for this study, we used Dr. Silva's scaling factors for both KCSC and WSSC scaling because they have a convenient numerical expression that can be used to adjust the coefficients of the selected empirical attenuation relationships. As a result, 20 alternative scaled empirical attenuation relationships were used to model horizontal ground motions at the site. The fourth column of Table F-1 lists the re-normalized weights for these relationships.

A similar process was used to specify empirical attenuation relationships for vertical motions. Table F-2 lists the empirical attenuation relationships for vertical motions considered by the Yucca Mountain Ground Motion Expert Panel. There are fewer relationships available for vertical motions. One panel member chose to apply a vertical/horizontal ground motion ratio

for rock sites to the Boore and others (1997) attenuation relationship as an option for specifying vertical motions. The second column of Table F-2 lists the scaling relationships to adjust the empirical models to normal faulting conditions. Dr. Abrahamson developed a separate set of empirical adjustment factors for vertical motions. The stress drop scaling factors for horizontal motions developed by Drs. Campbell and Silva were assumed by the panel members to also apply to vertical motions. Figure F-2 compares the resulting scaling relationships for vertical motions.

The third column of Table F-2 lists the relative weights applied to each of the scaled empirical attenuation relationships averaged over the seven ground motion panel experts. The fourth column of Table F-2 lists the re-normalized weights for those relationships selected for use in this study. Again, we have used Dr. Silva's scaling factors for both KCSC and WSSC scaling because they have a convenient numerical expression that can be used to adjust the coefficients of the selected empirical attenuation relationships. The scaling of the Boore and others (1997) horizontal relationship by vertical to horizontal ratios was not used because it was given limited weight by the experts. As a result, eleven alternative attenuation relationships were used to evaluate vertical ground motions.

MODIFICATIONS FOR CRUSTAL PATH EFFECTS

The rate of attenuation of ground motion level with distance from the source is controlled by geometric spreading of the wave front and anelastic energy absorption by the crustal rocks along the travel path. Given that the earthquakes of interest to the Skull Valley site are expected to occur in the upper portion of the earth's crust in similar geometries to California earthquakes, we assume that similar geometric spreading effects occur in both regions. The energy absorption along the travel path is usually represented by the quality factor, Q. Crustal rocks in California generally have a relatively low value of Q, that is often modeled by the relationship $Q = 150f^{0.6}$, where f is the frequency of the seismic wave. Singh and Herrmann (1983) assessed Q for the Utah region to be $Q = 500f^{0.2}$. This higher value of Q may result in less attenuation of seismic waves with distance compared to California. The difference in Q is expected to have no significant effect for nearby sources because the travel path is only a few kilometers. However, the most active source of large earthquakes in the region is the Wasatch fault, located approximately 80 km to the east of the site. For this source, the effects of differences in crustal attenuation may be important.

The effect of differences in Q between California and Utah was assessed using the technique applied for the Yucca Mountain study. The point source stochastic ground motion model

(Hanks, 1979; Hanks and McGuire, 1981; Boore, 1983, 1986) was used to simulate spectral accelerations for a magnitude 7 earthquake at a range of distances using the Q expressions for California and Utah (a magnitude 7 earthquake was chosen as the likely size of earthquakes on the Wasatch fault that may have a significant contribution to hazard at the site). All other parameters were set at appropriate values for California earthquakes. Figure F-3 shows the results of these simulations.

The difference between the ground motion levels as a function of distance, r, can be modeled by the expression (Youngs and others, 1987):

$$SA(\text{Utah } Q) / SA(\text{California } Q) = 1.0 + \gamma r \qquad \textbf{(F-1)}$$

The values of parameter γ obtained from the simulations are:

Crustal Path Adjustment Factors

Period (sec)	γ
PGA	0.0046
0.05	0.0039
0.075	0.0036
0.1	0.0042
0.15	0.0048
0.2	0.0052
0.3	0.0053
0.4	0.0052
0.5	0.0050
0.75	0.0046
1.0	0.0044
1.5	0.0039
2.0	0.0036
3.0	0.0031
4.0	0.0028

These values, together with Equation **(F-1)** were used to adjust the selected empirical attenuation relationships to account for the expected difference in crustal attenuation between California and north central Utah.

MODIFICATIONS FOR LOCAL SITE CONDITIONS

The process followed by the Yucca Mountain Ground Motion Expert Panel to correct for local site conditions was to assess the relative response of the Yucca Mountain site compared to that of a generic site representative of the empirical strong motion attenuation relationships. That concept is followed here using a combination of two approaches. The first approach uses a site

response model to compute the relative response to vertically propagating shear waves of the Skull Valley site compared to sites representative of the empirical ground motion models. The second approach compares recorded strong motion data for sites with similar classifications to the Skull Valley site to the motions predicted by the empirical ground motion models to develop an empirical site adjustment factor.

SKULL VALLEY SITE CONDITIONS

The surficial soils consist of approximately 5 feet of eolian silty soils. These are underlain by Lake Bonneville lacustrine soils to a depth of approximately 50 feet. The soils above a depth of approximate 26 feet consist of predominately deep-water deposits of clayey silts and silty clays. These are underlain by near shore deposits of very dense fine sand and very dense silts with gravel and sand layers. An erosional unconformity marked by the Promontory soil lies at a depth of 45 to 55 feet below the surface. The soils below this unconformity consist of the Little Valley lacustrine deposits, inter-bedded gravely and clayey sands and sandy silts. These soils are dense to hard with refusal conditions often encountered in site borings.

A second erosional unconformity at a depth of 85 to 95 feet marks the boundary between Quaternary and Tertiary sediments. Below this boundary lies the Salt Lake group, a mid- to late-Miocene sequence of semi-consolidated siltstones, claystones and sandstones. These sediments are presumed to continue to bedrock, which is a west dipping surface lying at a depth of 600 to 800 feet beneath the site. Ground water is estimated to lie at a depth of approximately 125 feet. The underlying bedrock consists of hard limestone and dolomite.

Geomatrix (2001) developed a "best estimate" set of dynamic properties for the subsurface materials at the Skull Valley site. This profile is shown on Figure F-4 and is given in Table F-3. Nine general sediment layers were identified. Six of these are located within the upper 35 feet. The shear wave velocities for these layers are based on the statistical analysis of measured velocities in 16 seismic cone tests and one down-hole velocity measurement. The shear wave velocities for layers between 35 and 105 feet in depth are based on the down-hole velocity measurement at the Canister Transfer Building boring CTB-05 and CTB-05A. The velocities obtained from these detailed measurements are generally consistent with earlier results obtained in seismic refraction and reflection surveys. Geosphere Midwest (1997) indicate a shear wave velocity of 700 to 790 fps for the soils above a depth of 45 to 55 feet and 1700 to 2400 fps for soils below this depth. Bay Geophysics (1999) reported an average velocity of 800 fps for the soil above the Promontory soil boundary and 1,100 ft/sec for soil above the Quaternary/Tertiary boundary. Using the layer average velocities listed in Table F-3, the

average velocity of the soils above the Promontory soil (depth 45 to 55 feet) is 863 fps and the average velocity of soils above the Tertiary unconformity (depth 85 to 95 feet) is 1,123 fps. In addition, the measured velocity within the upper portion of the Tertiary Salt Lake group is consistent with the range of values of 1,000 to 1,750 m/sec (3,280 to 5,741 fps) reported for this unit in the Salt Lake Valley (Tinsley and others, 1991; Williams and others, 1993; Wong and Silva, 1993).

As indicated in Table F-3, two alternative velocity profiles are considered for the Tertiary sediments below a depth of 125 feet. The first assumes that the velocity remains constant with depth until bedrock is reached at a depth of approximately 700 feet. The second assumes that the velocity increases with depth to a value representative of the upper range of values reported for this unit.

The crustal velocity profile used for earthquake location in north-central Utah consists of the following (J. Pechmann, University of Utah, personal communication, 1999):

Utah Crustal Velocity Profile

Depth Range (km)	P-Velocity (km/sec)	S-Velocity (km/sec)
0 – 1.4	3.4	1.95
1.4 – 15.5	5.9	3.39

These values were used to set the velocities for the bottom two layers of the crustal model (Table F-3).

Finally, the top five feet of the soil profile is to be replaced by soil-cement throughout the entire pad emplacement area and around the Canister Transfer Building. Because of the large extent of the soil-cement placement, the soil-cement layer is considered to be part of the free field profile. The best estimate velocity for this material was set at the minimum requirement specified in the initial design (Geomatrix, 2001). Preliminary site response calculations indicate that the computed surface motions are not sensitive to increases in the shear wave velocity of the soil-cement layer above 1,500 fps.

CLASSIFICATION OF THE SKULL VALLEY PFSF SITE CONDITIONS

The 1994 NEHRP Provisions for seismic design (Table 1.4.2.1 of FEMA, 1995) classify site conditions primarily in terms of the average shear wave velocity, $\overline{v_s}$, in the upper 100 feet of the soil profile. Based on the best estimate velocity profile presented in Table F-3, the average

shear wave velocity in the upper 100 feet of sediments is 1,196 fps. This values lies at the boundary between Class C (very dense soil and soft rock with 1,200 ft/sec $\leq \overline{v_s} \leq$ 2,500 ft/sec) and Class D (stiff soil with 600 ft/sec $\leq \overline{v_s} \leq$ 1,200 ft/sec).

Silva et al. (1998) developed generalized velocity profiles representative of the generic site classifications "rock" and "soil" used to develop Western US (WUS) empirical attenuation relationships, such as that of Abrahamson and Silva (1997). (Note that "California" and "WUS" are used interchangeably to represent ground motion models based primarily on California strong motion data.) Figure F-4 compares these velocity profiles to the best estimate velocity profile developed for the Skull Valley site. The average shear wave velocities for the top 100 feet of these two profiles are 530 m/sec (1,740 fps) and 284 m/sec (933 fps) for "rock" and "soil", respectively, placing "rock" within NEHRP Class C and "soil" within NEHRP Class D. The designation of generic "rock" sites in the WUS strong motion database as NEHRP Class C is consistent with the recommendations of Campbell (1997) and Boore et al., (1997). Abrahamson and Silva (1997) combine data from rock and shallow soil sites into their "rock" site category.

Based on these comparisons, the Skull Valley site can be classified as a shallow soil site, with shear wave velocities that reach rock-like levels at a depth of 85 to 95 feet. The deeper velocities appear to lie between those for generic "rock" and "soil" sites in the WUS, although they may be closer to those of "rock." The initial evaluation of the relative site response of the Skull Valley site (Rev 0 of this document, dated February, 1999) likened the Skull Valley site to generic WUS deep "soil" sites based on the presence of soil at the surface and a thick Tertiary section. However, the low level of damping in the shallow soils (documented in Geomatrix, 2001), the rapid increase in shear wave velocity with depth, and the fact that the Yucca Mountain Ground Motion Expert Panel used empirical rock attenuation relationships as their starting point, suggests that it is more appropriate to compare the relative response of the Skull Valley site to generic WUS "rock". Furthermore, the site conditions in Skull Valley may fall within the range of those included within the databases used to develop some of the empirical rock ground motion models.

SITE ADJUSTMENT FACTOR BASED ON SITE RESPONSE MODEL

The site adjustment factor developed by the Yucca Mountain Ground Motion Panel was obtained by computing the response of the Yucca Mountain profile and a generic WUS rock profile to vertically propagating waves. The ratio of the surface motions for these two profiles

defined the site adjustment factor. That concept was implemented in this study using the following approach:

1. Select a set of rock site recordings from earthquakes within the appropriate magnitude range and scale the recordings to ground motion levels relevant to evaluating the site hazard.

2. Deconvolve the recordings to a depth where the crustal velocities in California and Utah are similar, removing the average rock site amplification.

3. Compute the response of the WUS generic rock sites and the Skull Valley site using the deconvolved rock motions from step 2.

4. Compute the ratio of the response spectra for the surface motions obtained from the site response analyses of step 3. Use the statistics of these response spectral ratios to assess the expected difference between the response of WUS rock sites and the Skull Valley site.

Selection of Rock Site Recordings

It is expected that the major contribution to the hazard will be from large magnitude earthquakes occurring on the nearby Skull Valley and Stansbury faults. Therefore, twelve rock recordings from magnitude ~6.5 to 7 earthquakes were selected for the site response analyses. Table F-4 lists the selected recordings. Six of the recordings are from California earthquakes and six are from large normal faulting earthquakes recorded in Italy.

The recordings were scaled to ground motion levels corresponding to maximum magnitude events on the two nearby faults. The mean maximum magnitude for the Stansbury fault is **M** 7. Using the rock-site attenuation relationship developed by Abrahamson and Silva (1997) scaled to normal faulting conditions, the resulting median peak ground acceleration is 0.32g. Figure F-5 shows the corresponding response spectrum. Each of the rock recordings was scaled so that its response spectrum matches the target spectrum on average by minimizing the area between the two spectra. The mean maximum magnitude for the East fault is **M** 6.5. Using the rock-site attenuation relationship developed by Abrahamson and Silva (1997) scaled to normal faulting conditions, the resulting median peak ground acceleration is 0.57g. Figure F-6 shows the corresponding response spectrum and the rock recordings scaled to match this event.

Deconvolution of Rock Motions

The recorded rock surface motions were deconvolved to a depth where the crustal velocities are comparable for the generic WUS rock site and the Utah crustal model. Figure F-7 compares the generic WUS rock profile from Silva et al. (1998) and the Skull Valley profile. It was

judged that the two profiles reached sufficiently similar velocities at a depth of 5 km to use this depth as the appropriate base point for site response analyses.

The deconvolution calculations were performed using the one-dimensional wave propagation computer program SHAKE (Schnabel and others, 1972). Figure F-8 shows the normalized shear modulus and damping curves recommended by Silva and others (1998) for use at shallow depths in weathered and fractured rock typical of the velocity profile shown on Figure F-4. Once the rock velocity reaches 4,000 ft/sec (at a depth of about 350 feet), the rock is assumed to behave linearly (no modulus reduction).

The material damping in the rock below a depth of 350 ft was estimated using the observed high frequency attenuation at rock site recording stations. Anderson and Hough (1984) have show that the high frequency attenuation of ground motions in the near surface can be modeled by the attenuation parameter κ. Silva and Darragh (1996) indicate that κ is related to the near surface shear wave quality factor, Q_s by the expression:

$$\kappa = \frac{H}{Q_s V_s} \qquad \textbf{(F-2)}$$

where H is the portion of the crust over which the energy loss occurs and V_s is the average shear wave velocity over H. The appropriate value of H is 1 to 2 km (Silva and Darragh, 1996). For this calculation, the total thickness H over which the energy loss is assumed to occur was set to ~1.5 km.

Q_s is, in turn, related to the material damping, λ, used in liner viscoelastic wave propagation modeling (such as the site response analyses performed for this study using the program SHAKE) by the expression:

$$\lambda = \frac{1}{2Q_s} \qquad \textbf{(F-3)}$$

Silva and Darragh (1996) found that a average value of $\kappa = 0.04$ sec is appropriate for WUS rock site strong motion recording stations. This κ value represents the total damping in the upper portion of the crustal profile, including that portion to which the damping relationships shown on Figure F-8 apply. To calculate the damping to be applied to the rock layers below a depth of 350 feet, the κ contributed by the low strain damping in the shallower materials is removed. Table F-5a shows this calculation. Equation **(F-2)** is used to compute the value of Q_s

for each layer from the low strain damping shown on Figure F-8 (~10^{-3}%), and Equation **(F-1)** is used to compute the layer contribution to κ.

Silva and Darragh (1996) found that Q_s for WUS rocks is proportional to shear wave velocity. Using the assumption that $Q_s \propto V_S$, damping values can be obtained for each layer by substituting for Q_s the term γV_S in Equation **(F-2)**, resulting in the following expression for the total κ.

$$\kappa = \frac{1}{\gamma} \sum_i \frac{H_i}{V_{s\,i}^2} \qquad \textbf{(F-4)}$$

The values of $H_i / V_{s\,i}^2$ are summed for all layers and then Equation **(F-4)** solved for the value of γ that produces the desired value of κ. The appropriate values of Q_s are then computed as γV_S and Equation **(F-3)** is used to compute the value of damping to use for each layer in the SHAKE computation. Table F-5b lists the resulting values of material damping for the WUS rock profile. Below a depth of ~1.5 km, damping was set using Equation **(F-3)** and the California crustal Q for a frequency of 3 Hz (~300).

The unit weights assigned to the WUS profile by Silva et al. (1998) begin at 125 pcf at the surface, increasing to 132 pcf at a depth of 100 feet, then gradually to 168 pcf at crustal depths.

The deconvolution analysis assumes that all of the surface rock motions are a result of vertically propagating shear waves. However, Silva (1986) found that some of the surface motions consist of higher mode surface waves. He recommended that surface motions be filtered to remove frequencies higher than about 15 Hz before deconvolution to reduce the potential for overestimation of the motions at depth. He also indicated that the motions should be removed using an anti-aliasing filter rather than the abrupt frequency cut-off employed in program SHAKE. Accordingly, the rock recordings were low-pass filtered with a Butterworth filter prior to being input into the deconvolution analysis. The filtering was preformed prior to scaling the records to the target rock motion response spectra shown on Figures F-5 and F-6. The records were also high-pass filtered above a frequency of 0.14 Hz (a period of 7.0 sec.) and base-line corrected to remove spurious low frequency motions. Twenty-four base motions were then computed at a depth of 5 km using the average WUS rock velocity profile shown on Figure F-4, 12 using surface motions scaled to a **M** 7 earthquake on the Stansbury fault (Figure F-5) and 12 using surface motions scaled to a **M** 6.5 earthquake on the East fault (Figure F-6).

Site Response Analyses for WUS Rock Sites

The intent of the relative site response analyses is to compare the average response of velocity profiles representative of generic WUS rock sites to that of profiles representative of the Skull Valley site. The empirical WUS rock ground motion models have been constructed using strong motion data recorded on a variety of sites velocity profiles that vary about the average profile shown on Figure F-4. To properly represent the average response of these sites one should include this variability in velocity. EPRI (1993) developed a model to represent the variability in shear wave velocity profiles about an average profile. This model has been refined by Silva et al. (1998). The Silva et al. (1998) model was used to generate 30 profiles representative of WUS "rock" sites by randomizing the velocities in the upper 100 feet of the generic WUS rock profile. These profiles are shown on Figure F-9 along with the average profile from Figure F-4.

The 24 base motions were combined with the 30 WUS rock profiles to generate 240 surface motions representative of WUS rock sites. The process was to sequentially select 4 input motions for each WUS rock profile: profile 1 was combined with input motions 1 through 4 with **M** 7 scaling; profile 2 was combined with input motions 5 through 8 with **M** 7 scaling; profile 3 was combined with input motions 9 through 12 with **M** 7 scaling; and profile 4 started over with input motions 1 through 4 with **M** 7 scaling. This was repeated until all 30 profiles had been combined with the base input motions based on surface motions scaled to a **M** 7 earthquake on the Stansbury fault producing a set of 120 site response analyses. The process was then repeated using the base motions input motions based on surface motions scaled to a **M** 6.5 earthquake on the East fault producing a second set of 120 site response analyses.

Site Response Analyses for the Skull Valley Site

The velocity profile at the Skull Valley site was examined for potential variability from location to location within the site area. As shown in Table F-3, the depth to the various layer boundaries varies by ±1 or 2 feet for the shallow layers and ±5 feet for the depths to the erosional unconformaties at depths of ~ 50 and ~ 90 feet. Table F-6 presents the statistics of the shear wave velocity data of the site for the top 35 feet of the soil profile for which multiple velocity profiles were obtained (Geomatrix, 2001). The data indicate only slight variability in shear wave velocity across the site. The reasonably uniform velocities across the site are not surprising given the lacustrine depositional environment.

The statistical data for the Skull Valley velocities and variability in layer depths were used to generate 30 random profiles representative of the skull valley site. Table F-7 lists the

parameters of the best estimate profile used to generate the 30 velocity profiles. The depth to each layer boundary was simulated by a uniform distribution within the range defined in Table F-7. The velocity in each layer was selected by generating correlated random normal deviates using the adjacent layer correlation coefficients listed in Table F-7 and setting all other correlation coefficients to 0. A nominal adjacent layer correlation coefficient of 0.25 was selected to represent the range of computed correlation coefficients listed in Table F-6. The correlation between the velocity in the soil-cement layer and the underlying soil was set to 0, as was the correlation across the erosional unconformity at a depth of 50 feet. The correlation between layers 4 and 5 was also set to 0 reflecting the very small computed correlation. The standard deviation in the soil-cement shear wave velocity was set to 0.1 times the average velocity reflecting that the material will be placed in a controlled manner. The standard deviation in layer 7 was estimated using the correlation coefficient 0. 076 obtained for layer 6. The standard deviation for the layer 8 sands was to set 0.1 times the average velocity reflecting the low correlation coefficients obtained for the other soil layers. In addition, layer 8 was divided into two sublayers with a relatively high degree of correlation between them to allow for variability in velocity with depth through this thick layer. The velocity of the Tertiary sediments was not varied. However, analyses were performed using both the constant velocity model and the increasing velocity model (Table F-3). The location of the velocity transitions within the Tertiary sediments was allowed to vary within the limits shown in Table F-3. Figure F-10 shows the resulting 30 velocity profiles compared to the best estimate velocity profile.

The influence of the uncertainty in the average velocity of the subsurface sediments at Skull Valley on the site response was examined by developing upper and lower range velocity profiles. Table F-6 lists the 90-percent confidence interval on the mean velocity within the top 35 feet based on the 17 velocity profiles developed at the site. These values were used to construct the upper and lower range velocities listed in Table F-8. The uncertainty in the average velocity in layer 8 (depth range of 50 to 90 feet) was assigned a value of ± 0.1 times the best estimate velocity, reflecting the low variability observed in the velocities of the shallower soils. The uncertainty in the average velocity of the soil-cement and the Tertiary sediments was assigned a value of $\pm\sqrt{1.5}$ times the best estimate velocity. This value is the minimum variability in shear wave velocity recommended by ASCE (1986) for soil-structure interaction and is likely to be a conservative value based on the data obtained at the site for other sediment layers. Thirty randomized profiles were constructed for both the upper range and lower range velocity profiles listed in Table F-8 using the standard deviations and adjacent layer correlation

coefficients given in Table F-7. These profiles look very similar to those shown on Figure F-10.

Figure F-11 presents the shear modulus reduction and damping relationships selected for the Skull Valley soil deposits above the Tertiary sediments (Geomatrix, 2001). The relationships for the 0 to 12-ft depth range and the 12 to 26-ft depth range are based on resonant column tests performed on samples of the site soils. For the sandy soils below a depth of 26 feet, the relationships used by Silva and others (1998) to calibrate ground motion models for alluvial soils in California were selected. Silva and others (1998) developed two alternative sets of relationships. The curves selected for this analysis represent the stiffer (less modulus reduction and lower damping) set. This set was selected because of the low level of modulus reduction and low damping exhibited by the site test data.

The Tertiary sediments and the underlying bedrock were assumed to remain linear during shaking. Damping in these materials was developed following the approach described above for the WUS rock profile. There is no information on the value of κ appropriate for this site. Silva et al. (1998) list κ values for various sites in California, indicating the general site classification. These data suggest that the distribution of κ is similar for rock and shallow soil sites. In addition, Wong and Silva (1993) used a κ of 0.04 seconds in simulating ground motions in Utah for both rock and soil sites. Therefore, the average total site κ of 0.04 seconds for California rock sites was used to characterize the Skull Valley site.

Table F-9 shows the contribution of the low strain damping values in the upper 90 feet of soil to the total κ at the Skull Valley site. Table F-10 shows the damping values obtained for the best estimate and upper and lower range velocity profiles in the Tertiary sediments and the underlying first layer of the crustal model.

Thirty randomized profiles were generated for each of the six Skull Valley profile cases defined above. For each case, the 24 base motions were combined with the 30 randomized profiles to generate 240 surface motions representative of the response of Skull Valley following the same process used for the WUS rock profile.

Relative Site Response Results

The relative response of the Skull Valley site compared to WUS rock sites was assessed by computing the ratio of the 5-percent damped response spectra for a paired set of surface motions one computed using a Skull Valley profile and one computed using a WUS rock

profile. Each pair of surface motions is computed using the same base motion. As a result, there are 240 spectral ratios for each Skull Valley profile case, 120 computed using base motions derived from scaling to a **M** 7 earthquake on the Stansbury fault and 120 computed using base motions derived from scaling to a **M** 6.5 earthquake on the East fault. The following sets of spectral ratios were computed.

Spectral Ratio Cases

Scaling Level for Input Motion	Skull Valley Profile	WUS Profile
M 7 on Stansbury fault	Best Estimate – Constant Tertiary Velocity	Generic Rock
M 6.5 on East fault	Best Estimate – Constant Tertiary Velocity	Generic Rock
M 7 on Stansbury fault	Best Estimate – Increasing Tertiary Velocity	Generic Rock
M 6.5 on East fault	Best Estimate – Increasing Tertiary Velocity	Generic Rock
M 7 on Stansbury fault	Lower Range – Constant Tertiary Velocity	Generic Rock
M 6.5 on East fault	Lower Range – Constant Tertiary Velocity	Generic Rock
M 7 on Stansbury fault	Lower Range – Increasing Tertiary Velocity	Generic Rock
M 6.5 on East fault	Lower Range – Increasing Tertiary Velocity	Generic Rock
M 7 on Stansbury fault	Upper Range – Constant Tertiary Velocity	Generic Rock
M 6.5 on East fault	Upper Range – Constant Tertiary Velocity	Generic Rock
M 7 on Stansbury fault	Upper Range – Increasing Tertiary Velocity	Generic Rock
M 6.5 on East fault	Upper Range – Increasing Tertiary Velocity	Generic Rock

The site adjustment factor for each Skull Valley profile case and level of input motion was defined as the mean of the logs of the 120 spectral ratios computed at each spectral frequency. The mean log spectral ratio is considered appropriate because the empirical ground motion attenuation relationships are defined in terms of the expected log amplitude of ground motion and the purpose of the site adjustment factor is to correct this expected log amplitude to Skull Valley site conditions. In addition, the computed spectral ratios are approximately lognormally distributed. Figure F-12 compares the empirical 16^{th}, 50^{th}, and 84^{th} percentiles for the best estimate-constant Tertiary velocity case (combined **M** 7 and **M** 6.5 scaling) to the mean log [spectral ratio] and the mean log[spectral ratio] ± one standard deviation of log[spectral ratio]. The empirical percentiles were computed by ordering the computed ratios at each spectral period and locating the appropriate percentiles of the empirical distribution.

Figure F-13 presents the results of the 12 analysis cases defined above. Each curve represents the mean log[spectral ratio] of the 120 paired site response calculations. The spectral ratios computed using the two levels of input motion are very similar, indicating that the site adjustment factor can be considered to be independent of ground motion amplitude in the range of interest for this study. In addition, the spectral ratios for periods less than about 0.3 seconds (spectral frequencies greater than about 3 Hz) are insensitive to whether or not the Tertiary velocity remains constant or increases with depth. The spectral ratios for spectral periods

greater than 0.3 seconds (spectral frequencies less than 3 Hz) are sensitive to the variation of velocity with depth in the Tertiary sediments. However, the WUS rock profiles used to compute the spectral ratios did not include randomization at depths below 100 feet and the randomization of the Tertiary velocity profiles was restricted to variability in the location of the abrupt velocity steps for the increasing velocity cases. It is expected that including deeper randomization of the velocity profiles, particularly for the WUS rock profile, would smooth out the topography on the spectral ratios for spectral periods greater than 0.3 seconds. Given these arguments, it was judged appropriate to compute the spectral ratios combining the results for the constant and increasing Tertiary velocity cases.

Figure F-14 compares the combined spectral ratios for the best estimate, upper range and lower range velocity profiles. Again, the primary area of sensitivity is for spectral periods greater than 0.3 seconds, reflecting the uncertainty in the Tertiary sediment velocity. A symmetrical uncertainty factor was applied to the measured velocity to examine the sensitivity of the results to variations in the average velocity. However, the lower range velocity is considered much less likely that the upper range velocity because of the age of the sediments and the fact that the measured velocity in Skull Valley is at the lower end of the range of values reported for this geologic unit elsewhere in Utah. Accordingly, is was judged appropriate to compute the mean log[spectral ratio] for all profile cases, which yields results that are essentially equivalent to the best estimate profile (see upper plot on Figure F-14).

Finally, the combined mean log[spectral ratio] curve was conservatively smoothed by eye to produce the selected site adjustment factors at the spectral periods used for ground motion calculation. These selected factors are designated "site response model" adjustment factors, and are shown on the lower plot on Figure F-14.

As this analysis was being finalized, it was determined that the maximum thickness of soil cement under the pads is to be 2 feet. In addition, the minimum thickness is to be 1 foot. These constraints limit the range in the thickness of the soil-cement layer to 4 to 5 feet in the pad emplacement area instead of the 3 to 7 feet variability used to develop the soil profiles for the site response analyses. Additional site response analyses performed using this more limited variation in thickness in the best estimate velocity profile case produced relative site response factors that differ by 0 to 2 percent from those shown on Figure F-13. Thus, the "site response model" site adjustment factors presented on Figure F-14 are appropriate for the narrower range in the thickness of the soil-cement layer.

SITE ADJUSTMENT FACTOR BASED ON EMPIRICAL STRONG MOTION DATA

As discussed above, the Skull Valley site is classified as a shallow soil site located at the boundary between NEHRP Class C and Class D sites. As such, the velocity characteristics fall within the range of sites that are included in many of the empirical WUS "rock" strong motion data bases used to develop the ground motion models described in Section F.2. In particular, the Abrahamson and Silva (1997) attenuation relationship explicitly includes these types of sites within their "rock" classification. On this basis, ground motions for sites like Skull Valley may be directly assessed using WUS rock attenuation relationships.

The Pacific Earthquake Engineering Research Center (PEER) publishes on the internet a strong motion database developed by Pacific Engineering and Analysis that explicitly identifies shallow soil sites. Table F-11 lists 97 strong motion recordings from that data base that are categorized as shallow soil over rock (depth to rock < ~20 meters). These recordings are for magnitude **M** 5 and greater earthquakes recorded at sites within 50 km of the earthquake rupture in instrument shelters or light buildings.

Using these data, empirical spectral ratios were computed by dividing the spectral accelerations for the recorded motions by the spectral accelerations predicted by the six empirical rock site ground motion models discussed above. Figures F-15 and F-16 show the computed mean log[spectral ratios] and their 90-percent confidence intervals for horizontal and vertical motions, respectively. The confidence intervals are much wider for the Spudich et al. (1997) relationship because the applicable data were limited to the recordings from the Oroville, Mammoth Lakes, and Chalfant Valley earthquakes. The plotted results indicate that the shallow soil site data are on average well predicted by the WUS rock attenuation relationships, with a tendency to under predict for spectral periods greater than about 0.3 seconds.

The empirical spectral ratios shown on Figures F-15 and F-16 were used to develop empirical site adjustment factors. A weighted combination of the spectral ratios for each period was computed as follows. First, all individual spectral ratios less that 1.0 were set to 1.0, under the assumption that WUS rock attenuation models are not expected to over predict shallow soil site ground motions. The adjusted spectral ratios were then combined using the sum of the weights assigned to each attenuation relationship in Tables F-1 and F-2. The resulting "empirical" site adjustment factors are compared to the "site response model" adjustment factors on Figure F-17 and in Table F-12. It should be noted that the empirical site adjustment factors are equivalent in concept to the empirical source adjustment factors used by the Yucca Mountain Ground Motion Panel (see Section F.2).

RELATIVE WEIGHTING OF SITE RESPONSE MODEL AND EMPIRICAL SITE CORRECTION FACTORS

Both the site response modeling and the empirical data approaches presented above for developing site adjustment factors have advantages that tend to favor their use in predicting earthquake hazards for a given site. The "site response model" is based on data that reflect soil conditions at the site, and its use is in line with the common use of site response analyses to assess site-specific ground motions. On the other hand, the "empirical model" has the advantage that it employs actual strong motion data recorded at shallow soil sites. In fact, the approach that has been used in the past to develop "site-specific" ground motions for nuclear power plants is based on statistical analysis of recorded strong ground motions from sites with subsurface conditions similar to the site in question (Standard Review Plan, Rev. 2, Section 2.6.2.6; Kimball, 1983).

Because of the relative advantages of both methods, it is appropriate to incorporate the results obtained from each into the hazard calculation. The question becomes what relative weight to give to the site adjustment factors generated by each model. A similar question was addressed by the Yucca Mountain Ground Motion Expert Panel in their development of source adjustment factors in order to apply California strong motion attenuation relationships to the Yucca Mountain site. That panel incorporated source adjustment factors based on both analytical ground motion models and comparisons with empirical data. The Expert Panel generally favored the use of source adjustments based on modeling results over those based on empirical corrections. Excluding the weights assigned to Abrahamson and Silva (1997) and Spudich et al. (1997) in Table F-1, the average combined relative weight assigned to the empirical adjustment factors by the Expert Panel are 0.36 to the empirical scaling factors A-E and ½A-E and 0.64 to the modeling adjustment factors KCSC and WSSC. Empirical scaling of the Abrahamson and Silva (1997) attenuation relationships was favored by the Expert Panel, perhaps because the empirical source scaling factors were developed specifically using this relationship by Dr Abrahamson. No source scaling was strongly favored by the Expert Panel for the Spudich et al. (1997) relationship because it was specifically developed for normal faulting earthquakes.

In line with the relative preference for analytical compared to empirical ground motion adjustment factors used by the Yucca Mountain Ground Motion Expert Panel, we assign twice as much weight (0.67) to the site response site adjustment factors than to the empirical site adjustment factors (0.33) in computing the hazard at the Skull Valley site. This correlation of relative weights is reasonable because the subsurface soil conditions at most of the sites listed

in Table F-11 are not well known. In addition, the soils at many of these sites may show a greater degree on nonlinear behavior (modulus reduction and damping increase) than the Skull Valley soils exhibit at high levels of shaking (large shear strains). However, this is counter balanced by the fact that the level of ground shaking recorded at these sites is, in general, lower than that at the hazard levels of interest in this study. The lower level of shaking suggests that most of the sites listed in Table F-11 would have experienced, on average, a relatively low level of nonlinear behavior. Thus, the uncertainties associated with the potential for non-linear behavior at the sites listed in Table F-11 are balanced by the lower levels of ground shaking experienced at those sites.

TABLE F-1

EMPIRICAL ATTENUATION RELATIONSHIPS FOR HORIZONTAL MOTIONS AND SEISMIC SOURCE SCALING FACTORS FROM THE YUCCA MOUNTAIN GROUND MOTION EXPERT PANEL

Private Fuel Storage Facility
Skull Valley, Utah

Rock Site Attenuation Relationship	Earthquake Source Scaling Method	Average Weight Across Yucca Mountain Expert Panel	Re-normalized Weights Combining Numerical Modeling Scaling Factors
Abrahamson and Silva (1997)	None	0	0
	A-E	0.222	0.223
	½ A-E	0.036	0.036
	KCSC	0.051	--
	WSSC	0.014	0.065
Boore and others (1997)	None	0.006	0.006
	A-E	0.014	0.014
	½ A-E	0.036	0.036
	KCSC	0.042	--
	WSSC	0.050	0.092
Campbell (1997)	None	0.006	0.006
	A-E	0.029	0.029
	½ A-E	0.036	0.036
	KCSC	0.051	--
	WSSC	0.036	0.087
Idriss (1991, 1997)	None	0.006	0.006
	A-E	0.014	0.014
	½ A-E	0	0
	KCSC	0.051	--
	WSSC	0.021	0.072
Sadigh and others (1997)	None	0.006	0.006
	A-E	0.029	0.029
	½ A-E	0.036	0.036
	KCSC	0.051	--
	WSSC	0.021	0.072
Spudich and others (1997)	None	0.115	0.116
	KCSC	0.018	0.018
Sabetta and Pugliese (1996)	None	0.006	--

TABLE F-2

EMPIRICAL ATTENUATION RELATIONSHIPS FOR VERTICAL MOTIONS AND SEISMIC SOURCE SCALING FACTORS FROM THE YUCCA MOUNTAIN GROUND MOTION EXPERT PANEL

Private Fuel Storage Facility
Skull Valley, Utah

Rock Site Attenuation Relationship	Earthquake Source Scaling Method	Average Weight Across Yucca Mountain Expert Panel	Re-normalized Weights Combining Numerical Modeling Scaling Factors
Abrahamson and Silva (1997)	None	0.000	0
	A-E	0.321	0.333
	½ A-E	0.036	0.037
	KCSC	0.095	--
	WSSC	0.026	0.126
Boore and others (1997)	None	0.000	
	A-E	0.000	
	½ A-E	0.036	
	KCSC	0.000	--
	WSSC	0.000	
Campbell (1997)	None	0.014	0.014
	A-E	0.041	0.042
	½ A-E	0.036	0.037
	KCSC	0.095	--
	WSSC	0.074	0.175
Sadigh and others (1997)	None	0.014	0.014
	A-E	0.041	0.042
	½ A-E	0.036	0.037
	KCSC	0.095	--
	WSSC	0.042	0.142

TABLE F-3

BEST ESTIMATE PROFILE FOR SKULL VALLEY PFSF SITE CONSTANT TERTIARY SEDIMENT VELOCITY

Private Fuel Storage Facility
Skull Valley, Utah

Layer	Depth to Base of Layer (ft)	Average Layer Shear Wave Velocity (fps)	Average Layer Compression Wave Velocity (fps)	Unit Weight (pcf)
Eolian silts	5±2	560	1,117	
Lacustrine silt	10±1	528	1,131	80
Lacustrine silt	12±1	727	1,260	80
Lacustrine sand	18±1	854	1,472	100
Lacustrine silt	26±1	871	1,440	94
Lacustrine sands	35±1	1,022	1,667	115
Lacustrine sands	50±5	1,190	2,085	115
Dense sands and silty sands capped by Promontory Soil	90±5	1,800	3,400	120
Tertiary Salt Lake group – unsaturated	125	2,900	5,023	135
Tertiary Salt Lake group – saturated	700±100	2,900	5,023	145
Shallow crustal rocks	4,593	6,398	11,155	165
Crustal rocks	15 km	11,122	19,357	170

Increasing Tertiary Sediment Velocity

Layer	Depth to Base of Layer (ft)	Average Layer Shear Wave Velocity (fps)	Average Layer Compression Wave Velocity (fps)	Unit Weight (pcf)
Eolian silts	5±2	560	1,117	
Lacustrine silt	10±1	528	1,131	80
Lacustrine silt	12±1	727	1,260	80
Lacustrine sand	18±1	854	1,472	100
Lacustrine silt	26±1	871	1,440	94
Lacustrine sands	35±1	1,022	1,667	115
Lacustrine sands	50±5	1,190	2,085	115
Dense sands and silty sands capped by Promontory Soil	90±5	1,800	3,400	120
Tertiary Salt Lake group – unsaturated, Layer 1	125	2,900	5,023	135
Tertiary Salt Lake group – saturated, Layer 1	300±33	2,900	5,023	145
Tertiary Salt Lake group – saturated, Layer 2	500±67	4,000	6,928	145
Tertiary Salt Lake group – saturated, Layer 4	700±100	5,000	8,660	145
Shallow crustal rocks	4,593	6,398	11,155	165
Crustal rocks	15 km	11,122	19,357	170

TABLE F-4

ROCK RECORDINGS USED IN SITE RESPONSE ANALYSES

Private Fuel Storage Facility
Skull Valley, Utah

Record	Earthquake	M	Station	Comp (°)	Distance (km)	PGA (g)
1	San Fernando, CA	6.6	Pacoima Dam [279]	254	2.8	1.16
2	1971/02/09		Lake Hughs #12 [128]	021	20.3	0.37
3	Victoria, Mexico	6.4	Cerro Prieto	045	34.8	0.62
	1980/06/09					
4	Irpinia, Italy	6.9	Bagnoli Irpinio	000	10.9	0.14
5	1980/11/23		Bagnoli Irpinio	270		0.20
6			Sturno	000	16.2	0.25
7			Sturno	270		0.36
8	Irpinia, Italy aftershock	6.2	Calitri	000	8.4	0.18
9	1980/11/23		Calitri	270		0.17
10	Loma Prieta, CA	7.0	Gilroy #1	090	11.2	0.47
11	1989/10/17		Corratilos	000	5.1	0.64
12			Corratilos	090		0.48

TABLE F-5A

CONTRIBUTION TO κ FROM TOP 350 FT OF WUS ROCK PROFILE

Private Fuel Storage Facility
Skull Valley, Utah

Layer	h (ft)	Total h (ft)	Vs (fps)	Lambda	Qs	kappa (sec)
1	5	5	800	0.040	12.5	0.00050
2	8	13	1000	0.040	12.5	0.00064
3	7	20	1200	0.040	12.5	0.00047
4	10	30	1400	0.033	15.2	0.00047
5	14	44	1750	0.033	15.2	0.00053
6	11	55	2070	0.033	15.2	0.00035
7	14	69	2350	0.033	15.2	0.00039
8	19	88	2750	0.033	15.2	0.00046
9	22	110	3170	0.033	15.2	0.00046
10	108	218	3281	0.033	15.2	0.00218
11	131	349	3904	0.033	15.2	0.00222
					Total	0.00866

TABLE F-5B

MATERIAL DAMPING FOR WUS ROCK PROFILE

Private Fuel Storage Facility
Skull Valley, Utah

Layer	H (km)	Total Thickness (km)	Shear Wave Velocity (km/s)	H/Vs²	Q	Damping Ratio	Layer κ (sec)
1	0.065	0.065	1.36	0.035	15.1	0.0331	0.0032
2	0.1	0.165	1.53	0.043	17.0	0.0294	0.0038
3	0.115	0.28	1.72	0.039	19.1	0.0262	0.0035
4	0.16	0.44	1.89	0.045	21.0	0.0238	0.0040
5	0.237	0.677	2.07	0.055	23.0	0.0217	0.0050
6	0.228	0.905	2.3	0.043	25.6	0.0196	0.0039
7	0.55	1.455	2.55	0.085	28.3	0.0176	0.0076
			Sum	0.345		Sum	0.0310
			Gamma =	11.11			

TABLE F-6

STATISTICS OF SHEAR WAVE VELOCITIES AT SKULL VALLEY SITE (GEOMATRIX, 2001)

Private Fuel Storage Facility
Skull Valley, Utah

Layer	Depth Range (ft)	Number of Velocity Profiles	Average Shear Wave Velocity (fps)	Standard Deviation in Shear Wave Velocity (fps)	Coefficient of Variation	90% Confidence Interval in Mean Velocity (fps)	Computed Correlation Coefficient with Layer Above
1	0-5	15	560	57	0.10	±24	--
2	5-10	17	528	70	0.13	±28	0.13
3	10-12	17	727	100	0.14	±40	0.34
4	12-18	17	854	55	0.06	±22	0.21
5	18-26	17	871	32	0.04	±13	-0.05
6	26-35	7	1,022	78	0.08	±48	0.58

TABLE F-7

STATISTICAL MODEL FOR BEST ESTIMATE PROFILE FOR SKULL VALLEY PFSF SITE CONSTANT TERTIARY SEDIMENT VELOCITY

Private Fuel Storage Facility
Skull Valley, Utah

Layer	Depth to Base of Layer (ft)	Average Layer Shear Wave Velocity (fps)	Standard Deviation of Shear Wave Velocity (fps)	Correlation Coefficient with Layer Above
1	5±2	1,500	150	--
2	10±1	528	70	0.0
3	12±1	727	100	0.25
4	18±1	854	55	0.25
5	26±1	871	32	0.0
6	35±1	1,022	78	0.25
7	50±5	1,190	90	0.25
8a	70±5	1,800	180	0.0
8b	90±5	1,800	180	0.5
9	125	2,900	0	--
10	700±100	2,900	0	--
11	4,593	6,398	0	--
12	5 km	11,122	0	--

Increasing Tertiary Sediment Velocity

Layer	Depth to Base of Layer (ft)	Average Layer Shear Wave Velocity (fps)	Standard Deviation of Shear Wave Velocity (fps)	Correlation Coefficient with Layer Above
1	5±2	1,500	150	--
2	10±1	528	70	0.0
3	12±1	727	100	0.25
4	18±1	854	55	0.25
5	26±1	871	32	0.0
6	35±1	1,022	78	0.25
7	50±5	1,190	90	0.25
8a	70±5	1,800	180	0.0
8b	90±5	1,800	180	0.5
9	125	2,900	0	--
10	300±30	2,900	0	--
11	500±50	4,000	0	--
12	700±100	5,000	0	--
13	4,593	6,398	0	--
14	5 km	11,122	0	--

TABLE F-8

BEST ESTIMATE AND UPPER AND LOWER RANGE VELOCITY PROFILES FOR SKULL VALLEY PFSF SITE CONSTANT TERTIARY SEDIMENT VELOCITY

Private Fuel Storage Facility
Skull Valley, Utah

Layer	Depth to Base of Layer (ft)	Lower Range Average Layer Shear Wave Velocity (fps)	Best Estimate Average Layer Shear Wave Velocity (fps)	Upper Range Average Layer Shear Wave Velocity (fps)
1	5±2	1,225	1,500	1,837
2	10±1	500	528	556
3	12±1	687	727	767
4	18±1	832	854	876
5	26±1	858	871	884
6	35±1	974	1,022	1,070
7	50±5	1,034	1,190	1,248
8a	70±5	1,620	1,800	1,980
8b	90±5	1,620	1,800	1,980
9	125	2,368	2,900	3,552
10	700±100	2,368	2,900	3,552
11	4,593	6,398	6,398	6,398
12	5 km	11,122	11,122	11,122

Increasing Tertiary Sediment Velocity

Layer	Depth to Base of Layer (ft)	Lower Range Average Layer Shear Wave Velocity (fps)	Best Estimate Average Layer Shear Wave Velocity (fps)	Upper Range Average Layer Shear Wave Velocity (fps)
1	5±2	1,225	1,500	1,837
2	10±1	500	528	556
3	12±1	687	727	767
4	18±1	832	854	876
5	26±1	858	871	884
6	35±1	974	1,022	1,070
7	50±5	1,034	1,190	1,248
8a	70±5	1,620	1,800	1,980
8b	90±5	1,620	1,800	1,980
9	125	2,368	2,900	3,552
10	300±30	2,368	2,900	3,552
11	500±70	3,266	4,000	4,899
12	700±100	4,083	5,000	6,124
13	4,593	6,398	6,398	6,398
14	5 km	11,122	11,122	11,122

TABLE F-9

CONTRIBUTION TO κ FROM TOP 90 FT OF SKULL VALLEY PROFILE LOWER RANGE VELOCITIES

Private Fuel Storage Facility
Skull Valley, Utah

Lower Range Velocities

Layer	h (ft)	Total h (ft)	Vs (fps)	Lambda	Qs	kappa (sec)
1	5	5	538	0.009	55.6	0.00017
2	5	10	500	0.009	55.6	0.00018
3	2	12	687	0.009	55.6	0.00005
4	6	18	832	0.008	62.5	0.00012
5	8	26	858	0.008	62.5	0.00015
6	9	35	974	0.010	50.0	0.00018
7	15	50	1134	0.010	50.0	0.00026
8	40	90	1620	0.006	83.3	0.00030
					Total =	0.00141

Best Estimate Velocities

Layer	h (ft)	Total h (ft)	Vs (fps)	Lambda	Qs	kappa (sec)
1	5	5	562	0.009	55.6	0.00016
2	5	10	528	0.009	55.6	0.00017
3	2	12	727	0.009	55.6	0.00005
4	6	18	854	0.008	62.5	0.00011
5	8	26	871	0.008	62.5	0.00015
6	9	35	1022	0.010	50.0	0.00018
7	15	50	1190	0.010	50.0	0.00025
8	40	90	1800	0.006	83.3	0.00027
					Total =	0.00133

Upper Range Velocities

Layer	h (ft)	Total h (ft)	Vs (fps)	Lambda	Qs	kappa (sec)
1	5	5	586	0.009	55.6	0.00015
2	5	10	556	0.009	55.6	0.00016
3	2	12	767	0.009	55.6	0.00005
4	6	18	876	0.008	62.5	0.00011
5	8	26	884	0.008	62.5	0.00014
6	9	35	1070	0.010	50.0	0.00017
7	15	50	1246	0.010	50.0	0.00024
8	40	90	1980	0.006	83.3	0.00024
					Total =	0.00127

TABLE F-10

MATERIAL DAMPING FOR SKULL VALLEY

Private Fuel Storage Facility
Skull Valley, Utah

Best Estimate Profile - Constant Tertiary Velocity

Layer	H (km)	Total Thickness (km)	Shear Wave Velocity (km/s)	H/Vs²	Q	Damping Ratio	Layer κ (sec)
9-10	0.185	0.186	0.88392	0.237	12.7	0.0394	0.0165
11	1.214	1.4	1.95	0.319	28.0	0.0178	0.0222
			Sum =	0.556		Sum =	0.0387
			Gamma =	14.37			

Best Estimate Profile - Increasing Tertiary Velocity

Layer	H (km)	Total Thickness (km)	Shear Wave Velocity (km/s)	H/Vs²	Q	Damping Ratio	Layer κ (sec)
9-10	0.061667	0.061667	0.88392	0.079	10.6	0.0470	0.0066
11	0.061667	0.123333	1.2192	0.041	14.7	0.0340	0.0034
12	0.061667	0.185	1.524	0.027	18.4	0.0272	0.0022
13	1.214	1.399	1.95	0.319	23.5	0.0213	0.0265
			Sum=	0.466		Sum =	0.0387
			Gamma =	12.05			

Lower Range Profile - Constant Tertiary Velocity

Layer	H (km)	Total Thickness (km)	Shear Wave Velocity (km/s)	H/Vs²	Q	Damping Ratio	Layer κ (sec)
9-10	0.185	0.186	0.7217	0.355	12.6	0.0397	0.0203
11	1.214	1.4	1.95	0.319	34.1	0.0147	0.0183
			Sum=	0.674		Sum =	0.0386
			Gamma =	17.47			

Lower Range Profile - Increasing Tertiary Velocity

Layer	H (km)	Total Thickness (km)	Shear Wave Velocity (km/s)	H/Vs²	Q	Damping Ratio	Layer κ (sec)
9-10	0.061667	0.061667	0.7217	0.118	10.2	0.0491	0.0084
11	0.061667	0.123333	0.9555	0.068	13.5	0.0371	0.0048
12	0.061667	0.185	1.2443	0.040	17.6	0.0285	0.0028
13	1.214	1.399	1.95	0.319	27.5	0.0182	0.0226
			Sum =	0.545		Sum =	0.0386
			Gamma =	14.12			

TABLE F-10

MATERIAL DAMPING FOR SKULL VALLEY

Private Fuel Storage Facility
Skull Valley, Utah

Upper Range Profile - Constant Tertiary Velocity

Layer	H (km)	Total Thickness (km)	Shear Wave Velocity (km/s)	H/Vs²	Q	Damping Ratio	Layer κ (sec)
9-10	0.185	0.186	1.0826	0.158	13.3	0.0375	0.0128
11	1.214	1.4	1.95	0.319	24.0	0.0208	0.0259
			Sum=	0.477		Sum =	0.0387
			Gamma =	12.33			

Upper Range Profile - Increasing Tertiary Velocity

Layer	H (km)	Total Thickness (km)	Shear Wave Velocity (km/s)	H/Vs²	Q	Damping Ratio	Layer κ (sec)
9-10	0.061667	0.061667	1.0826	0.053	11.7	0.0428	0.0049
11	0.061667	0.123333	1.4932	0.028	16.1	0.0310	0.0026
12	0.061667	0.185	1.8335	0.018	19.8	0.0253	0.0017
13	1.214	1.4	1.95	0.319	21.1	0.0237	0.0296
			Sum=	0.418		Sum =	0.0387
			Gamma =	10.80			

TABLE F-11

STRONG MOTION RECORDINGS FOR SHALLOW SOIL SITES

Private Fuel Storage Facility
Skull Valley, Utah

Earthquake	Date	Time	Magnitude M	Station	Rupture Distance (km)	Average Horizontal PGA (g)	Vertical PGA (g)
Parkfield	6/28/66	4:26	6.1	Cholame #8	9.2	0.259	0.116
Parkfield	6/28/66	4:26	6.1	Cholame #12	14.7	0.061	0.053
Lytle Creek	9/12/70	14:30	5.4	Cedar Springs Pumphouse	23.7	0.073	0.037
Lytle Creek	9/12/70	14:30	5.4	Puddingstone Dam (Abutment)	32.8	0.019	0.014
Lytle Creek	9/12/70	14:30	5.4	Wrightwood - 6074 Park Dr	15.4	0.180	0.078
San Fernando	2/09/71	14:00	6.6	Castaic - Old Ridge Route	24.9	0.295	0.171
San Fernando	2/09/71	14:00	6.6	Lake Hughes #12	20.3	0.322	0.167
San Fernando	2/09/71	14:00	6.6	Pacoima Dam	2.8	1.193	0.699
San Fernando	2/09/71	14:00	6.6	Pearblossom Pump	38.9	0.118	0.050
Friuli, Italy	5/06/76	20:00	6.5	Barcis	49.7	0.030	0.014
Friuli, Italy	5/06/76	20:00	6.5	Tolmezzo	37.7	0.333	0.268
Fruili, Italy	9/11/76	16:31	5.5	Forgaria Cornino	18.2	0.102	0.046
Friuli, Italy	9/15/76	3:15	6.1	Forgaria Cornino	13.5	0.235	0.095
Tabas, Iran	9/16/78	0:00	7.4	Dayhook	17	0.365	0.183
Coyote Lake	8/06/79	17:05	5.7	Gilroy Array #6	3.1	0.370	0.146
Livermore	1/24/80	19:00	5.8	Del Valle Dam (Toe)	12.9	0.169	0.083
Livermore	1/24/80	19:00	5.8	Fremont - Mission San Jose	29.8	0.049	0.027
Livermore	1/24/80	19:00	5.8	San Ramon Fire Station	21.7	0.048	0.016
Livermore	1/24/80	19:00	5.8	San Ramon - Eastman Kodak	17.6	0.108	0.042
Livermore	1/27/80	2:33	5.4	Del Valle Dam (Toe)	12.9	0.042	0.028
Livermore	1/27/80	2:33	5.4	Fremont - Mission San Jose	29.8	0.037	0.017
Livermore	1/27/80	2:33	5.4	Livermore - Fagundas Ranch	3.6	0.245	0.098
Livermore	1/27/80	2:33	5.4	San Ramon - Eastman Kodak	17.6	0.171	0.037
Livermore	1/27/80	2:33	5.4	San Ramon Fire Station	21.7	0.054	0.022
Mammoth Lakes	6/11/80	4:41	5	Convict Lakes (CON)	7.6	0.187	0.091
Mammoth Lakes	6/11/80	4:41	5	Mammoth Elem School	12.3	0.015	0.000
Mammoth Lakes	6/11/80	4:41	5	USC Convict Lakes	9.1	0.037	0.038
Coalinga	5/02/83	23:42	6.4	Parkfield - Cholame 2E	40.5	0.031	0.017
Coalinga	5/02/83	23:42	6.4	Parkfield - Fault Zone 4	34.3	0.090	0.046
Coalinga	5/02/83	23:42	6.4	Parkfield - Fault Zone 6	32.8	0.056	0.026
Coalinga	5/02/83	23:42	6.4	Parkfield - Fault Zone 8	29.6	0.123	0.054
Coalinga	5/02/83	23:42	6.4	Parkfield - Fault Zone 9	31.9	0.053	0.026
Coalinga	5/02/83	23:42	6.4	Parkfield - Fault Zone 11	28.4	0.092	0.042
Coalinga	5/02/83	23:42	6.4	Parkfield - Fault Zone 15	29.9	0.140	0.084
Coalinga	5/02/83	23:42	6.4	Parkfield - Gold Hill 2W	36.6	0.078	0.036
Coalinga	5/02/83	23:42	6.4	Parkfield - Gold Hill 3W	38.8	0.129	0.067
Coalinga	5/02/83	23:42	6.4	Parkfield - Gold Hill 4W	41	0.074	0.029
Coalinga	5/02/83	23:42	6.4	Parkfield - Gold Hill 5W	43.7	0.063	0.034
Coalinga	5/02/83	23:42	6.4	Parkfield - Vineyard Cany 4W	34.6	0.054	0.024
Coalinga	5/02/83	23:42	6.4	Parkfield - Vineyard Cany 5W	37.1	0.062	0.048

TABLE F-11

STRONG MOTION RECORDINGS FOR SHALLOW SOIL SITES

Private Fuel Storage Facility
Skull Valley, Utah

Earthquake	Date	Time	Magnitude M	Station	Rupture Distance (km)	Average Horizontal PGA (g)	Vertical PGA (g)
Coalinga	5/09/83	2:49	5	Anticline Ridge - Palmer Ave	12.6	0.251	0.049
Coalinga	5/09/83	2:49	5	Oil City	13.3	0.267	0.098
Coalinga	5/09/83	2:49	5	Palmer Ave	12.7	0.242	0.095
Coalinga	7/09/83	7:40	5.2	Oil City	10	0.378	0.210
Coalinga	7/09/83	7:40	5.2	Palmer Ave	14	0.152	0.073
Coalinga	7/22/83	2:39	5.8	Oil City	8.2	0.622	0.568
Coalinga	7/22/83	2:39	5.8	Palmer Ave	12.2	0.281	0.201
Morgan Hill	4/24/84	21:15	6.2	Corralitos	22.7	0.094	0.040
Morgan Hill	4/24/84	21:15	6.2	Fremont - Mission San Jose	31.4	0.023	0.018
Morgan Hill	4/24/84	21:15	6.2	Gilroy Array #6	11.8	0.255	0.405
Morgan Hill	4/24/84	21:15	6.2	Gilroy Array #7	14	0.147	0.428
Morgan Hill	4/24/84	21:15	6.2	Gilroy - Gavilan Coll.	16.2	0.104	0.081
Hollister	1/26/86	19:20	5.4	SAGO South - Surface	14.9	0.063	0.053
N. Palm Springs	7/08/86	9:20	6	Cranston Forest Station	35.3	0.161	0.118
N. Palm Springs	7/08/86	9:20	6	Hurkey Creek Park	34.9	0.212	0.097
Chalfant Valley	7/20/86	14:29	5.9	Lake Crowley - Shehorn Res.	26	0.040	0.029
Chalfant Valley	7/21/86	14:42	6.2	Lake Crowley - Shehorn Res.	36	0.122	0.085
Whittier Narrows	10/01/87	14:42	6	Brea Dam (L Abut)	23.3	0.133	0.097
Whittier Narrows	10/01/87	14:42	6	Garvey Res. - Control Bldg	12.1	0.419	0.362
Whittier Narrows	10/01/87	14:42	6	LA - Baldwin Hills	27	0.150	0.114
Whittier Narrows	10/01/87	14:42	6	LA - Chalon Rd #	32.6	0.027	0.019
Whittier Narrows	10/01/87	14:42	6	LA - N Faring Rd #	28.5	0.050	0.034
Whittier Narrows	10/01/87	14:42	6	Malibu - Las Flores Canyon #	46.3	0.060	0.015
Whittier Narrows	10/01/87	14:42	6	Mill Creek, Angeles Nat For #	34.5	0.080	0.040
Whittier Narrows	10/01/87	14:42	6	Orange Co. Reservoir	23	0.191	0.126
Whittier Narrows	10/01/87	14:42	6	Pacific Palisades - Sunset #	38.6	0.049	0.035
Whittier Narrows	10/01/87	14:42	6	Pacoima Kagel Canyon	37.9	0.165	0.055
Whittier Narrows	10/01/87	14:42	6	Santa Monica - Second St #	32.6	0.034	0.021

TABLE F-11

STRONG MOTION RECORDINGS FOR SHALLOW SOIL SITES

Private Fuel Storage Facility
Skull Valley, Utah

Earthquake	Date	Time	Magnitude M	Station	Rupture Distance (km)	Average Horizontal PGA (g)	Vertical PGA (g)
Whittier Narrows	10/01/87	14:42	6	Sun Valley - Sunland #	29.3	0.075	0.043
Whittier Narrows	10/01/87	14:42	6	Tarzana - Cedar Hill	43	0.538	0.248
Whittier Narrows	10/01/87	14:42	6	Villa Park - Serrano Ave #	30.1	0.058	0.033
Whittier Narrows	10/01/87	14:42	6	West Covina - S Orange #	10.5	0.157	0.131
Whittier Narrows	10/04/87	10:59	5.3	LA - Baldwin Hills	27.6	0.093	0.040
Whittier Narrows	10/04/87	10:59	5.3	Tarzana - Cedar Hill	42.7	0.091	0.037
Loma Prieta	10/18/89	0:05	6.9	Corralitos	5.1	0.555	0.455
Loma Prieta	10/18/89	0:05	6.9	Fremont - Emerson Court	43.4	0.165	0.067
Loma Prieta	10/18/89	0:05	6.9	Fremont - Mission San Jose	43	0.115	0.080
Loma Prieta	10/18/89	0:05	6.9	Gilroy - Gavilan Coll.	11.6	0.341	0.191
Loma Prieta	10/18/89	0:05	6.9	Gilroy Array #6	19.9	0.146	0.101
Loma Prieta	10/18/89	0:05	6.9	Gilroy Array #7	24.2	0.270	0.115
Loma Prieta	10/18/89	0:05	6.9	SAGO South - Surface	34.7	0.070	0.060
Loma Prieta	10/18/89	0:05	6.9	UCSC	18.1	0.350	0.223
Loma Prieta	10/18/89	0:05	6.9	Woodside	39.9	0.081	0.050
Northridge	1/17/94	12:31	6.7	Burbank - Howard Rd.	20	0.140	0.085
Northridge	1/17/94	12:31	6.7	Castaic - Old Ridge Route #	22.6	0.540	0.217
Northridge	1/17/94	12:31	6.7	LA - Baldwin Hills #	31.3	0.200	0.091
Northridge	1/17/94	12:31	6.7	LA - Chalon Rd	23.7	0.204	0.174
Northridge	1/17/94	12:31	6.7	LA - N Faring Rd	23.9	0.257	0.191
Northridge	1/17/94	12:31	6.7	Lake Hughes #4 - Camp Mend #	32.3	0.069	0.053
Northridge	1/17/94	12:31	6.7	Lake Hughes #4B - Camp Mend #	32.3	0.048	0.042
Northridge	1/17/94	12:31	6.7	Malibu - Point Dume Sch #	35.2	0.105	0.087
Northridge	1/17/94	12:31	6.7	Pacific Palisades - Sunset	26.2	0.304	0.179
Northridge	1/17/94	12:31	6.7	Pacoima Kagel Canyon #	8.2	0.361	0.169
Northridge	1/17/94	12:31	6.7	Sandberg - Bald Mtn #	43.4	0.094	0.044
Northridge	1/17/94	12:31	6.7	Simi Valley - Katherine Rd	14.6	0.749	0.402
Northridge	1/17/94	12:31	6.7	Tarzana - Cedar Hill #	17.5	1.327	1.048
Kobe	1/16/95	20:46	6.9	KJMA	0.6	0.701	0.343

TABLE F-12

SITE ADJUSTMENT FACTORS

Private Fuel Storage Facility
Skull Valley, Utah

Period (sec)	Site Response Factor	Horizontal Empirical Factor	Vertical Empirical Factor
PGA	1.41	1.02	1.00
0.05	1.41	1.04	1.02
0.075	1.45	1.05	1.03
0.1	1.54	1.05	1.04
0.15	1.63	1.05	1.06
0.2	1.72	1.05	1.14
0.3	1.63	1.06	1.22
0.4	1.40	1.08	1.28
0.5	1.30	1.16	1.34
0.75	1.20	1.17	1.30
1.0	1.15	1.15	1.26
1.5	1.02	1.11	1.20
2.0	1.02	1.06	1.20
3.0	1.08	1.06	1.15
4.0	1.08	1.06	1.06

Non-GDS

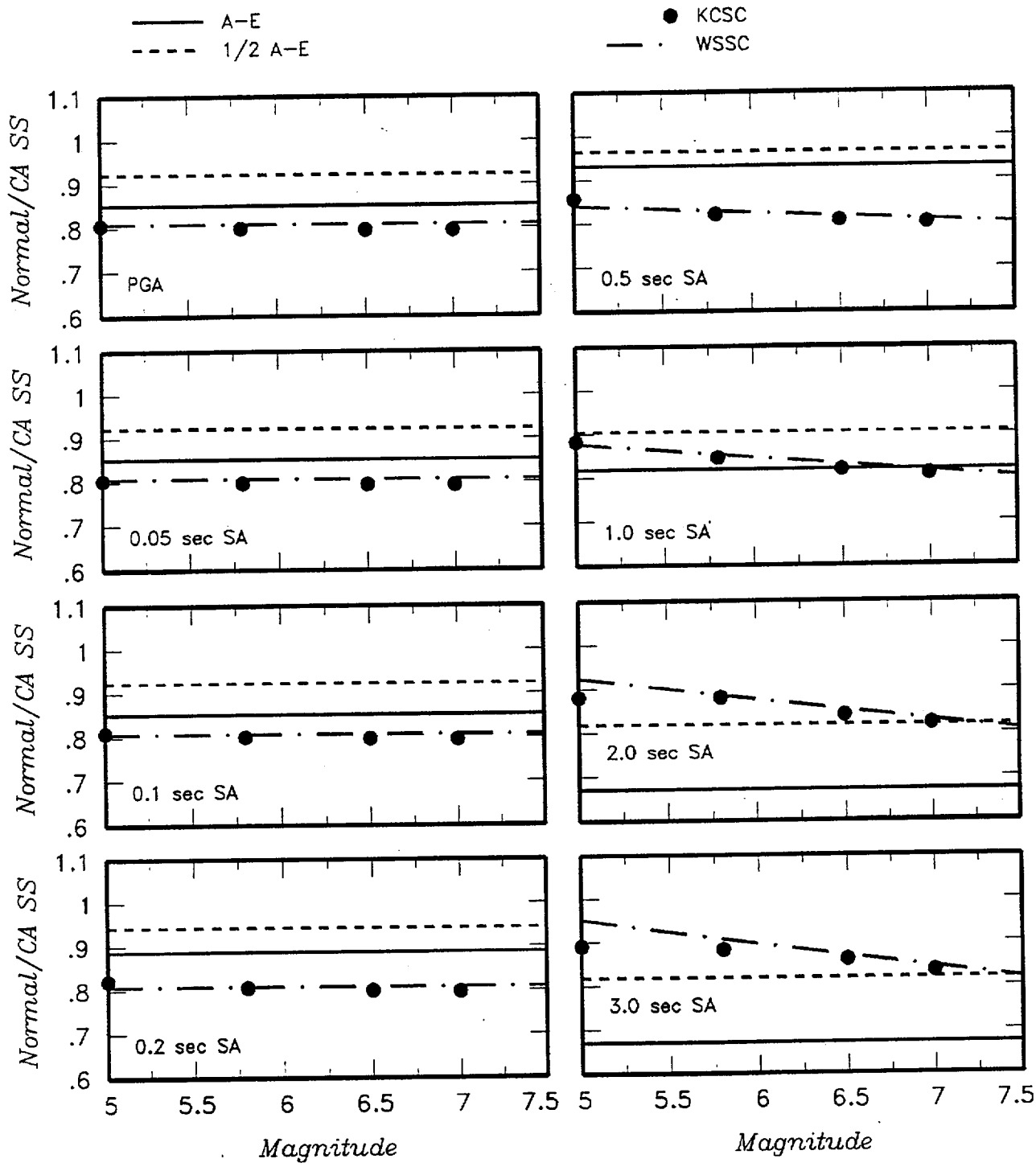

I:\DOC_SAFE\4000S\4790\4790-002\...F1-REV1

GEOMATRIX

SCALING RELATIONSHIPS DEVELOPED FOR THE YUCCA MOUNTAIN PROJECT (CRWMS M&O, 1998) FOR TRANSLATING HORIZONTAL GROUND MOTIONS FROM CALIFORNIA STRIKE-SLIP EARTHQUAKES TO EXTENSIONAL TECTONICS NORMAL FAULTING EARTHQUAKE MOTIONS.

Project No. 4790.002

Figure F-1

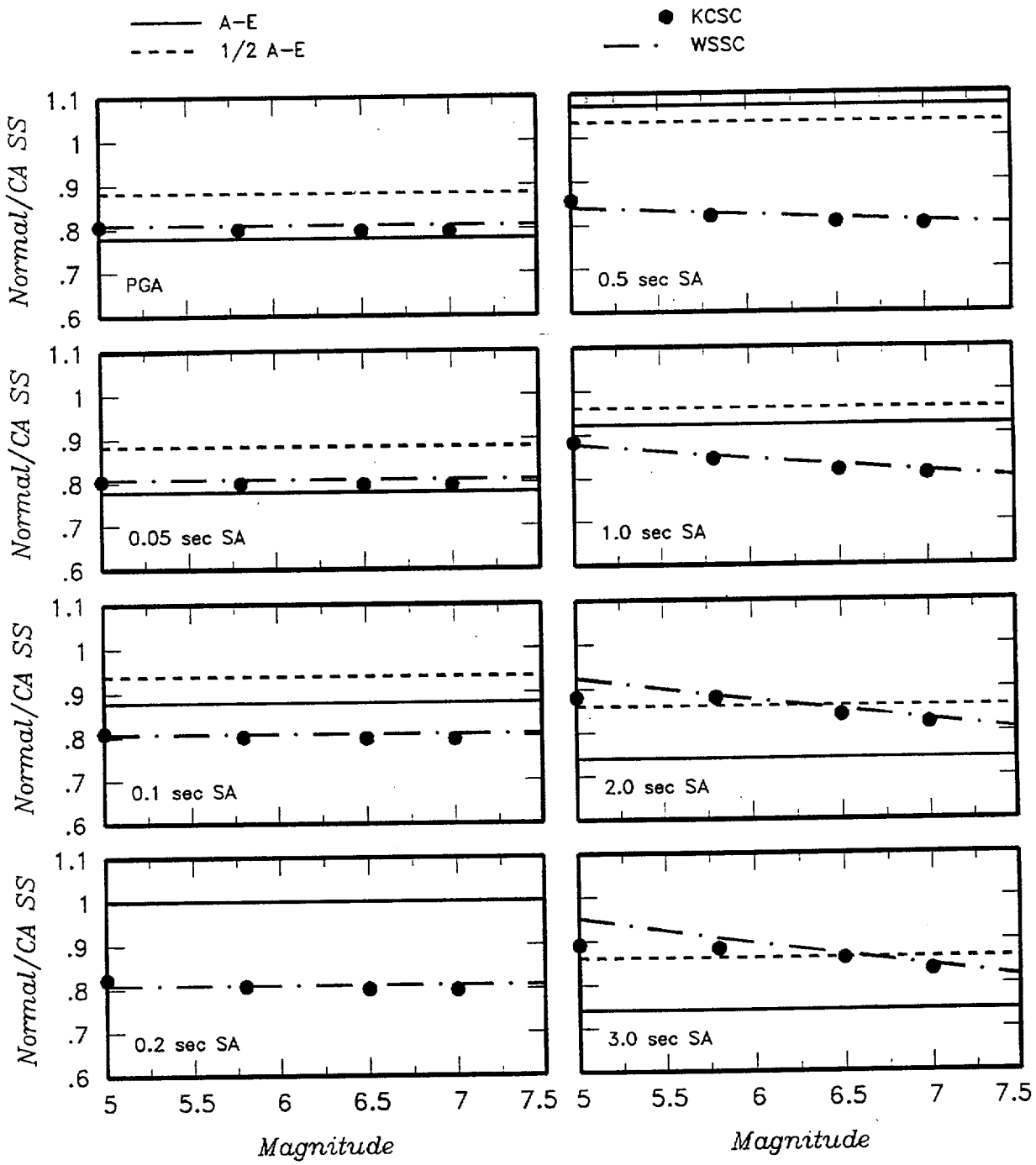

GEOMATRIX

SCALING RELATIONSHIPS DEVELOPED FOR THE YUCCA MOUNTAIN PROJECT (CRWMS M&O, 1998) FOR TRANSLATING VERTICAL GROUND MOTIONS FROM CALIFORNIA STRIKE-SLIP EARTHQUAKES TO EXTENSIONAL TECTONICS NORMAL FAULTING EARTHQUAKE MOTIONS.

Project No. 4790.002

Figure F-2

I:\DOC_SAFE\4000S\4790\4790-002\...F3-REV1

Non-GDS

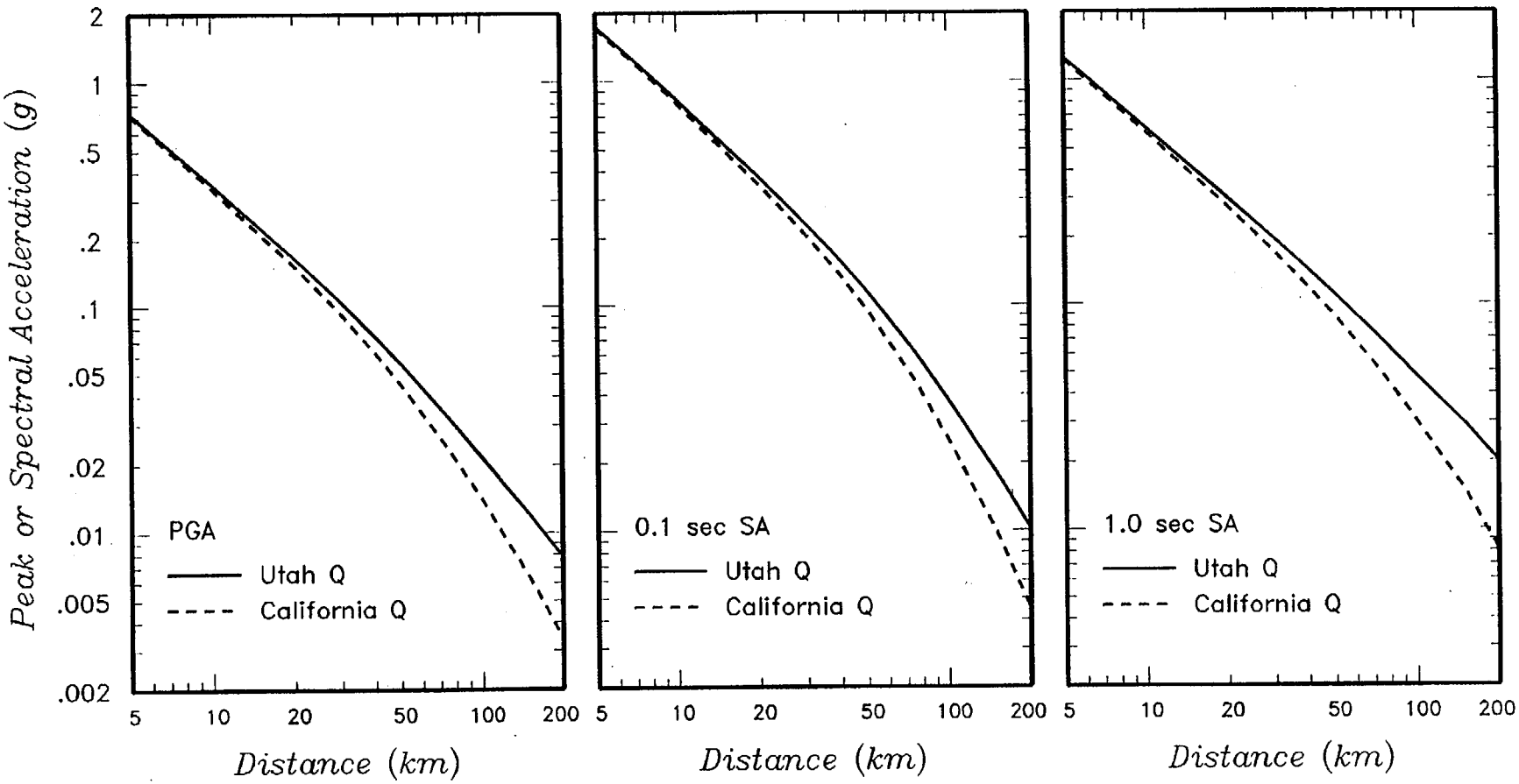

GEOMATRIX

SCALING RELATIONSHIPS DEVELOPED FOR THE YUCCA MOUNTAIN PROJECT (CRWMS M&O, 1998) FOR TRANSLATING VERTICAL GROUND MOTIONS FROM CALIFORNIA STRIKE-SLIP EARTHQUAKES TO EXTENSIONAL TECTONICS NORMAL FAULTING EARTHQUAKE MOTIONS.

Project No. 4790.002

Figure **F-3**

Non-GDS

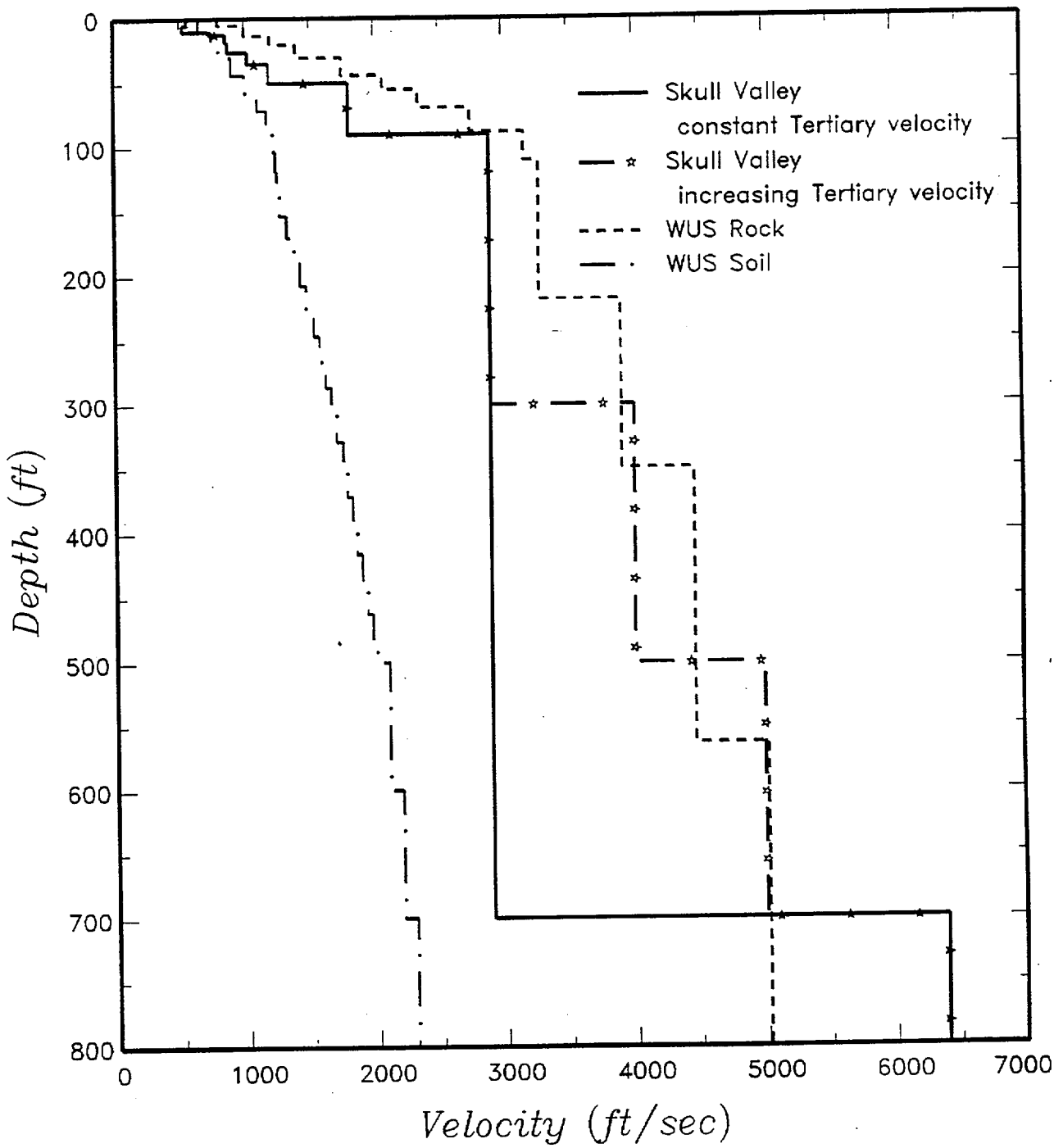

GEOMATRIX

COMPARISON OF BEST ESTIMATE VELOCITY PROFILE FOR SKULL VALLEY TO GENERIC WUS ROCK AND SOIL PROFILES DEVELOPED BY SILVA ET AL. (1998).

Project No. 4790.002

Figure F-4

I:\DOC_SAFE\4000S\4790\4790-002\...F4-REV1

I:\DOC_SAFE\4000S\4790\4790-002\...F5-REV1

Non-GDS

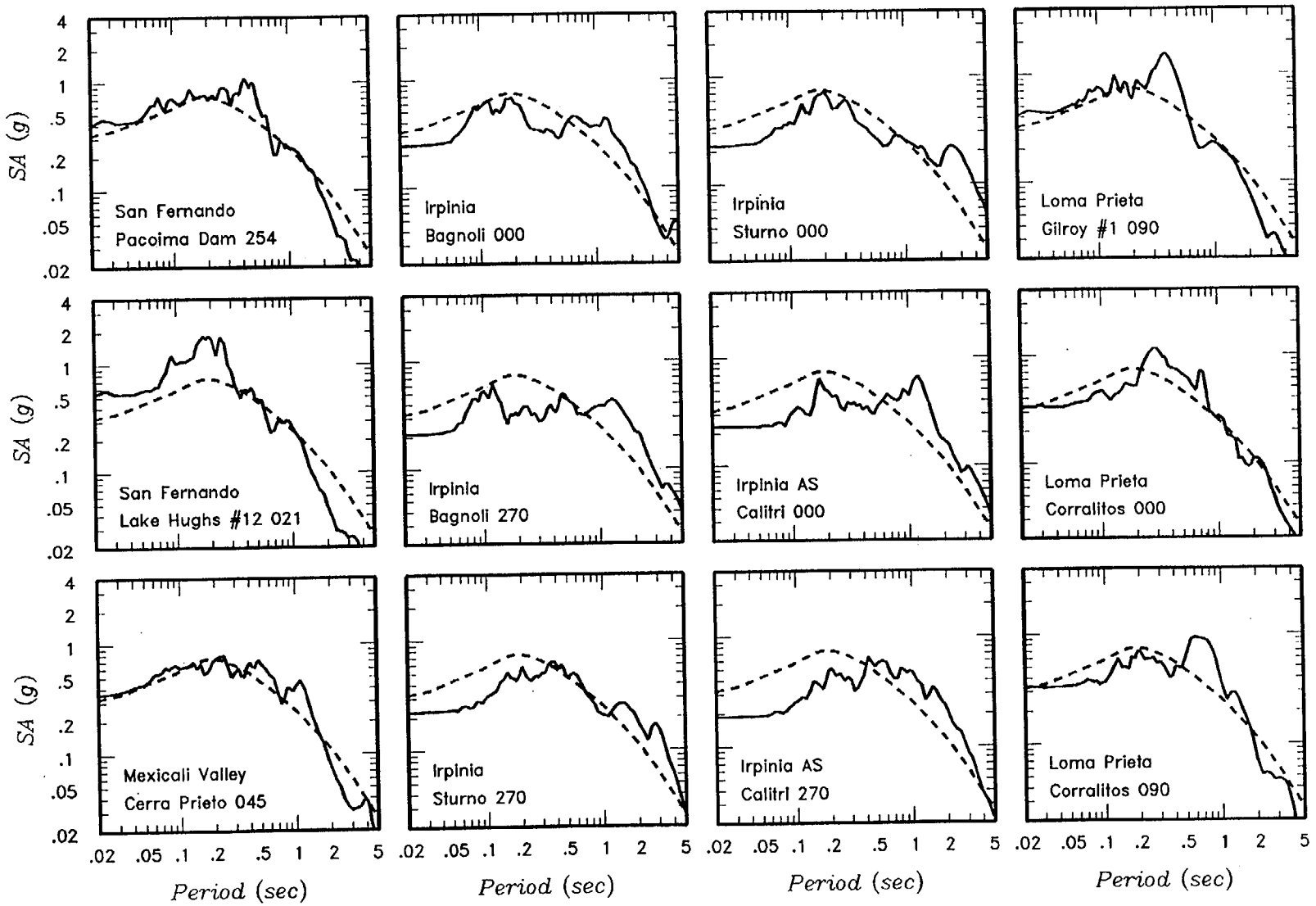

GEOMATRIX

ROCK SITE MOTIONS SCALED TO MEDIAN RESPONSE SPECTRUM
FOR A M 7 EARTHQUAKE ON THE STANSBURY FAULT.

Project No.
4790.002

Figure
F-5

I:\DOC_SAFE\4000S\4790\4790-002\...F6-REV1

Non-GDS

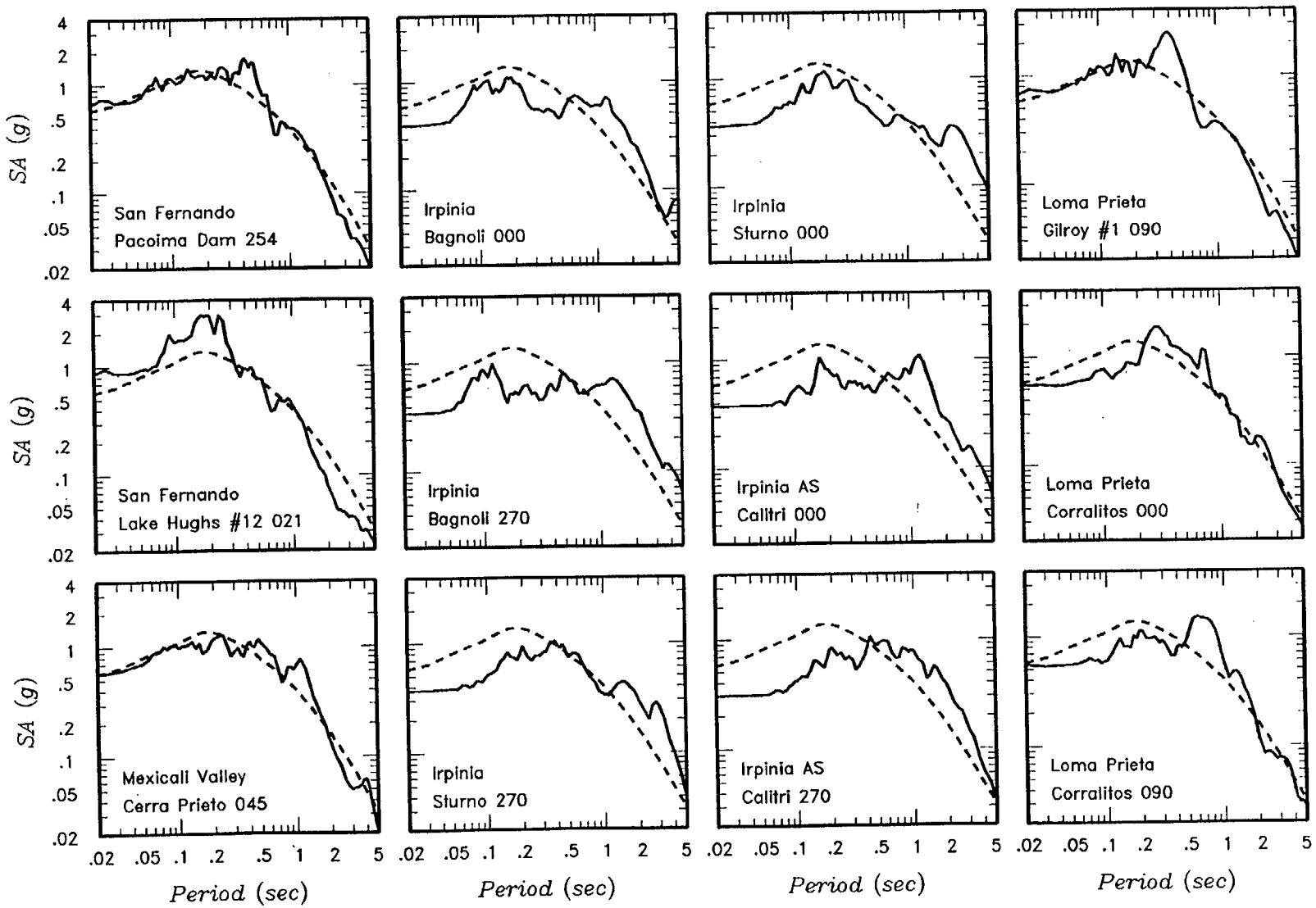

GEOMATRIX

ROCK SITE MOTIONS SCALED TO MEDIAN RESPONSE SPECTRUM
FOR A **M** 6.5 EARTHQUAKE ON THE EAST FAULT.

Project No.
4790.002

Figure
F-6

Non-GDS

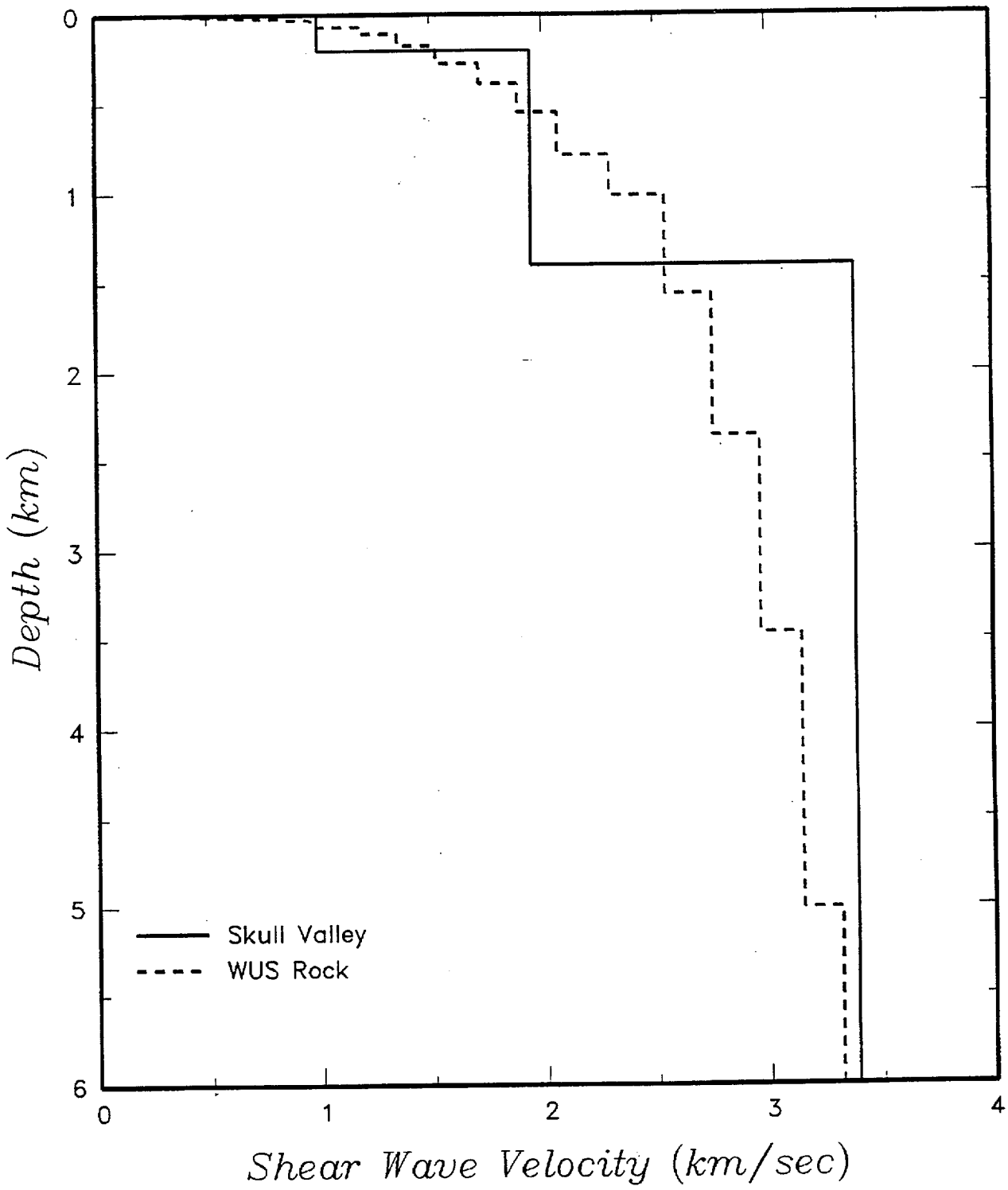

I:\DOC_SAFE\4000S\4790\4790-002\...F7-REV1

GEOMATRIX

COMPARISON OF CRUSTAL VELOCITY PROFILES FOR SKULL VALLEY AND GENERIC WUS ROCK FROM SILVA ET AL. (1998).

Project No. 4790.002

Figure F-7

Non-GDS

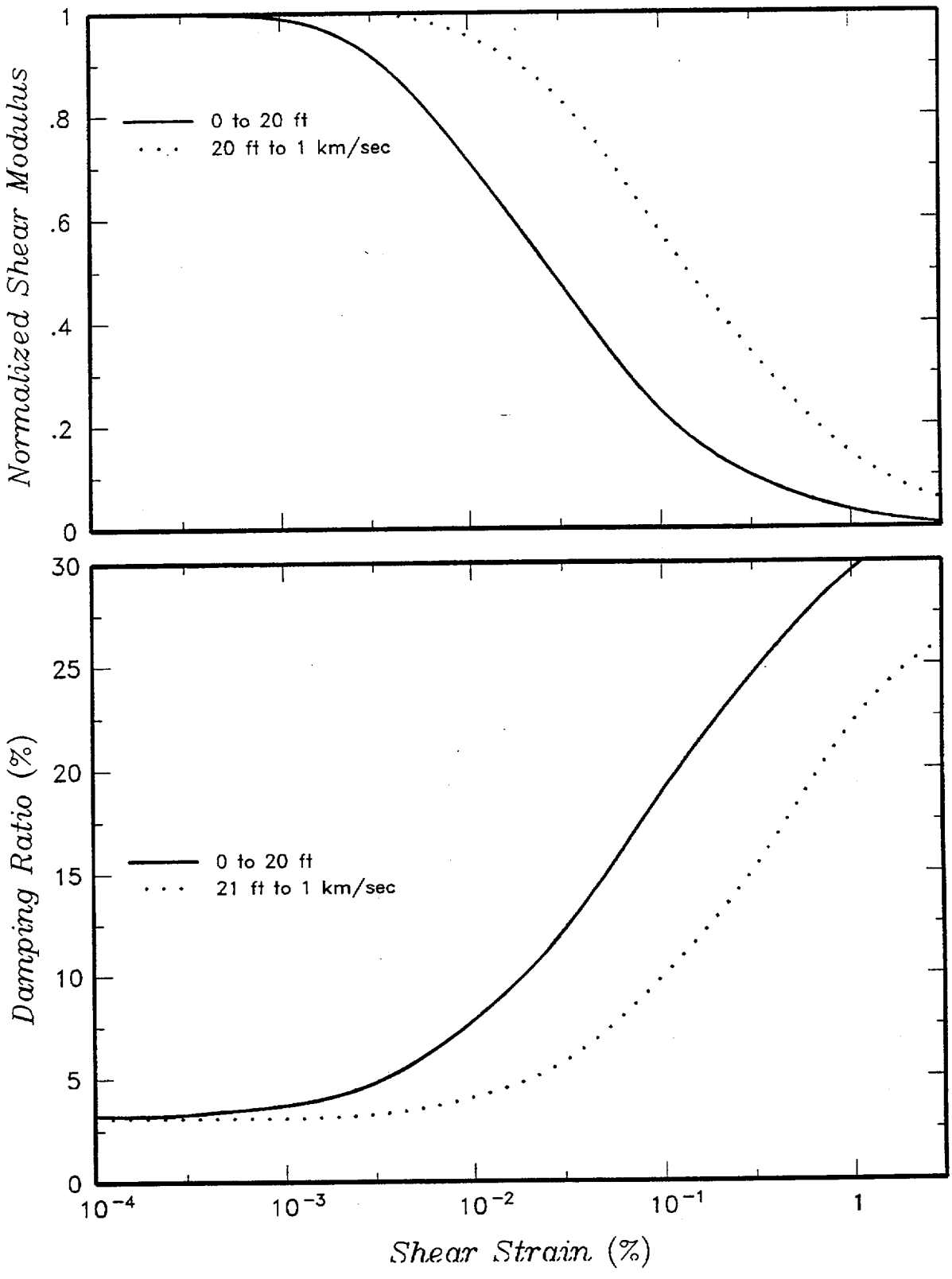

GEOMATRIX

MODULUS REDUCTION AND DAMPING RELATIONSHIPS FOR WEATHERED ROCK (SILVA AND OTHERS, 1998).

Project No. 4790.002

Figure F-8

I:\DOC_SAFE\4000S\4790\4790-002\...F8-REV1

Non-GDS

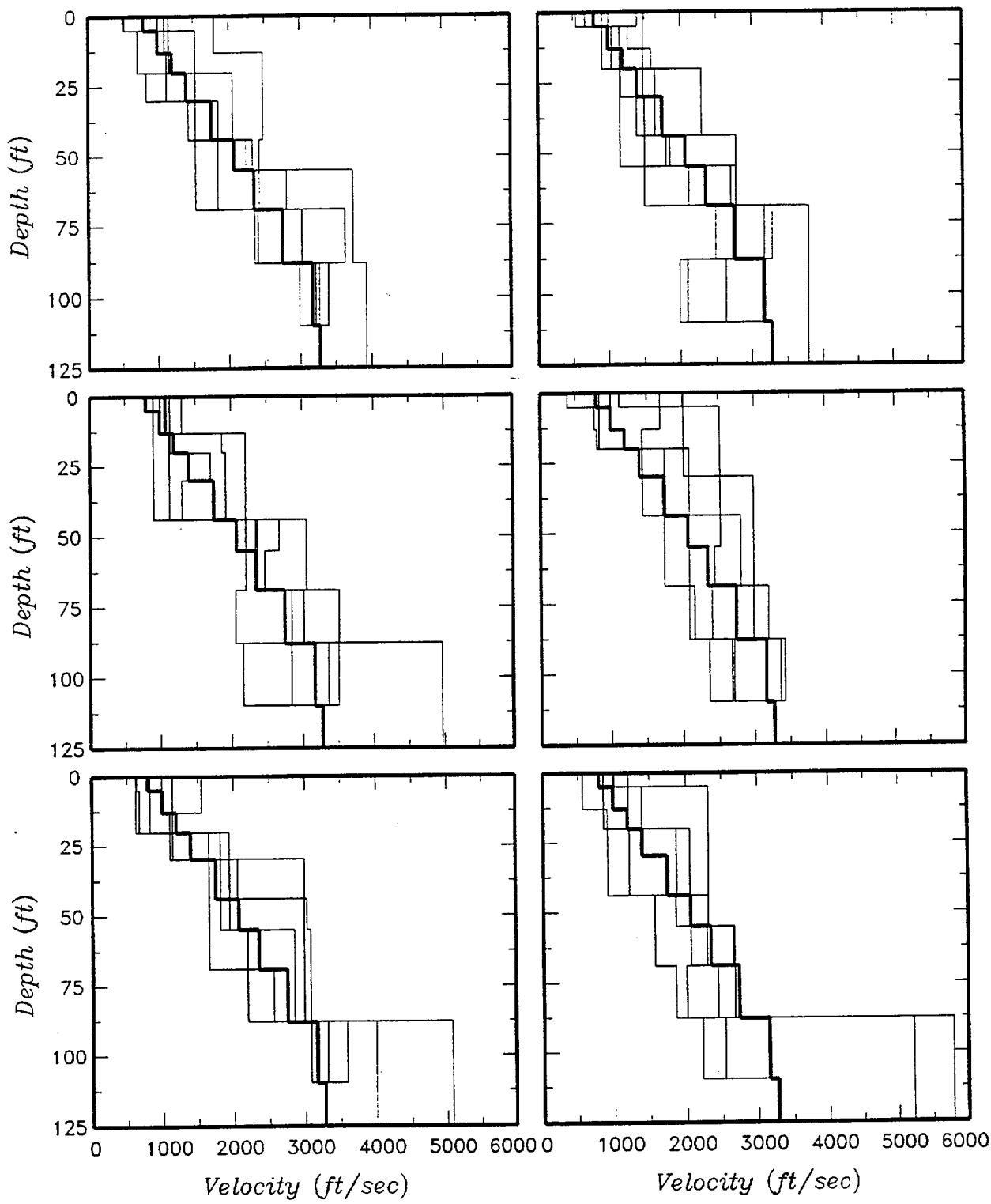

GEOMATRIX

THIRTY RANDOMIZED WUS ROCK VELOCITY PROFILES.

Project No.
4790.002

Figure
F-9

I:\DOC_SAFE\4000S\4790\4790-002\...F9-REV1

Non-GDS

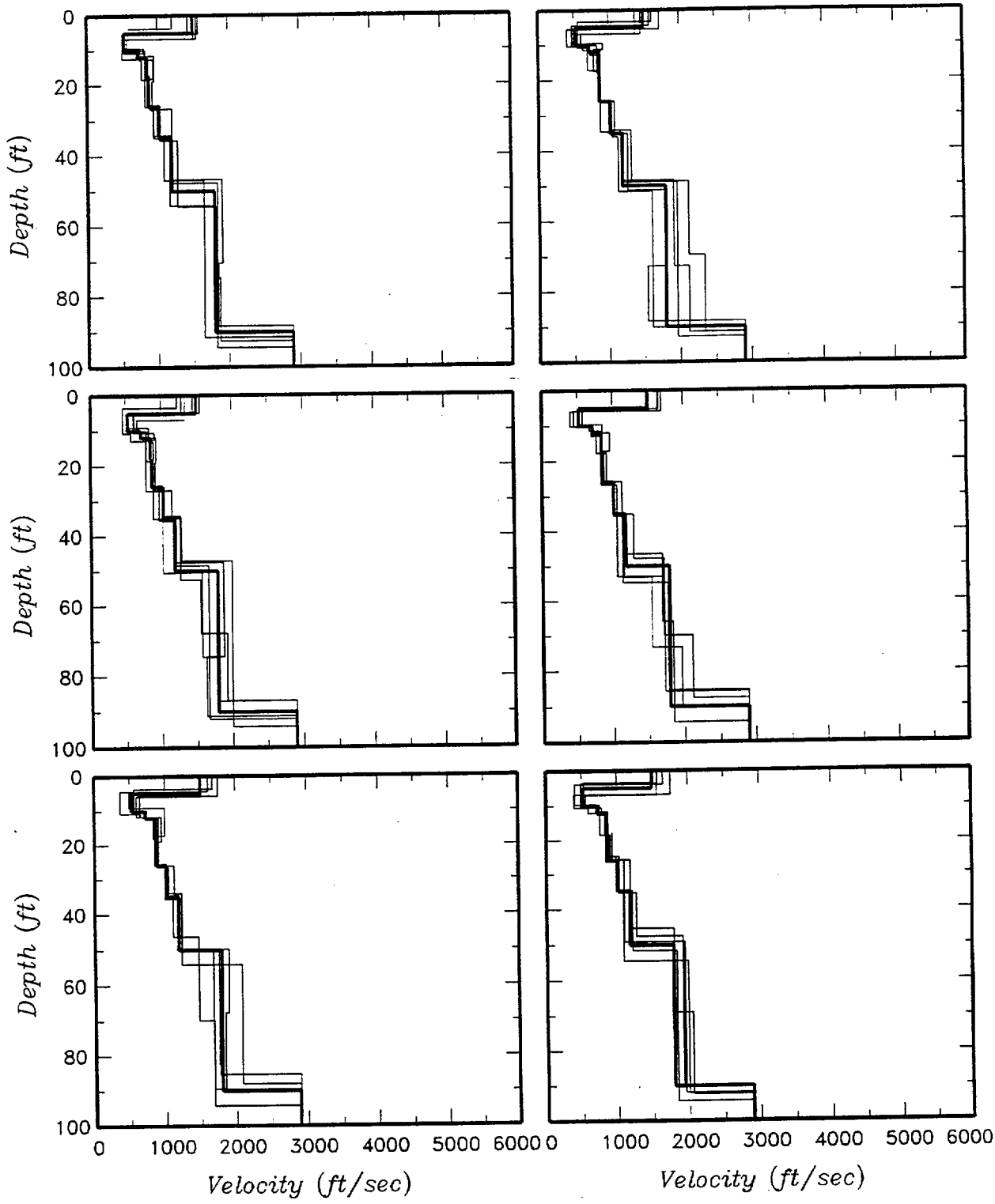

GEOMATRIX

THIRTY RANDOMIZED SKULL VALLEY VELOCITY PROFILES USING BEST ESTIMATE VELOCITY PROFILE.

Project No. 4790.002

Figure F-10

I:\DOC_SAFE\4000SI\4790\4790-002\...F10-REV1

Non-GDS

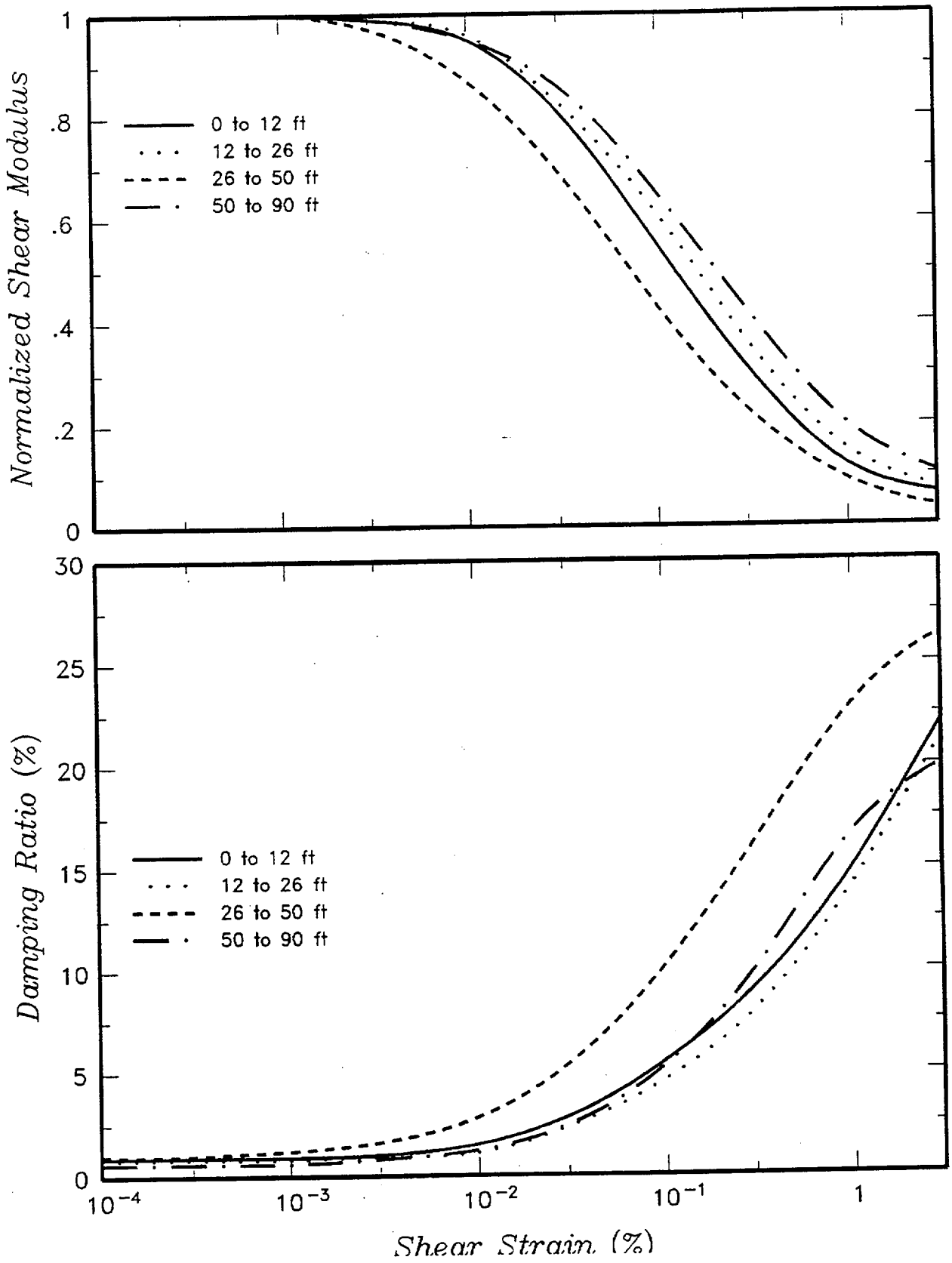

GEOMATRIX

MODULUS REDUCTION AND DAMPING RELATIONSHIPS FOR SKULL VALLEY SOILS.

Project No. 4790.002

Figure **F-11**

I:\DOC_SAFE\4000S\4790\4790-002\...F11-REV1

Non-GDS

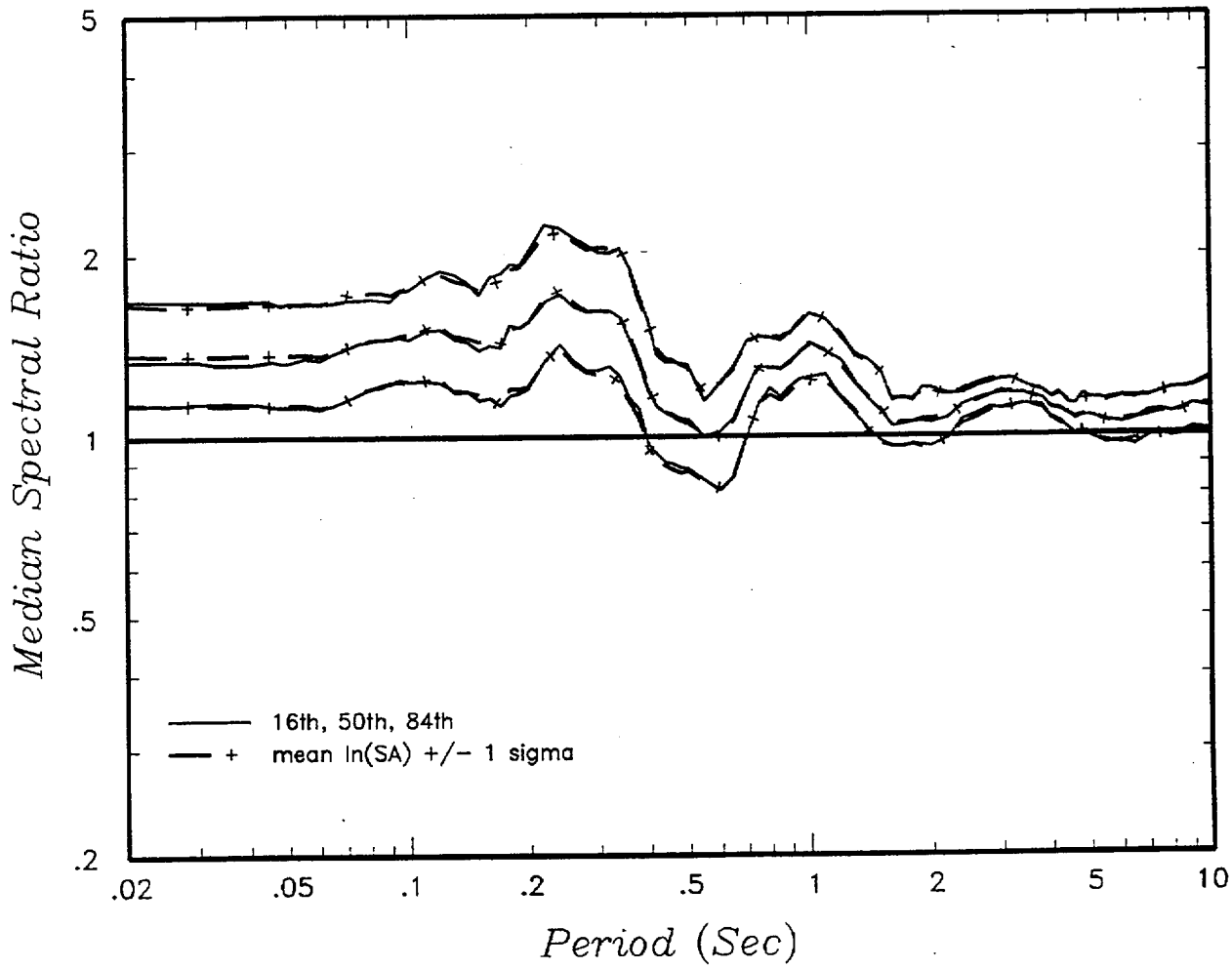

I:\DOC_SAFE\4000S\4790\4790-002\...F12-REV1

GEOMATRIX

COMPARISON OF EMPERICAL PERCENTILES OF SPECTRAL RATIO DISTRIBUTION TO MEAN LOG[SPECTRAL RATIO] AND MEAN LOG[SPECTRAL RATIO] ± ONE STANDARD DEVIATION OF LOG[SPECTRAL RATIO].

Project No. 4790.002

Figure F-12

Non-GDS

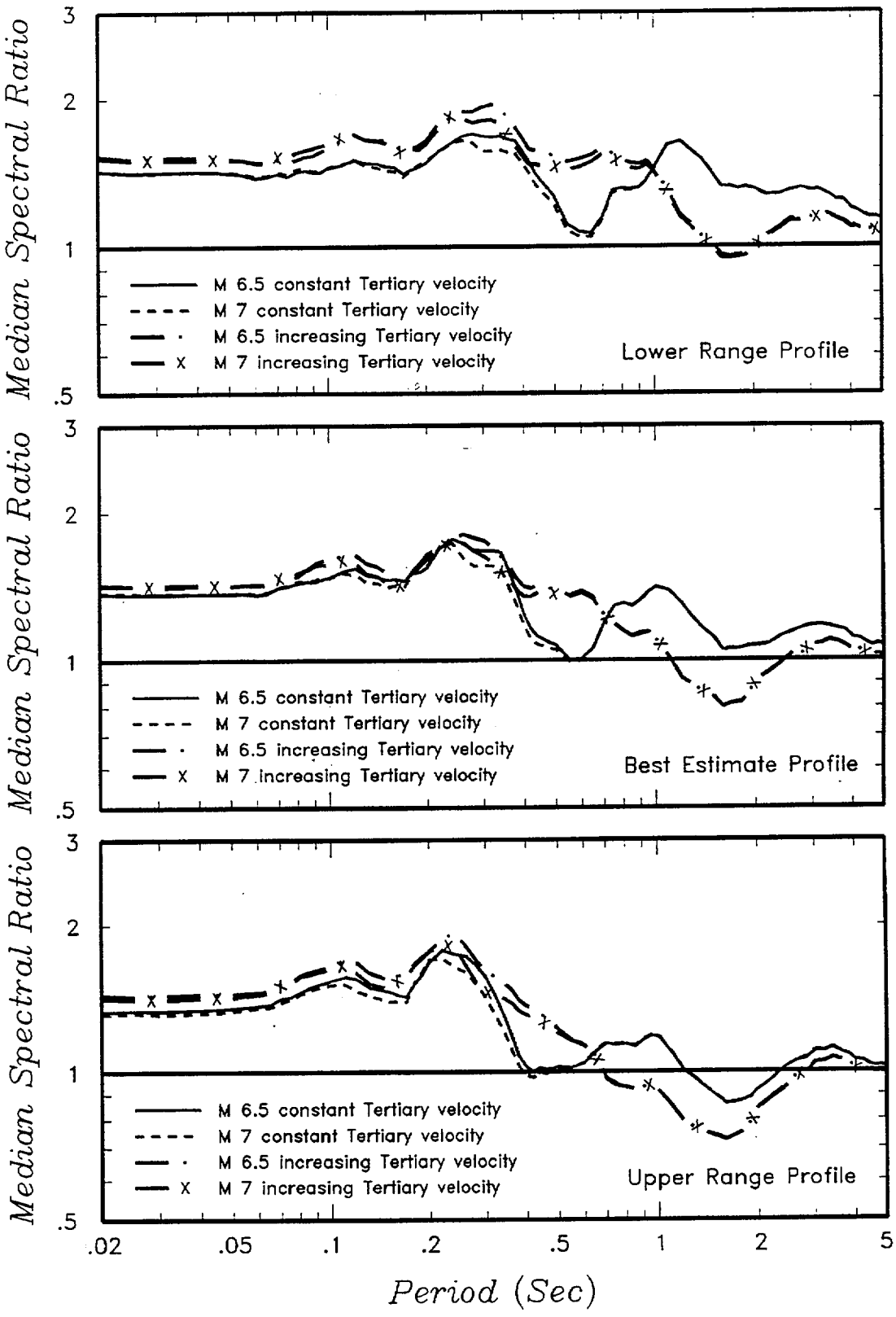

I:\DOC_SAFE\4000S\4790\4790-002\...F13-REV1

GEOMATRIX

RELATIVE SITE RESPONSE
SPECTRAL RATIOS FOR 12 ANALYSIS CASES.

Project No.
4790.002

Figure
F-13

Non-GDS

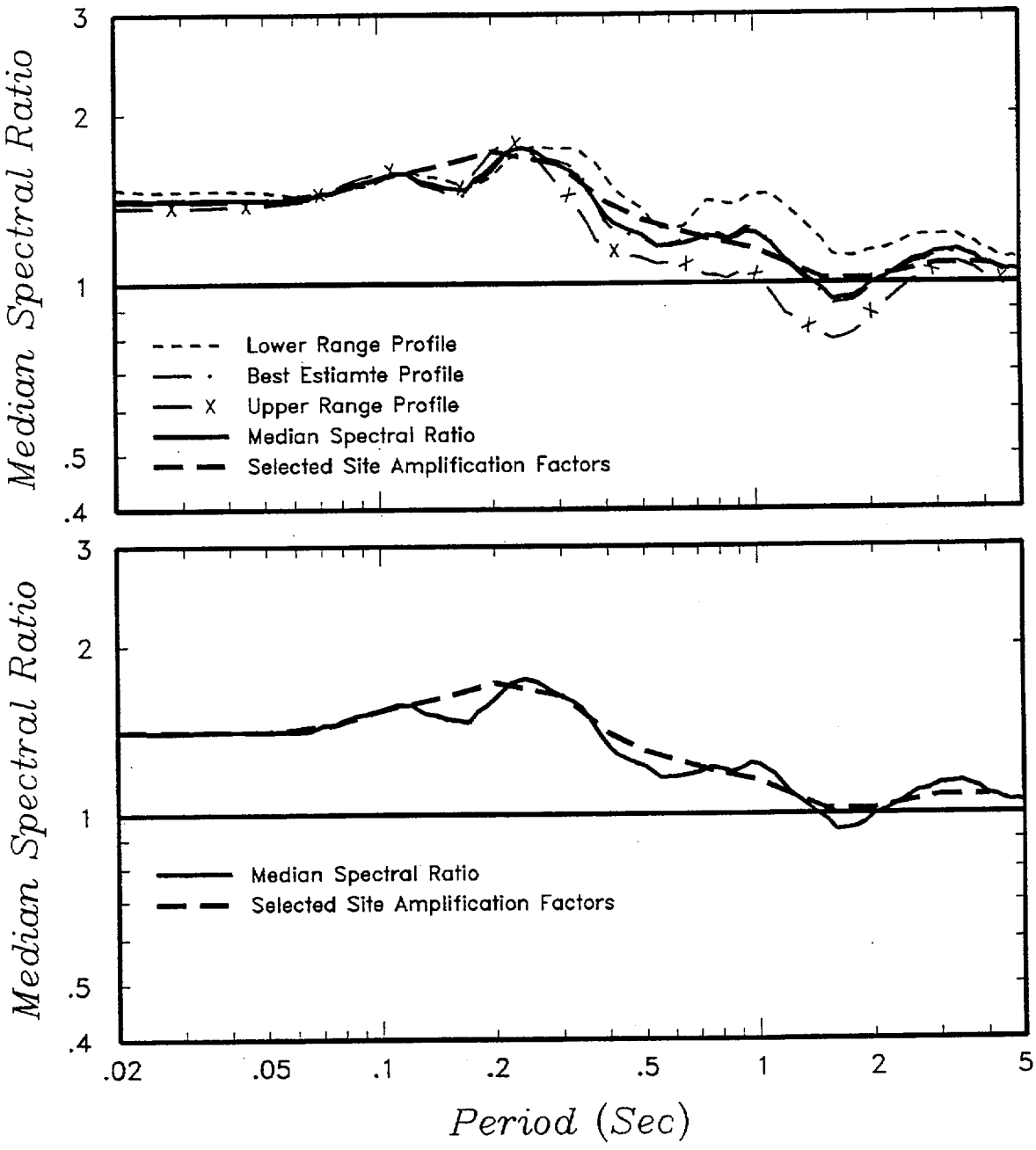

I:\DOC_SAFE\4000S\4790\4790-002\...F14-REV1

GEOMATRIX

COMBINED SPECTRAL RATIOS FOR BEST ESTIMATE, UPPER RANGE AND LOWER RANGE PROFILES AND SELECTED SITE AMPLIFICATION FACTORS BASED ON SITE RESPONSE MODEL.

Project No. 4790.002

Figure **F-14**

Non-GDS

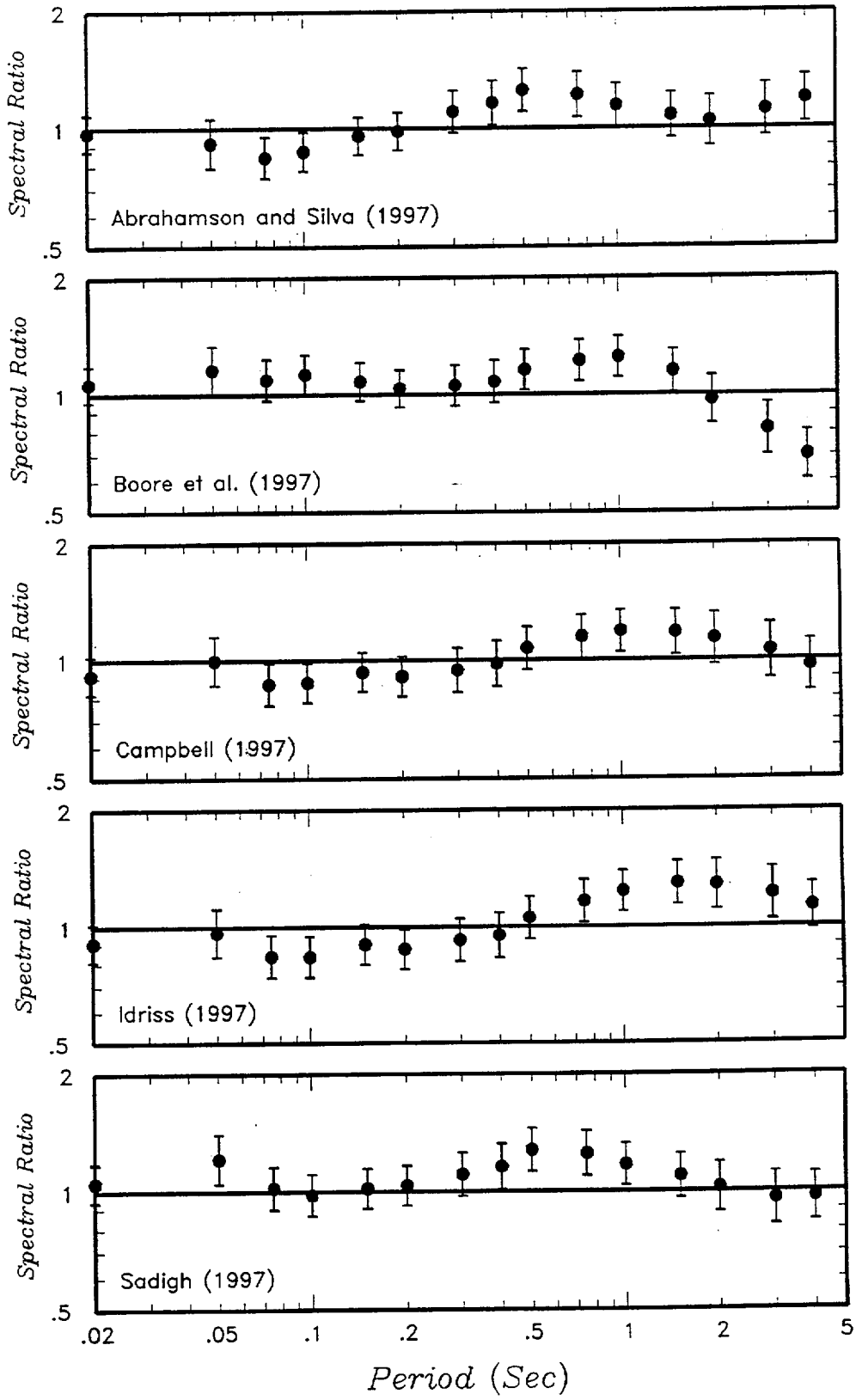

I:\DOC_SAFE\4000S\4790\4790-002\...F15-REV1

GEOMATRIX

EMPIRICAL SPECTRAL RATIOS OF RECORDED SHALLOW SOIL SITE GROUND MOTIONS DIVIDED BY PREDICTED ROCK SITE GROUND MOTION FOR WUS HORIZONTAL ATTENUATION RELATIONSHIPS.

Project No. 4790.002

Figure F-15

Non-GDS

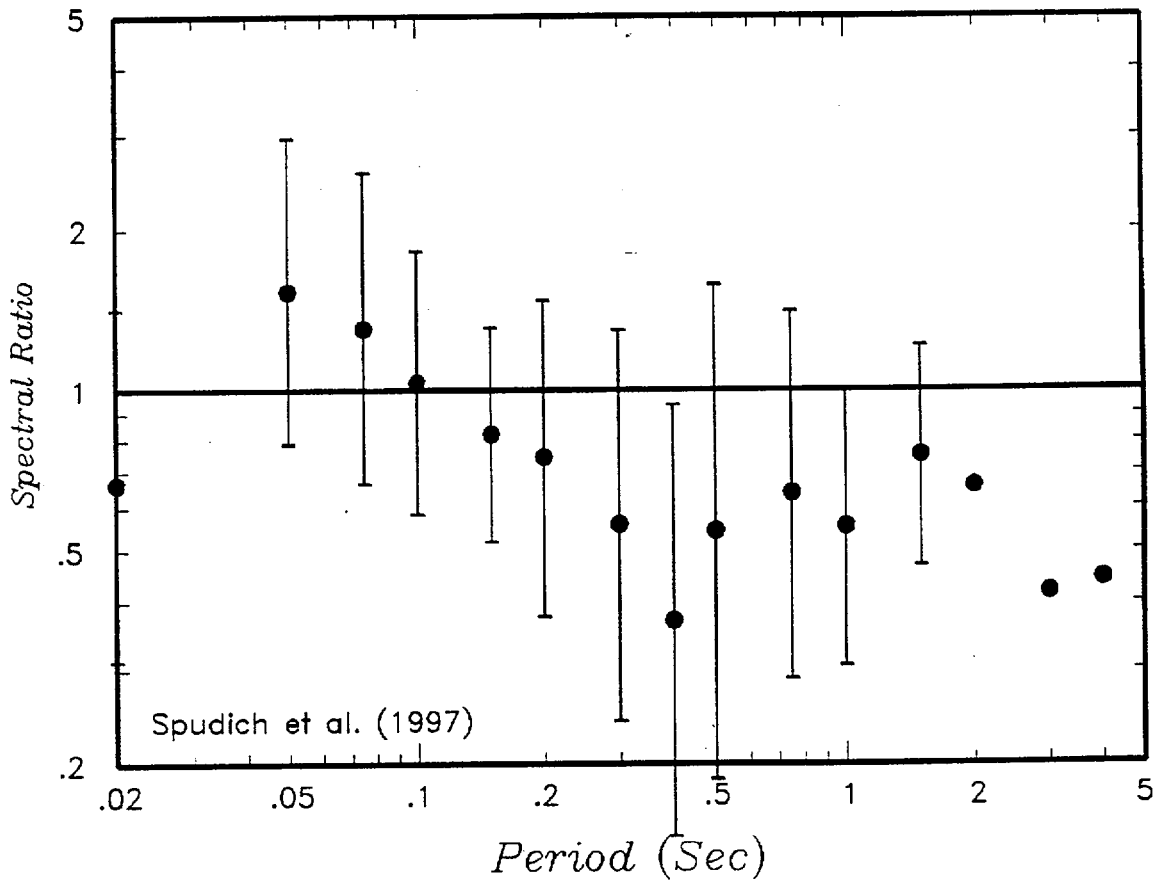

I:\DOC_SAFE\4000S\4790\4790-002\...F15a-REV1

GEOMATRIX

EMPIRICAL SPECTRAL RATIOS OF RECORDED SHALLOW SOIL SITE GROUND MOTIONS DIVIDED BY PREDICTED ROCK SITE GROUND MOTION FOR WUS HORIZONTAL ATTENUATION RELATIONSHIPS.

Project No. 4790.002

Figure **F-15 (cont.)**

Non-GDS

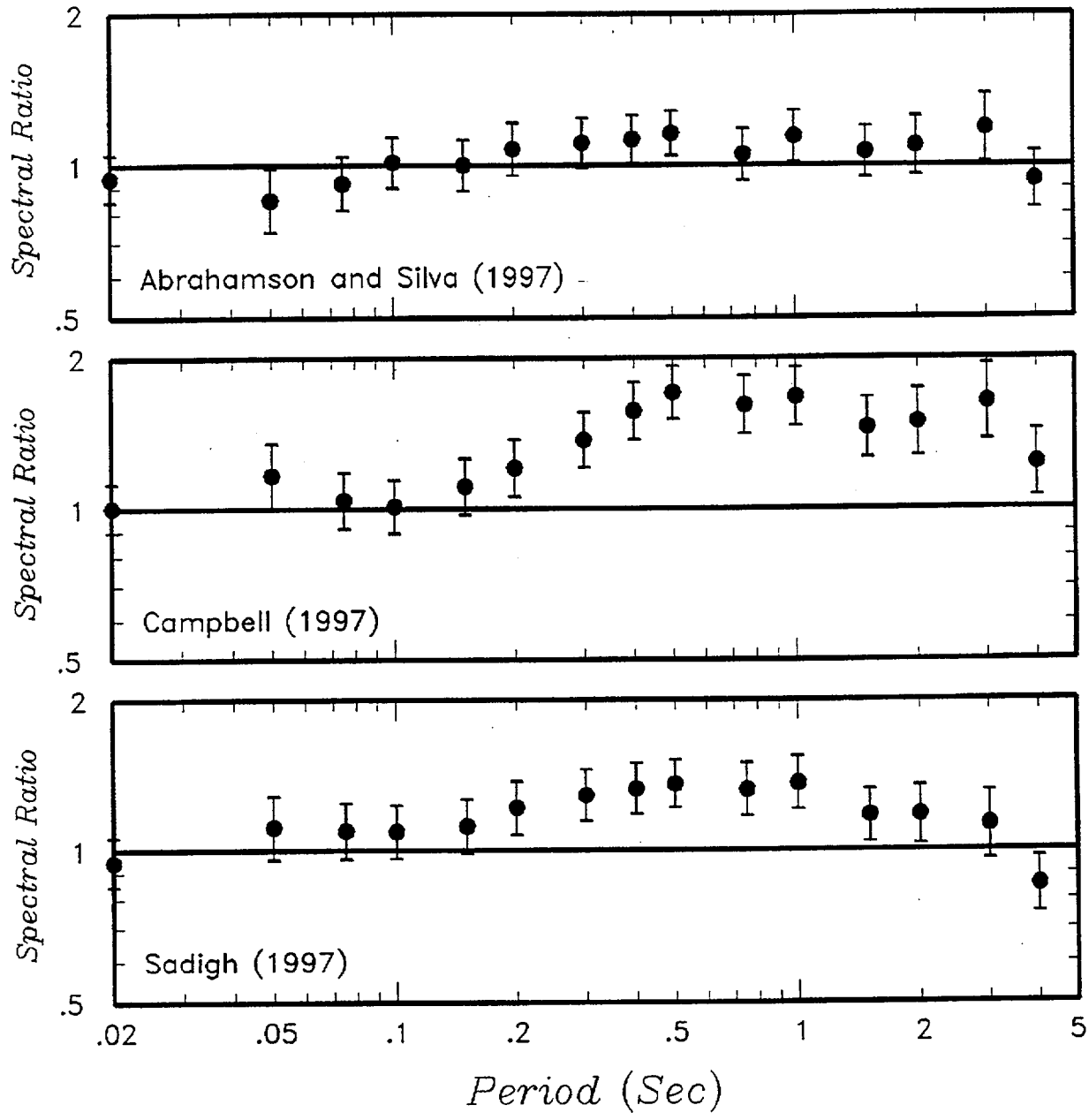

GEOMATRIX

EMPIRICAL SPECTRAL RATIOS OF RECORDED SHALLOW SOIL SITE GROUND MOTIONS DIVIDED BY PREDICTED ROCK SITE GROUND MOTION FOR WUS VERTICAL ATTENUATION RELATIONSHIPS.

Project No. 4790.002

Figure F-16

I:\DOC_SAFE\4000S\4790\4790-002\...F16-REV1

Non-GDS

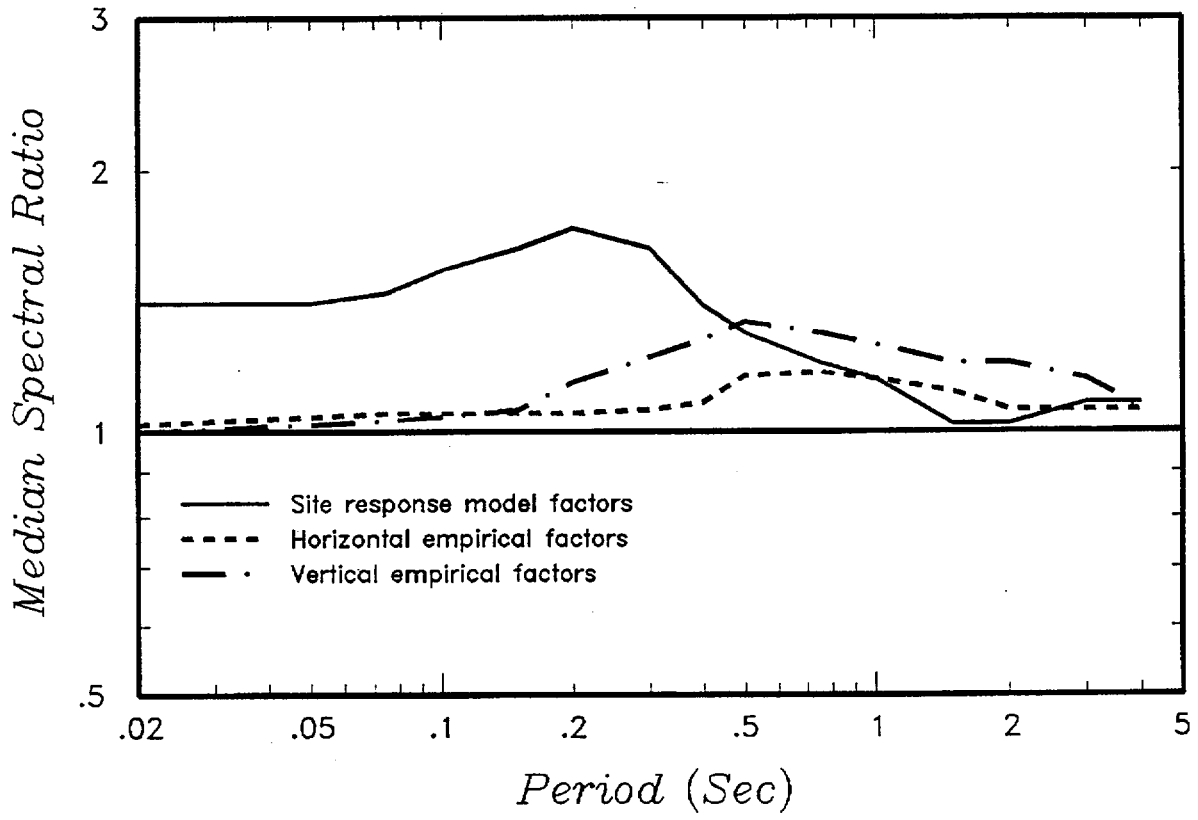

GEOMATRIX	SITE RESPONSE MODEL AND EMPIRICAL SITE ADJUSTMENT FACTORS USED TO COMPUTE GROUND MOTION HAZARD AT THE SKULL VALLEY SITE.	Project No. 4790.002 Figure F-17

I:\DOC_SAFE\4000S\4790\4790-002\...F17-REV1

Development of Design Ground Motions for the Private Fuel Storage Facility, Revision 1

Private Fuel Storage Facility

Skull Valley, Utah

Prepared for:

Stone & Webster Engineering Corporation
P.O. Box 5406
Denver, Colorado 80217-5406

Prepared by:

Geomatrix Consultants, Inc.
2101 Webster Street, Suite 1200
Oakland, California 94612
(510) 663-4100

March 2001

Project No. 4790.002

TABLE OF CONTENTS

TABLES

FIGURES

DEVELOPMENT OF DESIGN GROUND MOTIONS

Private Fuel Storage Facility
Skull Valley, Utah
Rev 01

1.0 INTRODUCTION

This report documents the development of design ground motion response spectra for the Skull Valley Private Fuel Storage site based on the result of the revised probabilistic seismic hazard analysis conducted for the site (Geomatrix Consultants, Inc., 2001). The transformation from the equal-hazard response spectra to design ground motions involves application of USNRC Regulatory Guide 1.165 (USNRC, 1997) procedures and, for this site, incorporation of near-source ground motion effects.

2.0 APPLICATION OF REGULATORY GUIDE 1.165

2.1 APPROACH

Appendix F of USNRC Regulatory Guide 1.165 describes how design ground motion response spectra are to be defined based on a probabilistic seismic hazard analysis. The steps involved when using site-specific response spectra are:

1. Using the specified probability level, develop an equal-hazard response spectrum from the results of a probabilistic seismic hazard analysis (PSHA) for the site.

2. From the results of the PSHA, determine the mean magnitude, $\overline{M}$, and mean distance, $\overline{D}$, for events contributing to the design ground motion level hazard at spectral frequencies of 5 to 10 Hz and 1 to 2.5 Hz. The procedure to be used is described in Appendix C of USNRC Regulatory Guide 1.165.

3. Develop appropriate site-specific response spectra shapes for the events defined by $\overline{M}$ and $\overline{D}$ from step 2. Scale these spectral shapes to the spectral acceleration levels for the average of motions for 5 to 10 Hz and the average of motions for 1 to 2.5 Hz. The envelop of the scaled spectra and the equal-hazard spectra then defines the design-basis ground motion response spectrum.

2.2 STEP 1: EQUAL-HAZARD SPECTRA

Geomatrix Consultants, Inc. (2001) presents the PSHA analysis for the Skull Valley Private Fuel Storage Facility site. The hazard results presented in that analysis are for free-field motions at the ground surface accounting for the estimated local site effects. Using these

results, equal-hazard response spectra were developed for a return period of 2,000 years (mean annual probabilities of exceedance of 5×10^{-4}). These spectra are shown on Figure 1.

2.3 STEP 2: DETERMINATION OF $\overline{M}$ AND $\overline{D}$

The procedure to be used for determining $\overline{M}$ and $\overline{D}$ is described in Appendix C of USNRC Regulatory Guide 1.165. The process involves computing the contribution to the total hazard at the specified design level from events in discrete magnitude and distance bins. These relative contributions are multiplied times the average magnitude and distance for each bin, and the product summed over all bins to compute a weighted average magnitude, $\overline{M}$, and log average distance, $\overline{D}$, of the events contributing to the design level hazard. Two spectral frequency ranges are used, the average of motions at 5 and 10 Hz (0.2 and 0.1 sec. periods, respectively) and the average of motions at 1 and 2.5 Hz (1.0 and 0.4 sec. periods, respectively). Appendix C of USNRC Regulatory Guide 1.165 specifies the size of the magnitude and distance bins appropriate for the evaluation of sites in the central and eastern United States and indicates that other bin sizes may be necessary. Because the hazard at the Skull Valley site is primarily due to magnitude 6 to 7.25 events occurring on the nearby faults, a reduced magnitude and distance bin size was used to provide a more accurate representation of the contributions to the hazard. The magnitude bin size was set to 0.25 magnitude units centered on each ¼ magnitude from 5 to 8, and the distance bins were set to: 0-5 km, 5-10, km, 10-15 km, 15-20 km, 20-25 km, 25-30 km, 30-50 km, 50-75 km, 75-100 km, 100-150 km, and 150-200 km.

Figure 2 shows the computed percent contributions to the hazard for each of the specified return periods, spectral frequency ranges, and horizontal and vertical motions. These results indicate that the hazard is due principally to earthquakes occurring within 15 km of the site. Because the contribution from events at distances greater than 100 km is less than 1 percent in all cases, the special provisions for distant sources described in Appendix C of USNRC Regulatory Guide 1.165 need not be applied. The computed values of $\overline{M}$ and $\overline{D}$ are:

Ground Motion Parameter	Spectral Frequency Range	$\overline{M}$	$\overline{D}$ (km)
2,000-year horizontal	5 – 10 Hz	6.4	5
	1 – 2.5 Hz	6.5	5
2,000-year vertical	5 – 10 Hz	6.5	6
	1 – 2.5 Hz	6.5	6

2.4 STEP 3: SCALING SITE-SPECIFIC SPECTRAL SHAPES TO EQUAL-HAZARD SPECTRA

Free-field ground surface response spectral shapes were developed for each of the $\overline{M}$ and $\overline{D}$ pairs listed above using the ground motion attenuation relationships developed for computing the hazard (Geomatrix Consultants, Inc., 2001). The spectral shapes were developed by computing 84th-percentile response spectra for each $\overline{M}$ and $\overline{D}$ using a weighted combination of the attenuation relationships and then dividing the resulting spectral accelerations by the computed 84th-percentile peak acceleration. The weights assigned to each of the relationships are given in Appendix F, Tables F-1 and F-2 of Geomatrix Consultants, Inc. (2001). These relationships have been adjusted for local site effects as described in Appendix F of Geomatrix Consultants, Inc. (2001).

Figure 3 shows the results of scaling these spectral shapes to the appropriate response spectral accelerations for each equal-hazard spectrum. In general, enveloping the three response spectra results in, at most, only minor increases in the ground motions above those specified by the equal hazard spectra. These increases arise, in part, from including more spectral frequencies in the spectral shapes than were used to compute the equal-hazard spectra, providing better interpolation and smoother spectral shapes.

3.0 INCORPORATION OF NEAR-SOURCE EFFECTS

The hazard at the Skull Valley site is due to the occurrence of large-magnitude earthquakes on nearby faults. Recent studies, focused primarily on strike-slip earthquakes, have indicated that there are effects of rupture directivity on strong ground motions that are observable and systematic in the near field of large earthquakes. These effects have been quantitatively defined by Somerville and others (1997) using empirical data. They describe two effects, one resulting from directivity of rupture (a Doppler effect) and one representing a systematic difference between fault-normal and fault-parallel motions (the horizontal response spectral

attenuation relationships used to define the equal-hazard response spectra and the spectral shapes shown on Figure 3 represent the geometric mean of the two horizontal components). The effects first become significant at a spectral frequency of 1.67 (0.6-second period) and increase with decreasing spectral frequency (increasing period).

The magnitude of these effects is related to the size of the earthquake and to the geometric relationship between the site, the length of the rupture, and the location of the point of rupture initiation. For dip-slip faults, these are parameterized by the term $y\cos(\phi)$, where ϕ is the angle between the rupture surface and a line drawn from the point of rupture initiation and the site and y is the distance from the point of rupture initiation to the site measured along the fault divided by the length of rupture measured in the direction of slip (for dip slip faults, the rupture width). Because most large normal faulting earthquakes appear to initiate near the base of the seismogenic crust, sites located on the fault trace will have $\phi = 0$ and y near 1.0, and will thus experience the maximum effect of both directivity and systematic fault-normal-to-fault-parallel differences in ground motion.

The impact of these effects on the spectra shown on Figure 3 was evaluated by considering the contributions of the different sources to the total hazard at a return period 2,000 years. From Figure 6-12 of Geomatrix Consultants, Inc. (1999), the majority of the hazard for horizontal motions comes from the four nearby faults: the East, West, Stansbury, and East Cedar Mountains faults. For each fault, the parameters ϕ and y were conservatively set to the values associated with rupture at the closest point on the faults, with rupture initiation occurring at the base of the seismogenic crust. Thus, y was set equal to 1.0 for all faults and ϕ was set to 1.6°, 3.0°, 19.5°, and 54.9° for the East, West, Stansbury, and East Cedar Mountains faults, respectively. The appropriate adjustment factor for each fault was computed using the relationships presented in Somerville and others (1997) and the mean magnitude contributing to the hazard for each fault. The hazard curves for each fault were then scaled in the horizontal (ground motion) direction by these factors and then reinterpreted to obtain frequencies of exceedance at common ground motion levels. These were, in turn, summed to obtain a new composite hazard curve for these faults and the result added to the hazard from all other sources to obtain an adjusted total hazard for horizontal ground motions. An additional source of some conservatism in this process is the fact that the standard deviation in the ground motions should be slightly reduced because the inclusion of a systematic directivity effect should improve the ability of the attenuation relationships to predict the observed ground motion data. However,

this effect has not been evaluated for dip-slip faults and has been conservatively ignored in this analysis.

The adjusted hazard curves were then interpolated to obtain spectral accelerations for a return period of 2,000 years. The resulting ratios of the adjusted to unadjusted spectral accelerations are:

Ratio of Near-Field Adjusted to Unadjusted Spectral Accelerations

Return Period	Spectral Period (sec)	Directivity only	Directivity plus Fault-Normal/ Average	Directivity plus Fault-Parallel/ Average
2,000 years	1.0	1.056	1.106	1.005
	2.0	1.161	1.307	1.019
	4.0	1.224	1.545	0.958

4.0 DESIGN GROUND MOTION RESPONSE SPECTRA

Design ground motion response spectra were developed by scaling the envelop of the response spectra shown on Figure 3 by the near-fault effects adjustment factors listed above. Ratios for intermediate frequencies were obtained by linear interpolation on log(period), with the ratio set to 1.0 for all periods less than 0.6 second (frequencies greater than 1.67 Hz). For vertical motions it was assumed that the near-fault effect for directivity only found for horizontal motions applies. The resulting response spectra are shown on Figures 4 and are tabulated in Table 1.

5.0 REFERENCES

Geomatrix Consultants, Inc., 2001, Fault evaluation study and seismic hazard assessment, Private Fuel Storage Facility, Skull Valley, Utah, Rev 01: report prepared for Stone & Webster Engineering Corporation, March.

Somerville, P.G., Smith, N.F., Graves, R.W., and Abrahamson, N.A., 1997, Modification of empirical strong ground motion attenuation relations to include the amplitude and duration effects of rupture directivity: Seismological Research Letters, v. 68, p. 199-222.

USNRC, 1997, Regulatory Guide 1.165 Identification and characterization of seismic sources and determination of safe shutdown earthquake ground motions: U.S. Nuclear Regulatory Commission, March.

TABLE 1

DESIGN GROUND MOTION RESPONSE SPECTRA FOR THE SKULL VALLEY PRIVATE FUEL STORAGE FACILITY

2,000-year Return Period Spectral Accelerations (g, 5% damping)				
	Horizontal			
Period (sec)	Fault Normal	Fault Parallel	Period (sec)	Vertical
PGA	0.711	0.711	PGA	0.695
0.03	0.711	0.711	0.02	0.695
0.05	0.985	0.985	0.05	1.293
0.075	1.246	1.246	0.075	1.638
0.1	1.541	1.541	0.1	1.761
0.15	1.889	1.889	0.15	1.635
0.2	2.011	2.011	0.2	1.426
0.3	1.699	1.699	0.3	0.959
0.4	1.291	1.291	0.4	0.663
0.5	1.050	1.050	0.5	0.509
0.75	0.693	0.664	0.75	0.324
1.0	0.525	0.477	1.0	0.237
1.5	0.314	0.260	1.5	0.145
2.0	0.223	0.174	2.0	0.104
3.0	0.147	0.0997	3.0	0.0668
4.0	0.103	0.0640	4.0	0.0468

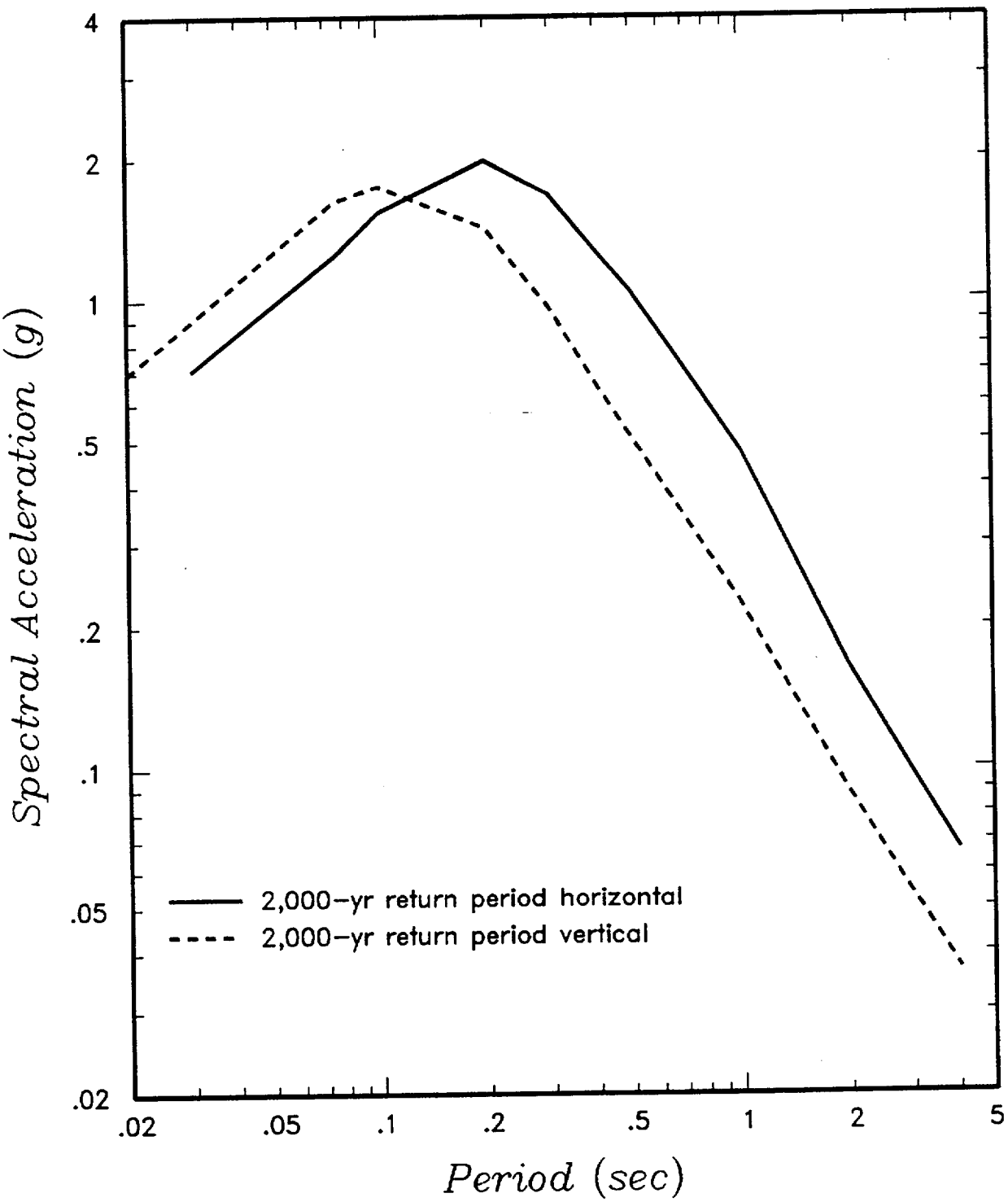

GEOMATRIX

EQUAL HAZARD RESPONSE SPECTRA (5% DAMPING) FOR THE SKULL VALLEY SITE
Private Fuel Storage Facility
Skull Valley, Utah

Project No.
4790.002

Figure
1

Non-GDS

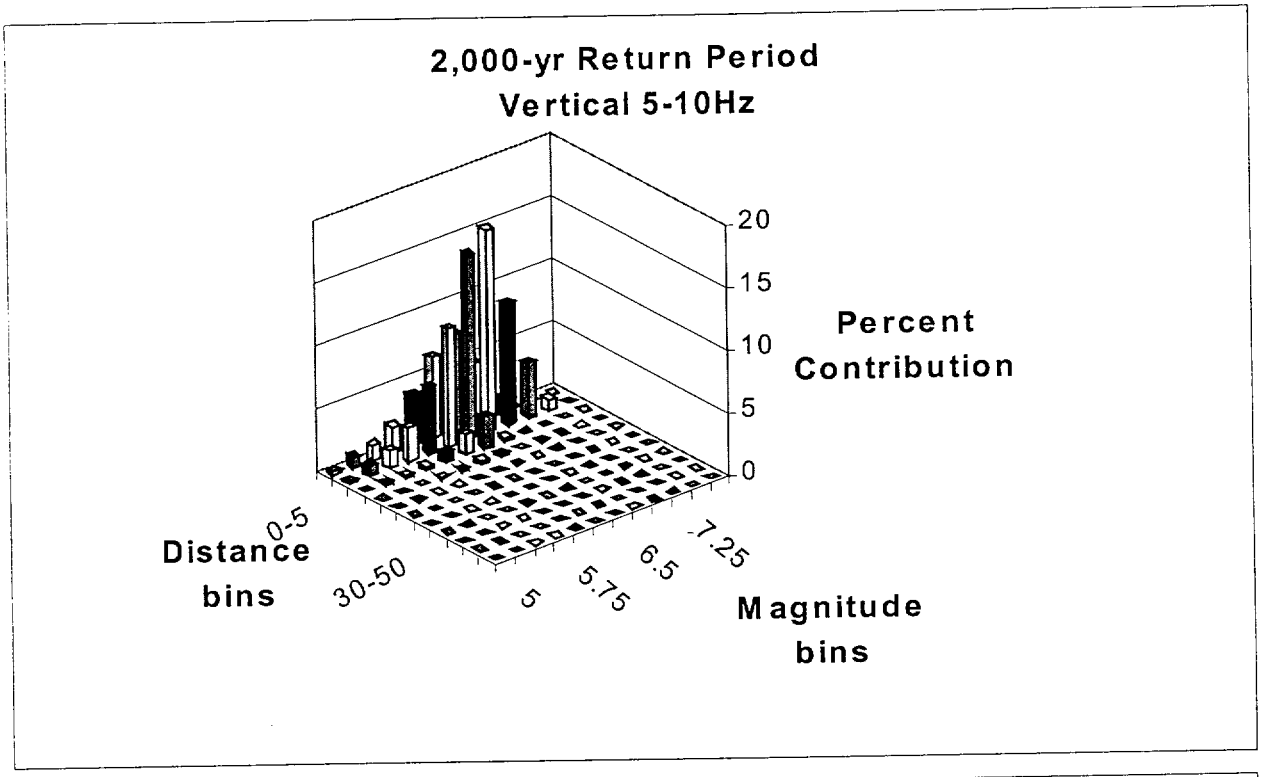

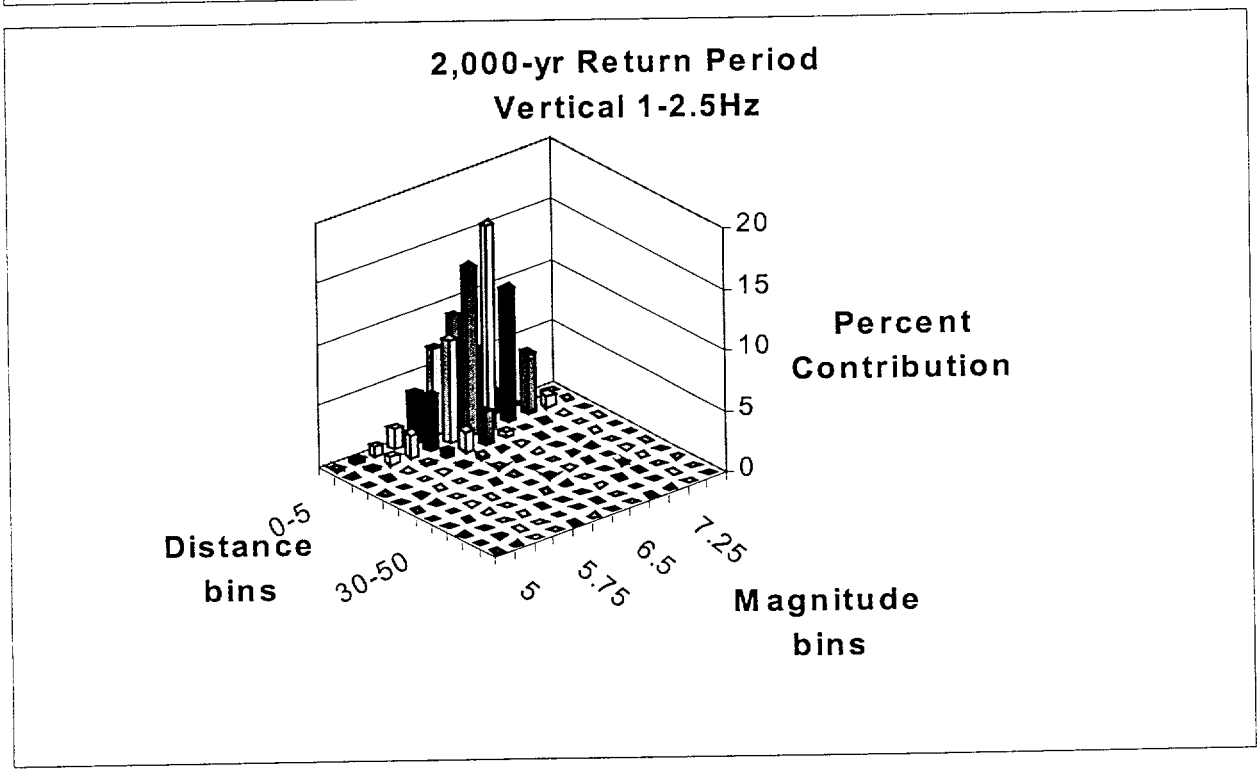

GEOMATRIX	PERCENT CONTRIBUTIONS OF EVENTS IN SPECIFIED MAGNITUDE AND DISTANCE BINS TO THE HAZARD. Private Fuel Storage Facility Skull Valley, Utah	Project No. 4790.002 Figure 2

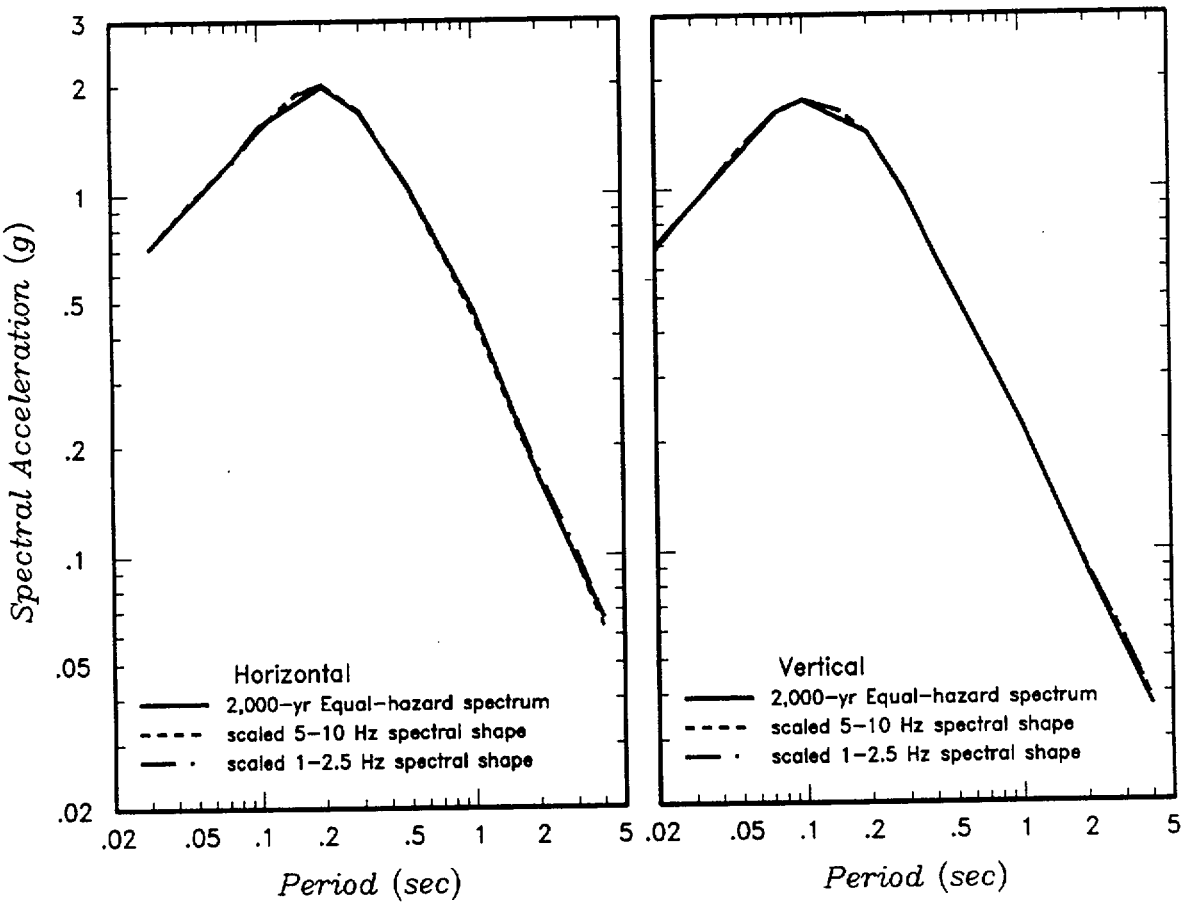

GEOMATRIX	COMPARISON OF EQUAL-HAZARD RESPONSE SPECTRA AND SCALED SPECTRAL SHAPES. Private Fuel Storage Facility Skull Valley, Utah	Project No. 4790.002 Figure 3

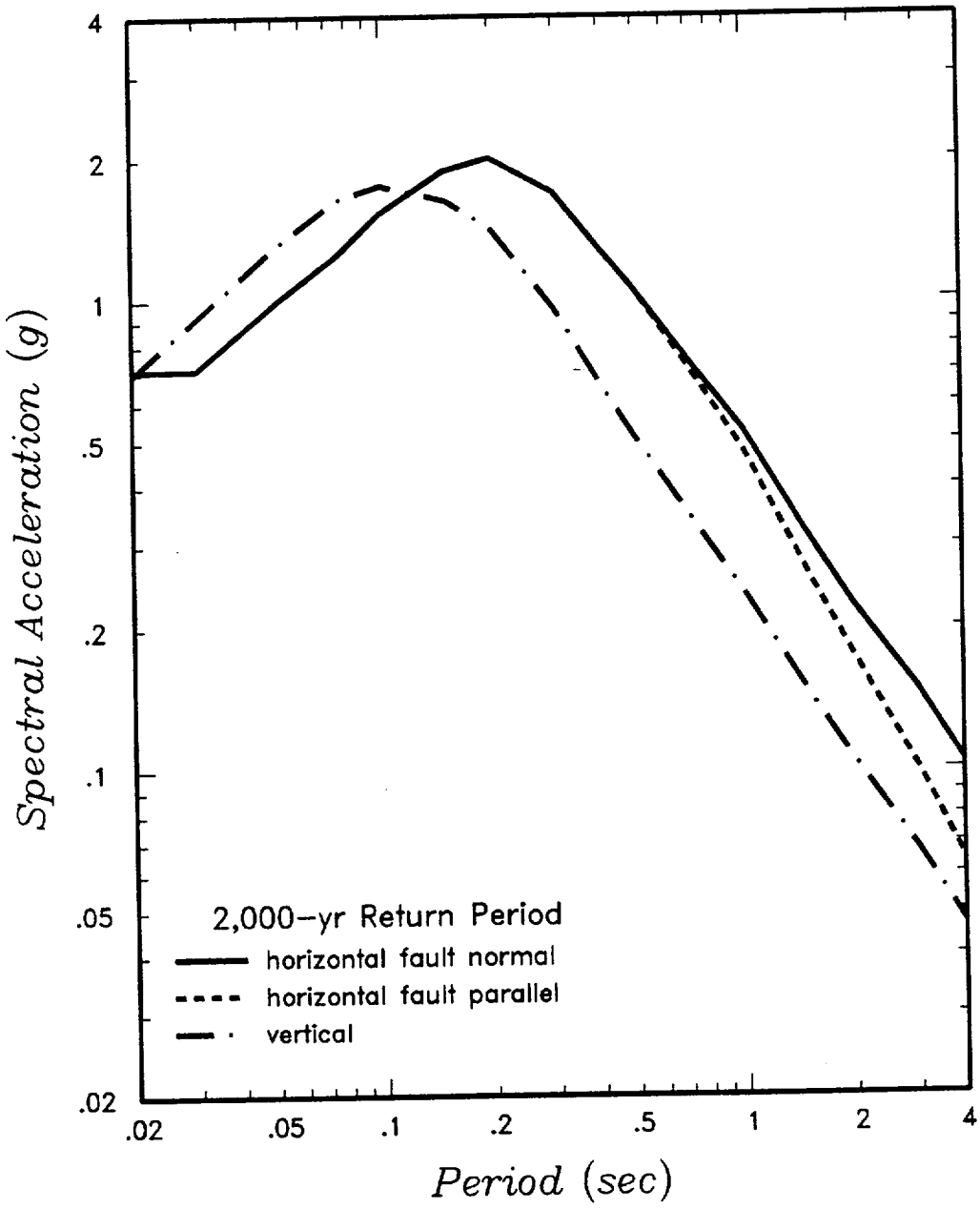

GEOMATRIX	DESIGN GROUND MOTION RESPONSE SPECTRA (5% DAMPING) BASED ON 2,000-YEAR RETURN PERIOD HAZARD. Private Fuel Storage Facility Skull Valley, Utah	Project No. 4790.002 Figure 4